Supported Metal Nanoparticles for The Selective Transformation of Bio-derived Molecules by Thermal Catalysis and Photocatalysis

Thesis submitted in accordance with the requirements of the University of Liverpool for the degree of Doctor of Philosophy

By

Edgar Osiris Gonzalez Yañez

April 2019

Acknowledgments

First of all, I would like to thank Prof. Jose A. Lopez-Sanchez for giving me the opportunity to carry out my PhD within his research group in the Chemistry Department at the University of Liverpool.

Especially, I would like to thank Dr. Alexander Cowan and Prof. Mario Pagliaro for their valuable suggestions and advice on my thesis and research work.

I would also like to thank Dr. Annarita Noschese for her support and guidance during this project. A special thanks goes to Dr. Thomas Davies for all his support, motivation, and patience with me at the early stages of my PhD. I would also like to thank Dr. Peter Priecel and Dr. Piera Demma Cara for your support and supervision during this project.

A special thanks goes to Javier and David, my best friends and brothers in this journey. I would like to thank all member of the JALS group for your support and friendship, I wish you all the best!. I would like to thank Elena, Laura, and Carmen who were my first students. I hope that you have enjoyed doing scientific research here in Liverpool. I wish you all the best and I hope to visit Spain soon.

I would like to thank the Mexican National Council for Science and Technology (CONACyT) for the financial support that was provided. I would like to thank the MicroBiorefinery (MBR), the Centre of Material Discovery (CMD), and the Research Complex at Harwell (RCaH) for access to state-of-the-art facilities.

Finally, I would like to thank my family, my Mum, Dad, Yutzi, and Melissa for your support during this PhD. A special thanks goes to Edith for her endless support and love.

Abstract

In this thesis, the catalytic activity of supported metal nanoparticles has been investigated in the selective conversion of bio-derived molecules using alternative technologies such as heterogeneous photocatalysis and microwave-assisted heating.

The first part of this Thesis presents the development of a new synthesis method (SASI) for the preparation of gold metal nanoparticles supported on conjugated microporous polymers (CMPs). The new method involves the preparation of metallic sols and their subsequent immobilization on the polymeric support in the presence of an organic solvent. For comparison, the traditional sol immobilisation method and the wet impregnation method were used to prepare gold catalysts. The catalytic activity of the catalysts was evaluated in the oxidation of glucose under microwave-assisted heating. The 2 wt% Au/CMP-SASI(ACN-W) catalyst showed the highest activity in the oxidation of glucose and demonstrated to be reusable after several runs without losing activity and selectivity.

The second part presents the evaluation of the photocatalytic activity of several gold catalysts in the oxidation of glucose under UV and visible light. Several support materials such as titanium dioxide (TiO_2), conjugated microporous polymers (CMPs), and multi-walled carbon nanotubes (CNTs) were used to prepare the gold catalysts. The initial experiments were carried out under alkaline conditions at atmospheric pressure, then a representative sample (2 wt% Au/CNTs) was used to catalyse the glucose oxidation in the presence of molecular oxygen as the oxidant under alkaline conditions. Interestingly, the results revealed that the Au/TiO_2 catalyst promotes the formation of several products during photocatalysis. Blank tests demonstrated the influence of the support material in the oxidation of glucose. These results contradict previous work which claims that the selective photo-oxidation of glucose into gluconic acid (as the main product) can be carried out using TiO_2-based gold catalysts under alkaline conditions. Additional experiments were carried out using gold nanoparticles supported on CMPs or CNTs. The results demonstrated the strong effect of the thermal reaction in the photocatalytic process regardless of the type of support used in this work.

The third part presents a new approach for the photocatalytic conversion of polysaccharides using noble metal nanoparticles supported on TiO_2. Parameters such as nature of the substrate, light intensity, irradiation time, and solvent composition were investigated in order to provide the optimal conditions to perform the photocatalysis. The results showed that organic solvents such as acetonitrile cannot be used during photocatalysis as it can undergo photodegradation over the gold catalysts. These results contradict previous work where it was established the positive effect of acetonitrile in the formation of carboxylic acids from glucose. The photoconversion of cellulose was carried out using water as a solvent in the presence of molecular oxygen as the oxidant under UV and visible light for 24 hours. Unfortunately, the formation of products was not observed. In order to improve the efficiency of the photocatalysts in the cellulose conversion, a promoter (NaOH) was added to the reaction mixture before the photocatalysis. The results showed that the presence of the base improves the cellulose reactivity allowing the formation of several oxidation products. On the other hand, additional experiments were carried using starch as starting material under visible light conditions, however, traces of oxidation products were observed along with high amounts of oligomers after photocatalysis, highlighting the complexity of the substrate.

Abbreviations

ACN	Acetonitrile
ACN–W	Acetonitrile–Water
ATR	Attenuated total reflectance
BDBA	Benzene diboronic acid
BE	Binding energy
BET	Brunauer–Emmett–Teller
CHN	CHN elemental analysis
CMD	Centre of Materials Discovery
CMPs	Conjugated microporous polymers
CNTs	Carbon nanotubes
DAD	Diode array detector
DMF	Dimethylformamide
DP	Degree of polymerization
DR UV–Vis	Diffuse reflectance UV–Vis spectroscopy
EtOAc	Ethyl acetate
FTIR	Fourier–transform infrared spectroscopy
GPC	Gel permeation chromatography
HMF	Hydroxymethylfurfural
HPLC–QTOF	High Performance Liquid Chromatography Time–of–Flight Mass Spectrometry
ICal	Imaging Centre at Liverpool
ICP–OES	Inductively Coupled Plasma – Optical Emission Spectrometry
LMCT	Ligand–to–metal charge–transfer
LUMOs	Lowest unoccupied molecular orbitals
MCC	Microcrystalline cellulose
MCNTs	Multi–walled carbon nanotubes
PPO	Poly(2,6–dimethyl–1,4–phenylene oxide)

PTFE	Polytetrafluoroethylene
PVA	Polyvinyl Alcohol
Q	Amount of swelling
RCaH	Research Complex at Harwell
RID	Refractive index detector
ROS	Reactive oxygen species
SASI	Solvent–assisted sol immobilisation
SI	Sol-immobilization method
SPR	Surface plasmon resonance
SPRB	Surface plasmon resonance band
TBB	Tetrabromobenzene
TCD	Thermal conductivity detector
TEM	Transmission electron microscopy
TiO_2	Titanium dioxide
TOC	Total organic carbon
TOF	Turnover frequency
UV–Vis	Ultraviolet–visible spectroscopy
WI	Wet impregnation
XPS	X-ray photoelectron spectroscopy
XRD	X-Ray Diffraction
ZrO_2	Zirconium dioxide

Table of Contents

List of Figures

Chapter 3

Chapter 5

Appendix B

List of Tables

List of Schemes

Chapter 1

Introduction

1.1 Catalysis

The concept of catalysis was developed in 1835 by Berzelius when he scrutinized the recorded observations of experimental work and denoted them as catalysis [1]. He defined the term catalysis to the substances that accelerate chemical reactions, and they are not consumed during the process. Later, in 1895 Ostwald provided a more accurate definition: catalysis is a process where a substance modifies the rate of a chemical reaction, and it is not consumed or transformed at the end. Now, this substance is called catalyst, and the IUPAC defines a catalyst as a substance that increases the rate of a reaction without modifying the thermodynamics [2]. A catalyst does not alter the standard Gibbs free energy, but only influences the energy barrier (the activation energy, E_a) between reactants and products. Figure 1.1 shows the energy diagram which compares a catalysed (red line) and uncatalysed (black line) reaction. For the uncatalysed reaction the activation energy (E_a) is high, and therefore sufficient energy must be applied to overcome this barrier in order to produce C from A + B. In the case of the catalysed reaction (red line), the presence of the catalyst provides an alternative reaction pathway where the formation of C from A + B is more favourable. This alternative path implies an activation energy ($E_{a,cat.}$) lower than the one for the uncatalysed process (E_a).

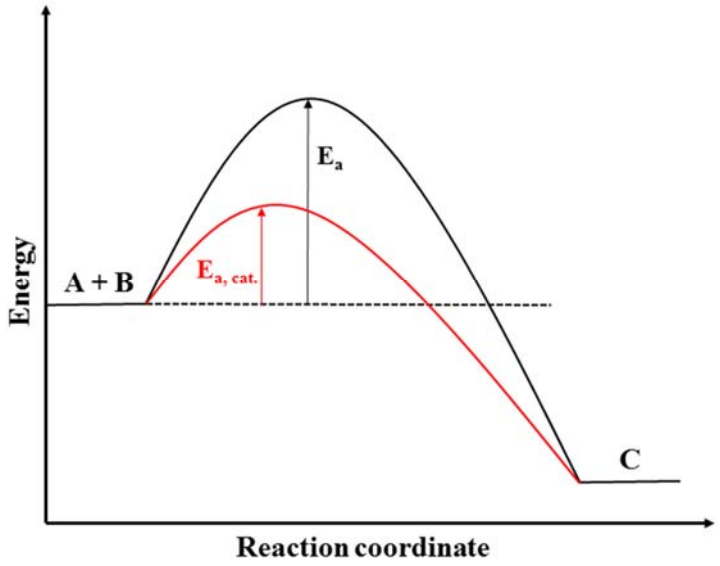

Figure 1.1 The energy diagram of a reaction catalysed (red line) and uncatalysed (black line). E_a corresponds to the activation energy, and $E_{a,cat.}$ is the activation energy for the catalysed reaction.

Catalysis can be categorized into two fields: homogeneous and heterogeneous catalysis. Typically, homogeneous catalysis implies that both the catalyst and reactant are presented in the same phase, for example, the decomposition of ozone in the presence of chlorine free radicals. In heterogeneous catalysis, both the catalyst and reactant are in a different phase; for example, the oxidation of carbon monoxide (gas phase) in the presence of a gold catalyst (solid phase) [3].

Heterogeneous catalysis is the most important type of catalysis, and it is estimated that nearly 90% of the chemical processes in the industry involves the use of a solid catalyst, ranging from the food to petrochemical industries [4, 5]. In heterogeneous catalysis, the reactants (in liquid or gas phase) can be converted into products over the surface or within the pores of the solid catalyst. In this scenario, it is clear that many reactions dependent on the effectiveness of the solid catalyst. Moreover, it is desirable that a catalyst can perform chemical transformations with high selectivity to the desired products and acceptable rates of reaction. At the same time, the catalyst should be stable at different reaction conditions without losing activity, but more importantly, it should provide good accessibility to the reactants in order to reach the active sites and being transformed. Therefore, the heterogeneous catalytic reactions involve a series of reaction steps in which the catalyst and reactants participate. For example:

1. Diffusion.- The reactants diffuse within the boundary layer to the catalyst surface.
2. Internal diffusion.- The reactants diffuse into the pores in order to reach the active centers of the catalyst.
3. Adsorption.- Adsorption of the reactants over the active centers.
4. Reaction.- Chemical transformation of the adsorbed reactants.
5. Desorption.- After the formation of the products, they are desorbed from the active centers of the catalyst.
6. Internal diffusion.- The products diffuse out of the pores.
7. Diffusion. The products diffuse out of the catalyst through the boundary layer.

Due to the presence of different reaction steps, the total rate of the reaction is affected by several parameters, including; a) film diffusion (steps 1 and 7), b) pore diffusion (steps 2 and 6), and c) the reaction kinetics (steps 3-5). In heterogeneous catalysis can also be presented mass and heat transfer effects for highly endothermic and exothermic systems [5].

1.2 Support Materials In Heterogeneous Catalysts

In heterogeneous catalysis, reactions are performed using reactants in liquid or gas phase and a solid catalyst, which is the heart of many catalytic processes in the industry. Typically, the catalytic activity of the solid catalysts is associated with metal surface sites (usually the active phase), and the presence of metal nanoparticles which are deposited on an inert support. As a result, it is desirable to increase the surface-to-volume ratio of the active phase in order to improve the catalytic activity of the final catalyst, thus the support material plays an important role in the catalyst development. The support material has several uses for the catalytic process: it increases the surface area available for the active phase, reduces the sintering process, and improves the chemical stability of the final catalyst [6]. Hence, the support stability is crucial as it can affect the lifetime of the catalyst, and consequently the catalytic activity. Common and novel support materials include metal oxides, carbon-based materials, zeolites, ordered mesoporous materials, polymers, and metal-organic frameworks [7-12]. In this thesis, support materials such as titanium dioxide, carbon nanotubes, and conjugated microporous polymer, were used to prepare solid catalysts. The following sections will be referred to these support materials.

1.2.1 Titanium Dioxide (TiO_2)

Titania or Titanium dioxide (TiO_2) is the most studied semiconductor material due to its high reactivity, thermal stability, nontoxicity, low cost and exceptional photoactivity under UV light irradiation [13]. TiO_2 has been widely investigated in the literature in several fields including, photocatalysis, sensors, heterogeneous catalysis, solar cells, and antimicrobial applications [14-17]. TiO_2 can be presented in three crystalline phases: brookite, rutile, and anatase (Figure 1.2). Brookite and anatase phases are less stable than rutile as they can undergo a phase transition at temperatures above 650 °C, forming the rutile phase [18]. Typically, the preparation of TiO_2 materials (brookite, anatase, or rutile) requires high temperatures to crystallize the amorphous material resulting in large particles and nonporous structures. However, it has been reported that crystalline TiO_2 with high porosity and well-defined mesostructure can be synthesized at low temperatures [19]. Moreover, crystalline TiO_2 structures have also been prepared by solution-based methods without thermal treatment forming particles below 10 nm [20].

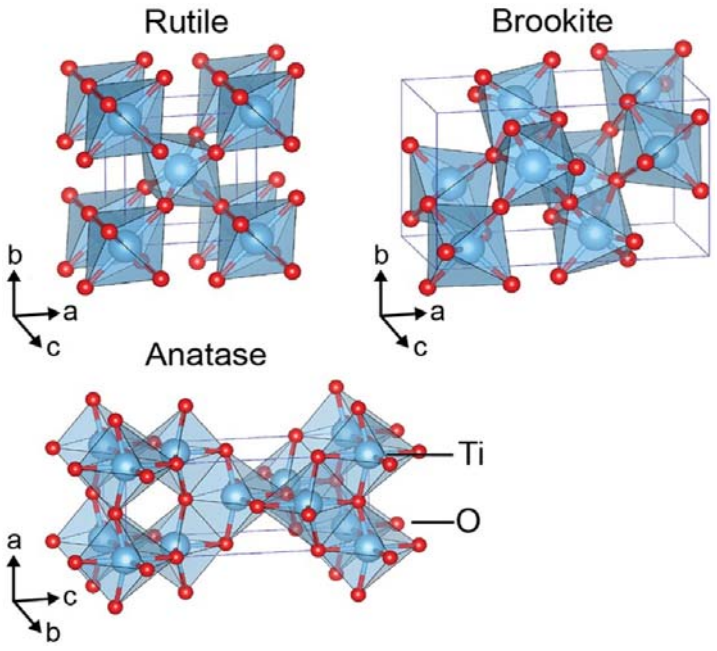

Figure 1.2 Crystalline phases of TiO_2: rutile, anatase, and brookite. Taken from Haggerty et al. [21].

As a support material, TiO_2 has demonstrated a positive effect on the catalytic activity of the TiO_2-based catalysts for several reactions, including oxygen reduction [22], hydrodesulfurization [23], propylene production [24], and dehydrogenation [25] among others. However, TiO_2 presents a few disadvantages that might limit its use in heterogeneous systems, for example, low adsorption, particle aggregation, and small surface area. Despite these limitations, a vast number of studies have used TiO_2 as support material for catalytic applications. In heterogeneous catalysis, noble metal nanoparticles (i.e. Au, Ag, Pt) [26-29] have been employed as active sites to catalyse several reactions using TiO_2 as a support material due to its high chemical and thermal stability as well as the promoting effect on the reaction performance as a result of the strong metal-support interactions [30]. However, the synthesis and activation method for the metal nanoparticles can also influence the catalytic activity of the final material. Therefore, the optimisation of the synthesis parameters and reactions conditions are directly related to the catalyst performance.

1.2.2 Carbon nanotubes (CNTs)

Carbon nanotubes (CNTs) were synthesized for the first time in 1991 by Iijima et al. [31] during the vaporization of carbon by an electric arc, and the following year they were produced at higher yield by varying the helium pressure in a reaction vessel [32]. The CNTs consist of graphite sheets (one graphite layer is donated as graphene) rolled up into a tube. CNTs can be classified into two main types: single-walled nanotubes (SWCNTs) and multi-walled nanotubes (MWCNTs). SWCNTs is an individual graphene sheet, while MWCNTs consist of concentric graphene sheets. Typically, CNTs are synthesized by three different methods:

1. The arc discharge method.- In this method, an arc discharge is generated between two carbon electrodes situated inside a reaction vessel under an inert atmosphere (helium or argon) with and without a catalyst [31, 33]. The method produces different materials such as fullerenes, MWCNTs, amorphous carbon and traces of graphene when pure graphite is used.

2. Laser vaporization (ablation).- A high power laser impinges on a graphite sample in the presence of transition metals (cobalt or nickel) under inert gas flow (helium or argon) at high temperature (1200 °C). The products are recovered using a water-cooled trap positioned outside the reactor [34, 35]. Moreover, it has been demonstrated that the use of transition metals such as cobalt or nickel promotes the formation of SWCNTs with yields ranging from 70 to 90 % [34]. However, the method produces small amounts of CNTs with high purity and is not economically viable for large-scale production.

3. Chemical vapor deposition (CVD).- The CVD method has been widely used for the preparation of CNTs due to its low-cost, high yields, and ease of scale-up. Typically, the method implies the use of a metal catalyst (i.e. cobalt, nickel, iron) at temperatures above 600-1200 °C while a hydrocarbon (i.e. ethylene, acetylene) vapor is passing through the tubular reactor. The metal catalyst decomposes the hydrocarbon vapor while at the same time the CNTs are growing over the metal catalyst, then they are collected after reaction [36, 37]. Moreover, liquid (i.e. benzene, ethanol) or solid (i.e. camphor, naphthalene, ferrocene) hydrocarbons can be used as starting material for the production of CNTs [38].

CNTs have attracted much attention since they were discovered by Iijima et al. [31], due to their exceptional mechanical, thermal and electrical properties which make them promising materials for a range of applications including hydrogen storage, field emission devices, photocatalysis, sensors, heterogeneous catalysis, and nanoelectronic devices among others [39-41]. In heterogeneous catalysis, CNTs have been used as a support material due to its high thermal stability and inert structure that allows them to be used under different conditions. CNTs have been defined as nanoreactors [41] where metal nanoparticles (i.e. Au, Pt, Ru) can be deposited either inside or outside the tubes aiming to catalyse chemical reactions, for example, hydrogenations [42], oxidations [43], hydroxylations [44], and photodegradation [45] among others. In general, MWCNTs are preferred over the SWCNTs as a support material because of their larger internal diameter which allows the diffusion of the reactants within the cavities.

1.2.3 Conjugated Microporous Polymers (CMPs)

Conjugated microporous polymers (CMPs) are amorphous materials which consist of a three-dimensional structure with extended π-conjugation [46]. CMPs are mainly composed of carbon-carbon and carbon-hydrogen bonds, and due to their organic structure, they can be produced in a range of compositions resulting in microporous structures with unique physical properties [47]. Moreover, chemical functionalities can be incorporated into the network allowing to fine-tune of the intrinsic properties for specific applications (i.e. synthesis of soluble CMPs) [48, 49]. CMPs have been synthesized using a wide range of organic reactions such as the Suzuki–Miyaura polycondensation [47], Sonogashira–Hagihara [50], and Yamamoto reaction [51] among others. The synthesis and design of conjugated microporous networks have gained much attention in recent years, and more particularly in the areas of gas adsorption [52], energy storage [53], light-harvesting [46], light emitting [54], and carbon capture [55].

In heterogeneous catalysis, CMPs have been recently used as a support material due to its ability to incorporate metal nanoparticles inside the microporous network. In this case, the pores provide spaces where metal particles can be confined, thus limiting particle aggregation and growth in particle size. To date, there are a few reports where CMPs were used as a support material for heterogeneous catalysts. Particularly, CMPs-based catalysts have been used to catalyse several reactions including oxidations, hydrogenations, Suzuki-coupling reactions, and Heck–Mizoroki coupling reactions [56-59]. In other cases, the CMP-based catalysts were not used under catalytic conditions, and their study was limited to the hydrogen sorption [10]. In all cases, palladium metal nanoparticles were used as active sites to perform chemical reactions, obtaining high conversion and remarkable selectivity to the desired products. Therefore, CMPs have demonstrated to be promising support materials that can be tuned to have specific properties which can produce heterogeneous catalysts with multiple functions.

1.3 Synthesis Methods for The Preparation of Heterogeneous Catalysts

In heterogeneous catalysis, the catalyst is considered the heart of any chemical transformation. In the chemical industry, it has been estimated that 90% of the chemical transformations employ a solid catalyst at some point during the process [5]. Therefore, the synthesis method is fundamental for the preparation of catalysts with high activity and stability, and more importantly, it is desirable that the catalysts can perform selective reactions avoiding the formation of side products. Typically, the catalysts consist of metal particles deposited on a support material, and since they are considered the active phase, it is essential to maximize the metal surface area in order to increase the catalytic activity. In this case, metal particles are usually synthesized in the range of 2 to 10 nm [60], then they are deposited on a support material with a high surface area, for example, activated carbon, CMPs, and silica among other. To date, there are several methodologies [60-62] for the preparation of supported nanoparticles, the most common methods used in the literature are impregnation, co-precipitation, deposition-precipitation, and sol immobilisation. These methods are briefly presented in the following sections.

1.3.1 Impregnation

The impregnation method is the most common synthetic procedure used in the preparation of metal catalysts. In this method, the appropriate amount of the metal precursor is dissolved in a solvent which allows the proper dissolution of the metal precursor. The freshly prepared solution is added to the support material, then it is aged and heated until the solvent is evaporated to form a thick paste. Finally, the solid is dried and calcined, in some cases, a reduction step is required afterwards [63]. Typically, there are two types of metal precursors: organic and inorganic. For example, inorganic precursors include metal salts/sulfates, carbonates or nitrates, and chlorides, while the organic precursors include metal acetylacetonates [62]. The most common solvent is water for the inorganic precursors, while organic solvents such as acetonitrile or hexane are used for organic precursors [12]. The impregnation method can be classified into two main types: incipient wetness or dry impregnation and wet

impregnation. For the incipient wetness impregnation, the volume of the metal solution is usually less than the pore volume of the support, whereas the wet impregnation method, the volume of the metal solution exceeds the pore volume.

1.3.2 Co-precipitation

In this method, salts of the metal precursor and support (typically nitrates) are dissolved in water and mixed in aqueous alkaline solution (i.e. Na_2CO_3, K_2CO_3), then the nucleation and growth processes simultaneously occur, resulting in a precipitate in the form of hydroxide or carbonate. Finally, the solid material is filtered, washed and then thermally treated [64]. During the synthesis, several parameters need to be controlled in order to avoid variations in the final solid: for example, temperature gradients, efficient mixing, the pH of the solution, ageing time and the sequence of the components [61]. The co-precipitation method is usually employed for the preparation of metal catalysts with high metal loading ranging from 10 to 15%.

1.3.3 Deposition-Precipitation

The deposition-precipitation method was first reported by Haruta et al. [3] in the preparation of gold catalysts for the carbon monoxide oxidation. In this method, the metal precursor is dissolved in a solvent (typically water), then the pH of the solution is adjusted to the desired value using a base in order to precipitate the metal precursor in the form of metal hydroxide or carbonate on the surface of the support material. Finally, the solid material is filtered, washed and thermally treated [64]. Due to the rapid nucleation and growth of the metal hydroxides particles in the solution, it is unlikely that they can be deposited inside the pores, and therefore they expected to be present on the surface of the support material [61]. In order to attain a homogeneous distribution of the particles during the synthesis, efficient mixing and gradual pH adjustment must be achieved. For the latter, it has been demonstrated that the use of urea is beneficial to the entire process as it can be added to the system at room temperature and when it is heated to 90 °C, slowly hydrolyses. As the rate of precipitation is higher than the rate of hydrolyses, the pH of the solution can be

considered constant through the synthesis [64]. However, the optimum pH is governed by the isoelectronic point (IEP) of the support material. In this case, acidic oxides such as SiO_2 (IEP = 2) cannot be used. Despite this, the deposition-precipitation method is still used in the literature, and more particularly it is used for the preparation of gold catalysts [65, 66].

1.3.4 Sol Immobilisation

The sol immobilisation method was first reported by Prati et al. [67] for the preparation of gold nanoparticles supported on activated carbon. In this method, an aqueous solution of the metal precursor is prepared by solubilizing the appropriate amount of the metal salt. Then, the metal precursor is reduced using a strong reducing agent (i.e. $NaBH_4$) in the presence of a stabilizer molecule (i.e. polymer, surfactant) [68]. Subsequently, the metallic sol is immobilized onto the support material. This step is the most important during the synthesis as the immobilization can be affected by the intrinsic properties of the support (i.e. surface area, IEP), and the concentration of the stabilizing agent [69]. In addition, it has been demonstrated that the nature of the protective agent can affect the metal dispersion on the support material.

There are two main advantages associated with the method: the colloidal synthesis allows control over the size, shape and even composition of the metal nanoparticles [70], and the method can be applied in most common support materials [64]. However, the main disadvantage of the method is the presence of the protecting agent due to it can affect the catalytic activity of the metal nanoparticles [69]. In this case, two post-treament methods have been used to partially or completely remove the protecting agent: calcination and solvent washing. The former might promote the sintering of the particles, whereas the latter has demonstrated a positive effect on the catalytic activity of the metal nanoparticles [26].

1.4 Biomass

1.4.1 Biomass as an alternative renewable resource for the production of chemicals

The majority of chemicals and fuels that are utilized by humankind up until the 21st century come from fossil fuels. However, several factors such as climate change, international conflicts, fluctuating fossil fuel prices, pollution from the petroleum refining processes and the depletion of fossil fuel reserves have motivated nations to search alternative sources to reduce our dependence on petroleum-based chemicals and fuels. The use of biomass offers an alternative as a substitute for fossil fuels due to its abundance, availability, and capability to be converted into useful products (electrical/heat energy, transport fuel, and chemical feedstocks). Biomass can be defined as all biologically produced matter, and its production is estimated at 146 billion metric tons a year [71], contributing to almost 10-14% of the world's energy supply [72]. Biomass can be obtained from a wide range of organic materials such as wood, agricultural crops, and their waste by-products, grass, algae [71] and animal wastes [73]. Therefore, biomass has considerable potential as raw material and sustainable resource to produce fuels and chemicals with zero carbon emissions.

1.4.2 Biomass composition

Biomass is the organic material derived from the reaction between CO_2, the air, water and sunlight that are activated via photosynthesis to produce several organic molecules such as carbohydrates, fats, proteins, oils, and other products. Particularly abundant are cellulose and hemicellulose which are the main components of the cell walls of plants bound within lignin, Figure 1.3 [74]. Typically, any material that is mainly composed by cellulose, hemicellulose, and lignin is usually referred to as lignocellulosic biomass.

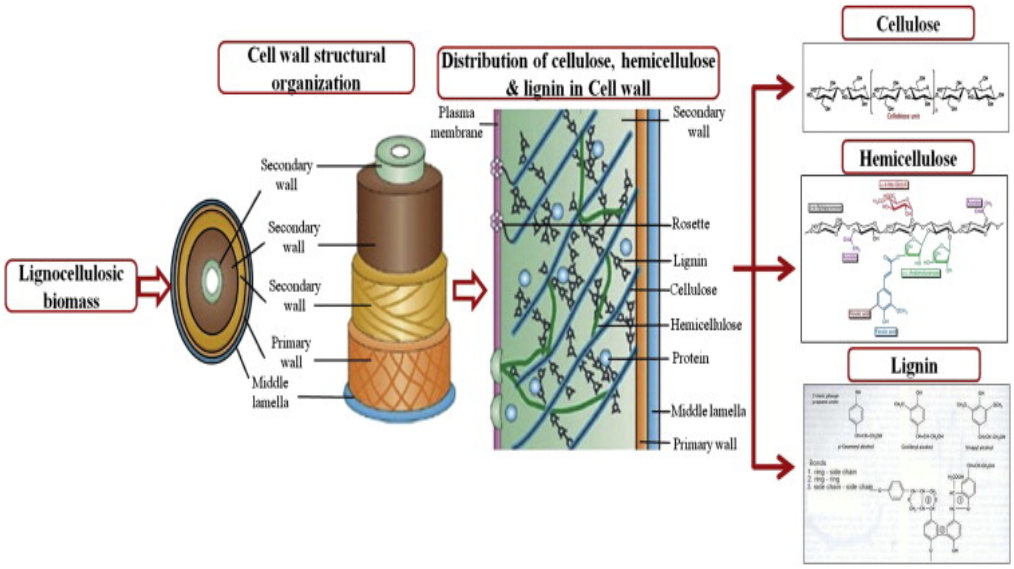

Figure 1.3 Structure of lignocellulosic biomass with cellulose, hemicellulose, and lignin as the main components. Take from Menon et al. [74].

Lignocellulosic biomass has been considered a good candidate for use as a renewable and sustainable source to produce chemicals and energy instead of fossil fuels [72, 75]. As a raw material, lignocellulosic biomass is mostly formed of three different polymeric units: lignin (15─20%), hemicellulose (25─35%) and cellulose (40─50%) [76]. Cellulose is the most abundant component among them, and it is mainly composed of linear D-glucose units which are bound to each other by β-1,4 linkages, forming long chains. Thus, due to the linear configuration of D-glucose and the enormous amount of hydroxyl groups, inter- and intramolecular hydrogen bonds are formed making the cellulose's structure more rigid (crystalline) and highly insoluble in water as well as most other common organic solvents [77]. Due to its crystallinity, cellulose presents seven different polymorphs (I_α, I_β, II, III_1, III_2, IV_1, IV_2), although in nature I_α and I_β are the most abundant, for example, the structure I_α is present in algae and bacteria, while the structure I_β is present in cotton and ramie fibers [78]. Cellulose presents the formula $(C_6H_{10}O_5)_n$, where "n" is the number of repeating units. The number of repeating units in cellulose is defined as the degree of polymerization (DP), Figure 1.4 [76]. The DP in cellulose normally depends on the type of material, although in raw cellulose the DP can achieve values up to 9000 units [79].

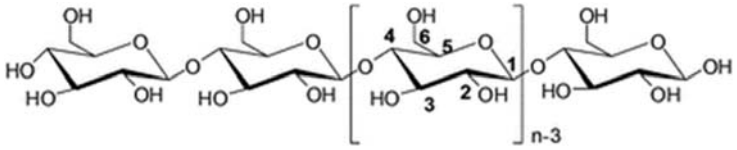

Figure 1.4 The chemical structure of cellulose with D-glucose as the repeating unit. Degree of polymerization n = DP. Taken from Huang et al. [76].

Hemicellulose is the second most abundant component of lignocellulosic biomass, and its structure may include several sugars that make it a complex polymer. Hemicelluloses are composed of different sugars such as hexoses (glucose, galactose, mannose) and pentoses (xylose and arabinose) that are branched throughout the polymeric matrix, Figure 1.5 [80].

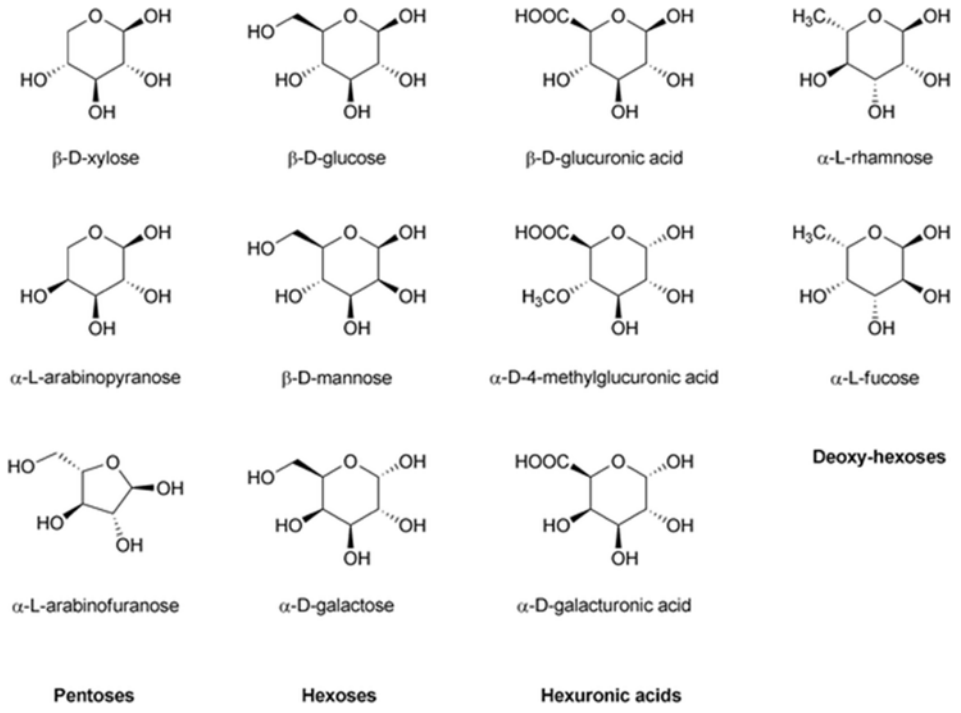

Figure 1.5 Functional groups in the structure of hemicelluloses. Taken from Rinaldi et al. [80].

In general, the amount and type of sugars that are contained in hemicelluloses will depend on the raw material used and differs if derived from wood (hardwood or softwood), pulping liquors, plant gums and plants [78]. On the other hand, hemicelluloses do not possess a strong protected structure like cellulose so can be readily attacked by acids, bases or enzymes [80].

Lignin is the third most important component of the lignocellulosic biomass (cellulose, hemicellulose, and lignin) and the most complex. Lignin contributes to almost 15─20% of the biomass composition [76] and its structure, molecular weight, and abundance depends on the type of material, for example, the content of lignin in some materials decreases as follows softwoods > hardwoods > grasses [81]. The lignin structure is based on three different cinnamyl alcohols which are *p*-coumaryl alcohol, coniferyl alcohol, and sinapyl alcohol, Figure 1.6. These cinnamyl alcohols are responsible for the formation of the lignin by polymerization, producing a complex structure which due to the variety of sources, it can differ significantly and cannot be precisely determined, Figure 1.7 [82].

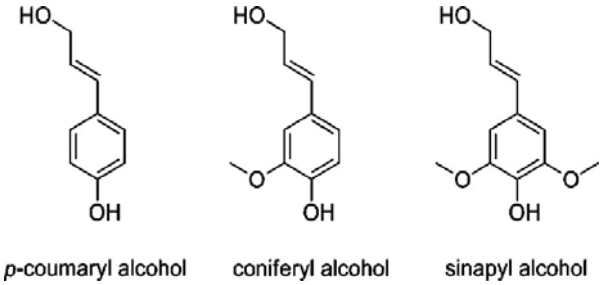

Figure 1.6 Functional groups in the structure of lignin. Taken from Dorrestijn et al. [82].

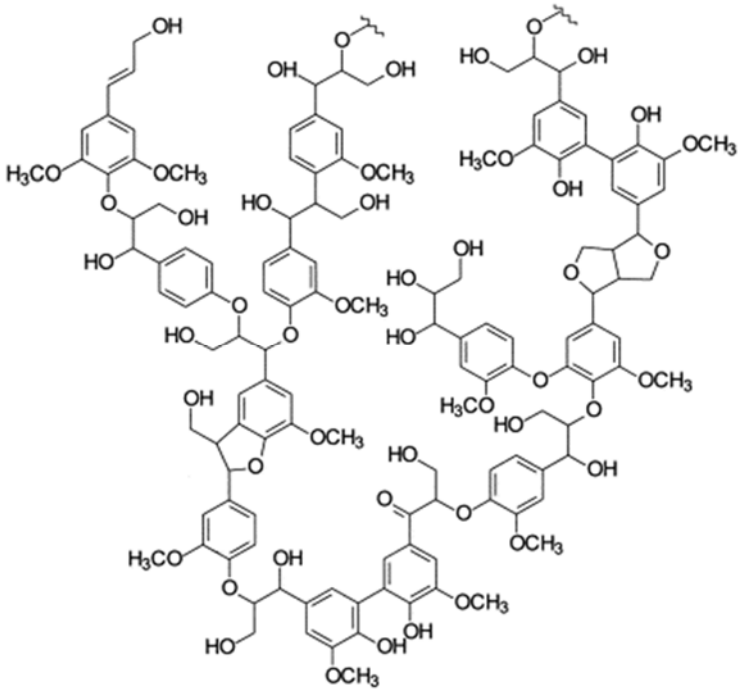

Figure 1.7 Possible structure of lignin. Taken from Dorrestijn et al. [82].

1.4.3 Biomass Transformation

Lignocellulosic biomass has a great potential as a substitute for petroleum-based chemicals and fuels due to its abundance, high availability and low cost. Given that cellulose is the most abundant component of the lignocellulosic biomass and, it is estimated that 50% of the organic carbon in the biosphere is presented in the form of cellulose [73], it represents the most promising natural source to be converted into chemicals and fuels. As mentioned in the previous section, cellulose presents a rigid structure making it highly insoluble in water and the most common solvents. Therefore, it is important to improve the reactivity and accessibility of the cellulose in order to allow its conversion into useful products.

In this case, different pretreatment methods have been developed to reduce the crystallinity of cellulose in order to increase its reactivity. Some of these methods are ball-milling [83, 84], ozonolysis [85], microwave irradiation (MWI) [86], ultrasound [87], the non-thermal atmospheric plasma method [88] and the solubilization in ionic liquids [89, 90], liquid acids [91, 92]. Although these pretreatment methods modify the cellulose's structure and increase its reactivity, the final result will depend on the type of process selected to transform cellulose into valuable products.

For the transformation of lignocellulosic biomass, several methods have been developed to convert these materials into useful forms. Some of these methods can be classified as thermochemical, chemical and biochemical [93]. Generally, it is necessary to take into account different factors before applying a specific method to convert biomass. For example, the thermochemical transformation normally involves temperatures above 700°C which can result in the decomposition of the formed products due to the high temperatures [94]. Thus, the use of high temperatures involves a considerable amount of energy input for this method that affects the cost-benefit of the process. In the case of acid hydrolysis (chemical method), problems arise with respect to the use of strong acids like HCl and H_2SO_4, such problems involve the handling and storage of acids, reactor corrosion, catalyst recovery and hazardous waste that require further treatment prior to final disposal [76].

On the other hand, enzymatic hydrolysis (biochemical method) of cellulose is typically carried out by cellulase enzymes (endoglucanase, cellobiohydrolase, and β-

glucosidase) which degrade cellulose to glucose at mild conditions (pH of 4.8 and temperature of 45–50 °C) [94, 95]. Despite this advantage in the process, the enzymatic hydrolysis presents different problems such as low activity, the process takes several days, the use of buffers to keep the pH and the high cost of the enzymes.

1.4.4 Application of Heterogeneous Photocatalysis for Biomass Transformation

1.4.4.1 General Principles of Photocatalysis

The term photocatalysis was first used in 1921 by Baly et al. [96] in the photoconversion of carbon dioxide to formaldehyde, the authors associated the results obtained to the presence of light which acts as a promoter accelerating the reaction. Later, in 1964 Doerffler et al. [97] used the term photocatalysis to describe a process in which a solid catalyst and light can influence a reaction. The main breakthrough occurred in 1972 when Fujishima and Honda reported the photoelectrochemical water splitting on TiO_2 electrodes [13]. This publication has been crucial in many research areas as it has promoted the application of photocatalysis in emerging fields such as solar energy conversion, hydrogen production, and heterogeneous photocatalysis among others.

A semiconductor material such as TiO_2, as stated by the band theory [98], presents a valence band (VB) and a conduction band (CB), and the separation between the VB and CB is called the band gap (or energy gap – E_g). In order to promote an electron (e^-) from the VB to the CB, a photon with energy ($h\upsilon$) that exceeds the band gap (E_g) of the semiconductor is required. The absorption of this photon excites an electron which is promoted from the VB to the CB, leaving a positive hole (h^+) in the VB (Figure 1.8). The electrons and holes are known as charge carriers.

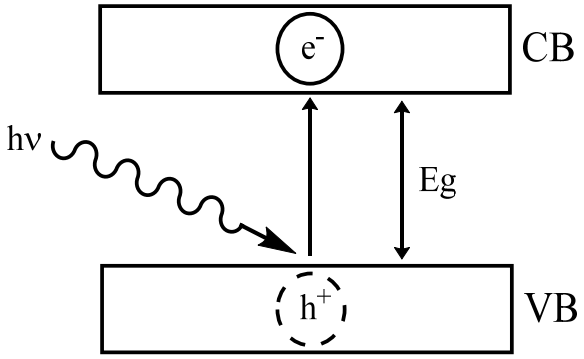

Figure 1.8 Light-induced excitation of electrons from the VB to CB with energy $h\upsilon \geq E_g$.

After the electron-hole generation, the charge carriers can be trapped by defect sites within or on the surface of the TiO_2 [99]. Also, they can recombine and dissipate energy as heat. More importantly, these electrons and holes can migrate to the surface of the semiconductor and initiate reduction and oxidation reactions respectively, as shown in Figure 1.9 [100]. Therefore, the efficient separation and an increase in the lifetime of the photogenerated charge carriers are of crucial importance for an effective photocatalyst.

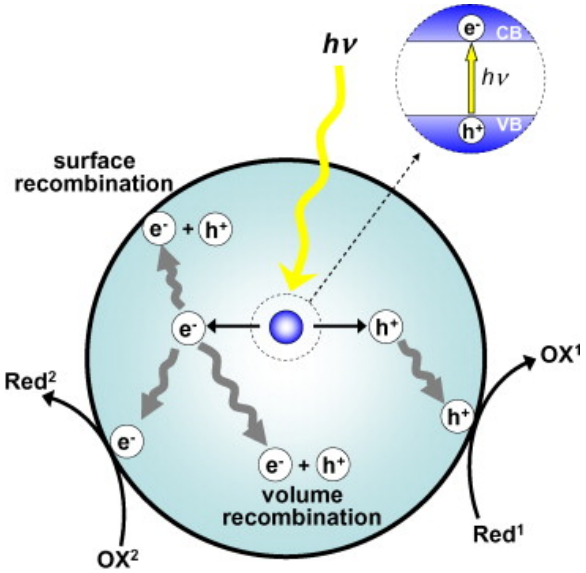

Figure 1.9 Photocatalytic mechanism on a TiO_2 particle. Reduction and oxidation reactions promoted by electrons (e^-) and holes (h^+) respectively, and the recombination of the charge carriers. Taken from Yasuhiro et al. [100].

Typically, the TiO_2 photocatalyst has been used as the reference material in photocatalytic applications due to its non-toxicity, strong oxidizing power, long-term photostability, low cost, and remarkable photocatalytic activity [101]. However, TiO_2 can only be activated under UV light irradiation ($\lambda < 388$ nm, 5% of the incident solar radiation) due to its wide band gap (3.0–3.2 eV, the values depend on the phase) [102]. Furthermore, the TiO_2 photocatalyst presents high electron-hole recombination rate which affects its photocatalytic activity [103]. In this scenario, various strategies have been investigated in order to extend the photoresponse of the TiO_2-based photocatalysts to the visible region and reduce the fast electron-hole recombination rate, for example, sensitization using an organic dye [104], non-metal doping (i.e. N, F, S) [105-107], the peroxo-TiO_2 synthesis (oxygen-rich materials) [108], coupled semiconductors [109, 110], and deposition of noble metals (i.e. Au, Ag) [27, 111]. Thus, the presence of some dopants has shown a significant shift in the absorption band of TiO_2 towards the visible region, and reduced the recombination of charge carriers, allowing an increase or a decrease of the photocatalytic activity in some cases.

Particularly, the modification of the TiO_2 photocatalyst with noble metals has attracted interest due to nanoparticles of noble metals can strongly absorb visible light as a result of their surface plasmon resonance (SPR) [112], which can be tuned by varying the size, shape, and even composition of the particles [113]. Moreover, the use of noble metal nanoparticles can be advantageous to the entire system as they can serve as an electron trap and active centers, reducing the recombination rate and increase the photoactivity. Generally, noble metal nanoparticles are supported on metal oxides (i.e. TiO_2, ZnO, CeO_2), and more recently, alternative materials such as carbon nanotubes, carbon quantum dots, and reduced graphene have been used as supports or charge carriers due to their electronic and structural properties [114-116]. Therefore, the combination of noble metal nanoparticles and semiconductors materials offers an alternative route to catalyse reactions using visible light irradiation at room temperature [117], in fact, some of them have already demonstrated remarkable activity for thermal-driven reactions (i.e. Au/C) [118].

1.4.4.2 Surface Plasmon Resonance

The surface plasmon resonance (SPR) is defined as the resonant photon-induced coherent oscillation of the conduction electrons at the metal-dielectric interface that is established when the frequency of the incident photons has the same frequency of metal surface electrons oscillating against the restoring force of their positive nuclei [119-121]. In other words, the SPR is the collective oscillations of the free electrons in the conduction band of the metal nanoparticles induced by the incident electromagnetic radiation (Figure 1.10). As a result of the SPR, metallic nanoparticles can absorb visible, infrared and near-infrared light in particular regions [122], for example, metal nanoparticles of Au, Ag, and Cu absorb visible light at 530, 400, and 580 nm respectively [123].

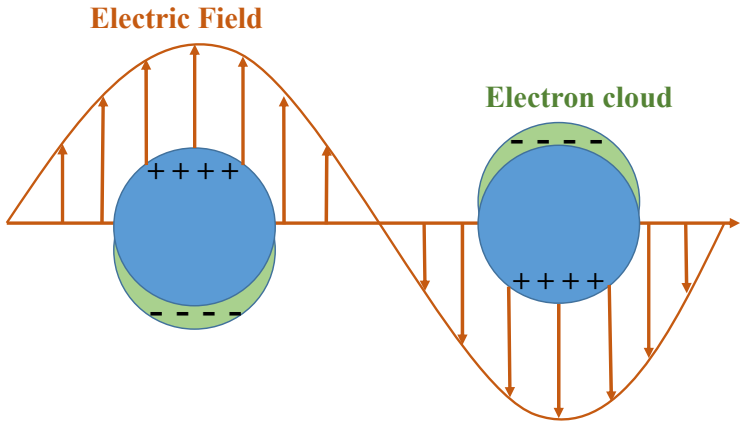

Figure 1.10 Schematic representation of the surface plasmon resonance (SPR).

In addition, the intensity and position of the SPR might be influenced by several factors such as the dielectric properties of the metal nanoparticles, the surrounding medium, metal-support interactions, electronic interactions with the protective agent, the size, and shape of the nanoparticles [102, 124]. In particular, it has been observed that the SPR effect is strongly related to the particle size, for example, gold nanoparticles with a particle size < 5 nm do not present an SPR absorption [125], while gold nanoparticles larger than 5 nm show a strong band in the 520–580 nm region [66, 123, 126-128]. In this case, as the particle size increases the absorption band broadens and shifts to longer wavelengths. Therefore, the SPR

absorption that distinguishes noble metal nanoparticles from other nanoplatforms has been applied in different research areas including surface-enhanced Raman spectroscopy [129], sensors [130], solar cells [131], and nanomedicine [132] among others.

More recently, the SPR property of the noble metal nanoparticles has been introduced into the emerging field of plasmonic photocatalysis, where noble metal nanoparticles are supported on a semiconductor material (usually TiO_2) and used to catalyse chemical reactions under light irradiation conditions [27, 111, 133]. More interestingly, noble metal nanoparticles in contact with a semiconductor lead to the formation of the so-called Schottky junction which allows for the build-up of an internal electric field close to the metal/support interface [134]. As a result, the electrons and holes can move freely in different directions reducing the electron-hole recombination and consequently increase their lifetime.

In addition to the SPR effect which promotes light absorption, metal nanoparticles can also absorb UV light as a result of the inter-band electron transitions, for example, from 5d to 6sp for gold nanoparticles [125, 135].

1.4.4.3 Major Mechanisms in Plasmonic Nanoparticles

The SPR in metallic nanoparticles is a complex process that is accompanied by a number of physical effects such as optical near-field enhancement, hot electron injection and photothermal conversion [136-138]. The first is a result of plasmon resonances, while the second and third are originated from the non-radiative damping of plasmon resonances [138].

- Optical near field enhancement

Upon illumination, the free electrons in a metal nanoparticle oscillate at the frequency of the incident electric field. Then, this oscillation is further enhanced when the SPR of the metal nanoparticle matches the frequency of the incident light. As a result of this oscillation, the metal nanoparticle acts as an electromagnetic

dipole re-emitting light at the same frequency [136]. Therefore, a fraction of this emitted light is scattered into the far-field, while the other is concentrated at the metal surface, producing a local electric field [138]. The local electric field enhancement is strongly dependent on the shape of the nanoparticles, for example, non-spherical nanostructures (i.e. nanocubes, nanoprisms) generate a high concentration of charges localized at the edges or sharp corners [139-141]. In addition, the enhancement of the electric field intensity can also be affected by the presence of metal nanoparticles in close proximity to each other. In the case of two silver nanocubes of 75 nm separated by ~1 nm, the electric field intensity is estimated to be 3 orders of magnitude (10^6) larger than the one in an isolated nanocube (~10^3) [119]. The areas between plasmonic nanoparticles with high-intensity fields are called "hot spots" [119, 120]. Electromagnetic simulations using the finite-difference time-domain method have demonstrated that the electric field intensity in the hot spot regions is 1000 times higher than the incident electric field [142].

When a semiconductor is integrated with a plasmonic metal nanoparticle, the excited SPR generates an intense electric field that can increase the rate of electron-hole generation in the semiconductor that is in close proximity to the photo-excited plasmonic metal nanoparticle [119]. However, the near field effect is limited by the band gap of the semiconductor, and therefore the energy of plasmonic fields should be higher than the band gap in order to enhance the electron-hole generation in the semiconductor [143].

Due to the SPR effect implies enhanced local electromagnetic fields, such oscillating fields can also interact with polar molecules adsorbed on the metal surface. This conclusion was demonstrated in the oxidation of formaldehyde, methanol and cyclohexane utilising the Au/ZrO_2 catalyst under illumination conditions. The results showed that molecules with similar structural features react in accordance with their polarity, that is, the molecule with higher polarity can be easily activated on the metal surface [144]. Furthermore, plasmonic metal nanoparticles supported on zeolites have demonstrated to enhance the polarized electrostatic field in the support due to the SPR effect. As a result, the enhanced polarized electrostatic field is able to polarize molecules adsorbed on the surface or within the porous matrix in zeolites, thus reducing the energy required for electron transfer or the activation of reactants [145].

- Hot electron injection

Following the light absorption and the SPR excitation in plasmonic nanostructures, electromagnetic decay occurs in a femtosecond timescale, either radiatively through re-emitted photons [146] or non-radiatively by transferring the energy to hot electrons [147-149]. In the non-radiative process, surface plasmons decay via the Landau damping process, which causes the formation of hot electron-hole pairs [150, 151]. Landau damping is a quantum mechanical process, which has been widely investigated using femtosecond spectroscopy and it can occur on a timescale ranging from 1–100 fs [152, 153]. The hot electrons generated by the damping of surface plasmons are not in thermal equilibrium and are characterised by high effective temperatures [154, 155].

In the non-radiative decay in noble metal nanostructures, the generation of hot electrons can occur through intraband excitations within the conduction band (i.e. from occupied *s* band to empty *s* band) or through interband excitations (i.e. from the *d* band to the *sp* conduction band) [150, 154]. In the case of the most common plasmonic metals such as Au and Ag, the interband transitions energy levels are 2.4 eV and 4 eV respectively. However, these energy levels lie below the Fermi energy levels for Au and Ag, suggesting that interband excitations are more unlikely to occur than intraband excitations [156, 157]. The hot electrons generated from plasmon decay will ultimately relax *via* electron–electron scattering and electron–phonon collisions, and then converted into heat [158].

In order to efficiently capture hot electrons, a plasmonic nanostructure can be integrated with an appropriate semiconductor to form a Schottky barrier. Typically, TiO_2 is used as semiconductor due to it has a high density of states in its conduction band and permits rapid electron injection [154]. The Schottky barrier blocks the electron transfer between the metal and the semiconductor. However, upon excitation of the SPR of the metal nanostructures, hot electrons generated from plasmon decay can have sufficient energy to overcome the Schottky barrier and then be injected into the conduction band of the semiconductor [159-162]. The necessary energy for hot electrons to overcome the Schottky barrier is smaller than the band gap of the semiconductor [159, 163]. After the injection of hot electrons into the semiconductor, the plasmonic nanostructures are left with a positive charge (hole, h^+).

On the other hand, hot electrons can also be injected into the lowest unoccupied molecular orbitals (LUMOs) of adsorbed molecules via two mechanisms (indirect and direct electron transfer). In the indirect electron transfer mechanism, the hot electrons are first generated in the metal nanostructure and then transferred into the LUMOs of the adsorbed molecules, potentially inducing chemical transformations [150, 164]. For the direct electron transfer mechanism, hot electrons generated from plasmon decay are directly injected into the adsorbed molecule, rather than first occupying available states in the metal [150, 164]. However, despite the differences between the indirect and direct electron transfer mechanism, it is likely that they can occur simultaneously in real photocatalytic reactions [150].

- Photothermal conversion

In the non-radiative process, hot electrons generated from plasmon decay can be transferred from the metal nanoparticles to an electron acceptor (i.e. adsorbate, semiconductor) [150, 164]. However, in another non-radiative pathway, these hot electrons can also relax through electron–electron and electron–phonon collisions [158]. This process of energy exchange between the electrons and the phonon modes of the nanoparticles results in an increase in the temperature of the metal nanoparticles, followed by heat transfer to the environment [150, 154, 164]. This ability of the metal nanoparticles to convert light into heat is described by the photothermal conversion efficiency (μ), which correlates the absorption (σ_{abs}) and extinction (σ_{ext}) cross-sections of a plasmonic nanostructure by the following expression: $\mu = \sigma_{abs}/\sigma_{ext}$ [137].

The photothermal conversion is strongly dependent on the size and shape of the nanoparticles. Particularly, it has been reported that metal nanoparticles smaller than ~10 nm results in a photothermal conversion efficiency of nearly 96% [165]. In the case of nanoparticles with a specific geometry such as flat, elongated or sharp nanostructures, have demonstrated to be more efficient heaters than nanoparticles with other shapes with the same volume [166]. In this study, the authors concluded that the incident electric field can more easily penetrate the thin nanostructures, and therefore the whole geometry is integrated into heat generation [166]. The steady-state temperature of the nanoparticles depends on the absorbed light power (Q =

$\sigma_{abs}I$, where I is the light intensity) and the thermal diffusion efficiency of the surrounding medium. In the case of metal nanoparticles dispersed in liquid solvents under continuous light irradiation, the steady-state temperature is almost constant because of liquids normally have larger thermal conductivities [121]. For example, a gold nanosphere (20 nm) dispersed in water is 5 °C hotter than the surrounding medium when it is illuminated with an irradiance of I = 1 $mW\mu m^{-2}$ [121, 167]. Moreover, metal nanoparticles in an aqueous environment have also been investigated under laser illumination. For example, it has been demonstrated that gold nanorods in solution can increase the solution temperature from ambient to 76°C when they are illuminated with a laser light power of 2 W [165].

On the other hand, the reaction rate (k) of most chemical reactions follows the Arrhenius equation [168], $k = A \exp(-E_a/RT)$, in which is described the relation between the rate of reaction and temperature. As mentioned before, plasmonic metal nanoparticles can efficiently convert light into heat, and consequently, this thermal energy can potentially be used to accelerate and control the reaction rate of chemical reactions [144, 169-172].

1.4.4.4 Proposed Mechanisms for Plasmonic Photocatalysis

Plasmonic photocatalysis has emerged as a promising technology for the conversion of photons into charge carriers (e^- and h^+) which can perform chemical reactions, resulting in an efficient conversion of light energy into chemical energy [173-175]. However, this technology is still in its infancy, and fundamental questions have been partially explained or remain unsolved, for example, how plasmon-mediated visible light photocatalysis work?. In this case, three main mechanisms have been proposed to understand the plasmon-mediated photocatalysis.

(i) The most widely accepted mechanism establishes that noble metal nanoparticles absorb the visible light, then the photogenerated charge carriers are separated by the metal-semiconductor interface and finally, the oxidation and/or reduction reactions occur on the surface of the catalyst. In this mechanism, electrons and/or holes are transferred from the noble metal nanoparticles to the semiconductor material [174, 176-179].

(ii) In the case of metal nanoparticles which are separated by a thin non-conductive material layer (~2–6 nm) from the semiconductor, a different mechanism is proposed by Linic et al. [119]. The radiative energy transfer from the noble metal nanoparticles to the semiconductor is a result of the interaction between the semiconductor and the plasmon-induced electric field concentrated in the vicinity of the metal nanoparticles [119]. The plasmon-induced electric field can improve the formation of charge carriers on the surface of the semiconductor, and consequently, they can be transferred to the semiconductor-liquid interface, improving the efficiency of the plasmonic photocatalyst.

(iii) For noble metal nanoparticles deposited on insulating oxides such as ZrO_2 and SiO_2, it has been proposed that the metal nanoparticles can be subjected to rapid heating (~3–5 °C per second) by absorbing visible light and as a result, chemical reactions can take place [144].

1.4.4.5 Photocatalytic Transformation of Biomass Model Compounds

Biomass is an attractive and sustainable source which can contribute to reduce our dependency on fossil fuels in the production of high-value chemicals and fuels. Biomass is an inexpensive and highly available source which is mainly composed of polysaccharides, lipids, and amino acids. Several methods have been used to convert biomass into useful products, for example, steam gasification [180], supercritical fluids [181], and pyrolysis [182]. However, these technologies require high energy input resulting in expensive processes. In this scenario, heterogeneous photocatalysis provides an alternative route to perform chemical transformations driven by sunlight at mild conditions. In this application, TiO_2-based photocatalysts have been widely used due to its non-toxicity, thermal stability, and high reactivity in different conditions.

To date, biomass model compounds such as carbohydrates have been investigated under photocatalytic conditions as they represent the most abundant component in real biomass (40─50%) [76]. Carbohydrates are of great interest as they can be converted into valuable products such as platform molecules, pharmaceuticals, detergents, and polymers [183, 184]. In order to transform carbohydrates into molecules of interest, they can be subjected to chemical modifications such as reduction, isomerization, and oxidation reactions. Therefore,

the photocatalytic conversion of carbohydrates and other biomass model compounds represents the most promising alternative to produce high-value chemicals from renewable sources in an environmentally responsible manner.

1.4.4.5.1 Photocatalytic Oxidation of Glucose

The photocatalytic oxidation of carbohydrates such as glucose was first reported using TiO_2-based catalysts due to its thermal stability, low cost, non-toxicity, and remarkable activity under UV light irradiation. Particularly, the oxidation of glucose has been widely investigated as it leads to the formation of carboxylic acids which are used as a food additive, in pharmaceuticals and soluble detergents [185]. In heterogeneous photocatalysis, the glucose photo-oxidation was reported for the first time by Colmenares et al. [186] using TiO_2-based catalysts under UV light irradiation. An ultrasound-mediated sol-gel synthesis was used to prepare two different catalysts (TiO_2(US) and TiO_2(R)) which were compared to the reference material (TiO_2-P25, Evonik) under photocatalytic conditions. The results showed that the TiO_2(US) catalyst displayed a modest glucose conversion of 11%, but more importantly this material showed the highest selectivity to the organic products with 71% after 10 minutes of light irradiation in the presence of a 50/50 v/v water/acetonitrile mixture. Under these conditions, gluconic acid, glucaric acid, and arabitol were detected in the liquid phase, while CO_2 was observed in the gas phase along with light hydrocarbons. Colmenares et al. [186] suggested that the presence of the acetonitrile in the water/acetonitrile mixture is beneficial to the system as a lower amount of water might result in a low concentration of radical species which could promote the mineralization reaction limiting the formation of the organic acids.

Later, Colmenares et al. [187] reported the photocatalytic activity of TiO_2 nanoparticles supported on zeolite Y synthesized by an ultrasound-mediated sol-gel synthesis. The photocatalysts were tested in the glucose oxidation and the degradation of phenol under UV light irradiation. The results showed that gluconic acid and glucaric acid were produced after 10 minutes of UV light irradiation. The glucose conversion was 15.5% with a total selectivity to the organic acids of 68% in the presence of a 50/50 v/v water/acetonitrile mixture. In this case, the small improvement in the glucose conversion was associated with the support material as it

has been reported that zeolites can promote electron transfer reactions and reduce the electron-hole recombination [188].

More recently, Da Và et al. [117] reported for the first time the glucose oxidation under visible light conditions using TiO_2-based catalysts. Several parameters such as substrate concentration, lamp power, type of light, reaction time and TiO_2 crystalline phases were evaluated under photocatalytic conditions. The results showed a glucose conversion of 42% with a gluconic acid selectivity of 7% after 4 hours of reaction under visible light irradiation. Moreover, it was found that the photo-oxidation of glucose using the TiO_2 photocatalyst produces short-chain aldoses (i.e. arabinose, glyceraldehyde, erythrose) and formic acid. The photoactivity of the TiO_2 material under visible light irradiation was attributed to the formation of a glucose-TiO_2 charge transfer complex as a result of the interaction between the metal and substrate. More interestingly, Da Và et al. [117] demonstrated for the first time that the glucose photo-oxidation can be carried out under natural light. Therefore, the results reported by Da Và are promising as they provide evidence that the use of natural light is an attractive alternative to produce high-value chemicals.

Despite the results obtained by Colmenares and Da Và in the photo-oxidation of glucose, the production of valuable molecules such as gluconic acid is limited due to the low efficiency of the TiO_2 photocatalyst even when the photoreactions were performed under UV light irradiation. Moreover, the composition of the solvent showed to be fundamental during photocatalysis as the presence of acetonitrile led to the formation of organic acids, however, the use of water as a green solvent is more desirable as the separation of the products could involve an additional cost if a second solvent is used.

In order to overcome these drawbacks, Colmenares et al. [189] reported the preparation of Fe-doped TiO_2 nanoparticles supported on silica or zeolite. Particularly, the use of the Fe^{+} ion might be advantageous as it can be incorporated into the crystal lattice of TiO_2 due to its similar size with the Ti^{4+} ion resulting in a positive effect on the electron-hole separation. The Fe-TiO_2/SiO_2 and Fe-TiO_2/Ze catalysts were prepared using the ultrasound-mediated impregnation method. The results showed that the incorporation the Fe^{+} ion into the TiO_2 structure was achieved as evidenced by red-shift in the absorption bands of the catalysts compared to the undoped ones. The catalysts were tested in the glucose oxidation in the presence of a 50/50 v/v water/acetonitrile mixture under UV light irradiation. The photocatalytic

results showed that gluconic acid and glucaric acid were formed in the presence of both catalysts. However, a glucose conversion of 7.2% with a selectivity of 94.3% to the organic products was achieved after 20 minutes of reaction using the Fe-TiO_2/Ze catalyst under optimized conditions. Following this line, Colmenares et al. [190] reported the use of the Cr^{3+} ion for the preparation of the Cr-TiO_2/SiO_2 and Cr-TiO_2/Ze catalysts. These materials were prepared using the ultrasound-mediated impregnation method as reported in their previous work [189]. Unfortunately, the result showed a glucose conversion of 7% with a selectivity of 87% to the organic acids (gluconic acid and glucaric acid) after 20 minutes of light irradiation. Therefore, these results demonstrate that transition metals such as Fe and Cr cannot promote the photo-oxidation of glucose despite the significant reduction of the band gap of TiO_2.

On the other hand, Bellardita et al. [191] reported a different approach in the preparation of photoactive materials for the photo-oxidation of glucose under light irradiation. In this case, two heteropolyacids were deposited on TiO_2, the commercial Keggin heteropolyacid ($H_3PW_{12}O_{40}$) and the home-prepared $K_7PW_{11}O_{39}$ salt. Heteropolyacids (HPAs) have been used as homogeneous photocatalysts due to their significant photoresponse under UV light irradiation. Light absorption by the HPA produces a charge transfer-excited state HPA^* which is more efficient oxidant compared to the HPA ground state [192]. The HPA/TiO_2 catalysts were prepared by the wet impregnation method and the solvothermal method. The photo-oxidation of glucose was carried out under UV light irradiation using a 1 mM aqueous glucose solution. The results showed that the product distribution and selectivity were strongly dependent on the catalysts used. Despite this, gluconic acid, fructose, arabinose, erythrose, and formic acid were detected in all cases. Moreover, glucaric acid and glyceraldehyde were observed in particular cases.

- **Selective Photocatalytic Oxidation of Glucose by Noble Metal Nanoparticles**

The photo-oxidation of glucose was first reported using TiO_2-based photocatalysts, however, these materials can only be activated under UV light irradiation, and therefore their activity was limited. In this case, noble metal nanoparticles (i.e. Ag, Au) have been used to extend the light absorption of the photocatalysts to the visible region in order to improve the photocatalytic activity as a result of the surface plasmon resonance effect (SPR) [112]. Recently, Da Vià et al. [27] reported the photo-oxidation of glucose under both UV and visible light using silver nanoparticles supported on TiO_2. The Ag/TiO_2 photocatalysts were prepared by the wet impregnation method. Several parameters such as the metal/substrate ratio, irradiation time, lamp power, type of light and substrate concentration were evaluated under photocatalytic conditions. The results showed that the photo-oxidation of glucose led to the formation of several products such as gluconic acid, arabinose, erythrose, glyceraldehyde, and formic acid under both UV and visible light conditions. Surprisingly, it was also observed that the bare TiO_2 and Ag/TiO_2 catalysts produced the same compounds under both UV and visible light conditions. Particularly, it was found that under UV light irradiation, the concentration of the organic products decreased as a result of the mineralization reaction. Under optimized conditions, the results showed that the 0.5 wt% Ag/TiO_2 catalyst was the most selective to the formation of gluconic acid (20%), however, the glucose conversion was 6% after 2 hours of reaction under visible light irradiation. Nevertheless, the obtained results under both UV and visible light suggested the presence of two mechanisms which could be responsible for the formation of the products. The Ruff degradation and the α-scission process were combined to explain the presence of the products formed under both UV and visible light, Figure 1.11.

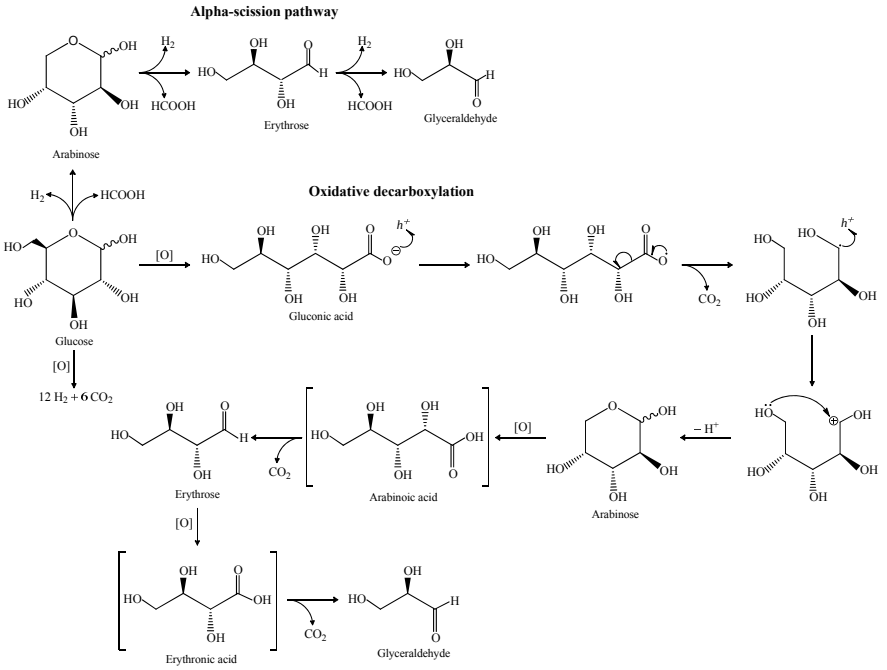

Figure 1.11 Mechanism proposed for the photo-oxidation of glucose under both UV and visible light. Adapted from Da Vià et al. [27].

On the other hand, Zhou et al. [111] reported for the first time the selective photo-oxidation of glucose under both UV and visible light using gold nanoparticles supported on TiO_2. The Au/TiO_2 catalysts were prepared by the deposition-precipitation method with a metal loading of 3 wt%. Several parameters were investigated in order to determine their influence during photocatalysis, for example, light intensity, type of light, the presence of a promoter, temperature and irradiation time. Interestingly, the results showed complete glucose oxidation under both UV and visible light (conversion > 99%) after 4 hours of reaction. More importantly, gluconic acid was the main product with a selectivity of 94% and 99% for the reactions under UV and visible light respectively. In this case, the authors demonstrated that the addition of a base such as Na_2CO_3 improves the oxidation process, achieving high conversion values and selectivity [111]. It was proposed that the base acts as a promoter [193] under visible light, accelerating the oxidation process, whereas under UV light it might serve as a sacrificial agent for the radical species formed. The role of the base under both UV and visible light was confirmed by electron paramagnetic resonance (EPR) analysis.

Based on the experimental results, Zhou et al. [111] proposed two possible mechanisms for the oxidation process under light irradiation conditions. (i) Under visible light, the photoactivated electrons from the metal nanoparticles generated by the SPR, are injected into the conduction band of the TiO_2. Then, these electrons reduce molecular oxygen (O_2) in the form of radical ($^{\bullet}O_2^-$), which is involved in the oxidation process. (ii) Under UV light conditions, the electrons are promoted from the VB to the CB of the TiO_2, then they are trapped by the metal nanoparticles. Finally, molecular oxygen is first activated over the surface of the metal nanoparticles by the photoactivated electrons and then participated in the oxidation process.

In a similar work, Omri et al. [133] reported the use of gold catalysts in the photo-oxidation of glucose under standard conditions (A.M. 1.5G, 100 mW/cm^2). The Au/TiO_2, Au/Al_2O_3, and Au/CeO_2 catalysts were prepared using the deposition-precipitation method with a metal loading between 0.4 and 0.7 wt%. The photocatalytic tests were carried out using water as a solvent and hydrogen peroxide as the oxidant (1.1 equiv.) under alkaline conditions (1 equiv.). Under photocatalytic conditions, the Au/CeO_2 catalyst was the most active among them, achieving a glucose conversion of 99% with a gluconic acid selectivity of 95% after 10 minutes of light irradiation. Moreover, the Au/CeO_2 catalyst demonstrated to be reusable as it retained its photocatalytic activity after five runs under the same experimental conditions. The remarkable photocatalytic activity of the Au/CeO_2 catalyst was attributed to the electronic and structural properties of the CeO_2 support combined with the presence of the gold nanoparticles.

Furthermore, the authors [133] demonstrated that carbohydrates with a degree of polymerization from 1 to 6 (mono- and oligosaccharides) can be converted into their corresponding mono- and hexa-aldonates. The work reported by Omri et al. [133] represents the first example of selective photo-oxidation of oligosaccharides under light irradiation conditions.

1.4.4.5.2 Photocatalytic Conversion of Polysaccharides

In the photocatalytic conversion of complex polysaccharides like cellulose a few attempts have been made in this field. Lina et al. [194] reported the photocatalytic conversion of cellulose under visible light irradiation using gold nanoparticles supported on zeolites. Prior to reaction, cellulose was dissolved in 1-ethyl-3-methylimidazolium chloride (ionic liquid) for 1 hour at 130 °C. Parameters such as temperature, light intensity, and wavelength were analysed in order to determine the optimal conditions in the system. The main products in the reaction were glucose and 5-hydroxymethylfurfural (HMF) with a total yield of 60% at 130 °C after 24 hours of reaction.

On the other hand, cellulose has also been used as a sacrificial agent to produce valuable chemicals and H_2 from water, when it was immobilized onto TiO_2 and exposed under UV light irradiation [195]. In addition, the photocatalytic conversion of cellulose under UV light was performed using a concentrated zinc chloride solution and a cylindrical corrugated plate photoreactor [196]. It was found that a $ZnCl_2$ solution dissolves and helps to break down the glycosidic linkages allowing the cellulose depolymerisation. 5-Hydroxymethylfurfural (HMF) was mainly favoured when a corrugated plate was used instead of a flat plate configuration in the photoreactor.

The other examples are related to the photocatalytic degradation of the contaminants of wastewater from the lignocellulosic industries (Paper and Pulp Industry). Some examples include the use of TiO_2 [197], Pt/TiO_2 [198], TiO_2/ZnO [199] and ferrous ions (Fe^{2+}) [200] on the degradation of lignin and other organic compounds, the Cu/TiO_2 catalyst has also been used during the degradation of lignocellulosic components (lignin, cellulose, and hemicellulose) of the coffee pulp [201].

1.5 Aim of the Work

This work will focus on the investigation of the catalytic activity of supported metal nanoparticles for the selective oxidation of bio-derived molecules and their application in heterogeneous photocatalysis and thermal catalysis. The aim of this PhD is to obtain basic information in the application of supported noble metal nanoparticles for the selective conversion of glucose and cellulose into valuable products using alternative technologies such as photocatalysis and microwaves. The project can be divided in the following objectives:

- Development of a synthesis method for the preparation of gold nanoparticles supported on conjugated microporous polymers (CMPs), and evaluation of the obtained catalysts in the oxidation of glucose.

- Assessment of the photocatalytic activity of gold catalysts (Au supported on TiO_2, CNTs, and CMPs) in the oxidation of glucose under UV and visible light.

- Evaluation of the photocatalytic activity of noble metal nanoparticles supported on TiO_2 in the photoconversion of cellulose under UV and visible light using molecular oxygen as the oxidant at high-pressure conditions.

1.6 References

[1] B. Lindström, L.J. Pettersson, A Brief History of Catalysis, CATTECH, 7 (2003) 130-138.

[2] IUPAC. Compendium of Chemical Terminology, 2nd ed. (the "Gold Book"). Compiled by A. D. McNaught and A. Wilkinson. Blackwell Scientific Publications, Oxford (1997). Online version (2019-) created by S. J. Chalk.

[3] M. Haruta, S. Tsubota, T. Kobayashi, H. Kageyama, M.J. Genet, B. Delmon, Low-Temperature Oxidation of CO over Gold Supported on TiO_2, α-Fe_2O_3, and Co_3O_4, J. Catal., 144 (1993) 175-192.

[4] G. Rothenberg, Catalysis: Concepts and Green Applications. Heterogeneous Catalysis, 2008.

[5] J.A. Dumesic, G.W. Huber, M. Boudart, Principles of Heterogeneous Catalysis, Handbook of Heterogeneous Catalysis(2008).

[6] Y.I. Matatov-Meytal, M. Sheintuch, Catalytic Abatement of Water Pollutants, Ind. Eng. Chem. Res., 37 (1998) 309-326.

[7] J.C. Védrine, Heterogeneous Catalysis on Metal Oxides, Catalysts, 7 (2017) 341.

[8] L. Prati, A. Villa, A.R. Lupini, G.M. Veith, Gold on carbon: one billion catalysts under a single label, Physical Chemistry Chemical Physics, 14 (2012) 2969-2978.

[9] W. Li, Q. Yue, Y. Deng, D. Zhao, Ordered Mesoporous Materials Based on Interfacial Assembly and Engineering, Adv. Mater., 25 (2013) 5129-5152.

[10] T. Hasell, C.D. Wood, R. Clowes, J.T.A. Jones, Y.Z. Khimyak, D.J. Adams, A.I. Cooper, Palladium Nanoparticle Incorporation in Conjugated Microporous Polymers by Supercritical Fluid Processing, Chemistry of Materials, 22 (2010) 557-564.

[11] E. Koohsaryan, M. Anbia, Nanosized and hierarchical zeolites: A short review, Chin. J. Catal., 37 (2016) 447-467.

[12] A. Dhakshinamoorthy, A.M. Asiri, H. Garcia, Metal Organic Frameworks as Versatile Hosts of Au Nanoparticles in Heterogeneous Catalysis, ACS Catalysis, 7 (2017) 2896-2919.

[13] A. Fujishima, K. Honda, Electrochemical Photolysis of Water at a Semiconductor Electrode, Nature, 238 (1972) 37-38.

[14] A. Kubacka, M.S. Diez, D. Rojo, R. Bargiela, S. Ciordia, I. Zapico, J.P. Albar, C. Barbas, V.A.P. Martins dos Santos, M. Fernández-García, M. Ferrer, Understanding the antimicrobial mechanism of TiO_2-based nanocomposite films in a pathogenic bacterium, Sci. Rep., 4 (2014) 4134.

[15] L. Yan, L. Zhe, G. Michael, J. Michael, L. Yang Yang, C. Xiaobo, Titanium dioxide nanomaterials for photocatalysis, J. Phys. D: Appl. Phys., 50 (2017) 193003.

[16] H. Tang, K. Prasad, R. Sanjinés, F. Lévy, TiO_2 anatase thin films as gas sensors, Sens. Actuators, B, 26 (1995) 71-75.

[17] P.N. Amaniampong, X. Jia, B. Wang, S.H. Mushrif, A. Borgna, Y. Yang, Catalytic oxidation of cellobiose over TiO_2 supported gold-based bimetallic nanoparticles, Catal. Sci. Technol., 5 (2015) 2393-2405.

[18] C. Perego, Y.-h. Wang, O. Durupthy, S. Cassaignon, R. Revel, J.-P. Jolivet, Nanocrystalline Brookite with Enhanced Stability and Photocatalytic Activity: Influence of Lanthanum(III) Doping, ACS Appl. Mater. Interfaces, 4 (2012) 752-760.

[19] D. Grosso, G.J.d.A.A. Soler-Illia, E.L. Crepaldi, F. Cagnol, C. Sinturel, A. Bourgeois, A. Brunet-Bruneau, H. Amenitsch, P.A. Albouy, C. Sanchez, Highly Porous TiO2 Anatase Optical Thin Films with Cubic Mesostructure Stabilized at 700 °C, Chem. Mater., 15 (2003) 4562-4570.

[20] J. Wang, J. Polleux, J. Lim, B. Dunn, Pseudocapacitive Contributions to Electrochemical Energy Storage in TiO_2 (Anatase) Nanoparticles, J. Phys. Chem. C, 111 (2007) 14925-14931.

[21] J.E.S. Haggerty, L.T. Schelhas, D.A. Kitchaev, J.S. Mangum, L.M. Garten, W. Sun, K.H. Stone, J.D. Perkins, M.F. Toney, G. Ceder, D.S. Ginley, B.P. Gorman, J. Tate, High-fraction brookite films from amorphous precursors, Sci. Rep., 7 (2017) 15232.

[22] J. Li, H. Zhou, H. Zhuo, Z. Wei, G. Zhuang, X. Zhong, S. Deng, X. Li, J. Wang, Oxygen vacancies on TiO2 promoted the activity and stability of supported Pd nanoparticles for the oxygen reduction reaction, J. Mater. Chem. A,, 6 (2018) 2264-2272.

[23] R. Palcheva, L. Dimitrov, G. Tyuliev, A. Spojakina, K. Jiratova, TiO_2 nanotubes supported NiW hydrodesulphurization catalysts: Characterization and activity, Appl. Surf. Sci., 265 (2013) 309-316.

[24] W. Limsangkass, S. Chaemchuen, S. Phatanasri, P. Praserthdam, K. Suriye, Synergistic effect of additional TiO_2 support on metathesis activity of ethylene and 2-butene over supported tungsten-based catalysts for propylene production, Kinet. Catal., 55 (2014) 676-682.

[25] D. Tilgner, M. Friedrich, J. Hermannsdörfer, R. Kempe, Titanium Dioxide Reinforced Metal–Organic Framework Pd Catalysts: Activity and Reusability Enhancement in Alcohol Dehydrogenation Reactions and Improved Photocatalytic Performance, ChemCatChem, 7 (2015) 3916-3922.

[26] J.A. Lopez-Sanchez, N. Dimitratos, C. Hammond, G.L. Brett, L. Kesavan, S. White, P. Miedziak, R. Tiruvalam, R.L. Jenkins, A.F. Carley, D. Knight, C.J. Kiely,

G.J. Hutchings, Facile removal of stabilizer-ligands from supported gold nanoparticles, Nat. Chem., 3 (2011) 551.

[27] L. Da Già, C. Recchi, T.E. Davies, N. Greeves, J.A. Lopez-Sanchez, Visible-Light-Controlled Oxidation of Glucose using Titania-Supported Silver Photocatalysts, ChemCatChem, 8 (2016) 3475-3483.

[28] M. Haruta, Size- and support-dependency in the catalysis of gold, Catal. Today, 36 (1997) 153-166.

[29] G.R. Bamwenda, S. Tsubota, T. Nakamura, M. Haruta, The influence of the preparation methods on the catalytic activity of platinum and gold supported on TiO_2 for CO oxidation, Catal. Lett., 44 (1997) 83-87.

[30] S.J. Tauster, S.C. Fung, R.T.K. Baker, J.A. Horsley, Strong Interactions in Supported-Metal Catalysts, Science, 211 (1981) 1121-1125.

[31] S. Iijima, Helical microtubules of graphitic carbon, Nature, 354 (1991) 56-58.

[32] T.W. Ebbesen, P.M. Ajayan, Large-scale synthesis of carbon nanotubes, Nature, 358 (1992) 220-222.

[33] A. Loiseau, H. Pascard, Synthesis of long carbon nanotubes filled with Se, S, Sb and Ge by the arc method, Chem. Phys. Lett., 256 (1996) 246-252.

[34] T. Guo, P. Nikolaev, A. Thess, D.T. Colbert, R.E. Smalley, Catalytic growth of single-walled manotubes by laser vaporization, Chem. Phys. Lett., 243 (1995) 49-54.

[35] T. Guo, P. Nikolaev, A.G. Rinzler, D. Tomanek, D.T. Colbert, R.E. Smalley, Self-Assembly of Tubular Fullerenes, J. Phys. Chem., 99 (1995) 10694-10697.

[36] A. Aqel, K.M.M.A. El-Nour, R.A.A. Ammar, A. Al-Warthan, Carbon nanotubes, science and technology part (I) structure, synthesis and characterisation, Arabian J. Chem., 5 (2012) 1-23.

[37] Y. Ando, X. Zhao, T. Sugai, M. Kumar, Growing carbon nanotubes, Materials Today, 7 (2004) 22-29.

[38] M. Kumar, Y. Ando, Chemical Vapor Deposition of Carbon Nanotubes: A Review on Growth Mechanism and Mass Production, J. Nanosci. Nanotechnol., 10 (2010) 3739-3758.

[39] R.H. Baughman, A.A. Zakhidov, W.A. de Heer, Carbon Nanotubes--the Route Toward Applications, Science, 297 (2002) 787-792.

[40] R. Leary, A. Westwood, Carbonaceous nanomaterials for the enhancement of TiO2 photocatalysis, Carbon, 49 (2011) 741-772.

[41] S.A. Miners, G.A. Rance, A.N. Khlobystov, Chemical reactions confined within carbon nanotubes, Chem. Soc. Rev., 45 (2016) 4727-4746.

[42] M. Ran, W. Chu, Y. Liu, A. Borgna, Nano Ru catalysts supported on carbon nanotubes for cellobiose conversion to sugar alcohols: effects of CNT channel size, RSC Adv., 5 (2015) 103669-103673.

[43] J. Liu, R. Liu, H. Li, W. Kong, H. Huang, Y. Liu, Z. Kang, Au nanoparticles in carbon nanotubes with high photocatalytic activity for hydrocarbon selective oxidation, Dalton Transactions, 43 (2014) 12982-12988.

[44] H. Zhang, X. Pan, X. Han, X. Liu, X. Wang, W. Shen, X. Bao, Enhancing chemical reactions in a confined hydrophobic environment: an NMR study of benzene hydroxylation in carbon nanotubes, Chem. Sci., 4 (2013) 1075-1078.

[45] X. Cui, Y. Wang, G. Jiang, Z. Zhao, C. Xu, A. Duan, J. Liu, Y. Wei, W. Bai, The encapsulation of CdS in carbon nanotubes for stable and efficient photocatalysis, J. Mater. Chem. A, 2 (2014) 20939-20946.

[46] L. Chen, Y. Honsho, S. Seki, D. Jiang, Light-Harvesting Conjugated Microporous Polymers: Rapid and Highly Efficient Flow of Light Energy with a Porous Polyphenylene Framework as Antenna, J. Am. Chem. Soc., 132 (2010) 6742-6748.

[47] R.S. Sprick, J.-X. Jiang, B. Bonillo, S. Ren, T. Ratvijitvech, P. Guiglion, M.A. Zwijnenburg, D.J. Adams, A.I. Cooper, Tunable Organic Photocatalysts for Visible-Light-Driven Hydrogen Evolution, J. Am. Chem. Soc., 137 (2015) 3265-3270.

[48] R. Dawson, A. Laybourn, R. Clowes, Y.Z. Khimyak, D.J. Adams, A.I. Cooper, Functionalized Conjugated Microporous Polymers, Macromolecules, 42 (2009) 8809-8816.

[49] C. Ge, H. Tom, T. Abbie, A.D. J., C.A. I., Soluble Conjugated Microporous Polymers, Angewandte Chemie International Edition, 51 (2012) 12727-12731.

[50] J.-X. Jiang, F. Su, A. Trewin, C.D. Wood, H. Niu, J.T.A. Jones, Y.Z. Khimyak, A.I. Cooper, Synthetic Control of the Pore Dimension and Surface Area in Conjugated Microporous Polymer and Copolymer Networks, J. Am. Chem. Soc., 130 (2008) 7710-7720.

[51] J.-X. Jiang, A. Trewin, D.J. Adams, A.I. Cooper, Band gap engineering in fluorescent conjugated microporous polymers, Chem. Sci., 2 (2011) 1777-1781.

[52] C.A. I., Conjugated Microporous Polymers, Advanced Materials, 21 (2009) 1291-1295.

[53] Y. Kou, Y. Xu, Z. Guo, D. Jiang, Supercapacitive Energy Storage and Electric Power Supply Using an Aza-Fused π-Conjugated Microporous Framework, Angew. Chem. Int. Ed., 50 (2011) 8753-8757.

[54] D. Xiao, Y. Li, L. Liu, B. Wen, Z. Gu, C. Zhang, Y.S. Zhao, Two-photon fluorescent microporous bithiophene polymer via Suzuki cross-coupling, Chem. Commun., 48 (2012) 9519-9521.

[55] R. Dawson, E. Stöckel, J.R. Holst, D.J. Adams, A.I. Cooper, Microporous organic polymers for carbon dioxide capture, Energy Environ. Sci., 4 (2011) 4239-4245.

[56] T. Ishida, Y. Onuma, K. Kinjo, A. Hamasaki, H. Ohashi, T. Honma, T. Akita, T. Yokoyama, M. Tokunaga, M. Haruta, Preparation of microporous polymer-encapsulated Pd nanoparticles and their catalytic performance for hydrogenation and oxidation, Tetrahedron, 70 (2014) 6150-6155.

[57] J. Schmidt, J. Weber, J.D. Epping, M. Antonietti, A. Thomas, Microporous Conjugated Poly(thienylene arylene) Networks, Adv. Mater., 21 (2009) 702-705.

[58] F. Wang, J. Mielby, F.H. Richter, G. Wang, G. Prieto, T. Kasama, C. Weidenthaler, H.-J. Bongard, S. Kegnæs, A. Fürstner, F. Schüth, A Polyphenylene Support for Pd Catalysts with Exceptional Catalytic Activity, Angewandte Chemie International Edition, 53 (2014) 8645-8648.

[59] P. Ju, S. Wu, Q. Su, X. Li, Z. Liu, G. Li, Q. Wu, Salen–porphyrin-based conjugated microporous polymer supported Pd nanoparticles: highly efficient heterogeneous catalysts for aqueous C–C coupling reactions, J. Mater. Chem. A, 7 (2019) 2660-2666.

[60] A. Corma, H. Garcia, Supported gold nanoparticles as catalysts for organic reactions, Chem. Soc. Rev., 37 (2008) 2096-2126.

[61] F. Pinna, Supported metal catalysts preparation, Catal. Today, 41 (1998) 129-137.

[62] P. Munnik, P.E. de Jongh, K.P. de Jong, Recent Developments in the Synthesis of Supported Catalysts, Chem. Rev. , 115 (2015) 6687-6718.

[63] R.J. White, R. Luque, V.L. Budarin, J.H. Clark, D.J. Macquarrie, Supported metal nanoparticles on porous materials. Methods and applications, Chem.Soc.Rev., 38 (2009) 481-494.

[64] L. Prati, A. Villa, The Art of Manufacturing Gold Catalysts, Catalysts, 2 (2012) 24.

[65] M.Á. Centeno, I. Carrizosa, J.A. Odriozola, Deposition–precipitation method to obtain supported gold catalysts: dependence of the acid–base properties of the support exemplified in the system TiO_2–TiO_xN_y–TiN, Appl. Catal. A. : Gen., 246 (2003) 365-372.

[66] R. Zanella, S. Giorgio, C.-H. Shin, C.R. Henry, C. Louis, Characterization and reactivity in CO oxidation of gold nanoparticles supported on TiO_2 prepared by deposition-precipitation with NaOH and urea, J. Catal., 222 (2004) 357-367.

[67] L. Prati, G. Martra, New gold catalysts for liquid phase oxidation, Gold Bulletin, 32 (1999) 96-101.

[68] L. Prati, A. Villa, Gold Colloids: From Quasi-Homogeneous to Heterogeneous Catalytic Systems, Acc. Chem. Res., 47 (2014) 855-863.

[69] A. Villa, D. Wang, G.M. Veith, F. Vindigni, L. Prati, Sol immobilization technique: a delicate balance between activity, selectivity and stability of gold catalysts, Catal. Sci. Technol., 3 (2013) 3036-3041.

[70] A.R. Tao, S. Habas, P. Yang, Shape Control of Colloidal Metal Nanocrystals, Small, 4 (2008) 310-325.

[71] A. Demirbaş, Biomass resource facilities and biomass conversion processing for fuels and chemicals, Energy Convers. Manage., 42 (2001) 1357-1378.

[72] P. McKendry, Energy production from biomass (part 1): overview of biomass, Bioresour. Technol., 83 (2002) 37-46.

[73] C.-H. Zhou, X. Xia, C.-X. Lin, D.-S. Tong, J. Beltramini, Catalytic conversion of lignocellulosic biomass to fine chemicals and fuels, Chem. Soc. Rev., 40 (2011) 5588-5617.

[74] V. Menon, M. Rao, Trends in bioconversion of lignocellulose: Biofuels, platform chemicals & biorefinery concept, Prog. Energy Combust. Sci., 38 (2012) 522-550.

[75] A. Corma, S. Iborra, A. Velty, Chemical Routes for the Transformation of Biomass into Chemicals, Chem. Rev., 107 (2007) 2411-2502.

[76] Y.-B. Huang, Y. Fu, Hydrolysis of cellulose to glucose by solid acid catalysts, Green Chem., 15 (2013) 1095-1111.

[77] A. Carlmark, E. Larsson, E. Malmström, Grafting of cellulose by ring-opening polymerisation – A review, Eur. Polym. J., 48 (2012) 1646-1659.

[78] P. Mäki-Arvela, T. Salmi, B. Holmbom, S. Willför, D.Y. Murzin, Synthesis of Sugars by Hydrolysis of Hemicelluloses- A Review, Chem. Rev., 111 (2011) 5638-5666.

[79] A. Cabiac, E. Guillon, F. Chambon, C. Pinel, F. Rataboul, N. Essayem, Cellulose reactivity and glycosidic bond cleavage in aqueous phase by catalytic and non catalytic transformations, Appl. Catal. A. : Gen., 402 (2011) 1-10.

[80] R. Rinaldi, F. Schuth, Design of solid catalysts for the conversion of biomass, Energy Environ. Sci., 2 (2009) 610-626.

[81] J. Zakzeski, P.C.A. Bruijnincx, A.L. Jongerius, B.M. Weckhuysen, The Catalytic Valorization of Lignin for the Production of Renewable Chemicals, Chem. Rev., 110 (2010) 3552-3599.

[82] E. Dorrestijn, L.J.J. Laarhoven, I.W.C.E. Arends, P. Mulder, The occurrence and reactivity of phenoxyl linkages in lignin and low rank coal, J. Anal. Appl. Pyrolysis, 54 (2000) 153-192.

[83] M. Yabushita, H. Kobayashi, K. Hara, A. Fukuoka, Quantitative evaluation of ball-milling effects on the hydrolysis of cellulose catalysed by activated carbon, Catal. Sci. Technol., 4 (2014) 2312-2317.

[84] R. Schmidt, S. Fuhrmann, L. Wondraczek, A. Stolle, Influence of reaction parameters on the depolymerization of H_2SO_4-impregnated cellulose in planetary ball mills, Powder Technol., 288 (2016) 123-131.

[85] R. Travaini, J. Martín-Juárez, A. Lorenzo-Hernando, S. Bolado-Rodríguez, Ozonolysis: An advantageous pretreatment for lignocellulosic biomass revisited, Bioresource Technology, 199 (2016) 2-12.

[86] H. Li, Y. Qu, Y. Yang, S. Chang, J. Xu, Microwave irradiation – A green and efficient way to pretreat biomass, Bioresource Technology, 199 (2016) 34-41.

[87] Q. Zhang, M. Benoit, K. De Oliveira Vigier, J. Barrault, G. Jegou, M. Philippe, F. Jerome, Pretreatment of microcrystalline cellulose by ultrasounds: effect of particle size in the heterogeneously-catalyzed hydrolysis of cellulose to glucose, Green Chem., 15 (2013) 963-969.

[88] M. Benoit, A. Rodrigues, Q. Zhang, E. Fourré, K. De Oliveira Vigier, J.-M. Tatibouët, F. Jérôme, Depolymerization of Cellulose Assisted by a Nonthermal Atmospheric Plasma, Angew. Chem. Int. Ed., 50 (2011) 8964-8967.

[89] R.P. Swatloski, S.K. Spear, J.D. Holbrey, R.D. Rogers, Dissolution of Cellose with Ionic Liquids, J. AM. CHEM. SOC., 124 (2002) 4974-4975.

[90] W.-H. Hsu, Y.-Y. Lee, W.-H. Peng, K.C.W. Wu, Cellulosic conversion in ionic liquids (ILs): Effects of H_2O/cellulose molar ratios, temperatures, times, and different ILs on the production of monosaccharides and 5-hydroxymethylfurfural (HMF), Catal. Today, 174 (2011) 65-69.

[91] F. Camacho, P. González-Tello, E. Jurado, A. Robles, Microcrystalline-cellulose hydrolysis with concentrated sulphuric acid, J. Chem. Tech. Biotechnol., 67 (1996) 350-356.

[92] D.R. Thompson, H.E. Grethlein, Design and Evaluation of a Plug Flow Reactor for Acid Hydrolysis of Cellulose, Ind. Eng. Chem. Prod. Res. Dev., 18 (1979) 166-169.

[93] M.M. Küçük, A. Demirbaş, Biomass conversion processes, Energy Convers. Mgmt, 38 (1997) 151-165.

[94] P.L. Dhepe, A. Fukuoka, Cellulose Conversion under Heterogeneous Catalysis, ChemSusChem, 1 (2008) 969-975.

[95] S.J.B. Duff, W.D. Murray, Bioconversion of forest products industry waste cellulosics to fuel ethanol: A review, Bioresour. Technol., 55 (1996) 1-33.

[96] E.C.C. Baly, I.M. Heilbron, W.F. Barker, CX.—Photocatalysis. Part I. The synthesis of formaldehyde and carbohydrates from carbon dioxide and water, J. Chem. Soc., Trans., 119 (1921) 1025-1035.

[97] W. Doerffler, K. Hauffe, Heterogeneous photocatalysis I. The influence of oxidizing and reducing gases on the electrical conductivity of dark and illuminated zinc oxide surfaces, J. Catal., 3 (1964) 156-170.

[98] G.L. Miessler, P.J. Fischer, D.A. Tarr, Inorganic Chemistry, 5th Edition, Pearson, (2014), 229-233.

[99] Y. Liu, Z. Li, M. Green, M. Just, Y.Y. Li, X. Chen, Titanium dioxide nanomaterials for photocatalysis, J. Phys. D: Appl. Phys., 50 (2017) 193003.

[100] Y. Shiraishi, T. Hirai, Selective organic transformations on titanium oxide-based photocatalysts, J. Photochem. Photobiol. C: Photochem. Rev., 9 (2008) 157-170.

[101] M.A. Henderson, A surface science perspective on photocatalysis, Surf.Sci.Rep., 66 (2011) 185-297.

[102] A. Bumajdad, M. Madkour, Understanding the superior photocatalytic activity of noble metals modified titania under UV and visible light irradiation, Phys.Chem.Chem.Phys., 16 (2014) 7146-7158.

[103] D.Y.C. Leung, X. Fu, C. Wang, M. Ni, M.K.H. Leung, X. Wang, X. Fu, Hydrogen Production over Titania-Based Photocatalysts, ChemSusChem, 3 (2010) 681-694.

[104] P. Chowdhury, H. Gomaa, A.K. Ray, Dye-Sensitized Photocatalyst: A Breakthrough in Green Energy and Environmental Detoxification, Sustainable Nanotechnology and the Environment: Advances and Achievements, American Chemical Society(2013), pp. 231-266.

[105] X. Fang, Z. Zhang, Q. Chen, H. Ji, X. Gao, Dependence of nitrogen doping on TiO2 precursor annealed under NH3 flow, J. Solid State Chem., 180 (2007) 1325-1332.

[106] A.M. Czoska, S. Livraghi, M. Chiesa, E. Giamello, S. Agnoli, G. Granozzi, E. Finazzi, C.D. Valentin, G. Pacchioni, The Nature of Defects in Fluorine-Doped TiO2, J. Phys. Chem. C, 112 (2008) 8951-8956.

[107] P. Periyat, D.E. McCormack, S.J. Hinder, S.C. Pillai, One-Pot Synthesis of Anionic (Nitrogen) and Cationic (Sulfur) Codoped High-Temperature Stable, Visible Light Active, Anatase Photocatalysts, J. Phys. Chem. C, 113 (2009) 3246-3253.

[108] V. Etacheri, M.K. Seery, S.J. Hinder, S.C. Pillai, Oxygen Rich Titania: A Dopant Free, High Temperature Stable, and Visible-Light Active Anatase Photocatalyst, Adv. Funct. Mater., 21 (2011) 3744-3752.

[109] J.C. Yu, L. Wu, J. Lin, P. Li, Q. Li, Microemulsion-mediated solvothermal synthesis of nanosized CdS-sensitized TiO_2 crystalline photocatalyst, Chem. Commun., (2003) 1552-1553.

[110] C. Yu, L. Wei, J. Chen, Y. Xie, W. Zhou, Q. Fan, Enhancing the Photocatalytic Performance of Commercial TiO_2 Crystals by Coupling with Trace Narrow-Band-Gap Ag2CO3, Ind. Eng. Chem. Res. , 53 (2014) 5759-5766.

[111] B. Zhou, J. Song, Z. Zhang, Z. Jiang, P. Zhang, B. Han, Highly selective photocatalytic oxidation of biomass-derived chemicals to carboxyl compounds over Au/TiO2, Green Chem., 19 (2017) 1075-1081.

[112] V. Amendola, R. Pilot, M. Frasconi, O.M. Maragò, M.A. Iatì, Surface plasmon resonance in gold nanoparticles: a review, J. Phys.: Condens. Matter, 29 (2017) 203002.

[113] A. Gołąbiewska, A. Malankowska, M. Jarek, W. Lisowski, G. Nowaczyk, S. Jurga, A. Zaleska-Medynska, The effect of gold shape and size on the properties and visible light-induced photoactivity of Au-TiO_2, Appl. Catal. B: Environ., 196 (2016) 27-40.

[114] R. Liu, H. Huang, H. Li, Y. Liu, J. Zhong, Y. Li, S. Zhang, Z. Kang, Metal Nanoparticle/Carbon Quantum Dot Composite as a Photocatalyst for High-Efficiency Cyclohexane Oxidation, ACS Catal., 4 (2014) 328-336.

[115] J. Liu, R. Liu, H. Li, W. Kong, H. Huang, Y. Liu, Z. Kang, Au nanoparticles in carbon nanotubes with high photocatalytic activity for hydrocarbon selective oxidation, Dalton Trans., 43 (2014) 12982-12988.

[116] P. Kar, S. Sardar, B. Liu, M. Sreemany, P. Lemmens, S. Ghosh, S.K. Pal, Facile synthesis of reduced graphene oxide–gold nanohybrid for potential use in industrial waste-water treatment, Sci. Technol. Adv. Mater., 17 (2016) 375-386.

[117] L. Da Vià, C. Recchi, E.O. Gonzalez-Yañez, T.E. Davies, J.A. Lopez-Sanchez, Visible light selective photocatalytic conversion of glucose by TiO_2, Appl. Catal., B: Environ., 202 (2017) 281-288.

[118] S. Biella, L. Prati, M. Rossi, Selective Oxidation of D-Glucose on Gold Catalyst, J. Catal., 206 (2002) 242-247.

[119] S. Linic, P. Christopher, D.B. Ingram, Plasmonic-metal nanostructures for efficient conversion of solar to chemical energy, Nat. Mater., 10 (2011) 911.

[120] S. Sarina, E.R. Waclawik, H. Zhu, Photocatalysis on supported gold and silver nanoparticles under ultraviolet and visible light irradiation, Green Chem., 15 (2013) 1814-1833.

[121] R. Jiang, J. Wang, Plasmon-assisted Chemical Reactions, Nanomaterials for Photocatalytic Chemistry (2016), pp. 155-193.

[122] H.A. Atwater, A. Polman, Plasmonics for improved photovoltaic devices, Nat. Mater., 9 (2010) 205.

[123] C. Wang, D. Astruc, Nanogold plasmonic photocatalysis for organic synthesis and clean energy conversion, Chem. Soc. Rev., 43 (2014) 7188-7216.

[124] S. Peiris, J. McMurtrie, H.-Y. Zhu, Metal nanoparticle photocatalysts: emerging processes for green organic synthesis, Catal. Sci. Technol., 6 (2016) 320-338.

[125] K. Yamada, K. Miyajima, F. Mafuné, Thermionic Emission of Electrons from Gold Nanoparticles by Nanosecond Pulse-Laser Excitation of Interband, J. Phys. Chem. C, 111 (2007) 11246-11251.

[126] X. Pan, Y.-J. Xu, Fast and spontaneous reduction of gold ions over oxygen-vacancy-rich TiO2: A novel strategy to design defect-based composite photocatalyst, Appl. Catal. A: Gen., 459 (2013) 34-40.

[127] M.V. Dozzi, L. Prati, P. Canton, E. Selli, Effects of gold nanoparticles deposition on the photocatalytic activity of titanium dioxide under visible light, Phys.Chem. Chem.Phys., 11 (2009) 7171-7180.

[128] Ş. Neaţu, B. Cojocaru, V.I. Pârvulescu, V. Şomoghi, M. Alvaro, H. Garcia, Visible-light C–heteroatom bond cleavage and detoxification of chemical warfare agents using titania-supported gold nanoparticles as photocatalyst, J. Mater. Chem., 20 (2010) 4050-4054.

[129] L. Brus, Noble Metal Nanocrystals: Plasmon Electron Transfer Photochemistry and Single-Molecule Raman Spectroscopy, Acc. Chem. Res., 41 (2008) 1742-1749.

[130] K.M. Mayer, J.H. Hafner, Localized Surface Plasmon Resonance Sensors, Chem. Rev., 111 (2011) 3828-3857.

[131] K.L. Kelly, E. Coronado, L.L. Zhao, G.C. Schatz, The Optical Properties of Metal Nanoparticles: The Influence of Size, Shape, and Dielectric Environment, J. Phys. Chem. B, 107 (2003) 668-677.

[132] P.K. Jain, I.H. El-Sayed, M.A. El-Sayed, Au nanoparticles target cancer, Nano Today, 2 (2007) 18-29.

[133] M. Omri, F. Sauvage, Y. Busby, M. Becuwe, G. Pourceau, A. Wadouachi, Gold Catalysis and Photoactivation: A Fast and Selective Procedure for the Oxidation of Free Sugars, ACS Catal., (2018) 1635-1639.

[134] M.R. Khan, T.W. Chuan, A. Yousuf, M.N.K. Chowdhury, C.K. Cheng, Schottky barrier and surface plasmonic resonance phenomena towards the

photocatalytic reaction: study of their mechanisms to enhance photocatalytic activity, Catal. Sci. Technol., 5 (2015) 2522-2531.

[135] B. Balamurugan, T. Maruyama, Evidence of an enhanced interband absorption in Au nanoparticles: Size-dependent electronic structure and optical properties, Appl. Phys. Lett., 87 (2005) 143105.

[136] G. Baffou, R. Quidant, Nanoplasmonics for chemistry, Chem. Soc. Rev., 43 (2014) 3898-3907.

[137] R. Long, Y. Li, L. Song, Y. Xiong, Coupling Solar Energy into Reactions: Materials Design for Surface Plasmon-Mediated Catalysis, Small, 11 (2015) 3873-3889.

[138] W.R. Erwin, H.F. Zarick, E.M. Talbert, R. Bardhan, Light trapping in mesoporous solar cells with plasmonic nanostructures, Energy Environ. Sci., 9 (2016) 1577-1601.

[139] M. Haggui, M. Dridi, J. Plain, S. Marguet, H. Perez, G.C. Schatz, G.P. Wiederrecht, S.K. Gray, R. Bachelot, Spatial Confinement of Electromagnetic Hot and Cold Spots in Gold Nanocubes, ACS Nano, 6 (2012) 1299-1307.

[140] M. Rycenga, X. Xia, C.H. Moran, F. Zhou, D. Qin, Z.-Y. Li, Y. Xia, Generation of Hot Spots with Silver Nanocubes for Single-Molecule Detection by Surface-Enhanced Raman Scattering, Angew. Chem. Int. Ed., 50 (2011) 5473-5477.

[141] B. Grześkiewicz, K. Ptaszyński, M. Kotkowiak, Near and Far-Field Properties of Nanoprisms with Rounded Edges, Plasmonics, 9 (2014) 607-614.

[142] Z. Liu, W. Hou, P. Pavaskar, M. Aykol, S.B. Cronin, Plasmon Resonant Enhancement of Photocatalytic Water Splitting Under Visible Illumination, Nano Lett., 11 (2011) 1111-1116.

[143] O. Ilic, M. Jablan, J.D. Joannopoulos, I. Celanovic, M. Soljačić, Overcoming the black body limit in plasmonic and graphene near-field thermophotovoltaic systems, Opt. Express, 20 (2012) A366-A384.

[144] X. Chen, H.-Y. Zhu, J.-C. Zhao, Z.-F. Zheng, X.-P. Gao, Visible-Light-Driven Oxidation of Organic Contaminants in Air with Gold Nanoparticle Catalysts on Oxide Supports, Angew. Chem. Int. Ed., 47 (2008) 5353-5356.

[145] X. Zhang, X. Ke, A. Du, H. Zhu, Plasmonic nanostructures to enhance catalytic performance of zeolites under visible light, Sci. Rep., 4 (2014) 3805.

[146] C. Sönnichsen, T. Franzl, T. Wilk, G. von Plessen, J. Feldmann, O. Wilson, P. Mulvaney, Drastic Reduction of Plasmon Damping in Gold Nanorods, Phys. Rev. Lett. ,88 (2002) 077402.

[147] J. Lehmann, M. Merschdorf, W. Pfeiffer, A. Thon, S. Voll, G. Gerber, Surface Plasmon Dynamics in Silver Nanoparticles Studied by Femtosecond Time-Resolved Photoemission, Phys. Rev. Lett., 85 (2000) 2921-2924.

[148] J. Hofmann, W. Steinmann, Plasma Resonance in the Photoemission of Silver, Phys. Status Solidi B, 30 (1968) K53-K56.

[149] J.G. Endriz, W.E. Spicer, Surface-Plasmon-One-Electron Decay and its Observation in Photoemission, Phys. Rev. Lett. , 24 (1970) 64-68.

[150] Y. Zhang, S. He, W. Guo, Y. Hu, J. Huang, J.R. Mulcahy, W.D. Wei, Surface-Plasmon-Driven Hot Electron Photochemistry, Chem. Rev., 118 (2018) 2927-2954.

[151] X. Li, D. Xiao, Z. Zhang, Landau damping of quantum plasmons in metal nanostructures, New J. Phys., 15 (2013) 023011.

[152] R. Bingham, J.T. Mendonça, J.M. Dawson, Photon Landau Damping, Phys. Rev. Lett., 78 (1997) 247-249.

[153] Y. Gao, Z. Yuan, S. Gao, Semiclassical approach to plasmon–electron coupling and Landau damping of surface plasmons, J. Chem. Phys., 134 (2011) 134702.

[154] C. Clavero, Plasmon-induced hot-electron generation at nanoparticle/metal-oxide interfaces for photovoltaic and photocatalytic devices, Nat. Photonics, 8 (2014) 95.

[155] M.L. Brongersma, N.J. Halas, P. Nordlander, Plasmon-induced hot carrier science and technology, Nat. Nanotechnol., 10 (2015) 25.

[156] T.P. White, K.R. Catchpole, Plasmon-enhanced internal photoemission for photovoltaics: Theoretical efficiency limits, Appl. Phys. Lett. , 101 (2012) 073905.

[157] C.N. Berglund, W.E. Spicer, Photoemission Studies of Copper and Silver: Experiment, Phys. Rev., 136 (1964) A1044-A1064.

[158] T. Inagaki, K. Kagami, E.T. Arakawa, Photoacoustic observation of nonradiative decay of surface plasmons in silver, Phys. Rev. B, 24 (1981) 3644-3646.

[159] M.W. Knight, H. Sobhani, P. Nordlander, N.J. Halas, Photodetection with Active Optical Antennas, Science, 332 (2011) 702-704.

[160] K. Wu, J. Chen, J.R. McBride, T. Lian, Efficient hot-electron transfer by a plasmon-induced interfacial charge-transfer transition, Science, 349 (2015) 632-635.

[161] M.W. Knight, Y. Wang, A.S. Urban, A. Sobhani, B.Y. Zheng, P. Nordlander, N.J. Halas, Embedding Plasmonic Nanostructure Diodes Enhances Hot Electron Emission, Nano Lett., 13 (2013) 1687-1692.

[162] S. Mubeen, J. Lee, W.-r. Lee, N. Singh, G.D. Stucky, M. Moskovits, On the Plasmonic Photovoltaic, ACS Nano, 8 (2014) 6066-6073.

[163] M. Moskovits, Hot Electrons Cross Boundaries, Science, 332 (2011) 676-677.

[164] S. Linic, U. Aslam, C. Boerigter, M. Morabito, Photochemical transformations on plasmonic metal nanoparticles, Nature Mater., 14 (2015) 567-576.

[165] H. Chen, L. Shao, T. Ming, Z. Sun, C. Zhao, B. Yang, J. Wang, Understanding the Photothermal Conversion Efficiency of Gold Nanocrystals, Small, 6 (2010) 2272-2280.

[166] G. Baffou, R. Quidant, C. Girard, Heat generation in plasmonic nanostructures: Influence of morphology, Appl. Phys. Lett., 94 (2009) 153109.

[167] G. Baffou, R. Quidant, Thermo-plasmonics: using metallic nanostructures as nano-sources of heat, Laser Photonics Rev., 7 (2013) 171-187.

[168] S.R. Logan, The origin and status of the Arrhenius equation, J. Chem. Educ., 59 (1982) 279.

[169] C.-W. Yen, M.A. El-Sayed, Plasmonic Field Effect on the Hexacyanoferrate (III)-Thiosulfate Electron Transfer Catalytic Reaction on Gold Nanoparticles: Electromagnetic or Thermal?, J. Phys. Chem. C, 113 (2009) 19585-19590.

[170] W.H. Hung, M. Aykol, D. Valley, W. Hou, S.B. Cronin, Plasmon Resonant Enhancement of Carbon Monoxide Catalysis, Nano Lett., 10 (2010) 1314-1318.

[171] C. Fasciani, C.J.B. Alejo, M. Grenier, J.C. Netto-Ferreira, J.C. Scaiano, High-Temperature Organic Reactions at Room Temperature Using Plasmon Excitation: Decomposition of Dicumyl Peroxide, Org. Lett., 13 (2011) 204-207.

[172] O. Neumann, A.S. Urban, J. Day, S. Lal, P. Nordlander, N.J. Halas, Solar Vapor Generation Enabled by Nanoparticles, ACS Nano, 7 (2013) 42-49.

[173] X. Zhang, Y.L. Chen, R.-S. Liu, D.P. Tsai, Plasmonic photocatalysis, Rep. Prog. Phys., 76 (2013) 046401.

[174] P. Wang, B. Huang, Y. Dai, M.-H. Whangbo, Plasmonic photocatalysts: harvesting visible light with noble metal nanoparticles, Phys. Chem. Chem. Phys., 14 (2012) 9813-9825.

[175] A. Primo, A. Corma, H. García, Titania supported gold nanoparticles as photocatalyst, Phys. Chem. Chem. Phys., 13 (2011) 886-910.

[176] Y. Tian, T. Tatsuma, Mechanisms and Applications of Plasmon-Induced Charge Separation at TiO2 Films Loaded with Gold Nanoparticles, J. Am. Chem. Soc., 127 (2005) 7632-7637.

[177] A. Furube, L. Du, K. Hara, R. Katoh, M. Tachiya, Ultrafast Plasmon-Induced Electron Transfer from Gold Nanodots into TiO2 Nanoparticles, J. Am. Chem. Soc., 129 (2007) 14852-14853.

[178] Y. Tian, T. Tatsuma, Plasmon-induced photoelectrochemistry at metal nanoparticles supported on nanoporous TiO_2, Chem. Commun., (2004) 1810-1811.

[179] S.T. Kochuveedu, Y.H. Jang, D.H. Kim, A study on the mechanism for the interaction of light with noble metal-metal oxide semiconductor nanostructures for various photophysical applications, Chem. Soc. Rev., 42 (2013) 8467-8493.

[180] S. Rapagnà, N. Jand, P.U. Foscolo, Catalytic gasification of biomass to produce hydrogen rich gas, Int. J. Hydrogen Energy, 23 (1998) 551-557.

[181] M. Watanabe, H. Inomata, K. Arai, Catalytic hydrogen generation from biomass (glucose and cellulose) with ZrO_2 in supercritical water, Biomass and Bioenergy, 22 (2002) 405-410.

[182] S. Li, S. Xu, S. Liu, C. Yang, Q. Lu, Fast pyrolysis of biomass in free-fall reactor for hydrogen-rich gas, Fuel Process. Technol., 85 (2004) 1201-1211.

[183] H. Kobayashi, A. Fukuoka, Synthesis and utilisation of sugar compounds derived from lignocellulosic biomass, Green Chem., 15 (2013) 1740-1763.

[184] C. Chatterjee, F. Pong, A. Sen, Chemical conversion pathways for carbohydrates, Green Chem., 17 (2015) 40-71.

[185] A.E. Koklin, T.A. Klimenko, A.V. Kondratyuk, V.V. Lunin, V.I. Bogdan, Transformation of aqueous solutions of glucose over the Pt/C catalyst, Kinet. Catal., 56 (2015) 84-88.

[186] J.C. Colmenares, A. Magdziarz, A. Bielejewska, High-value chemicals obtained from selective photo-oxidation of glucose in the presence of nanostructured titanium photocatalysts, Bioresour. Technol., 102 (2011) 11254-11257.

[187] J.C. Colmenares, A. Magdziarz, Room temperature versatile conversion of biomass-derived compounds by means of supported TiO_2 photocatalysts, J. Mol. Catal. A: Chem., 366 (2013) 156-162.

[188] S. Sankararaman, K.B. Yoon, T. Yabe, J.K. Kochi, Control of back electron transfer from charge-transfer ion pairs by zeolite supercages, J. Am. Chem. Soc., 113 (1991) 1419-1421.

[189] J.C. Colmenares, A. Magdziarz, O. Chernyayeva, D. Lisovytskiy, K. Kurzydłowski, J. Grzonka, Sonication-Assisted Low-Temperature Routes for the Synthesis of Supported Fe–TiO_2 Econanomaterials: Partial Photooxidation of Glucose and Phenol Aqueous Degradation, ChemCatChem, 5 (2013) 2270-2277.

[190] J.C. Colmenares, A. Magdziarz, K. Kurzydlowski, J. Grzonka, O. Chernyayeva, D. Lisovytskiy, Low-temperature ultrasound-promoted synthesis of

Cr–TiO_2-supported photocatalysts for valorization of glucose and phenol degradation from liquid phase, Appl. Catal. B: Environ., 134–135 (2013) 136-144.

[191] M. Bellardita, E.I. García-López, G. Marcì, B. Megna, F.R. Pomilla, L. Palmisano, Photocatalytic conversion of glucose in aqueous suspensions of heteropolyacid–TiO_2 composites, RSC Adv., 5 (2015) 59037-59047.

[192] C. Streb, New trends in polyoxometalate photoredox chemistry: From photosensitisation to water oxidation catalysis, Dalton Trans., 41 (2012) 1651-1659.

[193] G.-J.t. Brink, I.W.C.E. Arends, R.A. Sheldon, Green, Catalytic Oxidation of Alcohols in Water, Science, 287 (2000) 1636-1639.

[194] L. Wang, Z. Zhang, L. Zhang, S. Xue, W.O.S. Doherty, I.M. O'Hara, X. Ke, Sustainable conversion of cellulosic biomass to chemicals under visible-light irradiation, RSC Adv., 5 (2015) 85242-85247.

[195] G. Zhang, C. Ni, X. Huang, A. Welgamage, L.A. Lawton, P.K.J. Robertson, J.T.S. Irvine, Simultaneous cellulose conversion and hydrogen production assisted by cellulose decomposition under UV-light photocatalysis, Chem. Commun., 52 (2016) 1673-1676.

[196] H. Fan, G. Li, F. Yang, L. Yang, S. Zhang, Photodegradation of cellulose under UV light catalysed by TiO2, J. Chem. Technol. Biotechnol., 86 (2011) 1107-1112.

[197] K. Tanaka, R.C.R. Calanag, T. Hisanaga, Photocatalyzed degradation of lignin on TiO2, J. Mol. Catal. A: Chem., 138 (1999) 287-294.

[198] Y.-S. Ma, C.-N. Chang, Y.-P. Chiang, H.-F. Sung, A.C. Chao, Photocatalytic degradation of lignin using Pt/TiO_2 as the catalyst, Chemosphere, 71 (2008) 998-1004.

[199] S.K. Kansal, M. Singh, D. Sud, Studies on TiO_2/ZnO photocatalysed degradation of lignin, J. Hazard. Mater., 153 (2008) 412-417.

[200] E. Portjanskaja, S. Preis, Aqueous Photocatalytic Oxidation of Lignin: The Influence of Mineral Admixtures, Int. J. Photoenergy, 2007 (2007) 7.

[201] G. Corro, U. Pal, S. Cebada, Enhanced biogas production from coffee pulp through deligninocellulosic photocatalytic pretreatment, Energy Science & Engineering, 2 (2014) 177-187.

Chapter 2

Experimental

2.1 Chemicals

Table 2.1 List of chemicals used in this thesis and their supplier

Chemicals	Supplier
$AgNO_3$ (> 99%)	Sigma-Aldrich
$H_2PtCl_6 \cdot xH_2O$ (≥ 99.9%)	Sigma-Aldrich
$RuCl_3 \cdot xH_2O$ (99.98%)	Sigma-Aldrich
α-Cellulose	Sigma-Aldrich
Cellulose microcrystalline (Avicel® PH-101)	Sigma-Aldrich
Starch, soluble (ACS reagent)	Sigma-Aldrich
TiO_2, Aeroxide™ P25, ACROS Organics™	Fisher Scientific
Ethyl acetate (HPLC Grade)	Fisher Scientific
Tetrahydrofuran (HPLC Grade)	Fisher Scientific
Methanol (HPLC Grade)	Fisher Scientific
N,N-dimethylformamide (HPLC Grade), DMF	Fisher Scientific
Acetonitrile (HPLC Grade), ACN	Fisher Scientific
H_2SO_4 (> 95%)	Fisher Scientific
5-Keto-D-gluconic acid (98%)	Carbosynth
2-Keto-D-gluconic acid (98%)	Carbosynth
D-(-)-Arabinose (99%)	Alfa Aesar
D-(+)-Arabitol (99%)	Alfa Aesar
Nitrogen	BOC
Hydrogen	BOC
Oxygen	BOC
Carbon dioxide	BOC
Ultrapure water (Resistivity > 1MΩ.cm at 25°C)	Millipore Milli-DI®

Chemicals	Supplier
D-(+)-Glucose (≥ 99.5%, GC)	Sigma-Aldrich
D-(+)-Cellobiose (≥ 98%)	Sigma-Aldrich
D-Gluconic acid sodium salt (≥ 99%)	Sigma-Aldrich
Tartronic acid (≥ 97%)	Sigma-Aldrich
D-Sorbitol (≥ 98%)	Sigma-Aldrich
D-(-)-Fructose (≥ 99%)	Sigma-Aldrich
Formic acid (≥ 98%)	Sigma-Aldrich
Acetic acid (≥ 99%)	Sigma-Aldrich
DL-Glyceraldehyde (≥ 90%, GC)	Sigma-Aldrich
D-Saccharic acid potassium salt (≥ 98%)	Sigma-Aldrich
Glycolic acid (99%)	Sigma-Aldrich
D-(-)-Tartaric acid (99%)	Sigma-Aldrich
D-(+)-Gluconic acid δ-lactone	Sigma-Aldrich
D-(-)-Erythrose (≥ 75%)	Sigma-Aldrich
D-Mannitol (≥ 98%)	Sigma-Aldrich
Benzene-1,4-diboronic acid (≥ 95%)	Sigma-Aldrich
1,2,4,5-Tetrabromobenzene (97%)	Sigma-Aldrich
Tetrakis(triphenylphosphine)palladium(0) (99%), $Pd(PPh_3)$	Sigma-Aldrich
K_2CO_3 (99.9%)	Sigma-Aldrich
NaOH (≥ 98%)	Sigma-Aldrich
Na_2CO_3 (≥ 99.5%)	Sigma-Aldrich
Poly(2,6-dimethyl-1,4-phenylene oxide), (PPO)	Sigma-Aldrich
$NaBH_4$ (≥ 98%)	Sigma-Aldrich
Polyvinyl alcohol (M_w 9,000-10,000, 80% hydrolyzed), PVA	Sigma-Aldrich
Multi-walled carbon nanotubes (Lot #MKBT4011V)	Sigma-Aldrich
Ethanol (≥ 99.8%)	Sigma-Aldrich
$HAuCl_4 \cdot 3H_2O$ (≥ 99.9%)	Sigma-Aldrich

2.2 Definitions

$$\text{Conversion}\ (\%) = \frac{\text{Moles of substrate converted}}{\text{Initial moles of substrate}} * 100 \quad (2.1)$$

$$\text{Selectivity}_i(\%) = \frac{\text{Moles of product}_i}{\sum_{i=1}^{n} \text{Moles of product}_i} * 100 \quad (2.2)$$

$$\text{Yield}_i(\%) = \frac{\text{Moles of product}_i}{\text{Initial moles of substrate}} * 100 \quad (2.3)$$

$$\text{Carbon Mass Balance}\ (\%) = \frac{\text{Total moles of carbon detected}}{\text{Initial moles of carbon of substrate}} * 100 \quad (2.4)$$

$$\text{Turn Over Frequency (TOF)} = \frac{\text{Moles of substrate converted}}{\text{Total moles of metal x time}} \quad (2.5)$$

2.3 Synthesis of the Conjugated Microporous Polymer (CMP-1)

The conjugated microporous polymer (CMP-1) was prepared by the Suzuki–Miyaura polycondensation reaction [1]. The synthetic procedure followed the protocol reported by Sprick et al. [2]. In a typical synthesis, 829 mg of benzene-1,4-diboronic acid, 984 mg of 1,2,4,5-tetrabromobenzene, 15 mL of an aqueous solution of K_2CO_3 (2 M), 74 mL of N,N-dimethylformamide and 75 mg of $Pd(PPh_3)$ were charged in a two-neck flask (250 mL). Nitrogen was bubbled through the mixture for 30 minutes, and then the mixture was heated at 150 °C for 48 hours under reflux conditions. After the polycondensation reaction, a grey solid was formed and recovered by filtration (vacuum filtration), then it was washed with deionised water (250 mL) and methanol (250 mL). Subsequently, the solid was dried overnight under reduced pressure at 65 °C. The dried solid was then purified by Soxhlet extraction using tetrahydrofuran as a solvent for 48 hours under reflux conditions. After purification, the final solid was dried overnight under reduced pressure at 65 °C. Finally, the polymer was stored in a desiccator until further use. The CMP-1 structure can be found in Chapter 3, Section 3.2.1 (Scheme 3.1).

2.4 Catalyst preparation

2.4.1 Wet Impregnation Method (WI)

2.4.1.1 Synthesis of the Au/CMP-WI(ACN) and Au/PPO-WI(ACN) catalysts

An aqueous solution of the metal precursor ($HAuCl_4 \cdot 3H_2O$) was prepared by solubilising the appropriate amount of the metal salt in deionised water. Typically, 0.1 g of the support (CMP or PPO) was suspended in acetonitrile, 8 mL for CMP and 4 mL for PPO, in a vial under vigorous stirring for 12 hours in the absence of light (the vails were covered with aluminum foil to prevent degradation of the solvent). Subsequently, the appropriate volume of the metal solution was dropwise added, then the mixture was stirred at room temperature for 1 hour. The vial was placed in an oil bath at 70 °C until the solvent was evaporated. The final solid was dried overnight at 65 °C. Finally, the solid was treated under H_2 flow (50 mL min^{-1}) at 190 °C for 3 hours at 2 °C min^{-1}.

2.4.1.2 Synthesis of the TiO_2-supported noble metal catalysts

An aqueous solution of the appropriate metal precursor ($HAuCl_4 \cdot 3H_2O$ $H_2PtCl_6 \cdot xH_2O$, $AgNO_3$, $RuCl_3 \cdot xH_2O$) was prepared by solubilising the metal salt in deionised water. For the preparation of 0.5 g of a 1.5 wt% metal catalyst, the support (TiO_2-P25, Aeroxide^{TM}) was suspended in 4 mL of deionised water in a vial at room temperature under magnetic stirring. The appropriate volume of the metal solution was dropwise added, then the vial was heated using an oil bath at 80 °C until the solvent was evaporated. The solid was dried overnight at 110 °C under reduced pressure. In the case of the Au/TiO_2 and Ag/TiO_2 catalysts, they were calcined under static air at 400 °C for 3 hours at 2 °C min^{-1}. Prior to the reaction, the Pt/TiO_2 and Ru/TiO_2 catalysts were treated under H_2 flow (50 mL min^{-1}) at 400 °C for 4 hours with a heating rate of 2 °C min^{-1}.

2.4.2 Sol Immobilisation Method (SI)

2.4.2.1 Synthesis of the Au/CMP-SI, Au/PPO-SI, and Au/TiO_2-SI catalysts

The traditional sol immobilisation method was used to prepare the Au/CMP-SI, Au/PPO-SI, and Au/TiO_2-SI catalysts [3-5]. The gold catalysts with a metal loading of 2 wt% were prepared as follows: To an aqueous solution of the metal precursor ($HAuCl_4 \cdot 3H_2O$) of the desired concentration, the appropriate amount of PVA (1 wt%) was added (Au/PVA = 0.1 wt/wt) under vigorous stirring, then a freshly prepared solution of $NaBH_4$ (0.1 M) was added to form a red sol ($NaBH_4$/Au = 5 molar ratio). After 30 minutes of sol generation, the support (CMP-1, PPO, TiO_2) was added, and the mixture was acidified with H_2SO_4 to pH 1. After the immobilisation of the colloidal solution on the support (2 h), the slurry was filtered (vacuum filtration), and the obtained solid was washed with deionised water (2 L). The catalyst was dried overnight at 90 °C under reduced pressure. Finally, the catalyst was washed with water (250 mL) at 90 °C under reflux conditions and magnetic stirring (500 rpm) for 60 minutes [3], then it was dried overnight at 90 °C under reduced pressure.

2.4.3 Organic Solvent-Assisted Sol Immobilization (SASI)

2.4.3.1 Synthesis of the Au/CMP and Au/PPO catalysts using ACN and DMF as solvents

The organic solvent-assisted sol immobilisation method (SASI) was developed in order to prepare metal catalysts using conjugated microporous polymers (CMPs) as support. The SASI method consists of three separate steps: 1) Preparation of the pre-formed nanoparticles, 2) swelling of the polymer using an organic solvent under heat treatment, and 3) immobilisation of the colloid onto the support. Gold catalysts with a metal loading of 2 wt% were prepared as follows:

1) For the preparation of 0.4 g of a gold catalyst, the appropriate volume of the metal solution was added to 700 mL of deionised water under vigorous stirring (1100 rpm). Subsequently, 114 μL of an aqueous solution of PVA (1 wt%) was added to the mixture (Au/PVA = 0.1 wt/wt). Finally, a freshly prepared solution of $NaBH_4$ (0.1 M, 2.9 mL) was added to form a red sol ($NaBH_4$/Au = 5 molar ratio). The mixture was kept under stirring for 30 minutes.

2) The support (0.4 g, CMP or PPO) was suspended in 58 mL of an organic solvent (acetonitrile-ACN or N,N-dimethylformamide-DMF) under moderate stirring (400 rpm), then the mixture was heated at 90 °C under reflux conditions for 30 minutes.

3) Finally, the aqueous colloidal solution prepared in the step 1 was immobilized onto the swollen polymer (step 2) and the mixture was kept at 90 °C under vigorous stirring (1000 rpm) at reflux conditions for 2 hours. After the immobilisation of the colloid onto the support, the slurry was filtered (vacuum filtration) and the obtained solid was washed with dionised water (1 L). The solid was dried overnight at 60 °C under reduced pressure. The final solid was stored in a desiccator in the absence of light until further use. The SASI method was used to prepare the Au/CMP-SASI(DMF-W), Au/CMP-SASI(ACN-W), Au/PPO-SASI(DMF-W), and Au/PPO-SASI(ACN-W) catalysts.

2.4.3.2 Synthesis of the Au/CNTs catalyst

Multi-walled carbon nanotubes (CNTs) were used as a support for the immobilization of gold nanoparticles using the organic solvent-assisted sol immobilisation method (SASI) developed in the previous section. The synthetic procedure consists of the three steps mentioned in section 2.4.3.1, but an additional one was required for the preparation of the catalyst. Prior to the thermal treatment under reflux conditions (step 2), the CNTs (0.4 g) were sonicated in ethanol (58 mL) for 1 hour at room temperature in order to improve their dispersion in the liquid medium as reported in the literature [6-8]. After sonication in ethanol, the synthesis was carried out in the same manner as described in section 2.4.3.1.

2.5 Catalyst Recycling

Recycling tests for the Au/CMP-SASI(ACN-W) catalyst were performed using a pyramidal scheme as reported by Da Vià et al. [9]. The experiments were carried out at 130^0C and 10 bar of oxygen pressure using a SynthWAVE microwave reactor. In all cases, 50 mg of the catalyst was added to 5 mL of a glucose aqueous solution in a 40 mL glass vial. After the reaction, the catalyst was filtered (vacuum filtration) and washed with deionised water (400 mL), then it was dried overnight under reduced pressure at 110 °C. For the recycling tests, the first set of experiments were performed by running three simultaneous reactions, then the recovered catalyst was treated as mentioned above, and then it was used for two simultaneous reactions. After the second test, the catalyst was treated following the same procedure, and finally, it was used for one reaction.

2.6 Mechanical Treatment

Microcrystalline cellulose (Avicel® PH-101) and α-Cellulose were ball-milled in order to reduce their crystallinity and improves the catalyst performance. The samples (2.5 g) were separately pulverized with 18 ZrO_2 balls (10 mm) in a 45 mL grinding bowl (ZrO_2) for 48 hours at 600 rpm using a Planetary Micro Mill (Fritsch GmbH, PULVERISETTE 7 premium line). After the treatment, the samples were stored in a desiccator until further use.

2.7 Catalyst Characterization

2.7.1 X-Ray Diffraction (XRD)

X-ray diffraction measurements were carried out using a Panalytical X'Pert PRO HTS X-ray diffractometer using a Cu-Kα radiation (λ= 1.54Å) in the 2θ range of 4–90°. In all cases, the samples were ground to fine powder in an agate mortar before the analysis. The samples were analysed at the Centre of Materials Discovery (CMD) in the Chemistry Department, University of Liverpool, UK.

2.7.2 Transmission Electron Microscopy (TEM)

Transmission electron microscopy analysis was carried out using a JEOL JEM-2100F microscope operated at 200 kV. Samples were dispersed in ethanol under sonication and then deposited on a holey carbon coated 300 mesh copper grid (TAAB Laboratories Equipment Ltd). TEM analysis was performed at the Imaging Centre at Liverpool (ICal), University of Liverpool, UK.

2.7.3 UV-Vis Spectroscopy

UV-Vis analysis was carried out using a Thermo Scientific™ Evolution™ 220 spectrophotometer. Colloidal solutions were analysed in a 10 mm quartz cuvette in the range of 200-800 nm in order to confirm the presence of metal nanoparticles. Deionised water was used for the reference cuvette.

The solid catalysts were characterized by diffuse reflectance UV-Vis spectroscopy using a Thermo Scientific™ Evolution™ 220 spectrophotometer equipped with an ISA-220 Integrating Sphere (Thermo Scientific™) in the range of 200-800 nm. The baseline was calibrated using a PTFE reference disk. Prior to the analysis, the samples were finely ground in an agate mortar.

2.7.4 Infrared Spectroscopy

ATR-FTIR measurements were carried out using a Perkin Elmer Spectrum 100 Series FTIR spectrometer equipped with an attenuated total reflectance (ATR) accessory. Prior to the analysis, the solid samples were finely ground in an agate mortar. ATR-FTIR spectra were collected in the range of 4000-600 cm^{-1} with 32 scans per sample with a spectral resolution of 4 cm^{-1}.

2.7.5 Surface Area Measurements

The surface area was measured by nitrogen sorption using a Quantachrome NOVA 4200e gas sorption analyzer at 77 K. The Brunauer-Emmett-Teller (BET) equation was used to determine the surface area of the CMP support by 5 point measurements in the range of $0.05 < p/p_0 < 0.3$, where p and p_0 represent the equilibrium pressure and the saturation pressure of the adsorbate at the adsorption temperature respectively. Prior to the analysis, the sample (50 mg) was degassed overnight under vacuum at 150 °C.

2.7.6 Inductively Coupled Plasma – Optical Emission Spectrometry (ICP-OES)

ICP-OES analysis was performed by Mr. Stephen Moss at the Analytical Services in the Chemistry Department (University of Liverpool) using an Agilent 5110 ICP-OES spectrometer with SVDV detection. Prior to the analysis, the catalyst (10 mg) was suspended in aqua regia (nitric acid and hydrochloric acid in a molar ratio of 1:3) for digestion (2 mL), and then the mixture was treated under microwave conditions (15 W, 800 rpm) for 30 minutes. Subsequently, 0.5 mL of the mixture was diluted with 9.5 mL of deionised water. Finally, the samples were submitted by the author for analysis. Each sample was analysed in triplicate.

2.7.7 CHN Elemental Analysis

CHN analysis was performed by Mrs. Jean Ellis at the Analytical Services in the Chemistry Department (University of Liverpool) using a Thermo Scientific FlashEA^{TM} 1112 Series CHN Analyzer.

2.7.8 X-ray Photoelectron Spectroscopy (XPS)

XPS analysis was performed by Dr. Mark A. Isaacs at the Research Complex at Harwell (RCaH) using a Kratos SUPRA XPS fitted with a monochromated Al Kα X-ray source (1486.69 eV) and an electron flood gun. Samples were affixed to a glass microscope slide to ensure full electrical isolation from the system. Samples entered the analysis chamber at a pressure below 1 x 10^{-8} Torr. The XPS spectra were processed using the CasaXPS Version 2.1.34 software.

2.8 Product Analysis

2.8.1 High-Performance Liquid Chromatography (HPLC)

The reaction products were analysed using an Agilent Technologies 1200 Infinity HPLC equipped with a photodiode array detector (DAD) and a refractive index detector (RID). An Aminex HPX-87H column (300 x 7.8 mm) was used to separate the obtained products using a sulfuric acid aqueous solution of 25mM as a mobile phase with a flow rate of 0.65 mL min^{-1}. The retention times of the obtained products were compared to the known standards in order to confirm their presence in the reaction mixture. Calibration curves were used for the quantification of products and reactants after the reaction. The standard solutions were prepared by solubilising the appropriate amount of the compound in water at concentrations of 40, 30, 20, 10, 5, 1 and 0.5 mM. Table 2.2 shows the detection method and the retention times of the compounds used. However, some of these compounds were not observed under reaction conditions.

Table 2.2 Retention times and detection method for the compounds used in the HPLC analysis.

Compound	Detector	Retention time / min
Cellobiose	RID	6.9
Glucaric acid	DAD	7.2
2-Keto-Gluconic acid	DAD	7.72
5-Keto-Gluconic acid	DAD	7.86
Tartronic acid	DAD	7.97
Tartaric acid	DAD	8.16
D-(+)-Gluconic acid δ-lactone	DAD	8.18
Gluconic acid	DAD	8.21
Glucose	RID	8.5
Fructose	RID	9.3
Mannitol	RID	9.53
Sorbitol	RID	9.68
Arabinose	RID	10.1
Arabitol	RID	10.3
DL-Glyceraldehyde	RID	10.6
D-Erythrose	RID	10.8
Glycolic acid	RID	11.5
Formic acid	DAD	13.1
Acetic acid	DAD	14.2

2.8.2 Gas Chromatography

Gas phase products (H_2 and CO_2) were collected using a Tedlar® PLV Gas Sampling Bag (Sigma-Aldrich) and quantified using an Agilent Technologies 7890A Gas Chromatograph System equipped with a thermal conductivity detector (TCD). The product analysis was carried out using a Carboxen®-1010 PLOT capillary column (30 m x 0.53 mm, 30 μm, Sigma-Aldrich). The injection port was set at 280 °C with a split of 30:1. For the analysis of the gas phase products, the initial oven temperature was set at 40 °C and held for 1 minute, then the temperature was increased from 40 to 250 °C with a heating rate of 20 °C min^{-1} and held for 15 minutes. Calibration curves were prepared using 5 % hydrogen in nitrogen (BOC) and 9.6 % carbon dioxide in helium (BOC). The retention times and the formulas used to determine the amount of hydrogen and carbon dioxide are shown in Table 2.3.

Table 2.3 Retention time and calibration curves of the gases used in this work.

Compound	Retention time / min	Equation
Hydrogen (H_2)	1.1	y = 5E+09x + 362.02
Carbon dioxide (CO_2)	9.5	y = 1E+09x + 17.77

2.9 Description of Experimental Setup

2.9.1 Photocatalysis

Photocatalytic experiments were carried out using three different systems: a Luzchem Photoreactor, a 300 W Xenon Oriel Arc Lamp and a Parr Stirred Photo-reactor illuminated by a 1000 W Xenon Oriel Arc Lamp. These systems were used to perform the experiments described in Chapters 4 and 5.

2.9.1.1 Luzchem Photoreactor

Photocatalytic experiments under both UVA and visible light were carried out using a Luzchem Photoreactor (Mod. LZC-4, Luzchem Research Inc., CAN) equipped with 16 lamps for a total power of 128 W (Figure 2.1). The reactor consists of 8 top and 8 side lamps, which can be controlled independently. An internal temperature controller (FuzyPro 1/6 DIN, HCS Ltd, CAN) can be used to perform reactions from room temperature to 45 °C.

Figure 2.1 Luzchem Photoreactor equipped with 16 UVA lamps, typical experimental setup.

2.9.1.2 Photoreactor – 300 W Xenon Lamp

A 300 W Xenon oriel arc lamp (Mod. 6258, Newport, UK) controlled by a power supply (Mod. 69911 Newport, UK) was used to replicate the natural sunlight in the photocatalytic experiments (Figure 2.2). Due to its sun-like spectrum (Figure 2.3), the lamp was equipped with a UV filter with a cut-off value of 420 nm (Mod.FSQ-GG420) and a water filter to remove the infrared radiation (Mod.61945) and avoid overheating of the reaction mixture.

Figure 2.2 Typical experimental setup used for the 300 W Xenon lamp.

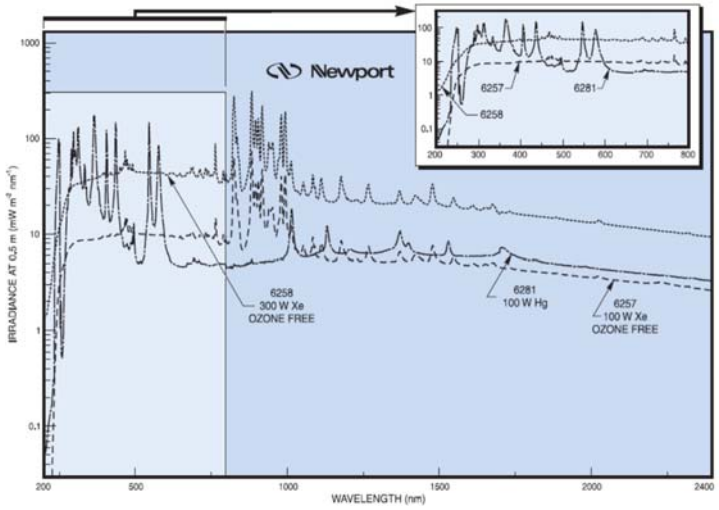

Figure 2.3 Spectral irradiance of the 300 W Xenon arc lamp [10].

2.9.1.3 Pressurized Photoreactor – 1000 W Xenon Lamp

Photocatalytic experiments at high-pressure conditions were carried out using a windowed Parr Micro Stirred Reactor (Mod. 4950, Parr Instrument Company, Illinois, USA) equipped with a Parr 4848 reactor controller (Figure 2.4). The reactor was irradiated at a 90^{o} angle through a sapphire oblong window using a 1000W Xenon oriel arc lamp (Mod. 6271, Newport, UK) as the light source (Figure 2.5). The lamp was equipped with a UV filter with a cut-off value of 420 nm (Mod.FSQ-GG420) and a water filter (Mod. 6123NS) to remove the infrared region and avoid overheating of the reaction mixture.

Figure 2.4 Experimental setup used for the 1000 W Xe lamp and the windowed Parr Stirred Reactor.

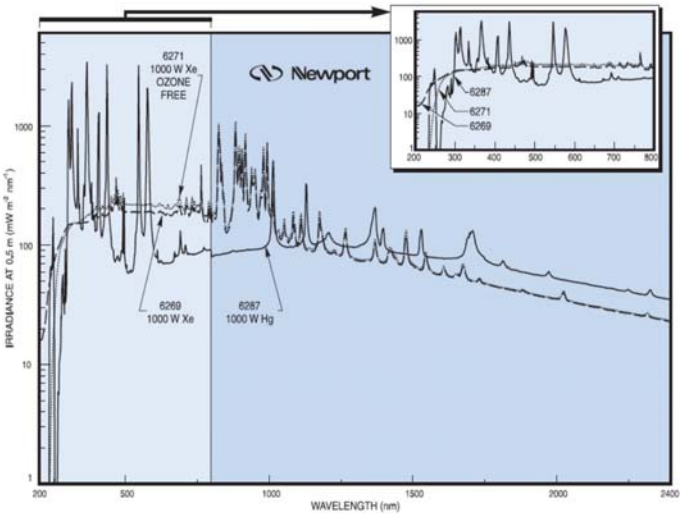

Figure 2.5 Spectral irradiance of the 1000 W Xenon arc lamp [10].

2.9.2 Microwave Assisted Heating

2.9.2.1 Catalytic Studies Under Microwave Conditions

Microwave technology has emerged as a green alternative route for a wide range of applications such as organic synthesis, sintering processes and heterogeneous catalysis [11-13]. The microwave heating process implies the conversion of electromagnetic energy to heat as a result of the combination of the dielectric properties of the irradiated material and the electromagnetic field applied [14]. Some advantages of microwave irradiation include fast heating, non-contact heating, efficient energy transfer and automation of the process among others [15].

In this work, catalytic experiments were carried out using a CEM Discover® SP microwave reactor equipped with a gas addition accessory (Mod. 908255, CEM Corporation, NC, USA). The experiments were performed using a 10 mL reaction vessel equipped with a fiber optic temperature probe mounted inside a quartz thermowell. This system was used for the catalytic studies on the glucose oxidation reaction described in Chapter 3 (Figure 2.6).

Figure 2.6 Image of the CEM Discover® SP microwave reactor used for the glucose oxidation reaction.

2.9.2.2 Catalyst Recycling under Microwave Conditions

Recycling tests for the Au/CMP-SASI(ACN-W) catalyst were carried out using a SynthWAVE microwave reactor (Milestone Srl, Italy) equipped with a recirculating chiller (Figure 2.7). The reactor allows performing one or multiple reactions at high temperature and pressure. For the recycling tests, the first set of experiments were performed by running three simultaneous reactions, then the recovered catalyst was used for two simultaneous reactions. Finally, the catalyst recovered from the second test was used for one reaction. The catalysts used during the second and third test were washed and dried before the reaction as described in section 2.5. The reactions were performed using a 40 mL glass vials fitted with a polytetrafluoroethylene (PTFE) cap which allows pressure equalization. The reaction conditions for the recycling tests were similar to ones for the CEM Discover® SP microwave reactor, 130 °C and 10 bar oxygen pressure.

Figure 2.7 Image of the SynthWAVE microwave reactor used for the recycling tests.

2.10 Catalyst Evaluation

2.10.1 Glucose Oxidation under Microwave Conditions

A 10 mL glass vial was charged with a glucose aqueous solution (55.5 mM, 2mL) and catalyst (substrate/metal = 438 molar ratio). The vial was sealed, pressurized (10 bar N_2) and purged three times, then it was pressurized with molecular oxygen at 10 bar. Finally, the vial was heated at 130 °C for 30 minutes under microwave conditions (70 W, 800 rpm). Samples were taken at fixed intervals, and the liquid products were separated from the catalyst using a PTFE filter (GILSON®, 0.22 μm) and quantified using HPLC analysis.

2.10.2 Glucose Photo-oxidation at Atmospheric Pressure With and Without Base

In a typical test, a 16 mL glass vial was charged with 14 mL of a glucose aqueous solution (20 mM or 1 mM) and 30 mg of the catalyst. The mixture was stirred at 700 rpm throughout the experiment, and it was irradiated at a constant distance by the 300 W Xenon lamp. In the case of the experiments performed using the Luzchem photoreactor, the vial was placed inside the chamber. In both cases, the system was allowed to reach equilibrium for 10 minutes in the absence of light before reaction. For the experiments under alkaline conditions, the base was added at the beginning of the reaction (substrate/base = 1:1 molar ratio). Samples were taken at fixed intervals, and the liquid products were separated from the catalyst using a PTFE filter (GILSON®, 0.22 μm) and quantified using HPLC analysis.

2.10.3 Glucose Photo-oxidation under Alkaline Medium at High-Pressure Conditions

A 100 mL glass liner was charged with 40 mL of a glucose aqueous solution (400 mM), Na_2CO_3 (substrate/base = 1:1 molar ratio) and 90 mg of the catalyst. The liner was placed inside the high-pressure reactor, and then the reactor was sealed. The system was pressurized (10 bar N_2) and purged three times, then it was

pressurized to the desired value with O_2. The reaction mixture was stirred at 500 rpm and heated from room temperature to 40 °C using a Parr 4848 reactor controller. The system was allowed to reach equilibrium for 10 minutes in the absence of light before reaction. Samples were taken at fixed intervals, and the liquid products were separated from the catalyst using a PTFE filter (GILSON®, 0.22 μm). The liquid samples were diluted 20 fold in water and analysed by HPLC.

2.10.4 Photocatalytic Conversion of Polysaccharides at High-Pressure Conditions With and Without Base.

A 100 glass liner was charged with 40 mL of deionised water, the substrate (50 mg or 150 mg), and catalyst (42 mg or 90 mg). The liner was placed inside the high-pressure reactor, and then the reactor was sealed. The system was pressurized (10 bar N_2) and purged three times with nitrogen, then it was pressurized to the desired value with O_2 or H_2. The reaction mixture was stirred at 500 rpm and heat from room temperature to 40 °C using a Parr 4848 reactor controller. Then, the system was allowed to reach equilibrium for 10 minutes in the absence of light before reaction. For the experiments under alkaline conditions, the based was added at the beginning of the reaction with a substrate/base = 1:1 molar ratio. Samples were taken at fixed intervals, and the liquid products were separated from the catalyst using a PTFE filter (GILSON®, 0.22 μm) and quantified using HPLC analysis.

2.11 References

[1] W. Huang, L. Su, Z. Bo, Hyperbranched Polymers with a Degree of Branching of 100% Prepared by Catalyst Transfer Suzuki−Miyaura Polycondensation, J. Am. Chem. Soc., 131 (2009) 10348-10349.

[2] R.S. Sprick, J.-X. Jiang, B. Bonillo, S. Ren, T. Ratvijitvech, P. Guiglion, M.A. Zwijnenburg, D.J. Adams, A.I. Cooper, Tunable Organic Photocatalysts for Visible-Light-Driven Hydrogen Evolution, J. Am. Chem. Soc., 137 (2015) 3265-3270.

[3] J.A. Lopez-Sanchez, N. Dimitratos, C. Hammond, G.L. Brett, L. Kesavan, S. White, P. Miedziak, R. Tiruvalam, R.L. Jenkins, A.F. Carley, D. Knight, C.J. Kiely, G.J. Hutchings, Facile removal of stabilizer-ligands from supported gold nanoparticles, Nat. Chem., 3 (2011) 551.

[4] A. Villa, D. Wang, G.M. Veith, F. Vindigni, L. Prati, Sol immobilization technique: a delicate balance between activity, selectivity and stability of gold catalysts, Catal. Sci. Technol., 3 (2013) 3036-3041.

[5] M. Comotti, W.-C. Li, B. Spliethoff, F. Schüth, Support Effect in High Activity Gold Catalysts for CO Oxidation, J. Am. Chem. Soc., 128 (2006) 917-924.

[6] Y. Yu, J.C. Yu, J.-G. Yu, Y.-C. Kwok, Y.-K. Che, J.-C. Zhao, L. Ding, W.-K. Ge, P.-K. Wong, Enhancement of photocatalytic activity of mesoporous TiO_2 by using carbon nanotubes, Appl. Catal. A: Gen., 289 (2005) 186-196.

[7] W. Wang, P. Serp, P. Kalck, J.L. Faria, Photocatalytic degradation of phenol on MWNT and titania composite catalysts prepared by a modified sol–gel method, Appl. Catal. B: Environ., 56 (2005) 305-312.

[8] Y. Luo, J. Liu, X. Xia, X. Li, T. Fang, S. Li, Q. Ren, J. Li, Z. Jia, Fabrication and characterization of TiO2/short MWNTs with enhanced photocatalytic activity, Mater. Lett., 61 (2007) 2467-2472.

[9] L. Da Vià, C. Recchi, T.E. Davies, N. Greeves, J.A. Lopez-Sanchez, Visible-Light-Controlled Oxidation of Glucose using Titania-Supported Silver Photocatalysts, ChemCatChem, 8 (2016) 3475-3483.

[10]https://www.newport.com/medias/sys_master/images/images/hfb/hdf/8797196451870/Light-Sources.pdf.

[11] C.O. Kappe, Controlled Microwave Heating in Modern Organic Synthesis, Angew. Chem. Int. Ed., 43 (2004) 6250-6284.

[12] M. Oghbaei, O. Mirzaee, Microwave versus conventional sintering: A review of fundamentals, advantages and applications, J. Alloys Comp., 494 (2010) 175-189.

[13] A. Kokel, C. Schäfer, B. Török, Application of microwave-assisted heterogeneous catalysis in sustainable synthesis design, Green Chem., 19 (2017) 3729-3751.

[14] E.T. Thostenson, T.W. Chou, Microwave processing: fundamentals and applications, Compos. Part A Appl. Sci. Manuf., 30 (1999) 1055-1071.

[15] D. Bogdal, S. Bednarz, K. Matras-Postolek, Microwave-Assisted Polymerization, Reference Module in Materials Science and Materials Engineering, Elsevier(2017).

Chapter 3

Development of Gold Catalysts on Polymeric Supports for the Glucose Oxidation: The Organic Solvent-assisted Sol Immobilisation (SASI) Method

3.1 Introduction

The sol-immobilization method (SI) is a widely used synthetic route to prepare supported-metal catalysts for catalytic applications [1-3]. The SI technique in comparison with traditional methods (*e.g., impregnation*) for catalyst synthesis, offers the possibility of controlling the particle size, shape and metal dispersion independently of the material used as support [1-7]. Typically, SI [1] implies the preparation of metal nanoparticles formed after the reduction of a metal precursor dissolved in water with a reducing agent in the presence of a stabilizer. Then in a second step, the pre-formed nanoparticles (the colloid) are immobilized on the support. The use of a reducing agent during the preparation of the colloid is beneficial to the entire system since it prevents additional catalyst reduction and changes in the material's properties. On the other hand, the use of a stabilizer can limit the catalytic activity by blocking actives metal sites [8-11] in some circumstances, but in other cases, its presence is required to avoid an increase in particle size [11, 12] or even necessary to make the metal nanoparticles more compatible in different environments by adding functionalities on the particle surface [13]. Therefore, the stabilizer plays an important role as protective agent for the metal nanoparticles and its removal should not compromise the catalytic activity of the final material.

To overcome this problem, the removal of the stabilizer from the metal nanoparticles surface has been addressed by different approaches such as thermal treatment under oxidative or inert atmosphere at elevated temperatures [14, 15], UV irradiation in presence of ozone [16-18], oxygen plasma treatment [19], and solvent washing [1, 11, 20]. Although these techniques could be useful to remove, partially or completely, the stabilizer from the nanoparticles surface, slight modifications in particle size, shape and distribution cannot be avoided [9]. Therefore, the use of the SI technique for the preparation of supported-metal catalysts is not a straightforward procedure, but its main advantage among other synthetic routes is that the nanoparticles formation is not affected by the support material [8].

Given that SI technique has shown superior control on the nanoparticles formation, model catalysts can be prepared to evaluate different parameters affecting the catalytic activity without considering the support effects. In particular for gold-based catalysts, supports such as metal oxides (e.g., TiO_2, ZrO_2) [1, 8, 11], silica [21-23] and activated carbon [5, 9, 24] are the most employed supports in the immobilization of gold nanoparticles. Although the aforementioned materials have shown good performance as supports for gold nanoparticles, several disadvantages have been observed during their application. For example, leaching of metal and increase in particle size were observed when gold on carbon was used under alkaline conditions [5], sintering during the activation of the catalyst and weak metal-support interaction are the main drawbacks associated to silica-based supports [25-28], and the support effect on the catalytic activity of gold nanoparticles for metal oxides [8, 29-32]. Therefore, it is clear that there is no "*universal"* support which could solve the above issues, but it would be desirable to find one that potentially minimize their impact on the catalytic activity of the gold nanoparticles. The search for new suitable supports able to enhance catalytic performance is therefore desirable.

A new class of porous organic materials, namely conjugated microporous polymers (CMPs) have emerged as promising supports where metal nanoparticles can be confined into the pores, thus providing good control of particle size as well as reducing particle aggregation [33-35]. CMPs can be composed of carbon-carbon and carbon-hydrogen bonds as well as nitrogen-rich pyridine units, and due to their organic structure, it is possible to introduce different chemical functionalities into the

network while conventional microporous materials such as zeolites and activated carbons do not allow it [36]. Hence, the use of microporous organic materials of tunable porosity such as CMPs could be advantageous for gold catalysis, since they offer potential for control of particle size which is important for gold nanoparticles due to their size-dependent catalytic activity. However, suitable preparation methods need to be devised.

To date, the impregnation method (by using supercritical CO_2 as a solvent or conventional synthesis with ethanol) [33, 35] and the polymer-encapsulated metal nanoparticles synthesis [34] have been reported as synthetic routes to deposit metal nanoparticles in CMPs. However, these techniques present some disadvantages, for example, the use of supercritical fluids requires high pressures [37], the conventional impregnation does not allow control of particle size as well as produce less active catalysts [38], and the encapsulation of metal nanoparticles is limited by the amount of metal entrapped into the polymeric matrix. Although there has been progress in the preparation of microporous polymer-based catalysts, the number of studies is limited, thus there is a necessity to develop new synthetic routes that produce more robust catalysts and fully exploited the intrinsic microporosity of the CMPs.

Schmidt et al. [35] reported that palladium nanoparticles can be deposited into CMPs networks by conventional impregnation with metal loadings up to 15 wt%. The catalysts were tested for the hydrogenation of diphenylacetylene to 1,2-diphenylethane with total conversion after 2 hours. The authors suggested that the accessibility of the metal nanoparticles within the polymeric network was responsible for the catalytic activity. Similarly, Pd catalysts were prepared by impregnation, however, supercritical CO_2 was used as solvent at pressures ranging from 7.38 to 28 MPa, producing palladium nanoparticles located at the surface (~5–10 nm) and within (~1–3 nm) the polymer as reported by Hasell et al. [33]. Unfortunately, the samples were not used in catalysis and the investigation was limited to the hydrogen sorption. A more detailed analysis of Pd catalysts using CMPs as support was reported by Ishida et al. [34]. The catalysts were prepared using the $Pd(PPh_3)_4$ complex which is typically used for the polymerization as the metal precursor to produce palladium nanoparticles within the polymeric network after thermal tratment with nitrogen (Pd/CMP-1-N_2) or hydrogen (Pd/CMP-1-H_2)

gas. The prepared catalysts were tested for the hydrogenation of 4-nitrostyrene to 4-ethylnitrobenzene where the Pd/CMP-1-H_2 catalysts showed conversion values of 99% and selectivity of 99% to the desired product. To further investigate the effect of functional groups on the CMP network during catalysis, hydroxyl groups were added by changing the monomer during the polymerization step. The Pd catalysts with (Pd/CMP-OH-H_2) and without (Pd/CMP-1-N_2, Pd/CMP-1-H_2) hydroxyl groups were tested for the hydrogenation of N-benzylideneaniline and oxidation of benzyl alcohol. The catalytic results showed that the catalysts with and without hydroxyl groups were active for the hydrogenation reaction. However, the oxidation of benzyl alcohol was improved by the addition of OH groups into the CMP network with a 73% yield of benzaldehyde compared to 34% for the catalysts without hydroxyl groups. Therefore, it is clear that the catalytic results demonstrate that the CMPs networks can serve as supports for the metal nanoparticles. Nevertheless, it is important that future studies will be directed to improve understanding of the metal-support interactions and their effect on the catalytic activity.

In the present chapter, we report for the first time a novel synthetic route to deposit metal nanoparticles onto microporous organic polymers and demonstrate their catalytic activity. The new route involves the preparation of colloidal sols and their immobilization on the support which was previously treated with an organic solvent (e.g., acetonitrile-ACN or dimethylformamide-DMF) under thermal conditions. The CMP-1 network [39] was used as support for the gold nanoparticles to produce the Au/CMP catalyst. For comparison, poly(2,6-dimethyl-1,4-phenylene oxide) (PPO), a commercial polymer, was used as support for the first time to produce the Au/PPO catalyst. In addition, the traditional sol-immobilisation and impregnation methods were used to prepare gold catalysts using the CMP and PPO supports, then the catalysts were compared with the organic solvent-assisted sol-immobilisation method. The bare supports and gold catalysts were characterized using different techniques such as TEM, XPS, XRD, Solid UV-Vis, ICP-OES, BET, CHN elemental analysis and FTIR. The gold catalysts were tested in the oxidation of glucose to gluconic acid using microwave assisted heating.

3.2 Results and discussion

In the early stages of the investigation, the CMP-1 network could be obtained from the Cooper group (Prof A. I. Cooper FRS, University of Liverpool, UK), however, we decided to carry out the synthesis of the polymer in our laboratory. The main aim was to have control over the synthetic procedure, and then integrated it with the preparation of the gold catalysts. Therefore, it was crucial that we got involved in the synthesis of the polymeric material. In the present work, we prepared 40 batches of the CMP network which were used for the preparation of the catalysts and characterization tests.

3.2.1 Synthesis and characterization of the CMP network

The conjugated microporous polymer CMP was prepared by the Suzuki—Miyaura polycondensation reaction [40] (Scheme 3.1) according to the protocol reported by Sprick et al [39]. Briefly, a two neck flask (250 mL) was charged with the following reagents under nitrogen flow: 1,4-benzene diboronic acid (BDBA) (829 mg, 5 mmol), 1,2,4,5-tetrabromobenzene (TBB) (984 mg, 2.5 mmol), K_2CO_3 (15 mL of 2M aqueous solution), dimethylformamide (75 mL) and $Pd(PPh_3)$ (75 mg, $6.49x10^{-2}$ mmol). Nitrogen was bubbled through the mixture for 30 minutes and then the mixture was heated at 150 °C for 48 hours.

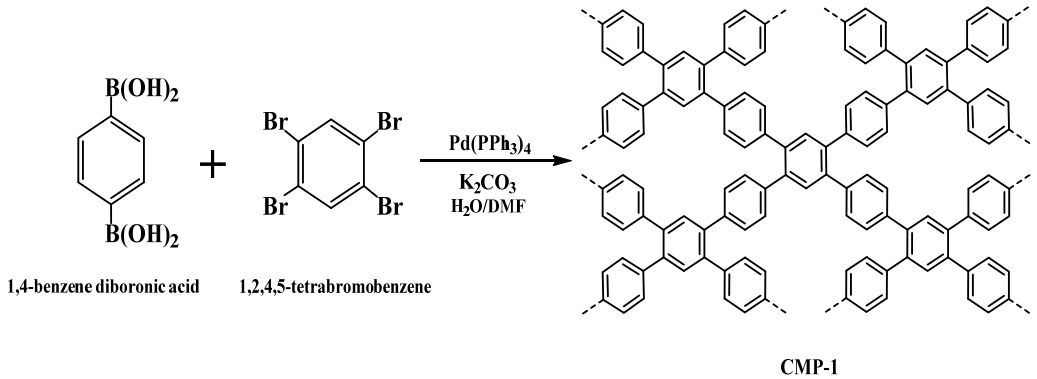

Scheme 3.1 Suzuki—Miyaura polycondensation reaction.

As a result, a grey solid was recovered by filtration (Figure 3.1), washed with water and methanol, and purified by Soxhlet extraction using tetrahydrofuran as solvent for 48 hours. After purification, the solid was dried overnight under reduced pressure, and stored in a desiccator until further use. The obtained polymer for each synthesis was about 500–600 mg. The CMP network was characterized with CHN elemental analysis, FTIR, XRD, ICP-OES, N_2 sorption and solid UV-Vis.

Figure 3.1 Solid CMP network (sample 32) prepared by the Suzuki—Miyaura polycondensation reaction.

To confirm the reproducibility of the as-prepared polymer during the synthesis, three separate batches were analysed by CHN elemental analysis and ICP-OES to determine the carbon, hydrogen and palladium content in the prepared samples. The results in Table 3.1 shows that a sample typically could consist of 88.6 wt% carbon, 4.6 wt% hydrogen and 1.2 wt% palladium. The obtained results are in good agreement with the reported values [39] and the standard deviation among the samples is less than 1% which is a good indicative of the reproducibility of the synthesis and the obtained material.

Table 3.1 Total carbon and hydrogen content measured by CHN elemental analysis, and palladium content measured by ICP-OES.[a]

Sample	C (%)	H (%)	Pd (%)
CMP	88.66±0.84	4.68±0.06	1.25±0.33

[a]Values represent the mean of three measurements ± SD (n = 3).

The nitrogen adsorption isotherm of the CMP (Figure 3.2a) suggest a type I isotherm according to the IUPAC classification that indicates the presence of microporosity (pores < 2 nm) [41]. The surface area of the CMP was calculated by using the Brunauer-Emmett-Teller method (BET), obtaining 671 m²/g which was similar to the reported value of 683 m²/g [42]. The powder X-ray diffraction analysis (Figure 3.2b) shows that the material is completely amorphous in agreement with previous reports [39].

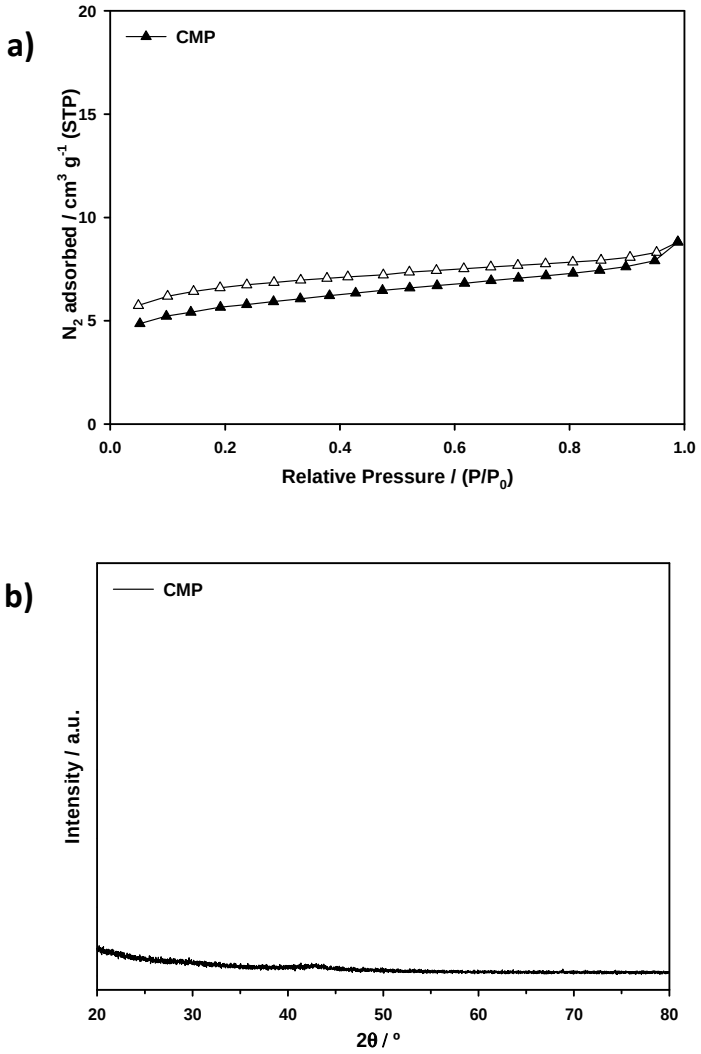

Figure 3.2 Nitrogen sorption isotherm (a, open symbol indicates desorption isotherm) and powder X-ray diffraction pattern (b) for the CMP network (sample 32).

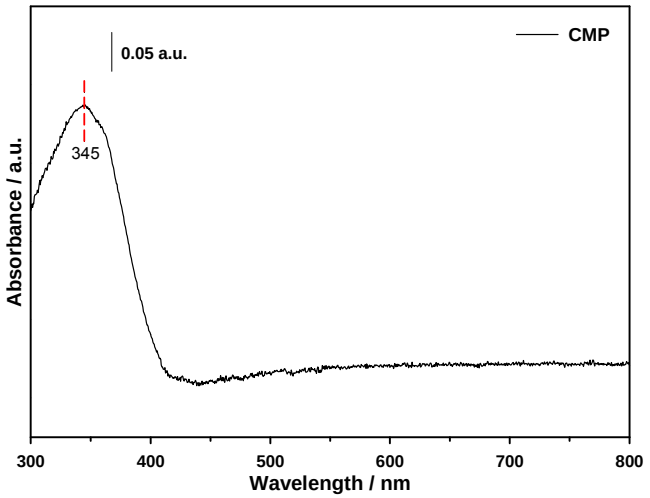

Figure 3.3 Solid UV-Vis spectrum of the CMP network (sample 32).

The solid UV-Vis spectrum of the polymer is displayed in Figure 3.3 where a strong absorption band is observed at 345nm in the UV region. This result is consistent with the literature since organic polymers with conjugated π-electrons such as linear poly(*p*-phenylene) have shown band gaps from 2 to 5 eV which correspond to light absorption in the UV range [39, 43].

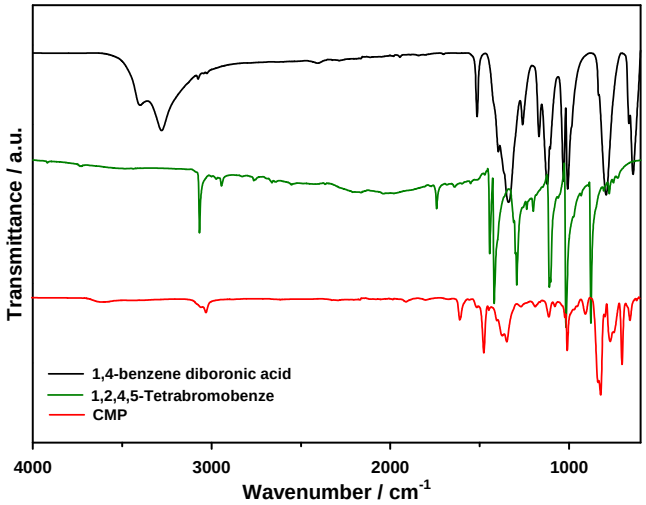

Figure 3.4 FT-IR spectra of the CMP network (sample 32) and the monomers (BDBA and TBB)

The FTIR analysis of the CMP network is displayed in Figure 3.4 and the absorption bands are reported in Table 3.2. The IR spectrum shows absorption bands of the C-H, B-O, C-Br and aromatic C-H bonds from the BDBA and TBB monomers as well as bands assigned to the C=C bond in aromatics (1604 cm^{-1}) and substituted

phenyl rings (1474 cm^{-1}). The band at 1187 cm^{-1} corresponds to the C-H in-plane bending bonds in the polymeric network, whereas the O-H stretch bond is observed as a weak band at 3647 cm^{-1} that has been assigned to the $B(OH)_2$ group from the monomer BDBA [44]. In conclusion, the experimental results showed that the CMP-1 network was successfully synthesized in this work and its application in heterogeneous catalysis will be discussed in the following sections.

Table 3.2 IR absorption frequencies of the CMP-1 network

Absorption bands (cm^{-1})			
[44]	**This work**	**Assignments**	**Monomer**
3645	3647	ν(O-H)	BDBA
3027, 2952	3031, 2952	Aromatic ν(C-H)	BDBA, TBB
1600	1604	Aromatic ν(C=C)	
1472	1474	ν(C=C)[a]	
1372	1370	ν(B-O)	BDBA
1185	1187	δ(C-H)	
1005	1006	ν(C-Br)	TBB
834	835	ν(C-H)[b]	BDBA
768, 746, 697	767, 745, 696	ν(C-H)[c]	TBB

[a]Vibrational modes of the substituted phenyl rings.
[b]Bending modes of the di-substituted, and [c]tetra-substituted phenyl rings.

3.2.2 Synthesis of the Au/CMP and Au/PPO catalysts by the WI, SI and SASI methods

Gold catalysts have been widely investigated in the catalysis field due to their remarkable activity and selectivity for many reactions [45], but since the early reports on the oxidation of carbon monoxide showed that the catalytic activity can be affected by the synthesis method and support used [46, 47], a lot effort has been made to improve understanding in the preparation method and its effect on the catalytic activity in gold catalysts. Therefore, the aim of this section is to provide an efficient route for the preparation of gold catalysts using microporous polymers as supports which present swelling properties. The catalysts were prepared using conventional methods, wet impregnation (WI) and sol-immobilisation (SI), and for the first time the organic solvent-assisted sol-immobilisation (SASI) method.

3.2.2.1 Wet impregnation (WI)

The WI method typically implies the contact of the support with an aqueous solution of the metal precursor where an excess amount of the solution is added. The gold catalysts prepared in this work by the WI method followed the same synthetic route as a typical impregnation does, however, acetonitrile was used as a solvent (Section 2.4.1). The aforementioned organic solvent is beneficial in two ways: it allows the swelling of the polymer facilitating the diffusion of the metal ions into the polymeric matrix and permits the solubilization of the metal precursor [48-50]. Therefore, the WI method with acetonitrile as solvent was used to prepare the 2 wt% Au/CMP-WI(ACN) and 2 wt% Au/PPO-WI(ACN) catalysts.

Figure 3.5 The CMP (sample 30) and PPO supports suspended in acetonitrile before being placed on a stirring plate for 12 hours.

In a typical synthesis, 0.1 g of the support (CMP or PPO) was suspended in acetonitrile (Figure 3.5), 8mL for CMP and 4 mL for PPO, in a vial under magnetic stirring for 12 hours in the absence of light (the vials were covered with aluminum foil to prevent degradation of the solvent). Then, an aqueous solution of the metal precursor ($HAuCl_4 \cdot 3H_2O$, Sigma-Aldrich) was dropwise added. The mixture was left under magnetic stirring at room temperature for 1 hour and then it was heated at 70 °C until the solvent was evaporated. The solid obtained was dried overnight at 60 °C. Finally, the samples were treated under H_2 flow (50 mL min^{-1}) at 190 °C for 3 hours at 2 °C min^{-1}.

3.2.2.2 Sol immobilisation (SI)

The sol immobilisation method (SI) is a well-known synthetic route that can be used for any type of support, producing metal-supported catalysts with notable catalytic activity. The SI method implies the preparation of a colloidal solution, then the pre-formed nanoparticles are immobilized onto the support [1-7].

The SI method was utilised to prepare gold catalysts using the CMP and PPO polymers as support as described in Section 2.4.2. Briefly, the appropriate amount of the metal precursor ($HAuCl_4 \cdot 3H_2O$) was dissolved in deionised water under magnetic stirring at room temperature, then it was reduced by a reducing agent (sodium borohydride-$NaBH_4$) in the presence of a stabilising polymer (Polyvinyl alcohol-PVA). After sol generation, the support (CMP or PPO) was added and the mixture was acidified with H_2SO_4 to pH 1. After the immobilisation of the colloidal solution on the support, the slurry was filtered, and the obtained catalyst was washed with deionised water and dried overnight. Then, the catalyst was washed with water at reflux conditions in order to remove the excess of the stabilising agent following the procedure reported by Lopez-Sanchez et al. [1]. Finally, the 2 wt% Au/CMP-SI and 2 wt% Au/PPO-SI were obtained.

3.2.2.3 Organic Solvent-Assisted Sol Immobilisation (SASI)

The organic solvent-assisted sol immobilisation (SASI) method was developed for the preparation of gold catalysts using conjugated microporous polymers as support. The advantage of using these polymers is due to metal nanoparticles can be confined into the porous network, allowing control of particle size as well as reducing particle aggregation. This synthetic procedure has not been reported in the current literature, thus it opens up routes to efficiently produce porous polymer-based catalysts for its application in heterogeneous catalysis. The SASI method consists of three separate steps: 1) Preparation of the pre-formed metal nanoparticles, 2) swelling of the polymer in the presence of an organic solvent under heat treatment and 3) immobilisation of the colloid onto the support. The general synthetic route of the SASI method is shown in Figure 3.6.

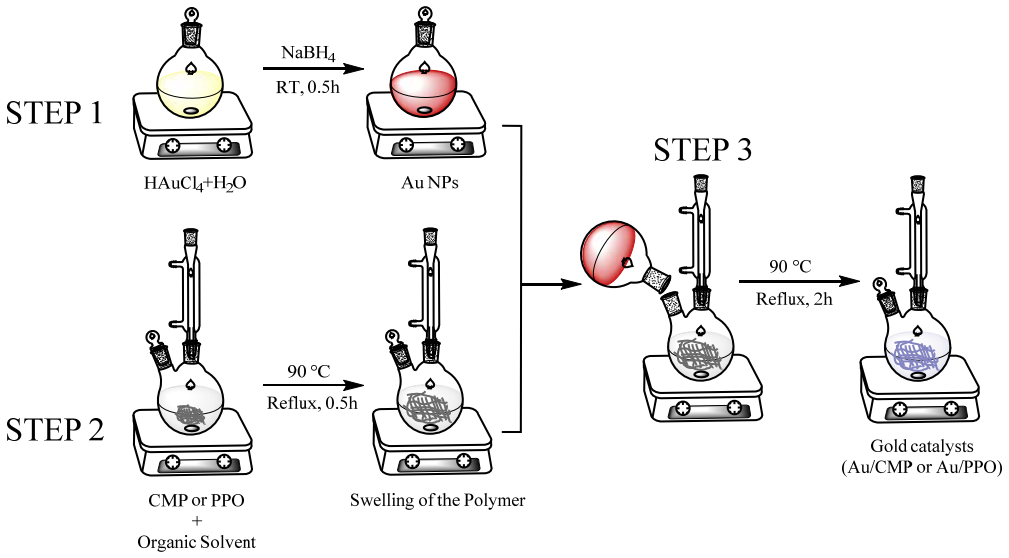

Figure 3.6 Schematic representation of the SASI method. 1) Preparation of the pre-formed nanoparticles, 2) swelling of the polymer, and 3) immobilisation of the colloid onto the support. RT = Room temperature, $NaBH_4$ = Sodium borohydride, Au NPs = Gold nanoparticles.

STEP 1: The first step in the SASI method includes the preparation of the gold nanoparticles by chemical reduction ($NaBH_4$ as reducing agent) of the gold precursor ($HAuCl_4 \cdot 3H_2O$) in the presence of a stabilising agent (Poly(vinyl alcohol)-PVA). The UV-Vis spectra of the aqueous $HAuCl_4$ solution used in this work is shown in Figure 3.7.

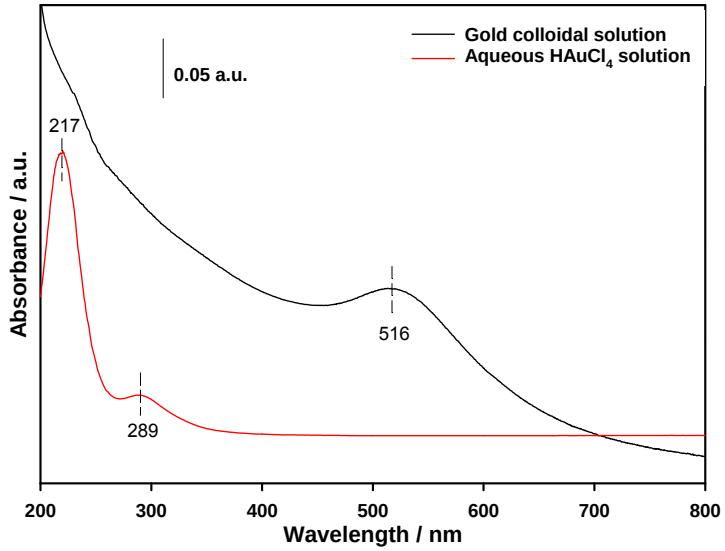

Figure 3.7 UV-Vis spectra of the aqueous $HAuCl_4$ solution before (red line) and after (black line) reduction.

The starting gold solution showed two bands at 217 and 289 nm which correspond to the ligand-to-metal charge transfer (LMCT) transition bands of the $[AuCl_4]^-$ ions (red line) [51, 52]. After chemical reduction by using sodium borohydride ($NaBH_4$) as reducing agent both bands decreased indicating that Au^{3+} ions were reduced into metallic state [53] and a broad band at 516 nm was formed (black line). This band is the surface plasmon resonance band (SPRB) which is due to the presence of spherical gold nanoparticles [54-56].

STEP 2: The second step in the SASI method corresponds to the swelling of the polymer with an organic solvent under heat treatment at reflux conditions. As mentioned before, the swelling of the polymeric network improves the diffusion of metal ions or metal nanoparticles onto the polymeric matrix due to the expansion of the network volume. In order to determine the organic solvent which maximizes the swellability of the CMP, a separate analysis was carried out following the same procedure described by Wilson et al. [57].

The swellability test was performed using the same procedure reported by Wilson et al. [57] in the study of hypercrosslinked polymer networks. The quantification of the swellability of the CMP network was evaluated using acetonitrile (ACN), dimethylformamide (DMF), and ethyl acetate (EtOAc) as the organic solvents. The method consists of adding a known amount of the polymer to an Eppendorf microcentrifuge tube, then the organic solvent is added, and the polymer is allowed to stand over an extended period of time. The resulted height of the swollen polymer in the microcentrifuge tube is measured for each solvent used. The amount of swelling (Q, mL/mg) is determined by using the equation 3.1 which was obtained during the calibration of a microcentrifuge tube with precise amounts of water, Figure 3.8.

$$y = 2.6304x^{0.551} \qquad (3.1)$$

The swelling tests for the CMP were carried out as follows: 1mg of the CMP network was placed into the Eppendorf tube, then 1mL of the organic solvent was added. The polymer was allowed to stand in the organic solvent for 20 hours in absence of light at room temperature. The height of the swollen polymer was

measured with a ruler and the obtained values were converted using the equation 3.1. The Q values were calculated as an average of three measurements, and the error was calculated as the standard deviation.

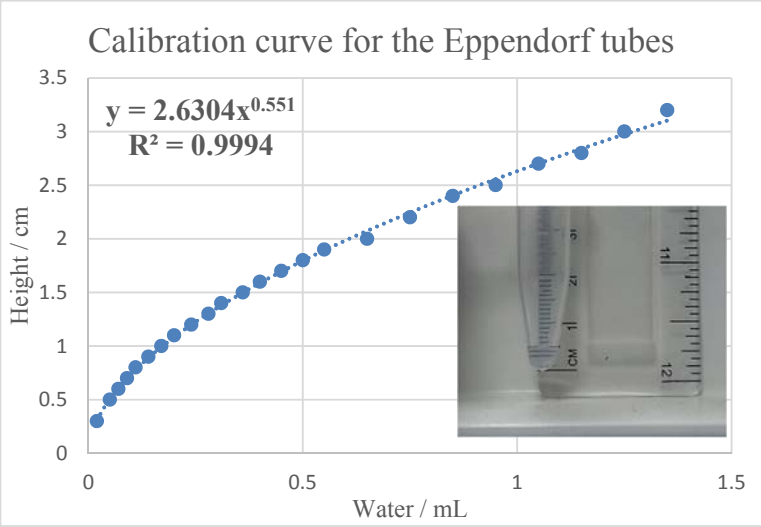

Figure 3.8 Calibration curve of the Eppendorf microcentrifuge tubes with water.

Figure 3.9 shows the amount of swelling (Q, mL/g) of the CMP network with different organic solvents. The test showed that DMF maximizes the swellability of the polymer by comparison with the other two solvents. The swelling values for the CMP network against the organic solvents are 72.3 mL/g for DMF, 70.7 mL/g for EtOAc and 65.4 mL/g for ACN.

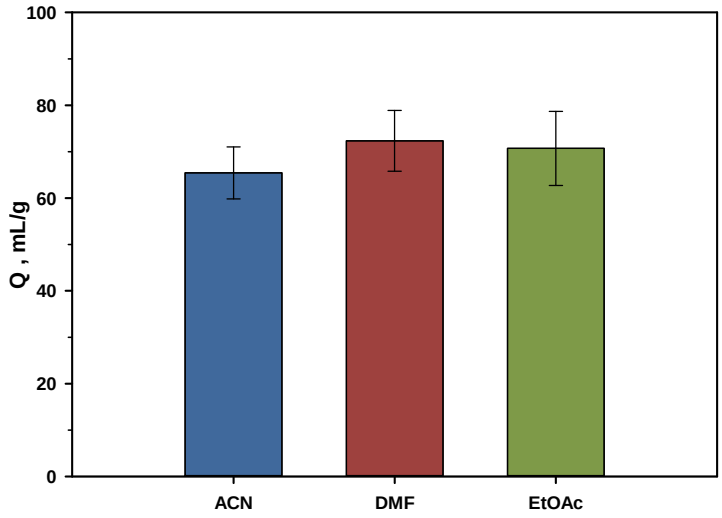

Figure 3.9 Swellability test for the CMP network (sample 32) utilising acetonitrile (ACN), dimethylformamide (DMF), and ethyl acetate (EtOAc). The Q values were calculated as an average of three measurements.

From Figure 3.9 it is clear that there is no solvent dependence in the swelling of the CMP network, hence the chosen solvent will depend on the final application. In the second step of the SASI method acetonitrile or dimethylformamide were used as solvent since ethyl acetate is not miscible with water. The miscibility between the organic solvents ACN or DMF and water allows the use of the PVA stabilized gold nanoparticles which were suspended in an aqueous solution. In a typical synthesis, 0.1 g of the support (CMP or PPO) was suspended in 15 mL of the organic solvent (ACN or DMF), then the mixture was heated at 90 °C under magnetic stirring at reflux conditions for 30 minutes.

STEP 3: Following the synthetic route in the SASI method, the aqueous colloidal solution prepared during the first step was immobilized onto the swollen polymer (step 2) and the mixture was kept at 90 °C under stirring at reflux conditions for 2 hours. Finally, the slurry was filtered, and the obtained catalyst was washed with deionised water. Then, the catalyst was dried overnight at 60 °C under reduced pressure and stored until further use. The SASI method was used to prepare the 2 wt% Au/CMP-SASI(ACN-W) and 2 wt% Au/CMP-SASI(DMF-W) catalysts using the organic solvents acetonitrile and dimethylformamide. The nomenclature for these catalysts includes the addition of the letter "W" which refers to the water used for the preparation of the colloidal solution and shows the presence of the mixtures water-acetonitrile and water-dimethylformamide during the preparation of the gold catalysts. The characterization and catalytic activity of the prepared catalysts will be discussed in the following sections.

3.2.3 Characterization of the Au/CMP and Au/PPO catalysts

3.2.3.1 The Au/PPO catalysts

The ICP-OES analysis of the Au/PPO catalysts was carried out to determine the real metal loading of the gold catalysts prepared by the WI, SI and SASI methods. Table 3.3 shows that the synthetic method has an effect on the amount of gold deposited on the samples. The Au/PPO-WI(ACN) catalyst showed that the WI method effectively deposited the desired amount (slightly higher due to the experimental error) of the metal on the support, whereas the SI method showed that the complete deposition of gold was not achieved for the Au/PPO-SI catalyst. The results suggest that the SI method was not a good technique and therefore we needed to develop the SASI method. The Au/PPO-SASI(DMF-W) catalyst showed that the SASI method successfully deposited the metal on the support and even high metal loading was achieved. The high metal content in this catalyst is associated to the experimental error during the preparation of the catalyst but it demonstrates that Au/PPO catalysts with high metal content can be prepared using the SASI method and DMF as solvent. Meanwhile, the Au/PPO-SASI(ACN-W) catalyst showed the lowest metal content among the catalysts in this series, indicating that the solvent (ACN) affects the deposition of the metal on the PPO support.

Table 3.3 Metal amount determined by the ICP-OES analysis for the Au/PPO catalysts

Catalysts	$[Au]_{nominal}$ / wt%	$[Au]_{real}$ / wt%
Au/PPO-SASI(ACN-W)	2	0.2
Au/PPO-SASI(DMF-W)	2	3.1
Au/PPO-SI	2	1.1
Au/PPO-WI(ACN)	2	2.6

The Au/PPO catalysts were characterized by diffuse reflectance UV-Vis spectroscopy (DR UV-Vis) with the aim of investigating any change on the metal nanoparticles after deposition on the PPO support. As shown in Figure 3.10, DR UV-Vis spectra were measured in the 400-800 nm range of the catalysts. The DR UV-Vis spectra of the Au/PPO catalysts showed the presence of the surface plasmon resonance (SPR) band of gold in the range between 524 and 578 nm.

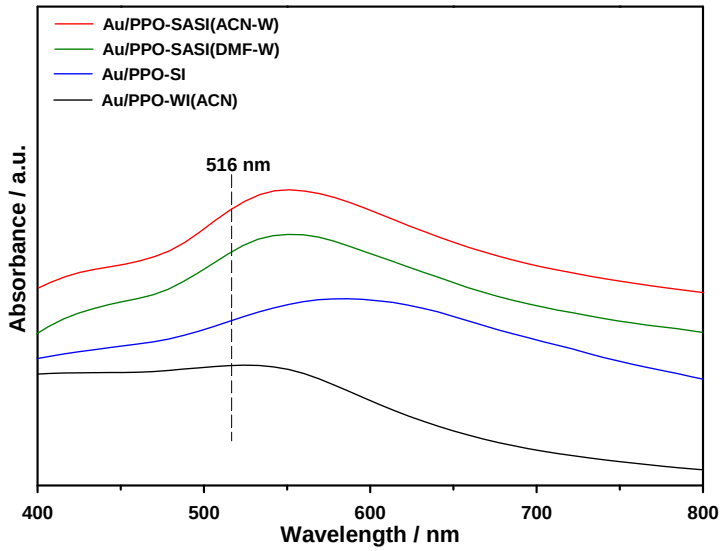

Figure 3.10 UV-Vis spectra of the Au/PPO catalysts prepared by the WI, SI and SASI (using ACN or DMF as solvents) methods.

Plasmonic peaks in the same range have been attributed to the presence of gold nanoparticles [58-65]. In Table 3.4 the SPR bands of the Au/PPO catalysts are reported. The SPR band of the Au/PPO catalysts prepared by the SI and SASI methods showed a red shift of the plasmonic peaks with respect to the SPR band (516 nm) of the gold nanoparticles in the colloidal solution. The red shift observed in the plasmon band for the gold catalysts might be due to an increase in particle size or a support effect [66, 67]. The catalyst prepared by the WI method showed a plasmonic peak centered at 524 nm which could indicate the presence of small gold nanoparticles [58-65].

Table 3.4 Gold surface plasmon resonance band for the Au/PPO catalysts.

Catalysts	$UV_{\lambda max}$ / nm
Au/PPO-SASI(ACN-W)	550
Au/PPO-SASI(DMF-W)	550
Au/PPO-SI	578
Au/PPO-WI(ACN)	524

XRD analysis was carried out on the Au/PPO catalysts prepared by the WI, SI and SASI methods with the aim to identify the presence of gold diffraction signal in the samples. The XRD analysis of the Au/PPO catalysts in the 2θ range of 20–80° is shown in Figure 3.11.

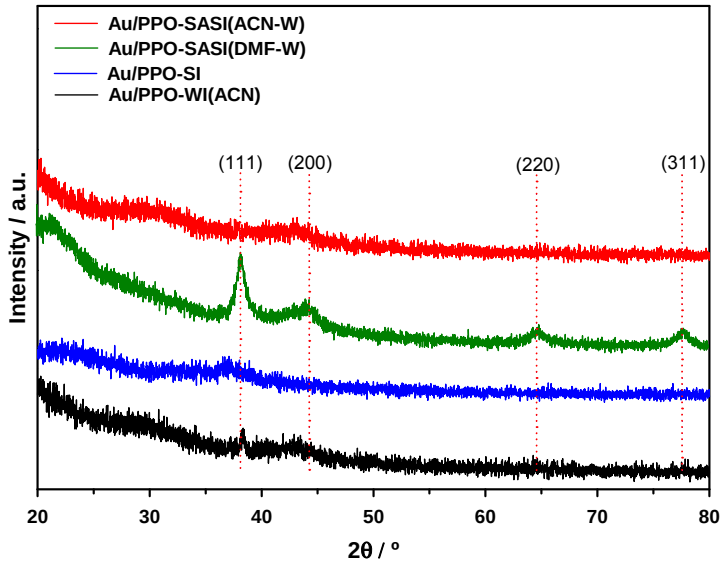

Figure 3.11 XRD patterns of the Au/PPO catalysts prepared by the WI, SI and SASI (using ACN or DMF as solvents) methods.

The XRD analysis on the PPO-supported gold catalysts showed the amorphous character of the polymeric support (Figure 3.11). The samples prepared by the WI, SI, and SASI(ACN-W) methods showed the presence of low-intensity reflection signals at 2θ ≈ 38.3° and/or 44.4° that correspond to the [1 1 1] and [2 0 0] planes of gold [68-70]. However, the Au/PPO-SASI(DMF-W) catalyst in this series showed the most intense reflection signals at 2θ ≈ 38.2°, 44.4°, 64.5º, and 77.7º that correspond to the [1 1 1], [2 0 0], [2 2 0] and [3 1 1] planes of gold with face-centered cubic (*fcc*) crystalline structure [68-70]. The increased intensity of the reflection signals for gold in the Au/PPO-SASI(DMF-W) catalyst could be associated to the high metal (3.1 wt%) content as evidenced by the ICP-OES analysis reported in Table 3.3.

X-ray photoelectron spectroscopy (XPS) analysis was carried out on the Au/PPO catalysts prepared by the WI, SI and SASI methods with the aim to determine the species present at the surface and the influence of the electronic properties of the polymer in the final material. Figure 3.12 shows the XPS spectrum (scattered points) of the gold catalysts over the Au 4f region. In order to determine the different gold species and their chemical state in the samples, the deconvolution of the Au 4f spectrum was performed using the CasaXPS Version 2.1.34 software. The spectra were fitted by using two spin-orbit split Au $4f_{7/2}$ and Au $4f_{5/2}$ components (asymmetric doublet), solid lines in Figure 3.12.

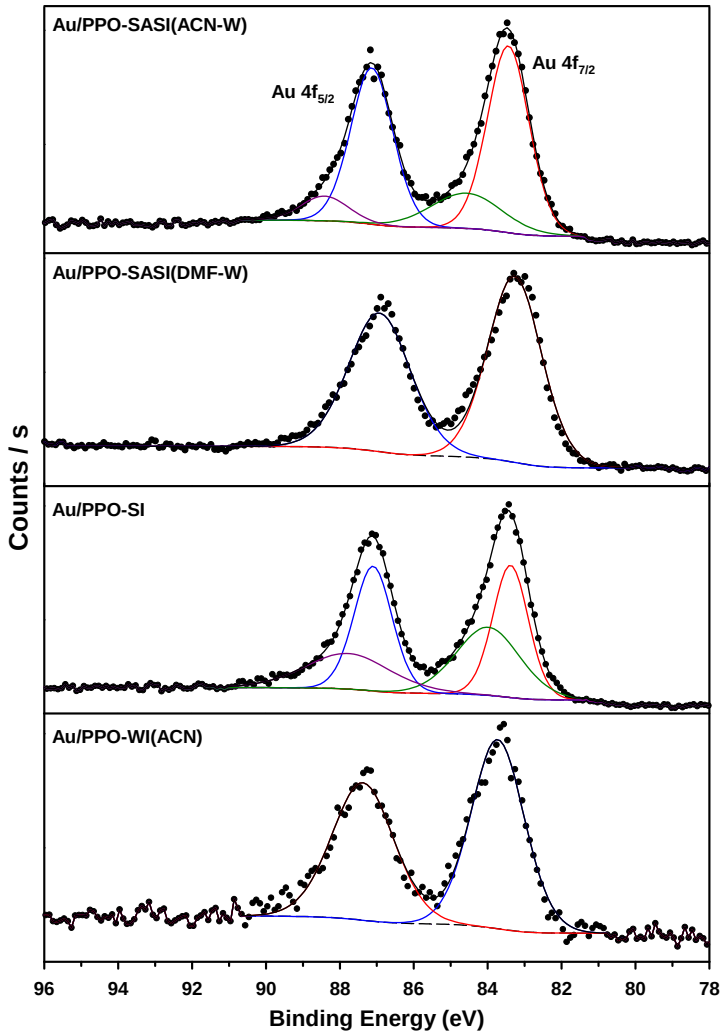

Figure 3.12 XPS spectra of the Au 4f region for the Au/PPO catalysts.

The Au $4f_{7/2}$ peak is generally used as binding energy reference to assign the chemical state of the gold species [71-74]. Hence, the binding energies (BE) values will be referred to the Au $4f_{7/2}$ core-level in this section. The assignments of the chemicals states for the Au/PPO catalysts were obtained from the literature, but they correspond to different materials. Table 3.5 shows the BE values and the relative surface composition for the Au/PPO catalysts. The XPS analysis of the Au/PPO-WI(ACN) catalyst showed that the Au $4f_{7/2}$ peak was located at 83.72 eV which can be assigned to the $Au^{\delta-}$ oxidation state [75, 76]. The XPS spectrum of the Au/PPO-SI catalyst showed the presence of two gold species after deconvolution of the Au 4f doublet, the $Au^{\delta-}$ (83.42 eV) and $Au^{\delta+}$ (84.69 eV) oxidation states [75-77]. For the catalysts prepared by the SASI method, the Au/PPO-SASI(DMF-W) catalyst showed the $Au^{\delta-}$ oxidation (83.26 eV) state [75, 76], whereas the Au/PPO-SASI(ACN-W)

catalyst showed the $Au^{\delta-}$ (83.44 eV) and $Au^{\delta+}$ (84.57 eV) oxidation states [75-77] after deconvolution of the Au 4f doublet. The results reported by the XPS analysis on the Au/PPO catalysts showed that the $Au^{\delta-}$ and $Au^{\delta+}$ oxidation states are mainly favoured on the PPO support.

Table 3.5 Binding energy (BE) values of the Au 4f region of the Au/PPO catalysts and relative surface composition.

Catalyst	Au $4f_{7/2}$ BE (eV)	Au $4f_{5/2}$ BE (eV)	Chemical State	Surface Composition (At%)		
				Au 4f	C 1s	O 1s
Au/PPO-SASI(ACN-W)	83.44	87.13	$Au^{\delta-}$	1.84	86.22	11.47
	84.57	88.41	$Au^{\delta+}$	0.46		
Au/PPO-SASI(DMF-W)	83.26	86.92	$Au^{\delta-}$	0.97	89.84	9.19
Au/PPO-SI	83.42	87.08	$Au^{\delta-}$	4.23	81.86	10.59
	84.69	88.16	$Au^{\delta+}$	3.31		
Au/PPO-WI(ACN)	83.72	87.36	$Au^{\delta-}$	0.09	89.52	10.39

3.2.3.2 The Au/CMP catalysts

The ICP-OES analysis was carried out on the Au/CMP catalysts in order to determine the real metal content of gold in the catalysts prepared by the WI, SI, and SASI methods. Table 3.6 shows that the metal content in the catalysts was affected by the synthesis method. The Au/CMP-WI(ACN) catalyst showed that the required amount of gold was deposited using the WI method with acetonitrile as solvent. In the case of the Au/CMP-SI catalyst, the concentration required was not achieved during the synthesis, indicating that the SI method is not a suitable route to produce gold catalysts and therefore we needed to develop the SASI method in order to use pre-formed metal nanoparticles more efficiently on polymeric supports. For the samples prepared by the SASI method, the use of DMF as solvent during the synthesis produced gold catalysts with high metal content (similar findings were observed for the Au/PPO-SASI(DMF-W)), whereas the use of ACN showed that the metal content was close to required value.

Table 3.6 Metal amount determined by the ICP-OES analysis for the Au/CMP catalysts

Catalysts	$[Au]_{nominal}$ / wt%	$[Au]_{real}$ / wt%
Au/CMP-SASI(ACN-W)	2	1.6
Au/CMP-SASI(DMF-W)	2	2.6
Au/CMP-SI	2	1.2
Au/CMP-WI(ACN)	2	2.1

The CMP-supported gold catalysts were characterized by diffuse reflectance UV-Vis spectroscopy (DR UV-Vis). Figure 3.13 shows the DR UV-Vis spectra of the samples in the 400-800 nm range. The Au/CMP catalysts showed the presence of the surface plasmon resonance (SPR) band of gold for the gold catalysts between 542 and 569 nm (Table 3.7), indicating the presence of gold nanoparticles [58-65]. In all cases, a red shift was observed in the plasmonic peaks that it can be associated to several factors such as solvent effect, metal-support interactions and particle growth [66, 67].

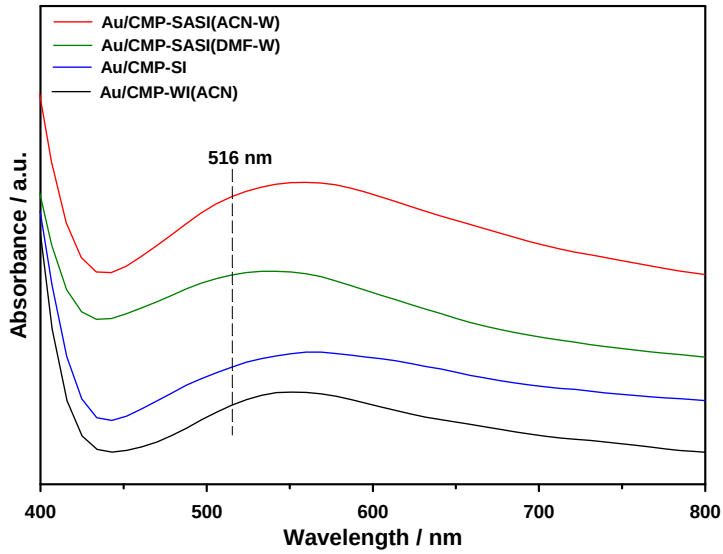

Figure 3.13 UV-Vis spectra of the Au/CMP catalysts prepared by the WI, SI and SASI (using ACN or DMF as solvents) methods.

Table 3.7 Gold surface plasmon resonance band for the Au/CMP catalysts.

Catalysts	$UV_{\lambda max}$ / nm
Au/CMP-SASI(ACN-W)	560
Au/CMP-SASI(DMF-W)	542
Au/CMP-SI	569
Au/CMP-WI(ACN)	551

X-ray diffraction analysis was performed on the Au/CMP catalysts prepared by the WI, SI and SASI methods. The aim was to identify the presence gold diffraction signals in the final materials. The samples were analysed in the 2θ range of 20–80°, and the results are reported in Figure 3.14. The diffraction patterns of the Au/CMP catalysts showed the amorphous character of the CMP polymer in agreement with previous reports [39, 44].

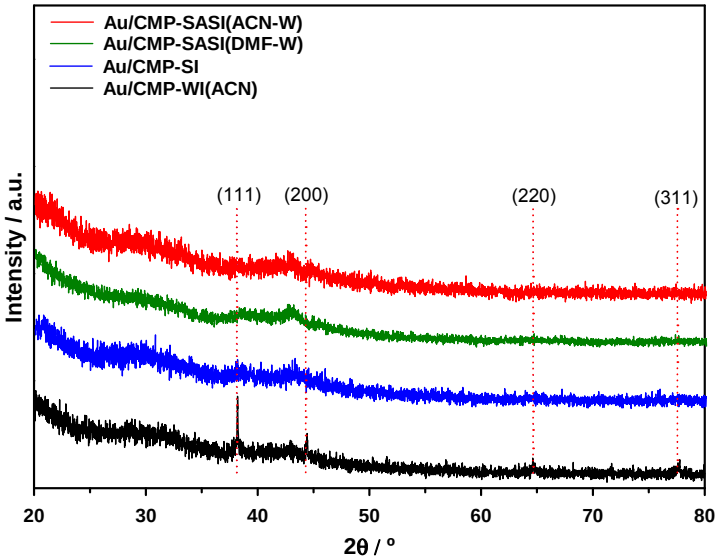

Figure 3.14 XRD patterns of the Au/CMP catalysts prepared by the WI, SI and SASI (using ACN or DMF as solvents) methods.

The CMP-supported gold catalysts (Figure 3.14) prepared by the SI and SASI methods showed low-intensity reflection signals of gold at 2θ ≈ 38.2° and/or 44.4° which correspond to the [1 1 1] and [2 0 0] planes, whereas the sample prepared by WI showed reflection signals at 2θ ≈ 38.2°, 44.4°, 64.5º, and 77.7º that correspond to the [1 1 1], [2 0 0], [2 2 0] and [3 1 1] planes of gold with face-centered cubic (*fcc*) crystalline structure [68-70].

XPS analysis was performed on the Au/CMP catalysts prepared by the WI, SI and SASI methods with the aim to identify the formed gold species and their chemical state in the final material. Figure 3.15 shows the XPS spectrum (scattered points) of the gold catalysts over the Au 4f region. The XPS analysis was carried out in the same manner as described in section 3.2.3.1 for the Au/PPO catalysts. The obtained spectra after deconvolution are presented as solid lines in Figure 3.15. The binding energies and the relative surface composition are reported in Table 3.8.

Table 3.8 Binding energy (BE) values of the Au 4f region of the Au/CMP catalysts and relative surface composition.

Catalyst	Au $4f_{7/2}$ BE (eV)	Au $4f_{5/2}$ BE (eV)	Chemical State	Surface Composition (At%)			
				Au 4f	Pd 3d	C 1s	O 1s
Au/CMP-SASI(ACN-W)	82.95	86.65	$Au^{\delta-}$	1.21	0.95	92.86	4.81
	84.13	88.15	Au^0	0.15			
Au/CMP-SASI(DMF-W)	83.27	86.98	$Au^{\delta-}$	0.85	0.96	93.78	4.24
	84.02	88.39	Au^0	0.16			
Au/CMP-SI	83.80	87.47	$Au^{\delta-}$	0.31	0.48	94.57	4.28
	84.38	88.07	Au^0	0.36			
Au/CMP-WI(ACN)	84.37	88.05	Au^0	0.06	ND	95.64	4.29

ND = No detected

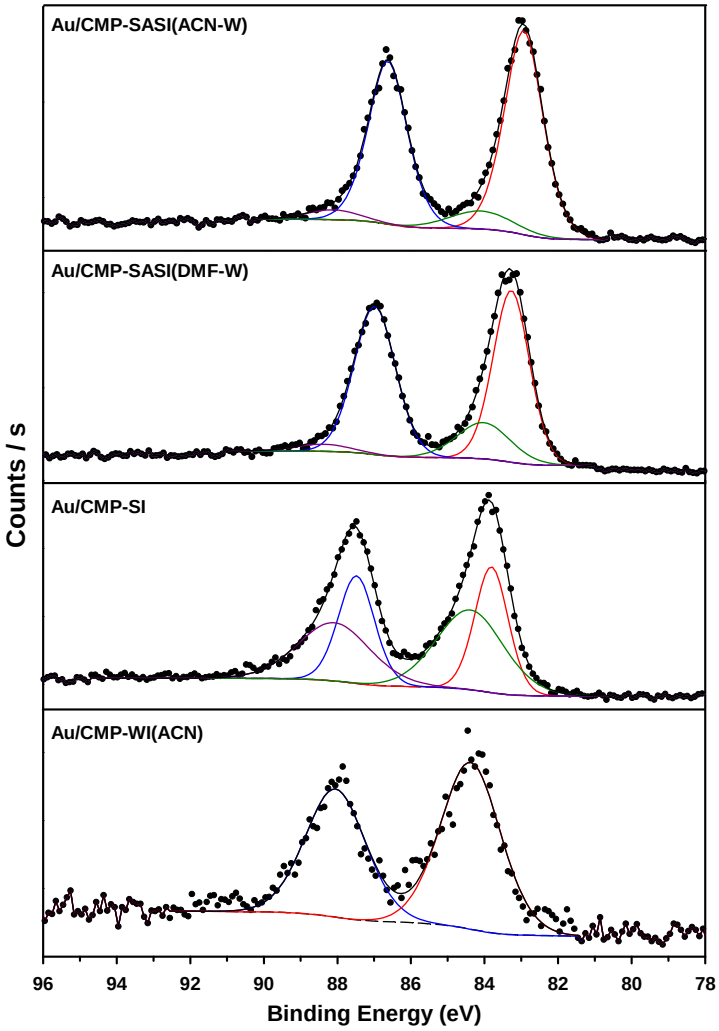

Figure 3.15 XPS spectra of the Au 4f region for the Au/CMP catalysts.

Similar to the Au/PPO catalysts, the assignments of the chemical states for the Au/CMP catalysts were obtained from the literature, but they correspond to different materials. In the CMP-supported gold catalysts, the presence of two gold species was observed for the samples prepared by SI and SASI methods. The Au $4f_{7/2}$ BE values for the Au/CMP-SI (83.8 and 84.38 eV), Au/CMP-SASI(DMF-W) (83.27 and 84.02 eV) and Au/CMP-SASI(ACN-W) (82.95 and 84.13 eV) catalysts showed the presence of the $Au^{\delta-}$ and Au^{0} species [75, 76, 78-80], whereas the BE value for the Au/CMP-WI(ACN) (84.37 eV) catalyst in this series is consistent with the presence of metallic gold (Au^{0}) [75, 78-80]. The XPS analysis on the Au/CMP catalysts showed that the $Au^{\delta-}$ and Au^{0} oxidation states are mainly favoured on the CMP support.

The Au/CMP-SASI(ACN-W) catalyst was characterised by transmission electron microscopy (TEM) as shown in Figures 3.16 and 3.17. Figure 3.16a shows that the gold nanoparticles were homogeneously dispersed on the CMP surface and the presence of agglomerated nanoparticles was not observed. Figure 3.16b shows that the gold nanoparticles retained their spherical shape after deposition onto the support, indicating that the nature of the CMP network does not have an effect on the metal nanoparticles. The presence of small gold nanoparticles with mean particle size of 3.7 nm was observed for the Au/CMP-SASI(ACN-W) catalyst (Figure 3.17).

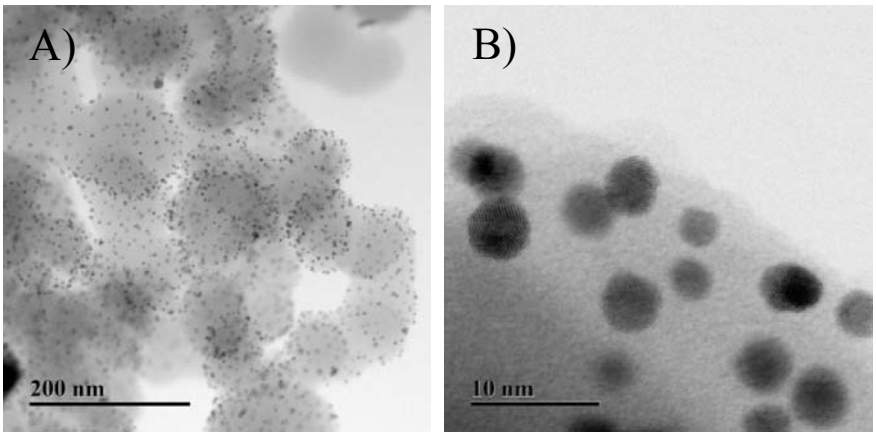

Figure 3.16 Bright field TEM micrographs from different regions of the fresh 1.6 wt % Au/CMP-SASI(ACN-W) catalyst.

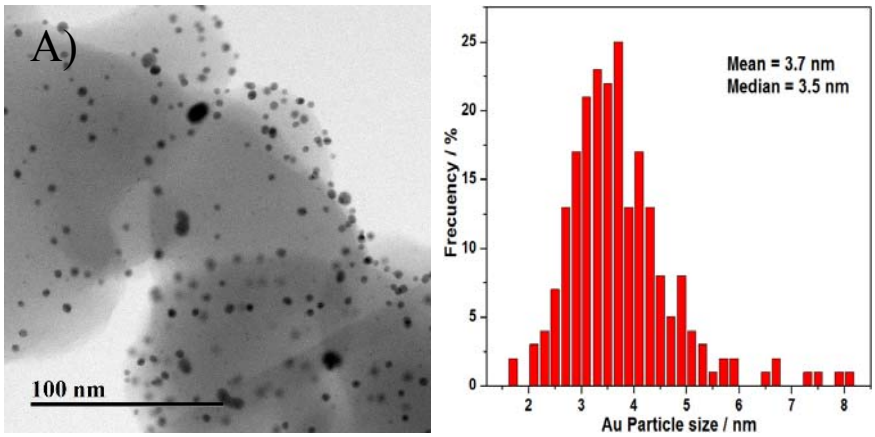

Figure 3.17 Particle size distribution obtained from the bright field TEM image (A) from the fresh 1.6 wt % Au/CMP-SASI(ACN-W) catalyst.

3.2.3.3 Final Comparative Remarks

Gold catalysts were prepared on polymeric supports using conventional methods (WI and SI) and novel synthesis as the SASI method. The catalysts were characterized using several techniques such as ICP-OES, Solid UV-Vis, XRD, TEM, and XPS. Since the materials presented in this work are reported for the first time, we decided to show the characterization of the catalysts in two sections, Section 3.2.3.1 for the Au/PPO catalysts and Section 3.2.3.2 for the Au/CMP catalysts. The aim was to show a more detailed analysis of the new materials using the above techniques. In this section, we will present a comparative examination of the catalysts prepared and the effect of the synthesis method in the final materials.

The ICP-OES analysis of the Au/PPO and Au/CMP catalysts showed that the synthesis method had an effect on the metal deposition (Table 3.9). Particularly, the catalysts prepared by the WI method, Au/PPO-WI(ACN) and Au/CMP-WI(ACN), showed that the desired amount of the metal was deposited on the support. In the case of the SI method, the Au/PPO-SI and Au/CMP-SI catalysts showed that approximately half of the metal amount was deposited in the samples, indicating the SI method is not a suitable route to prepare gold catalysts on polymeric supports. The new synthetic route, the SASI method, demonstrated that the use of an organic solvent during the synthesis improves the swelling of the polymer and metal deposition. Particularly, the use of DMF showed that catalysts with high metal content can be prepared, whereas the use ACN showed that the immobilization of the gold nanoparticles was favoured on the CMP.

Table 3.9 Metal amount determined by the ICP-OES analysis for the Au/PPO and Au/CMP catalysts.

Catalysts	$[Au]_{nominal}$ / wt%	$[Au]_{real}$ / wt%
Au/CMP-SASI(ACN-W)	2	1.6
Au/CMP-SASI(DMF-W)	2	2.6
Au/CMP-SI	2	1.2
Au/CMP-WI(ACN)	2	2.1
Au/PPO-SASI(ACN-W)	2	0.2
Au/PPO-SASI(DMF-W)	2	3.1
Au/PPO-SI	2	1.1
Au/PPO-WI(ACN)	2	2.6

The presence of the SPR band in supported gold catalysts derives from the presence of the SPR band of gold nanoparticles in solution. In the case of supported gold catalysts, the SPR band can change closely with the particle size, shape, and the support material [58-65]. The gold nanoparticles (in solution) used in this work presents a SPR band at 516 nm (Figure 3.7) which is in good agreement with the reported values [54-56]. After the immobilization of the gold nanoparticles onto the supports (CMP and PPO) using the SI and SASI methods, the SPR band was observed at higher wavelength in all cases (Figures 3.10 and 3.13). The catalysts prepared by the WI method showed a red shift of the SPR band as the ones prepared by colloidal methods. Based on the results reported in Table 3.10, it is clear that the synthesis method and solvent produced different particle size on the supports due to the shift of the SPR band as it has been demonstrated for supported gold catalysts which have shown SPR bands above 520 nm with a particle size between 2 and 20 nm [55-62]. The SPR band in the supported gold catalysts can also be influenced by the solvent during the preparation step. However, the effect of the solvent is difficult to compare among the systems because of the different dielectric properties of the solvents [81, 82]. Although, it should be noticed that the use of DMF as solvent during the synthesis of the Au/CMP-SASI(DMF) and Au/PPO-SASI(DMF) catalysts produced higher metal loadings than ACN as solvent (Table 3.9).

Table 3.10 Gold surface plasmon resonance band for the Au/PPO and Au/CMP catalysts.

Catalysts	$UV_{\lambda max}$ / nm
Au/CMP-SASI(ACN-W)	560
Au/CMP-SASI(DMF-W)	542
Au/CMP-SI	569
Au/CMP-WI(ACN)	551
Au/PPO-SASI(ACN-W)	550
Au/PPO-SASI(DMF-W)	550
Au/PPO-SI	578
Au/PPO-WI(ACN)	524

The XRD analysis on the CMP- and PPO-supported gold catalysts showed the amorphous character of the polymers. The supported gold catalysts in most cases showed very low-intensity reflection signals which may be due to the low amount of gold on the polymers or the gold nanoparticles are small. In fact, the Au/PPO-SASI(DMF-W) catalyst showed the effect of metal loading on the intensity of the

reflection peaks of gold as this catalyst presented the highest metal loading among the samples (Table 3.9). Although the metal content was high for the Au/PPO-SASI(DMF-W) catalyst, the average crystallite size was calculated to be 9.7 nm using the Scherrer equation [83], whereas the Au/CMP-WI(ACN) catalysts showed a crystallite size of 85.7 nm. These results once again support the use of colloidal methods in combination with organic solvents on the synthesis of polymer-supported catalysts.

The XPS analysis was performed on the fresh Au/PPO and Au/CMP catalysts synthesized by the WI, SI and SASI methods, Figures 3.12 and 3.15. The BE values of the Au 4f region ($4f_{7/2}$ and $4f_{5/2}$ components) and surface composition for the gold catalysts are summarized in Table 3.11. The curve-fitting of the Au 4f spectrum for the gold catalysts showed the presence of electropositive ($Au^{\delta+}$) and electronegative ($Au^{\delta-}$) oxidation states as well as metallic gold (Au^0). The observed chemical states in the samples were assigned as a function of the binding energy position. The gold catalysts with BE values between 84.02 and 84.38 eV showed the presence of metallic (Au^0) species [75, 78-80]. In the case of catalysts with BE values between 84.57 and 84.69 eV but lower than 85.0 eV (Au^+) have been attributed to species with a partial positive ($Au^{\delta+}$) charge resulting from the electron transfer from gold [75, 77].

Table 3.11 Binding energy (BE) values of the Au 4f region of the Au/PPO and Au/CMP catalysts and surface composition.

Catalyst	Au $4f_{7/2}$	Au $4f_{5/2}$	Chemical	Surface Composition (At%)			
	BE (eV)	BE (eV)	State	Au 4f	Pd 3d	C 1s	O 1s
Au/CMP-SASI(ACN-W)	82.95	86.65	$Au^{\delta-}$	1.21	0.95	92.86	4.81
	84.13	88.15	Au^0	0.15			
Au/CMP-SASI(DMF-W)	83.27	86.98	$Au^{\delta-}$	0.85	0.96	93.78	4.24
	84.02	88.39	Au^0	0.16			
Au/CMP-SI	83.80	87.47	$Au^{\delta-}$	0.31	0.48	94.57	4.28
	84.38	88.07	Au^0	0.36			
Au/CMP-WI(ACN)	84.37	88.05	Au^0	0.06	ND	95.64	4.29
Au/PPO-SASI(ACN-W)	83.44	87.13	$Au^{\delta-}$	1.84	—	86.22	11.47
	84.57	88.41	$Au^{\delta+}$	0.46			
Au/PPO-SASI(DMF-W)	83.26	86.92	$Au^{\delta-}$	0.97		89.84	9.19
Au/PPO-SI	83.42	87.08	$Au^{\delta-}$	4.23		81.86	10.59
	84.69	88.16	$Au^{\delta+}$	3.31			
Au/PPO-WI(ACN)	83.72	87.36	$Au^{\delta-}$	0.09	—	89.52	10.39

ND = No detected

In most cases, the gold catalysts showed the presence of an intense peak for the Au $4f_{7/2}$ level located at BE values between 82.95 and 83.80 eV, which are lower than the BE value of metallic gold (Au^0) at 84.0 eV [75, 78-80]. This negative shift in the binding energies could indicate that the gold species are more reduced than metallic gold, thus a partial negative ($Au^{\delta-}$) charge is observed [75, 76]. The presence of gold species with a partial negative charge has been attributed to electron transfer from the support to the gold nanoparticles. In particular, it has been reported that supports such as CeO_2 [76, 84], TiO_2 [85-87], γ-Al_2O_3 [71], and graphene [88] could act as electron donors to the gold particles. Therefore, it is possible that the presence of a partial negative charge on Au sites in the CMP- and PPO-supported gold catalysts is due to a metal-support interaction. This assumption can also be supported by the fact that gold does not easily donate electrons due to its high electronegativity and high ionization potential [89]. Hence, it can be assumed that the polymers (CMP or PPO) can act as electron donors to the gold particles, resulting in a partial negative ($Au^{\delta-}$) charge on Au sites. The presence of the $Au^{\delta-}$ oxidation state is still under debate in the literature, results obtained by Zwijnenburg et al. [90] using ^{197}Au-Mössbauer spectroscopy did not show negatively charged gold particles. Moreover, some groups have attributed the origin of this negative shift in the BE values to initial or final state effects [91, 92], while others attribute it to the changes in electron density to Coulombic forces [93]. In this scenario, it is clear that the assignment of chemical states in gold catalysts is complex and changes in binding energies could be associated to metal-support interactions or changes in particle size and shape, thus the information reported in the literature should be interpreted with caution. Nevertheless, we can conclude that the use of CMP as support clearly results in a partial negative charge in the gold particles and this could be due to its electronic properties.

3.2.4 Catalyst Testing

3.2.4.1 Au/CMP and Au/PPO catalysts for the oxidation of glucose

The catalytic performance of the CMP- and PPO-supported gold catalysts was investigated for the glucose oxidation reaction using microwave assisted heating. The oxidation of glucose has been widely investigated in the literature as alternative route to produce value added chemicals from sustainable sources as biomass. The selective oxidation of glucose to gluconic acid is an important reaction since the carboxylic acid and its salts are widely used as a food additive, in pharmaceuticals and as a raw material for biodegradable polymers [94]. The glucose oxidation is often carried out using molecular oxygen (Scheme 3.2) or air at atmospheric pressure in the presence of supported metal catalysts. Typically, palladium and platinum catalysts have been extensively studied in the glucose oxidation, however, the strong adsorption of oxygen on the metal surface have limited their catalytic activity [95]. In this scenario, gold catalysts have emerged as an alternative to the palladium and platinum catalysts due to their remarkable activity, and selectivity to gluconic acid [96-105]. The glucose oxidation using gold catalysts has shown that basic conditions are required to maintain high activity and selectivity as reported by Biella et al. [5]. Therefore, most studies on the glucose oxidation using gold catalysts have been carried out in two different ways, in basic media [5, 96, 99], and base-free conditions in the presence of molecular oxygen or air as the oxidant [103, 104, 106]. Since the catalytic transformation of glucose is well-known in the literature, it was selected as a test reaction to determine the effect of the synthesis method (WI, SI, and SASI) and support material (CMP and PPO) in the as-prepared catalysts.

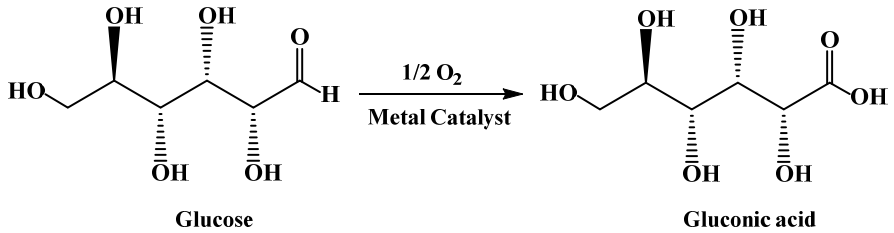

Scheme 3.2 The glucose oxidation in the presence of a metal catalyst with molecular oxygen as the oxidant.

The reaction was carried out using a 55.5 mM glucose stock solution in the presence of molecular oxygen as the oxidant (10 bar) and heated for 30 minutes at 130 ºC under microwave assisted heating (CEM Discover® SP, Section 2.9.2). In some cases, the oxidation process showed the formation of different products such as tartronic, glycolic, and formic acids, however, gluconic acid was the most abundant product in all cases. The blank test showed no formation of oxidation products when the bare CMP was used under reaction conditions, demonstrating that gold nanoparticles are needed to carry out the glucose oxidation (Table A.5, Appendix A). In the following sections, the glucose conversion, gluconic acid yield and the turnover frequency will only be presented in the discussion, unless stated otherwise. Conversion, mass balance and yields of products for the glucose oxidation are reported in Appendix A.

As an example, Table 3.12 shows conversion, product yield, mass balance and TOF values in the catalytic oxidation of glucose using the Au/PPO catalysts. Figure 3.18 shows (a) the glucose conversion and (b) gluconic acid yield for the Au/PPO catalysts. The results shows that the synthesis method had the strongest effect on the catalytic activity. The Au/PPO-SASI(DMF-W) and Au/PPO-SI catalysts were the most active in this series with conversion values of 28.5% and 35.4% and gluconic acid yields of 27.4% and 33.8% after 30 minutes of reaction time. However, the Au/PPO-SI catalyst showed the highest TOF value (68.8 min^{-1}) compared to the Au/PPO-SASI(DMF-W) catalyst (13.5 min^{-1}), indicating that the Au/PPO-SI catalyst was the most active among the catalysts prepared in this series.

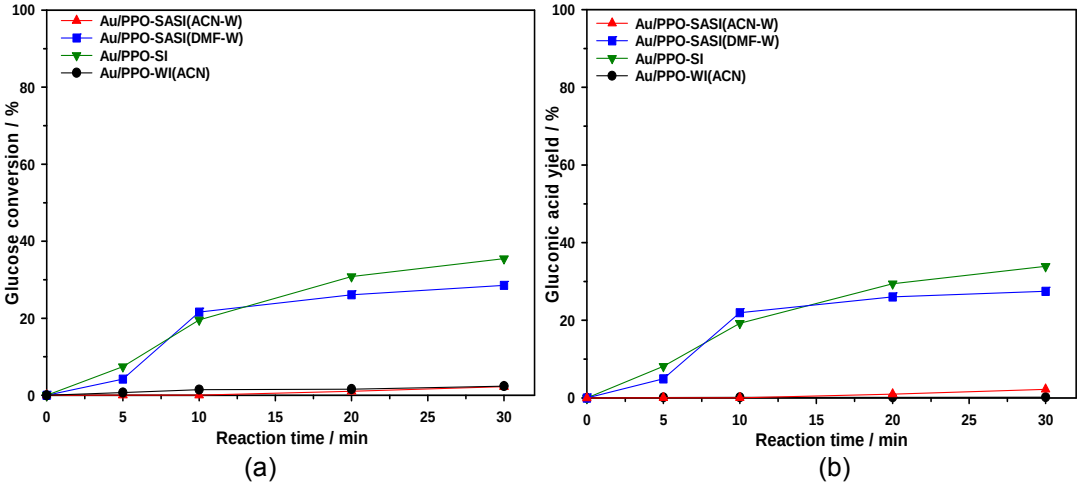

Figure 3.18 Glucose conversion (a) and gluconic acid yield (b) for the Au/PPO catalysts. Reaction conditions: Glucose/Au = 438 molar ratio, T = 130 ºC, Reaction time = 30 min, $P(O_2)$ = 10 bar.

Notably, the Au/PPO-SASI(ACN-W) catalyst showed the lowest glucose conversion (2.2% after 30 min.) among the catalysts synthesized by the SASI method. In this case, the poor activity of the Au/PPO-SASI(ACN-W) catalyst can be associated to the solvent (acetonitrile) used during the synthesis, which limits the immobilization of the gold nanoparticles onto the support. As a result, the Au loading of the catalyst was 0.2 wt % (Table 3.3), a value far below the desired metal content (2 wt %). On the other hand, the 2.6 wt % Au/PPO-WI(ACN) catalyst showed that high metal content did not improve the catalytic activity as the glucose conversion was 2.3% after 30 minutes of reaction time. Despite the high metal content in the Au/PPO-WI(ACN) catalyst, the catalytic activity was negligible, thus indicating that the WI method produced less active catalysts. A possible explanation for the low activity could be associated to the particle size which cannot be controlled by the WI method [38] and this represents the most important factor for the gold nanoparticles due to their size-dependent activity [32].

Table 3.12 Conversion, product yield and mass balance values in the catalytic oxidation of glucose with the Au/PPO catalysts under microwave conditions after 30 minutes reaction time.

Catalyst	Glucose Conversion (%)	Gluconic acid (%)	Tartronic acid (%)	Mass Balance (%)	TOF[a] (min^{-1})
Au/PPO-SASI(ACN-W)	2.2	2.2	-	99	1.8
Au/PPO-SASI(DMF-W)	28.5	27.4	-	98.9	13.5
Au/PPO-SI	35.4	33.8	0.13	98.5	68.8
Au/PPO-WI(ACN)	2.3	0.17	2.13	99	2.7

[a] TOF values were calculated at 5 minutes reaction time, TOF = (Moles of glucose converted)/(Moles of metal x Time).

For the first time, we report the oxidation of glucose to gluconic acid using novel Au/PPO catalysts with molecular oxygen as the oxidant. The results showed that the synthesis method had a strong effect in the catalytic activity of the final material. The SI method showed to be more efficient in the preparation of gold catalysts using the PPO as support, however, low conversion values and yields were observed in all cases. Based on the previous findings, it is clear that more robust materials (supports) need to be developed in order to improve the catalytic activity of metal nanoparticles. For this reason, we took advantage of conjugated microporous polymers where metal nanoparticles can be confined into the porous structure, thus providing particle size control and a protective environment for catalytic applications.

Gold catalysts were prepared by the WI, SI and SASI methods using the CMP as support. The catalysts were tested in the glucose oxidation under microwave assisted heating (similar conditions to the Au/PPO catalysts). Figure 3.19 shows the (a) glucose conversion and (b) gluconic acid yield for the Au/CMP catalysts. The Au/CMP-WI(ACN) catalyst showed 2.3% conversion and gluconic acid yield of 1.8% which were the lowest values observed in this series. This results once again confirm that catalysts synthesized by the WI method are less active than the ones prepared by the immobilization of colloidal nanoparticles (SI and SASI methods). The Au/CMP-SI catalysts showed 52.3% conversion and gluconic acid yield of 48.5%, indicating that the SI method can be an alternative in the preparation of gold catalysts on CMPs or any other material. However, the catalysts prepared by the novel SASI method showed superior activity than the ones prepared by the SI method. The Au/CMP-SASI(DMF-W) catalyst showed 85.3% conversion and gluconic acid yield of 70.6%, whereas the Au/CMP-SASI(ACN-W) showed 86.8% conversion and gluconic acid yield of 71.5%.

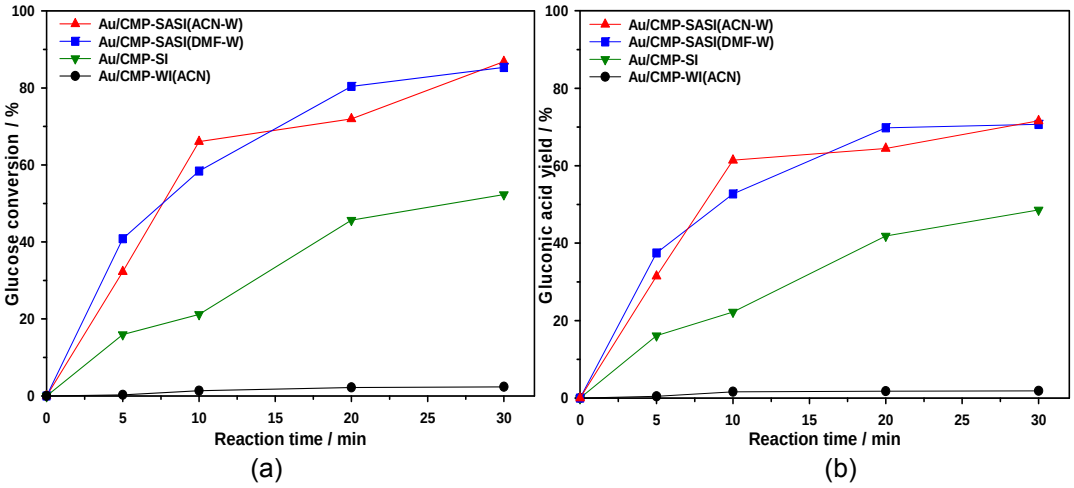

Figure 3.19 Glucose conversion (a) and gluconic acid yield (b) for the Au/CMP catalysts. Reaction conditions: Glucose/Au = 438 molar ratio, T = 130 ºC, Reaction time = 30 min, $P(O_2)$ = 10 bar.

The results showed similar conversion values and yields for the catalysts prepared by the SASI method. This trend could be due to the catalysts are very similar in composition despite the organic solvent used. Indeed, the XPS results (Table 3.11) showed that the Au/CMP-SASI(DMF-W) and Au/CMP-SASI(ACN-W) catalysts presented the $Au^{\delta-}$ and Au^{0} oxidation states at the surface. Although this is an indication that the catalysts present the same chemical species at the surface, other

effects such as particle size and preparation method could play a more important role on the catalytic activity. For a valid comparison, the turnover frequency (TOF) was used to measure the catalytic activity of the materials in the glucose oxidation (Section 2.2). The TOF values were calculated at 5 minutes of reaction time in all cases.

Figure 3.20 shows the TOF values of the CMP- and PPO-supported gold catalysts as a function of the synthesis method and solvent used. The results confirmed that the CMP-supported gold catalysts displayed superior activity than the PPO-based catalysts. The Au/CMP-WI(ACN) showed a TOF of 1.2 min^{-1}, which was the lowest value observed in this series, whereas the Au/CMP-SI catalyst showed a TOF of 131.2 min^{-1}, indicating that the SI method could be a suitable method to prepare gold catalysts using the CMP as support. However, we went one step further and developed the SASI method in order to increase the intrinsic activity (TOF) of the final material. As a result, the Au/CMP-SASI(DMF-W) showed a TOF of 162.7 min^{-1}, whereas the Au/CMP-SASI(ACN-W) showed the highest TOF value (201.8 min^{-1}) among the catalysts tested in this series and even more active than the Au/PPO-SI with a TOF of 68.8 min^{-1}

In the literature, the oxidation of glucose using polymers as supports for the gold nanoparticles has attracted limited attention due to the low conversion values and poor stability of the catalysts compared to metal oxides or carbon as supports [96-105].

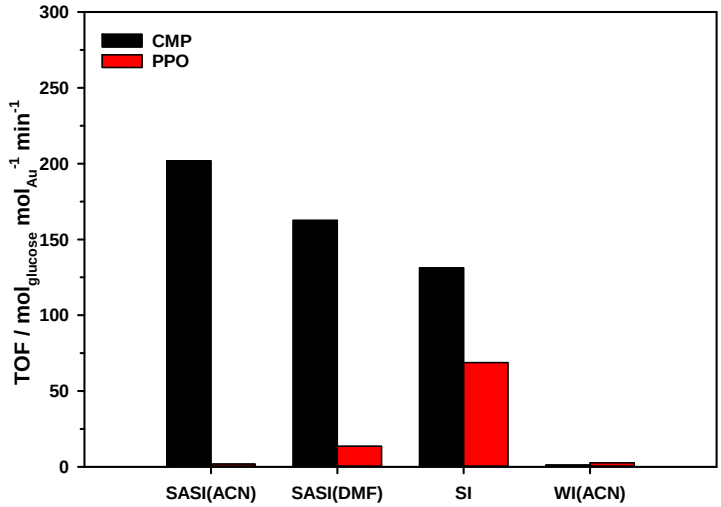

Figure 3.20 TOF values for the glucose oxidation in the presence of the Au/CMP and Au/PPO catalysts. Reaction conditions: Glucose/Au = 438 molar ratio, T = 130 ºC, $P(O_2)$ = 10 bar. TOF values were calculated at 5 minutes reaction time. TOF = $\frac{Moles\ of\ Glucose\ converted}{\text{Moles of metal} \times \text{time}}$

To the best of our knowledge, some groups have attempted the oxidation of glucose using polymeric materials as supports. Biffis et al. [107] reported the glucose oxidation using gold nanoclusters (2.5 nm) stabilized by polymer microgel supports at 50 °C and pH 9.5, obtaining a modest TOF of 7.5 min^{-1}. However, Ishida et al. [108] reported that gold nanoparticles supported on basic anion-exchange resins such as quaternary ammonium salt ($–N^{+}Me_3$) showed a TOF of 450 min^{-1} in the glucose oxidation at 60 °C and pH 9.5. Comparing the results reported by Biffis et al. [107] and Ishida et al [108], it is clear that the use of molecular oxygen and alkaline conditions promote the oxidation reaction. Nevertheless, the Au/CMP-SASI(ACN-W) catalyst showed better results in terms of catalytic activity (TOF = 201.8 min^{-1}) than the catalyst (TOF = 7.5 min^{-1}) reported by Biffis et al. [107] but it was less active than the catalyst (TOF = 450 min^{-1}) prepared by Ishida et al. [108], where the reactions conditions were carefully selected to obtain high TOF values (0.1 wt% Au catalyst, and glucose/Au = 32,000 molar ratio).

In Table 3.13 are reported several supports (metal oxides or carbon-based materials) which have been investigated using gold nanoparticles in the glucose oxidation. Among catalysts, gold supported on carbon (Au/C) has shown to be very active for the base-free glucose oxidation as reported by Biella et al. [5]. The catalyst showed total conversion and 100% selectivity to gluconic acid after 6 hours. However, leaching of the metal and changes in particle size were the main disadvantages of this catalyst. Other supports have been also studied in the glucose oxidation but different catalytic activities were reported, indicating that factors such as the synthesis method and metal-support interactions could affect the final material. Nevertheless, the SASI method has demonstrated that metal nanoparticles can be loaded on conjugated microporous polymers and the glucose oxidation reaction represents the first example of a gold-catalysed selective oxidation using synthetic organic networks as supports.

Table 3.13 Catalytic transformation of glucose to gluconic acid with molecular oxygen as the oxidant using gold catalysts under base-free conditions.

Catalyst	Catalyst ratio	Oxidant	T (°C)	Time (h)	Con. (%)	Selec. (%)	Ref.
Au/C	1000	3 bar O_2	100	6	100	100	[5]
Au/TiO_2	438	3 bar O_2	160	1	88	95	[109]
Au/Al_2O_3	100	1 bar O_2	120	18	76	95	[110]
Au/graphite	100	3 bar O_2	110	2	55	84	[104]
Au/CeO_2	140	2.3 bar O_2	65	2	77	98	[106]
Au/CMP-SASI(ACN-W)	438	10 bar O_2	130	0.5	87	89	This work

3.2.4.2 Optimisation of the Au/CMP-SASI(ACN-W) catalyst

As shown in Figures 3.19 and 3.20 the Au/CMP-SASI(ACN-W) catalyst displayed the best catalytic performance and intrinsic activity among the gold catalysts prepared. In this section, the optimisation of the catalyst preparation by the SASI method will be presented and evaluated in the glucose oxidation reaction. The optimisation of the catalyst is required in order to improve the catalytic performance of the final material and make it more attractive for its application in other reactions.

3.2.4.2.1 Effect of the Temperature on the Synthesis Method

The effect of the temperature on the preparation of the Au/CMP-SASI(ACN-W) catalyst was explored and the catalysts prepared were tested in the oxidation of glucose under identical reaction conditions. As described in Section 3.2.2.3, the SASI method (Figure 3.6) consists of three separate steps which are: 1) Preparation of the colloidal solution, 2) swelling of the polymer with an organic solvent under heat treatment and 3) immobilisation of the colloid onto the support. In the SASI method, the effect of temperature starts during the second step when the swelling of the polymer is carried out under thermal treatment with the aim of improving the diffusion of the metal nanoparticles onto the porous network. In this section, the effect of the temperature on the swelling of the polymer (step 2) was examined during the preparation of the catalyst.

The Au/CMP-SASI(ACN-W) catalyst presented in section 3.2.4.1 was synthesized as follows : The support (CMP, 0.1 g) was suspended in ACN (15 mL) and treated at 90 °C for 30 minutes under reflux conditions (step 2), then the immobilisation of the colloidal solution was carried out at the same temperature (90 °C) under reflux conditions for 30 minutes (step 3). For the catalysts prepared in this section, the temperature was modified during the steps 2 and 3. The Au/CMP-SASI(ACN-W)-RT catalyst was prepared at room temperature without reflux conditions during the steps 2 and 3, whereas the Au/CMP-SASI(ACN-W)-45°C catalyst was prepared at 45 °C, the temperature was the same during the steps 2 and 3, and no reflux conditions were used. Finally, the Au/CMP-SASI(ACN-W)-90°C

was prepared at 90 °C, the temperature was the same during the steps 2 and 3, and reflux conditions were used during the synthesis.

Table 3.14 shows the ICP-OES analysis of the Au/CMP-SASI(ACN-W)-RT, Au/CMP-SASI(ACN-W)-45°C and Au/CMP-SASI(ACN-W)-90°C catalysts. The results showed similar metal content in all cases, indicating that the temperature has no effect on the immobilisation of the colloidal gold nanoparticles.

Table 3.14 Solid UV-Vis and ICP-OES analysis for the Au/CMP-SASI(ACN-W) catalysts prepared by the SASI method at different temperatures.

Catalyst	T/ °C	$[Au]_{nominal}$ / wt%	$[Au]_{real}$ / wt%	$UV_{\lambda max}$ / nm	TOF[d]
Au/CMP-SASI(ACN-W)[b]	90[a]	2	2.23	534	273.6
	45[a]	2	2.32	532	275.4
	RT[c]	2	2.33	530	190.7

[a] Thermal treatment = 30 min., [b] Immobilisation time = 30 min., [c] RT = Room temperature and no reflux. [d] TOF values were calculated at 5 minutes reaction time, TOF = (Moles of glucose converted)/(Moles of metal x Time).

Solid UV-Vis analysis was carried out on the Au/CMP catalysts prepared at different temperatures as shown in Figure 3.21. The DR UV-Vis spectra of the Au/CMP catalysts showed the presence of the surface plasmon resonance (SPR) band of gold in the range between 530 and 534 nm (Table 3.14), indicating the presence of gold nanoparticles [58-65]. In all cases, a red shift was observed in the plasmonic peaks with respect to the SPR band (516 nm) of the gold nanoparticles in the colloidal solution. The SPR bands of the catalysts were located at similar position (Table 3.14), which might indicate that the particle size was the same in all cases.

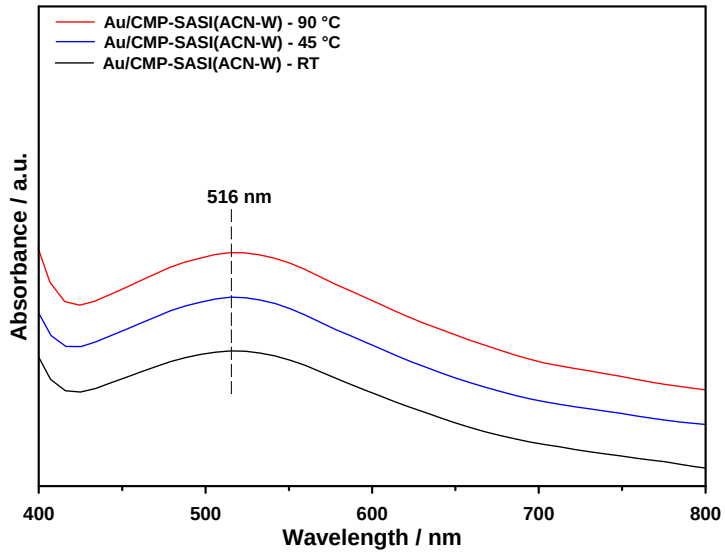

Figure 3.21 UV-Vis spectra of the Au/CMP catalysts prepared by SASI method at different temperatures.

Figure 3.22 shows the catalytic results in the oxidation of glucose at 5 minutes of reaction time with the catalysts prepared. The Au/CMP-SASI(ACN-W)-RT catalyst showed a glucose conversion of 42.8% and gluconic acid yield of 38.3%. The Au/CMP-SASI(ACN-W)-45°C showed 61.7% conversion and 56.1% gluconic acid yield, whereas the Au/CMP-SASI(ACN-W)-90°C displayed 58.9% conversion and gluconic acid yield of 55%. Therefore, it is clear that the catalytic activity of the gold nanoparticles was influenced by the effect of the temperature on the synthesis method. In particular, the catalyst synthesized at room temperature showed the lowest conversion and selectivity. Meanwhile, the Au/CMP-SASI(ACN-W)-45°C and Au/CMP-SASI(ACN-W)-90°C showed very similar values of conversion, selectivity and TOF (Table 3.14). The results showed that the temperature has an effect during the preparation of the catalyst as the final samples displayed different activity. This phenom requires more investigation but we can speculate that the immobilisation of the gold nanoparticles is really fast, and the use of high temperature might help to solubilise the stabilizer agent (PVA) present on the nanoparticles, resulting in gold nanoparticles with different activity. This speculation could be in agreement with previous reports [1], however, it needs to be demonstrated.

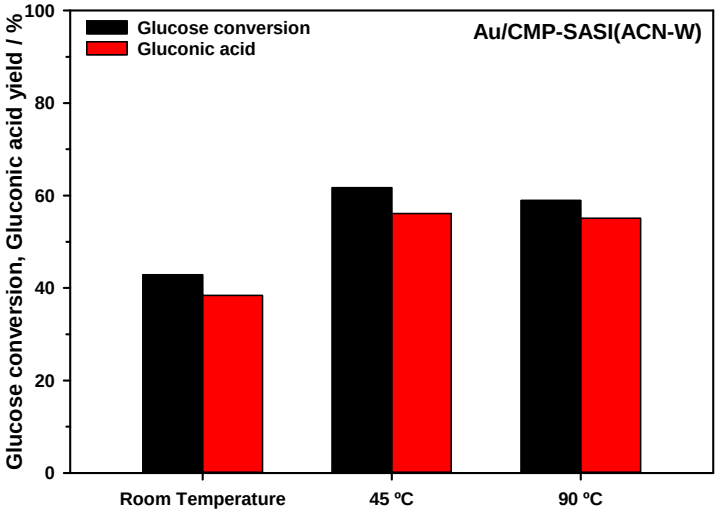

Figure 3.22 Influence of the temperature on the SASI method. Reaction conditions: Glucose/Au = 438 molar ratio, T = 130 ºC, $P(O_2)$ = 10 bar.

3.2.4.2.2 Effect of the Immobilisation Time

The catalysts presented in section 3.2.4.2.1 were synthesized as follows : The support (CMP, 0.1 g) was suspended in ACN (15 mL) and treated at 90 °C for 30 minutes under reflux conditions (step 2), then the immobilisation of the colloidal solution was carried out at the same temperature (90 °C) under reflux conditions for 30 minutes (step 3). The catalysts prepared in this section followed the same procedure described above but the immobilisation was carried out at different times during the step 3 (t = 0.5, 2, 5 and 24 hours). The temperature was fixed at 90 °C, based on the assumption that high temperature might help to solubilise the stabilizer agent (PVA). The fresh catalysts were tested in the oxidation of glucose under identical reaction conditions.

Table 3.15 shows the ICP-OES analysis of the fresh catalysts prepared by the SASI method at different immobilisation times. The results showed that desired metal content was achieved in all cases, although some catalysts presented slightly high metal content due to the experimental error during the synthesis.

Table 3.15 Solid UV-Vis and ICP-OES analysis for the Au/CMP-SASI(ACN-W) catalysts prepared by the SASI method at different immobilisation times.

Catalysts	Time / hr	$[Au]_{nominal}$ / wt%	$[Au]_{real}$ / wt%	$UV_{\lambda max}$ / nm
Au/CMP-SASI(ACN)[a]	0.5	2	2.23	534
	2	2	2.19	530
	5	2	2.33	541
	24	2	2.43	536

[a] Thermal treatment = 30 min. with ACN and reflux conditions at 90^0C.

Figure 3.23 shows the solid UV-Vis analysis of the Au/CMP catalysts prepared by the SASI method at different immobilisation times. The UV-Vis spectra of the Au/CMP catalysts showed the presence of the SPR band of gold in the range between 530 and 541 nm (Table 3.15), indicating the presence of gold nanoparticles [58-65]. The catalysts presented a red shift in all cases with respect to the SPR band (516 nm) of the gold nanoparticles in the colloidal solution. The SPR band of the catalysts were observed at different positions which might indicate that the catalysts presented different particle size.

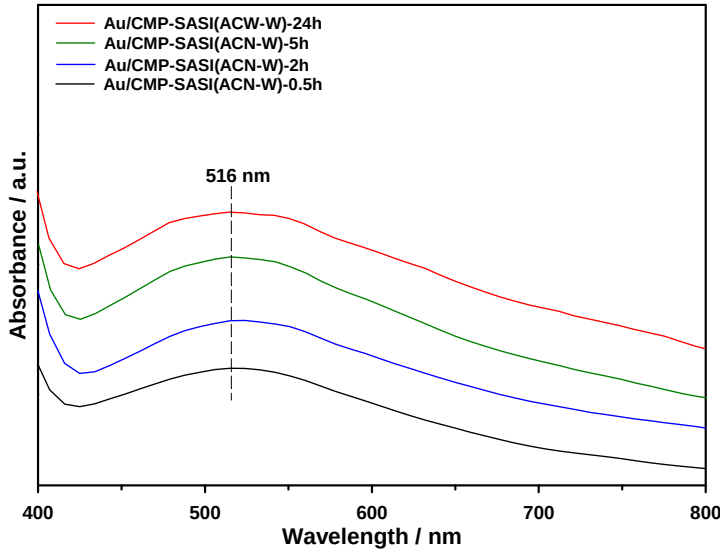

Figure 3.23 Solid UV-Vis spectra of the Au/CMP catalysts prepared by SASI method at different immobilisation times.

Figure 3.24 shows the effect of the immobilisation time on the preparation of the Au/CMP catalysts by the SASI method for the glucose oxidation at 5 minutes of reaction time. The results showed that the Au/CMP-SASI(ACN-W)-0.5h catalyst presented the lowest catalytic activity in this series with a TOF of 201.8 min^{-1} whilst the Au/CMP-SASI(ACN-W)-2h catalyst showed the highest catalytic activity with a TOF of 327.8 min^{-1}. The glucose conversion and gluconic acid yield were also dependent on the immobilization time and the highest values were observed for the Au/CMP-SASI(ACN-W)-2h catalyst with 69.2% conversion and 67.2% gluconic acid yield.

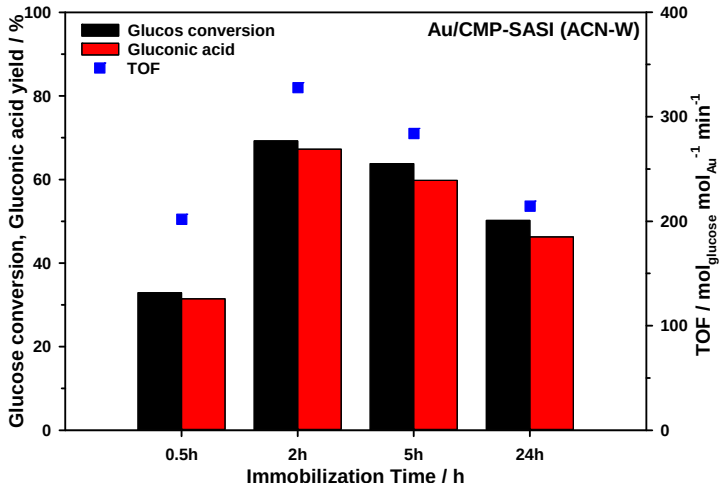

Figure 3.24 Effect of the immobilisation time on the preparation of the Au/CMP catalysts. Reaction conditions: Glucose/Au = 438 molar ratio, T = 130 ºC, $P(O_2)$ = 10 bar. TOF values were calculated at 5 minutes reaction time. TOF = $\frac{Moles\ of\ Glucose\ converted}{\text{Moles of metal} \times \text{time}}$

Although the catalysts presented slightly different metal content the results showed that the catalytic activity of the Au/CMP catalysts was mainly affected by the variation of the immobilisation time. Several explanations could be hypothesized in order to explain the differences observed on the catalytic activity of the Au/CMP catalysts. (i) Due to the preparation method implies the use of moderate temperature (90 °C), longer immobilisation times might help to solubilise the protecting agent (PVA) causing changes in the particle size and therefore affecting the catalytic activity, whereas (ii) at short times (below 2 hours) the amount of the protecting agent could be sufficient to limit the activity of the gold nanoparticles. (iii) As acetonitrile was used to improve the swellability of the polymer, longer immobilisation times might allow more metal nanoparticles to be deposited into the porous network affecting the availability of active sites. These speculations might be useful to understand the effect of the immobilisation time on the catalytic activity, however, they need to be demonstrated.

3.2.4.2.3 Effect of the Metal Loading

Gold catalysts were synthesized by the SASI method with different metal loadings (0.5, 1, 2 and 3 wt %) and tested in the oxidation of glucose under the following reaction conditions: temperature = 130 °C, pressure = 10 bar, reaction time = 30 minutes and glucose/Au = 438 molar ratio (the catalyst amount was adjusted according the metal loading to maintain the same substrate/metal ratio in all cases). The catalysts were synthesized using the optimal parameters determined in the previous sections: the support (0.1g) is suspended in ACN (15 mL) and treated at reflux conditions (90 °C) for 30 minutes (step 2), then the colloidal solution is added and the mixture is stirred for 2 hours (immobilisation time, step 3) at 90 °C.

The ICP-OES analysis of the catalysts prepared by the SASI method is reported in Table 3.16. The results showed that the CMP support was loaded with the desired metal content up to 3 wt %, indicating that the SASI method is a suitable technique to deposit gold nanoparticles onto conjugated microporous polymers.

Table 3.16 Solid UV-Vis and ICP-OES analysis for the Au/CMP-SASI(ACN-W) catalysts prepared by the SASI method with different metal loadings.

Catalysts	$[Au]_{nominal}$ / wt%	$[Au]_{real}$ / wt%	$UV_{\lambda max}$ / nm
Au/CMP-SASI(ACN)[a]	0.5	0.57	525
	1	1.18	536
	2	2.19	530
	3	3.39	528

[a] Thermal treatment = 30 min. with ACN at reflux conditions (90 ^{0}C), Immobilisation time = 2 hours.

Figure 3.25 shows the solid UV-Vis analysis of the Au/CMP catalysts prepared by the SASI method with different metal loadings. The UV-Vis spectra of the gold catalysts shows plasmonic peaks between 525 and 536 nm (Table 3.16), indicating the presence of gold nanoparticles [58-65]. All catalysts presented a red shift with respect to the SPR band (516 nm) of the gold nanoparticles in solution. The presence of plasmonic peaks at different wavelengths might indicate gold particles with different sizes. Moreover, the solid UV-Vis spectra of the Au/CMP catalysts showed that the SPR band was amplified as the gold content increased from 0.5 to 3 wt %. However, the position of the SPR band and its intensity could also depend on the particle size and shape, therefore, the solid UV-Vis analysis should be interpreted with caution.

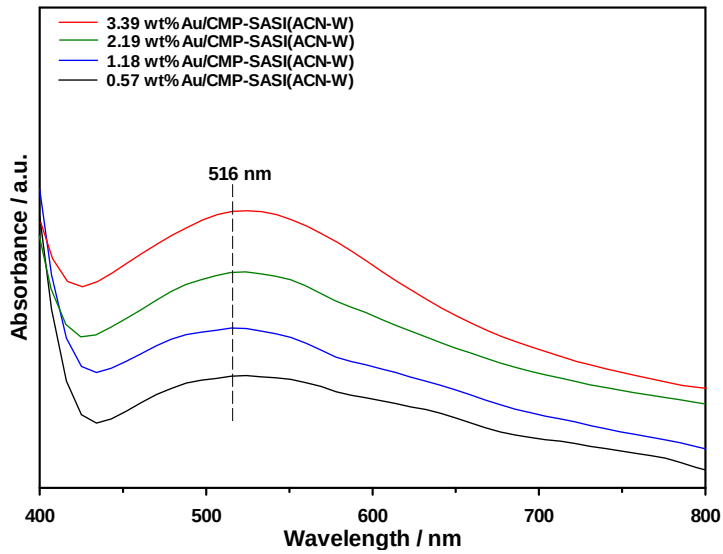

Figure 3.25 Solid UV-Vis spectra of the Au/CMP catalysts prepared by SASI method with different metal loading.

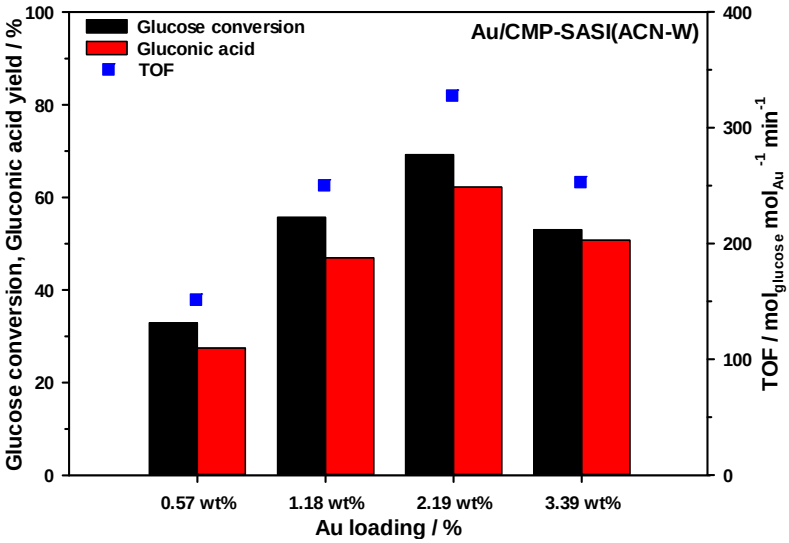

Figure 3.26 Effect of the metal loading on the oxidation of glucose catalysed by the CMP-supported gold catalysts. Reaction conditions: Glucose/Au = 438 molar ratio, T = 130 ºC, P(O_2) = 10 bar. TOF values were calculated at 5 minutes reaction time. TOF = $\frac{Moles\ of\ Glucose\ converted}{\text{Moles of metal} \times \text{time}}$

Figure 3.26 shows the catalytic results for the gold catalysts as function of the gold content. The 2.19 wt% Au/CMP-SASI(ACN-W) catalyst showed the highest activity with a TOF of 327.7 min^{-1}, whereas the 0.57 wt% Au/CMP-SASI(ACN-W) displayed the lowest activity with a TOF of 151.4 min^{-1}. Surprisingly, the 1.18 wt% Au/CMP-SASI(ACN-W) catalyst showed similar activity (TOF = 250.2 min^{-1}) to the 3.39 wt% Au/CMP-SASI(ACN-W) (TOF = 253 min^{-1}). A possible explanation for the low activity of the 3.39 wt% Au/CMP-SASI(ACN-W) catalyst could be associated to particle agglomeration due to the high metal loading. The glucose conversion and gluconic acid yield showed the same trend as the TOF where the 2.19 wt% Au/CMP-SASI(ACN-W) catalyst demonstrated to be the most active catalysts for the oxidation of glucose.

3.2.4.2.4 Catalyst Reusability

Given the improvement in the preparation of CMP-supported gold catalysts by the SASI method, recycling studies for the 2 wt% Au/CMP-SASI(ACN-W) catalyst were carried out. The catalyst was prepared using the optimal conditions determined in previous sections. The recycling tests were carried out using the SynthWAVE microwave reactor (Section 2.9.2.2) at 130^0C and 10 Bar of oxygen pressure. The catalyst (50 mg) catalyst was added to 5 mL of a glucose stock solution and placed in a 40 mL glass vial. The reaction mixture was vented three times with nitrogen gas before reaction, then it was vent two times with oxygen gas and finally the system was pressurized at 10 Bar of oxygen pressure. After reactions conditions, the reaction mixture was centrifuge for 5 minutes in order to separate the catalyst from the liquid phase, then a liquid sample was taken for the HPLC analysis (Section 2.8.1).

The mixture containing the spent catalyst was filtrated and washed three times with deionised water. Finally, the washed catalyst was dried overnight at 110 ^{0}C and then ground. The first run was performed by running three simultaneous reactions, then the recovered catalyst was treated following the previously mentioned procedure, and then it was used in a second run for two simultaneous reactions. After reaction, the catalyst was treated following the same procedure. For the third run, one reaction was performed. The oxidation of glucose was carried out for 20 minutes where the gluconic acid displayed the highest yield.

Table 3.17 Recycling tests of the 2 wt% Au/CMP-SASI(ACN-W) catalyst prepared by the SASI method for the oxidation of glucose to gluconic acid.[a]

Catalyst	Run	Conv. (%)	Product yield for the glucose oxidation (%)			
			Gluconic acid	Tartronic acid	Glycolic acid	Formic acid
Au/CMP-SASI(ACN-W)	1	90.3	71.7	3.12	0.46	4.14
	1	90.4	72.0	3.18	0.45	4.62
	1	90.0	71.7	3.08	0.47	3.89
	2	91.2	69.0	3.14	0.46	4.40
	2	91.3	70.5	3.19	0.54	4.14
	3	90.3	67.2	3.29	0.60	4.66

[a] Reaction conditions: Glucose/Au = 438 molar ratio, T = 130 ºC, P(O_2) = 10 Bar, Reaction time = 20 min.

The glucose conversion and product yield are shown in Table 3.17. The results once again have demonstrated that the 2 wt% Au/CMP-SASI(ACN-W) catalyst effectively transform glucose to gluconic acid without losing activity and stability after several reuses. Moreover, the ICP analysis showed that metal leaching was not observed during the experiments as shown in Table 3.18.

Table 3.18 Metal amount determined by the ICP-OES analysis before and after catalyst reusability [a].

Catalyst	Run	$[Au]_{real}$ / wt%	$[Pd]_{real}$ / wt%
Au/CMP-SASI(ACN-W)	Fresh	2.16	1.38
	1	2.15	1.37
	2	2.15	1.35
	3	2.15	1.33

3.3 Conclusions

In this chapter, we have investigated for the first time the utilisation of porous polymers as supports for the gold catalysts in the glucose oxidation reaction. The conjugated microporous polymer CMP-1 [39] and poly(2,6-dimethyl-1,4-phenylene oxide) (PPO, commercial polymer) were used as supports for the gold nanoparticles. To prepare the catalysts, we have developed the solvent-assisted sol immobilisation (SASI) method where the use of an organic solvent (dimethylformamide or acetonitrile) is essential to improve the swellability of the polymers allowing the immobilization of the gold nanoparticles into the support material.

The SASI method was compared with conventional methods such as the traditional sol immobilisation-SI and wet impregnation-WI. The catalytic results showed that the SASI method produced the most active catalysts among the preparation methods. With the addition of dimethylformamide as solvent, higher metal loading were achieved, however, the use of acetonitrile produced gold catalysts with superior activity. Recycling studies of the Au/CMP-SASI(ACN-W) catalyst demonstrated that the catalytic activity prevails after several reuses.

The XPS analysis showed that the predominant species were $Au^{\delta-}$ sites, which are associated with the electron transfer from the support to the gold nanoparticles. This assumption could be supported by the fact that the CMP and PPO supports present aromaticity in their structure which could contribute by donating electron density, although the presence of an electronegative oxidation state ($Au^{\delta-}$) is still under discussion in the literature, this work shows its presence.

Therefore, this work has demonstrated that porous polymers can serve as support materials for catalytic applications and the preparation method is of great importance as it can affect the catalytic performance of the final material.

3.4 References

[1] J.A. Lopez-Sanchez, N. Dimitratos, C. Hammond, G.L. Brett, L. Kesavan, S. White, P. Miedziak, R. Tiruvalam, R.L. Jenkins, A.F. Carley, D. Knight, C.J. Kiely, G.J. Hutchings, Facile removal of stabilizer-ligands from supported gold nanoparticles, Nat. Chem., 3 (2011) 551.

[2] A. Villa, G.M. Veith, L. Prati, Selective Oxidation of Glycerol under Acidic Conditions Using Gold Catalysts, Angew. Chem. Int. Ed., 49 (2010) 4499-4502.

[3] A. Villa, C.E. Chan-Thaw, G.M. Veith, K.L. More, D. Ferri, L. Prati, Au on Nanosized NiO: A Cooperative Effect between Au and Nanosized NiO in the Base-Free Alcohol Oxidation, ChemCatChem, 3 (2011) 1612-1618.

[4] L. Prati, A. Villa, C.E. Chan-Thaw, R. Arrigo, D. Wang, D.S. Su, Gold catalyzed liquid phase oxidation of alcohol: the issue of selectivity, Faraday Discuss., 152 (2011) 353-365.

[5] S. Biella, L. Prati, M. Rossi, Selective Oxidation of D-Glucose on Gold Catalyst, J. Catal., 206 (2002) 242-247.

[6] J. Kennedy, W. Jones, D.J. Morgan, M. Bowker, L. Lu, C.J. Kiely, P.P. Wells, N. Dimitratos, Photocatalytic hydrogen production by reforming of methanol using Au/TiO_2, Ag/TiO_2 and $Au-Ag/TiO_2$ catalysts, Catal. Struct. React., 1 (2015) 35-43.

[7] N. Dimitratos, C.D. Pina, E. Falletta, C.L. Bianchi, V. Dal Santo, M. Rossi, Effect of Au in $Cs_{2.5}H_{1.5}PVMo_{11}O_{40}$ and $Cs_{2.5}H_{1.5}PVMo_{11}O_{40}/Au/TiO_2$ catalysts in the gas phase oxidation of propylene, Catal. Today, 122 (2007) 307-316.

[8] M. Comotti, W.-C. Li, B. Spliethoff, F. Schüth, Support Effect in High Activity Gold Catalysts for CO Oxidation, J. Am. Chem. Soc., 128 (2006) 917-924.

[9] S. Campisi, C.E. Chan-Thaw, D. Wang, A. Villa, L. Prati, Metal nanoparticles on carbon based supports: The effect of the protective agent removal, Catal. Today, 278 (2016) 91-96.

[10] D. Li, C. Wang, D. Tripkovic, S. Sun, N.M. Markovic, V.R. Stamenkovic, Surfactant Removal for Colloidal Nanoparticles from Solution Synthesis: The Effect on Catalytic Performance, ACS Catal., 2 (2012) 1358-1362.

[11] A. Villa, D. Wang, G.M. Veith, F. Vindigni, L. Prati, Sol immobilization technique: a delicate balance between activity, selectivity and stability of gold catalysts, Catal. Sci. Technol., 3 (2013) 3036-3041.

[12] A. Villa, D. Wang, D.S. Su, L. Prati, Gold Sols as Catalysts for Glycerol Oxidation: The Role of Stabilizer, ChemCatChem, 1 (2009) 510-514.

[13] M.-A. Neouze, U. Schubert, Surface Modification and Functionalization of Metal and Metal Oxide Nanoparticles by Organic Ligands, Monatsh Chem, 139 (2008) 183-195.

[14] R.M. Rioux, H. Song, M. Grass, S. Habas, K. Niesz, J.D. Hoefelmeyer, P. Yang, G.A. Somorjai, Monodisperse platinum nanoparticles of well-defined shape: synthesis, characterization, catalytic properties and future prospects, Top Catal, 39 (2006) 167-174.

[15] J. Shen, X. Yin, D. Karpuzov, N. Semagina, PVP-stabilized mono- and bimetallic Ru nanoparticles for selective ring opening, Catal. Sci. Technol., 3 (2013) 208-221.

[16] C. Aliaga, J.Y. Park, Y. Yamada, H.S. Lee, C.-K. Tsung, P. Yang, G.A. Somorjai, Sum Frequency Generation and Catalytic Reaction Studies of the Removal of Organic Capping Agents from Pt Nanoparticles by UV−Ozone Treatment, J. Phys. Chem. C, 113 (2009) 6150-6155.

[17] P. Shufeng, K. Yousuke, K. Takeshi, K. Takeshi, Decomposition of Monolayer Coverage on Gold Nanoparticles by UV/ozone Treatment, Chem. Lett., 34 (2005) 544-545.

[18] W. Chen, J. Kim, S. Sun, S. Chen, Electro-oxidation of formic acid catalyzed by FePt nanoparticles, Phys. Chem. Chem. Phys., 8 (2006) 2779-2786.

[19] J. Gun, D. Rizkov, O. Lev, M.H. Abouzar, A. Poghossian, M.J. Schöning, Oxygen plasma-treated gold nanoparticle-based field-effect devices as transducer structures for bio-chemical sensing, Microchim. Acta, 164 (2009) 395-404.

[20] J.-D. Grunwaldt, C. Kiener, C. Wögerbauer, A. Baiker, Preparation of Supported Gold Catalysts for Low-Temperature CO Oxidation via “Size-Controlled” Gold Colloids, J. Catal., 181 (1999) 223-232.

[21] H. Shi, N. Xu, D. Zhao, B.-Q. Xu, Immobilized PVA-stabilized gold nanoparticles on silica show an unusual selectivity in the hydrogenation of cinnamaldehyde, Catal. Commun., 9 (2008) 1949-1954.

[22] P. Botella, A. Corma, M.T. Navarro, Single Gold Nanoparticles Encapsulated in Monodispersed Regular Spheres of Mesostructured Silica Produced by Pseudomorphic Transformation, Chem. Mater., 19 (2007) 1979-1983.

[23] J. Xie, Y. Wang, Y. Li, Y. Wei, Self-assembly preparation of Au/SiO2 catalyst and its catalysis for cyclohexane oxidation with air, Reac Kinet Mech Cat, 102 (2011) 143-154.

[24] J. Zhu, J.L. Figueiredo, J.L. Faria, Au/activated-carbon catalysts for selective oxidation of alcohols with molecular oxygen under atmospheric pressure: Role of basicity, Catal. Commun., 9 (2008) 2395-2397.

[25] J.P. Gabaldon, M. Bore, A.K. Datye, Mesoporous silica supports for improved thermal stability in supported Au catalysts, Top Catal, 44 (2007) 253-262.

[26] B. Lee, Z. Ma, Z. Zhang, C. Park, S. Dai, Influences of synthesis conditions and mesoporous structures on the gold nanoparticles supported on mesoporous silica hosts, Microporous Mesoporous Mater., 122 (2009) 160-167.

[27] M. Okumura, S. Nakamura, S. Tsubota, T. Nakamura, M. Azuma, M. Haruta, Chemical vapor deposition of gold on Al_2O_3, SiO_2, and TiO_2 for the oxidation of CO and of H_2, Catal. Lett., 51 (1998) 53-58.

[28] M. Okumura, S. Tsubota, M. Haruta, Preparation of supported gold catalysts by gas-phase grafting of gold acethylacetonate for low-temperature oxidation of CO and of H_2, J. Mol. Catal. A: Chem., 199 (2003) 73-84.

[29] M.M. Schubert, S. Hackenberg, A.C. van Veen, M. Muhler, V. Plzak, R.J. Behm, CO Oxidation over Supported Gold Catalysts—"Inert" and "Active" Support Materials and Their Role for the Oxygen Supply during Reaction, J. Catal., 197 (2001) 113-122.

[30] M. Haruta, N. Yamada, T. Kobayashi, S. Iijima, Gold catalysts prepared by coprecipitation for low-temperature oxidation of hydrogen and of carbon monoxide, J. Catal., 115 (1989) 301-309.

[31] M. Haruta, S. Tsubota, T. Kobayashi, H. Kageyama, M.J. Genet, B. Delmon, Low-Temperature Oxidation of CO over Gold Supported on TiO_2, α-Fe_2O_3, and Co_3O_4, J. Catal., 144 (1993) 175-192.

[32] M. Haruta, Size- and support-dependency in the catalysis of gold, Catal. Today, 36 (1997) 153-166.

[33] T. Hasell, C.D. Wood, R. Clowes, J.T.A. Jones, Y.Z. Khimyak, D.J. Adams, A.I. Cooper, Palladium Nanoparticle Incorporation in Conjugated Microporous Polymers by Supercritical Fluid Processing, Chemistry of Materials, 22 (2010) 557-564.

[34] T. Ishida, Y. Onuma, K. Kinjo, A. Hamasaki, H. Ohashi, T. Honma, T. Akita, T. Yokoyama, M. Tokunaga, M. Haruta, Preparation of microporous polymer-encapsulated Pd nanoparticles and their catalytic performance for hydrogenation and oxidation, Tetrahedron, 70 (2014) 6150-6155.

[35] J. Schmidt, J. Weber, J.D. Epping, M. Antonietti, A. Thomas, Microporous Conjugated Poly(thienylene arylene) Networks, Adv. Mater., 21 (2009) 702-705.

[36] R. Dawson, A. Laybourn, R. Clowes, Y.Z. Khimyak, D.J. Adams, A.I. Cooper, Functionalized Conjugated Microporous Polymers, Macromolecules, 42 (2009) 8809-8816.

[37] M. Türk, C. Erkey, Synthesis of supported nanoparticles in supercritical fluids by supercritical fluid reactive deposition: Current state, further perspectives and needs, J. Supercrit. Fluids, 134 (2018) 176-183.

[38] L. Prati, A. Villa, The Art of Manufacturing Gold Catalysts, Catalysts, 2 (2012) 24.

[39] R.S. Sprick, J.-X. Jiang, B. Bonillo, S. Ren, T. Ratvijitvech, P. Guiglion, M.A. Zwijnenburg, D.J. Adams, A.I. Cooper, Tunable Organic Photocatalysts for Visible-Light-Driven Hydrogen Evolution, J. Am. Chem. Soc., 137 (2015) 3265-3270.

[40] W. Huang, L. Su, Z. Bo, Hyperbranched Polymers with a Degree of Branching of 100% Prepared by Catalyst Transfer Suzuki−Miyaura Polycondensation, J. Am. Chem. Soc., 131 (2009) 10348-10349.

[41] K. S. W. Sing, D. H. Everett, R. A. W. Haul, L. Moscou, R. A. Pierotti, J. Rouquerol, T. Siemieniewska, Reporting physisorption data for gas/solid systems with special reference to the determination of surface area and porosity, Pure Appl. Chem., 57 (1985) 603-619.

[42] R.S. Sprick, B. Bonillo, M. Sachs, R. Clowes, J.R. Durrant, D.J. Adams, A.I. Cooper, Extended conjugated microporous polymers for photocatalytic hydrogen evolution from water, Chem. Commun., 52 (2016) 10008-10011.

[43] S. Yanagida, A. Kabumoto, K. Mizumoto, C. Pac, K. Yoshino, Poly(p-phenylene)-catalysed photoreduction of water to hydrogen, J. Chem. Soc., Chem. Commun., (1985) 474-475.

[44] L. Chen, Y. Honsho, S. Seki, D. Jiang, Light-Harvesting Conjugated Microporous Polymers: Rapid and Highly Efficient Flow of Light Energy with a Porous Polyphenylene Framework as Antenna, J. Am. Chem. Soc., 132 (2010) 6742-6748.

[45] G. Bond, C. Louis, D.T. Thompson, Catalysis by Gold, Imperial College Press, Catal. Sci. Series 2006, Vol. 6.

[46] H. Masatake, K. Tetsuhiko, S. Hiroshi, Y. Nobumasa, Novel Gold Catalysts for the Oxidation of Carbon Monoxide at a Temperature far Below 0 °C, Chem. Lett., 16 (1987) 405-408.

[47] G.R. Bamwenda, S. Tsubota, T. Nakamura, M. Haruta, The influence of the preparation methods on the catalytic activity of platinum and gold supported on TiO_2 for CO oxidation, Catal. Lett., 44 (1997) 83-87.

[48] L. Liu, X. Tai, G. Yu, H. Guo, Q. Meng, Gold and silver nanoparticles supported on metal-organic frameworks: a highly active catalyst for three-component coupling reaction, Chem. Res. Chin. Univ., 32 (2016) 443-450.

[49] Y.E. Cheon, M.P. Suh, Enhanced Hydrogen Storage by Palladium Nanoparticles Fabricated in a Redox-Active Metal–Organic Framework, Angew. Chem. Int. Ed., 48 (2009) 2899-2903.

[50] Y. Wei, S. Han, D.A. Walker, P.E. Fuller, B.A. Grzybowski, Nanoparticle Core/Shell Architectures within MOF Crystals Synthesized by Reaction Diffusion, Angew. Chem. Int. Ed., 51 (2012) 7435-7439.

[51] K. Esumi, A. Suzuki, A. Yamahira, K. Torigoe, Role of Poly(amidoamine) Dendrimers for Preparing Nanoparticles of Gold, Platinum, and Silver, Langmuir, 16 (2000) 2604-2608.

[52] Y.-G. Kim, S.-K. Oh, R.M. Crooks, Preparation and Characterization of 1−2 nm Dendrimer-Encapsulated Gold Nanoparticles Having Very Narrow Size Distributions, Chem. Mater., 16 (2004) 167-172.

[53] S. Yang, Y. Wang, Q. Wang, R. Zhang, B. Ding, UV irradiation induced formation of Au nanoparticles at room temperature: The case of pH values, Colloids Surf A Physicochem Eng Asp, 301 (2007) 174-183.

[54] S. Link, M.A. El-Sayed, Size and Temperature Dependence of the Plasmon Absorption of Colloidal Gold Nanoparticles, J. Phys. Chem. B, 103 (1999) 4212-4217.

[55] T. Shimizu, T. Teranishi, S. Hasegawa, M. Miyake, Size Evolution of Alkanethiol-Protected Gold Nanoparticles by Heat Treatment in the Solid State, J. Phys. Chem. B, 107 (2003) 2719-2724.

[56] N. Vo Ke Thanh, N. Hoang Phuong Uyen, H. Trong Phat, T. Nguyen Nguyen Pham, L. Quang Vinh, H. Thanh Dat, Preparation of gold nanoparticles by microwave heating and application of spectroscopy to study conjugate of gold nanoparticles with antibody E. coli O157:H7, Adv. Nat. Sci: Nanosci. Nanotechnol., 6 (2015) 035015.

[57] C. Wilson, M.J. Main, N.J. Cooper, M.E. Briggs, A.I. Cooper, D.J. Adams, Swellable functional hypercrosslinked polymer networks for the uptake of chemical warfare agents, Polymer Chemistry, 8 (2017) 1914-1922.

[58] A.M. Nadeem, G.I.N. Waterhouse, H. Idriss, The reactions of ethanol on TiO2 and Au/TiO2 anatase catalysts, Catal. Today, 182 (2012) 16-24.

[59] Y. Borensztein, L. Delannoy, A. Djedidi, R.G. Barrera, C. Louis, Monitoring of the Plasmon Resonance of Gold Nanoparticles in Au/TiO_2 Catalyst under Oxidative and Reducing Atmospheres, J. Phys. Chem. C, 114 (2010) 9008-9021.

[60] X. Pan, Y.-J. Xu, Fast and spontaneous reduction of gold ions over oxygen-vacancy-rich TiO_2: A novel strategy to design defect-based composite photocatalyst, Appl. Catal. A: Gen., 459 (2013) 34-40.

[61] R. Zanella, S. Giorgio, C.-H. Shin, C.R. Henry, C. Louis, Characterization and reactivity in CO oxidation of gold nanoparticles supported on TiO_2 prepared by deposition-precipitation with NaOH and urea, J. Catal., 222 (2004) 357-367.

[62] Á. Veres, T. Rica, L. Janovák, M. Dömök, N. Buzás, V. Zöllmer, T. Seemann, A. Richardt, I. Dékány, Silver and gold modified plasmonic TiO_2 hybrid films for photocatalytic decomposition of ethanol under visible light, Catal. Today, 181 (2012) 156-162.

[63] M.V. Dozzi, L. Prati, P. Canton, E. Selli, Effects of gold nanoparticles deposition on the photocatalytic activity of titanium dioxide under visible light, Phys.Chem. Chem.Phys., 11 (2009) 7171-7180.

[64] Ş. Neaţu, B. Cojocaru, V.I. Pârvulescu, V. Şomoghi, M. Alvaro, H. Garcia, Visible-light C–heteroatom bond cleavage and detoxification of chemical warfare agents using titania-supported gold nanoparticles as photocatalyst, J. Mater. Chem., 20 (2010) 4050-4054.

[65] J. Sá, S.F.R. Taylor, H. Daly, A. Goguet, R. Tiruvalam, Q. He, C.J. Kiely, G.J. Hutchings, C. Hardacre, Redispersion of Gold Supported on Oxides, ACS Catal., 2 (2012) 552-560.

[66] A. Villa, N. Dimitratos, C.E. Chan-Thaw, C. Hammond, G.M. Veith, D. Wang, M. Manzoli, L. Prati, G.J. Hutchings, Characterisation of gold catalysts, Chem. Soc. Rev., 45 (2016) 4953-4994.

[67] X. Ke, X. Zhang, J. Zhao, S. Sarina, J. Barry, H. Zhu, Selective reductions using visible light photocatalysts of supported gold nanoparticles, Green Chem., 15 (2013) 236-244.

[68] M.H. Majles Ara, Z. Dehghani, R. Sahraei, A. Daneshfar, Z. Javadi, F. Divsar, Diffraction patterns and nonlinear optical properties of gold nanoparticles, J. Quant. Spectrosc. Radiat. Transfer, 113 (2012) 366-372.

[69] Y. Chen, X. Gu, C.-G. Nie, Z.-Y. Jiang, Z.-X. Xie, C.-J. Lin, Shape controlled growth of gold nanoparticles by a solution synthesis, Chem. Commun., (2005) 4181-4183.

[70] N. Vo Ke Thanh, H. Trong Phat, N. Dang Giang, N. Hoang Phuong Uyen, L. Quang Vinh, H. Thanh Dat, Synthesis and spectroscopic characterization of gold nanobipyramids prepared by a chemical reduction method, Adv. Nat. Sci.: Nanosci. Nanotechnol., 6 (2015) 045017.

[71] Y.-F. Han, Z. Zhong, K. Ramesh, F. Chen, L. Chen, Effects of Different Types of γ-Al_2O_3 on the Activity of Gold Nanoparticles for CO Oxidation at Low-Temperatures, J. Phys. Chem. C, 111 (2007) 3163-3170.

[72] A.M. Venezia, V.L. Parola, B. Pawelec, J.L.G. Fierro, Hydrogenation of aromatics over Au-Pd/SiO_2-Al_2O_3 catalysts; support acidity effect, Appl. Catal. A: Gen., 264 (2004) 43-51.

[73] B. Pawelec, A.M. Venezia, V. La Parola, E. Cano-Serrano, J.M. Campos-Martin, J.L.G. Fierro, AuPd alloy formation in Au-Pd/Al_2O_3 catalysts and its role on aromatics hydrogenation, Appl. Surf. Sci., 242 (2005) 380-391.

[74] Z. Suo, C. Ma, M. Jin, T. He, L. An, The active phase of Au–Pd/Al_2O_3 for CO oxidation, Catal. Commun., 9 (2008) 2187-2190.

[75] L. Ilieva, G. Pantaleo, I. Ivanov, R. Zanella, J.W. Sobczak, W. Lisowski, A.M. Venezia, D. Andreeva, Preferential oxidation of CO in H_2 rich stream (PROX) over gold catalysts supported on doped ceria: Effect of water and CO_2, Catal. Today, 175 (2011) 411-419.

[76] C. Pischetola, L. Collado, M. Keane, F. Cárdenas-Lizana, Gas Phase Hydrogenation of Furaldehydes via Coupling with Alcohol Dehydrogenation over Ceria Supported Au-Cu, Molecules, 23 (2018) 2905.

[77] M. Li, X. Wang, F. Cárdenas-Lizana, M.A. Keane, Effect of support redox character on catalytic performance in the gas phase hydrogenation of benzaldehyde and nitrobenzene over supported gold, Catal. Today, 279 (2017) 19-28.

[78] C. Gentilini, F. Evangelista, P. Rudolf, P. Franchi, M. Lucarini, L. Pasquato, Water-Soluble Gold Nanoparticles Protected by Fluorinated Amphiphilic Thiolates, J. Am. Chem. Soc., 130 (2008) 15678-15682.

[79] Y. Du, R. Hu, Y. Jia, Q. Zhou, W. Meng, J. Yang, $CuCl_2$ promoted low-gold-content Au/C catalyst for acetylene hydrochlorination prepared by ultrasonic-assisted impregnation, Journal of Industrial and Engineering Chemistry, 37 (2016) 32-41.

[80] L. Abis, L. Armelao, D. Belli Dell'Amico, F. Calderazzo, F. Garbassi, A. Merigo, E.A. Quadrelli, Gold molecular precursors and gold–silica interactions, J. Chem. Soc., Dalton Trans., (2001) 2704-2709.

[81] S. Underwood, P. Mulvaney, Effect of the Solution Refractive Index on the Color of Gold Colloids, Langmuir, 10 (1994) 3427-3430.

[82] J. Fernández-Lodeiro, B. Rodríguez-González, H.M. Santos, E. Bertolo, J.L. Capelo, A.A. Dos Santos, C. Lodeiro, Unraveling the Organotellurium Chemistry Applied to the Synthesis of Gold Nanomaterials, ACS Omega, 1 (2016) 1314-1325.

[83] I.B.C. Gallo, E.A. Carbonio, H.M. Villullas, What Determines Electrochemical Surface Processes on Carbon-Supported PdAu Nanoparticles?, ACS Catal., 8 (2018) 1818-1827.

[84] S.-Y. Lai, Y. Qiu, S. Wang, Effects of the structure of ceria on the activity of gold/ceria catalysts for the oxidation of carbon monoxide and benzene, J. Catal., 237 (2006) 303-313.

[85] P. Rodriguez, D. Plana, D.J. Fermin, M.T.M. Koper, New insights into the catalytic activity of gold nanoparticles for CO oxidation in electrochemical media, J. Catal., 311 (2014) 182-189.

[86] S. Arrii, F. Morfin, A.J. Renouprez, J.L. Rousset, Oxidation of CO on Gold Supported Catalysts Prepared by Laser Vaporization: Direct Evidence of Support Contribution, J. Am. Chem. Soc., 126 (2004) 1199-1205.

[87] J. Radnik, C. Mohr, P. Claus, On the origin of binding energy shifts of core levels of supported gold nanoparticles and dependence of pretreatment and material synthesis, Physical Chemistry Chemical Physics, 5 (2003) 172-177.

[88] J. Li, C.-y. Liu, Y. Liu, Au/graphene hydrogel: synthesis, characterization and its use for catalytic reduction of 4-nitrophenol, J. Mater. Chem., 22 (2012) 8426-8430.

[89] M. Baron, O. Bondarchuk, D. Stacchiola, S. Shaikhutdinov, H.J. Freund, Interaction of Gold with Cerium Oxide Supports: CeO2(111) Thin Films vs CeOx Nanoparticles, J. Phys. Chem. C, 113 (2009) 6042-6049.

[90] A. Zwijnenburg, A. Goossens, W.G. Sloof, M.W.J. Crajé, A.M. van der Kraan, L. Jos de Jongh, M. Makkee, J.A. Moulijn, XPS and Mössbauer Characterization of Au/TiO2 Propene Epoxidation Catalysts, J. Phys. Chem. B, 106 (2002) 9853-9862.

[91] R. Meyer, C. Lemire, S.K. Shaikhutdinov, H.-J. Freund, Surface chemistry of catalysis by gold, Gold Bull., 37 (2004) 72-124.

[92] M.G. Mason, Electronic structure of supported small metal clusters, Phys. Rev. B, 27 (1983) 748-762.

[93] B.L. Mojet, J.T. Miller, D.E. Ramaker, D.C. Koningsberger, A New Model Describing the Metal–Support Interaction in Noble Metal Catalysts, J. Catal., 186 (1999) 373-386.

[94] Z. Zhang, G.W. Huber, Catalytic oxidation of carbohydrates into organic acids and furan chemicals, Chem. Soc. Rev., 47 (2018) 1351-1390.

[95] M. Besson, P. Gallezot, Selective oxidation of alcohols and aldehydes on metal catalysts, Catalysis Today, 57 (2000) 127-141.

[96] M. Comotti, C.D. Pina, M. Rossi, Mono- and bimetallic catalysts for glucose oxidation, J. Mol. Catal. A: Chem., 251 (2006) 89-92.

[97] M. Comotti, C. Della Pina, E. Falletta, M. Rossi, Aerobic Oxidation of Glucose with Gold Catalyst: Hydrogen Peroxide as Intermediate and Reagent, Adv. Synth. Catal., 348 (2006) 313-316.

[98] U. Prüße, M. Herrmann, C. Baatz, N. Decker, Gold-catalyzed selective glucose oxidation at high glucose concentrations and oxygen partial pressures, Appl. Catal. A. : Gen., 406 (2011) 89-93.

[99] P. Beltrame, M. Comotti, C. Della Pina, M. Rossi, Aerobic oxidation of glucose: II. Catalysis by colloidal gold, Appl. Catal. A. : Gen., 297 (2006) 1-7.

[100] S. Cattaneo, M. Stucchi, A. Villa, L. Prati, Gold Catalysts for the Selective Oxidation of Biomass-Derived Products, ChemCatChem, 0 (2018).

[101] R. Saliger, N. Decker, U. Prüße, d-Glucose oxidation with H_2O_2 on an Au/Al2O3 catalyst, Appl. Catal. B: Environ., 102 (2011) 584-589.

[102] T. Benkó, A. Beck, K. Frey, D.F. Srankó, O. Geszti, G. Sáfrán, B. Maróti, Z. Schay, Bimetallic Ag–Au/SiO_2 catalysts: Formation, structure and synergistic activity in glucose oxidation, Appl. Catal. A: Gen., 479 (2014) 103-111.

[103] P.J. Miedziak, H. Alshammari, S.A. Kondrat, T.J. Clarke, T.E. Davies, M. Morad, D.J. Morgan, D.J. Willock, D.W. Knight, S.H. Taylor, G.J. Hutchings, Base-free glucose oxidation using air with supported gold catalysts, Green Chem., 16 (2014) 3132-3141.

[104] P. Qi, S. Chen, J. Chen, J. Zheng, X. Zheng, Y. Yuan, Catalysis and Reactivation of Ordered Mesoporous Carbon-Supported Gold Nanoparticles for the Base-Free Oxidation of Glucose to Gluconic Acid, ACS Catal., 5 (2015) 2659-2670.

[105] J. Zhang, Z. Li, J. Huang, C. Liu, F. Hong, K. Zheng, G. Li, Size dependence of gold clusters with precise numbers of atoms in aerobic oxidation of d-glucose, Nanoscale, 9 (2017) 16879-16886.

[106] Y. Wang, S. Van de Vyver, K.K. Sharma, Y. Román-Leshkov, Insights into the stability of gold nanoparticles supported on metal oxides for the base-free oxidation of glucose to gluconic acid, Green Chem., 16 (2014) 719-726.

[107] A. Biffis, S. Cunial, P. Spontoni, L. Prati, Microgel-stabilized gold nanoclusters: Powerful “quasi-homogeneous” catalysts for the aerobic oxidation of alcohols in water, J. Catal., 251 (2007) 1-6.

[108] T. Ishida, S. Okamoto, R. Makiyama, M. Haruta, Aerobic oxidation of glucose and 1-phenylethanol over gold nanoparticles directly deposited on ion-exchange resins, Appl. Catal. A: Gen., 353 (2009) 243-248.

[109] Y. Cao, X. Liu, S. Iqbal, P.J. Miedziak, J.K. Edwards, R.D. Armstrong, D.J. Morgan, J. Wang, G.J. Hutchings, Base-free oxidation of glucose to gluconic acid using supported gold catalysts, Catal. Sci. Technol., 6 (2016) 107-117.

[110] C. Megías-Sayago, S. Ivanova, C. López-Cartes, M.A. Centeno, J.A. Odriozola, Gold catalysts screening in base-free aerobic oxidation of glucose to gluconic acid, Catal. Today, 279 (2017) 148-154.

Chapter 4

Catalytic Studies Under Light Irradiation

4.1 Introduction

Glucose is the most abundant and promising monosaccharide which has attracted much attention in recent years. It is a simple molecule which is highly water-soluble and more reactive than other complex polysaccharides. Glucose can be obtained from the depolymerisation of cellulose [1-3] or by enzymatic processes from sucrose [4]. As a feedstock, glucose has been used to produce high-value chemicals and fuels such as sorbitol [5], gluconic acid, glucaric acid, arabitol [6], hydroxymethylfurfural [7], formic acid [8], ethanol [9] and hydrogen [10]. Therefore, glucose is an extremely versatile molecule which can be converted into chemicals and fuels at different conditions. Particularly, the oxidation of glucose to gluconic acid has been widely investigated as the carboxylic acid and its salts are used as a food additive, in pharmaceuticals and soluble detergents [11]. Currently, gluconic acid is produced by fermentation of glucose, however, the accumulation of gluconic acid in the medium affects the microbes function and consequently low yields and reaction rates are observed [12]. An alternative approach for the oxidation of glucose is the use of heterogeneous photocatalysis which has been successfully applied for the selective oxidation of alcohols in the gas [13, 14] and liquid phase [15, 16] with promising results.

The photocatalytic oxidation of glucose was first reported using TiO_2-based photocatalysts [6, 17-20] and more recently metal nanoparticles (i.e., Au, Ag) were used to extend the light absorption of the photocatalyst to the visible region due to the surface plasmon resonance effect (SPR) [21-23]. In 2011 Colmenares et al. [17] reported for the first time the glucose oxidation under UV light using TiO_2-based photocatalysts prepared by an ultrasound-mediated sol-gel synthesis. The catalysts, TiO_2 (US) and TiO_2 (R), were tested and compared to the benchmark material, Degussa (Evonik) P25 (commercial TiO_2) [24]. The TiO_2 (US) photocatalyst displayed the highest selectivity to products such as gluconic acid, glucaric acid and arabitol in the liquid phase while CO_2 was detected in the gas phase. Later, the same authors reported the photocatalytic activity of different materials such as TiO_2 nanoparticles [6], Fe-TiO_2 [20], and Cr-TiO_2 [18], which were supported on zeolite or silica and tested for the oxidation of glucose under UV light. The results showed that the reaction conditions had a strong influence on the product distribution, particularly solvent composition and irradiation time. Gluconic acid and glucaric acid were detected in most cases while arabitol [6] was found under specific conditions.

The photocatalytic transformation of glucose to aldoses (arabinose and erythrose) was reported by Chong et al. [25] using TiO_2-based photocatalysts, however, oxidation products such as gluconic and formic acid were detected. Particularly, gluconic acid was obtained when the Rh/TiO_2-A and Rh/TiO_2-P25 photocatalysts were used. Chong et al. [25] also reported that arabinose and erythrose were formed through the C-C bond cleavage (α-scission) of glucose along with hydrogen and formic acid. The same mechanism (α-scission) was observed for arabinose and erythrose as starting materials.

In 2015 Bellardita et al. [26] reported the preparation of two heteropolyacid-TiO_2 (HPA/TiO_2) composites which were tested for the oxidation of glucose under UV light. The commercial Keggin heteropolyacid ($H_3PW_{12}O_{40}$) and home prepared $K_7PW_{11}O_{39}$ salt were supported on TiO_2. The results showed that products such as gluconic acid, arabinose, erythrose and formic acid were obtained using the HPA/TiO_2 catalysts and bare support (TiO_2). In some cases, traces of products such as glyceraldehyde, glucaric acid and fructose were detected.

The previous work showed that the photocatalytic transformation of glucose can produce a wide range of high-value chemicals. However, the initial studies were carried out under UV light which limits the application of photocatalysis in real conditions (UV light represents c. 4% of the solar spectrum). In 2016 we reported for the first time the selective photo-oxidation of glucose under visible light conditions using TiO_2 as photocatalyst [19]. In this work, we found that the ligand-to-metal charge-transfer (LMCT) complex, TiO_2-glucose, is responsible for the photocatalytic activity under visible light conditions. As a result, gluconic acid and other partial oxidation products (arabinose, erythrose, glyceraldehyde and formic acid) were obtained under visible light irradiation. Moreover, it was demonstrated that the photo-oxidation of glucose can be carried out under natural light. In the same year, we also presented a study on the photo-conversion of glucose using TiO_2-supported silver photocatalysts under visible light [21]. It was found that the reaction conditions affect the product distribution, particularly the use of UV light promotes the formation of CO_2 (mineralisation pathway) and limits the production of high-value chemicals.

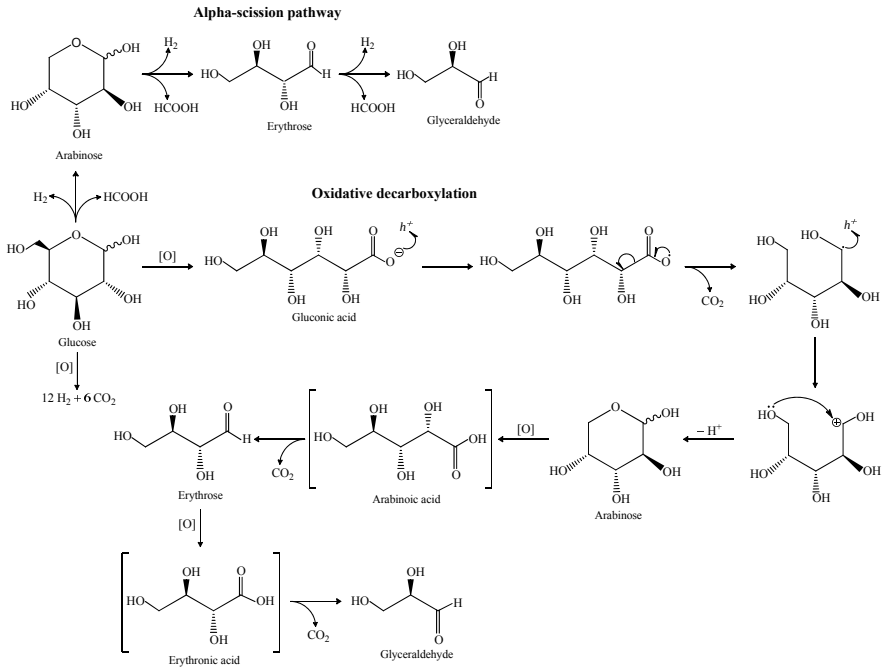

Scheme 4.1 Reaction mechanism for the photocatalytic conversion of glucose under UVA and visible light proposed by Da Vià et al., adapted from reference [21].

A mechanism (Scheme 4.1) which includes the Ruff degradation [27] reaction and the α-scission [25] process was proposed to explain the presence of gluconic acid, short-chain aldoses (arabinose, erythrose, and glyceraldehyde), and formic acid during the photocatalytic conversion of glucose under UV and visible light.

By the end of 2016, Zhou et al. [23] reported the selective photocatalytic oxidation of biomass derivatives using the Au/TiO_2 photocatalyst under UV and visible light. The authors showed that the photo-oxidation of the substrates under both UV and visible light only produces the carboxyl compounds with selectivities higher than 95% in alkaline conditions. In the case of the photo-oxidation of glucose, the results showed total conversion (>98%) and yields higher than 92% after 4 hours of irridation under both UV and visible light. The authors suggested that the base (Na_2CO_3) is responsible for the exceptional results as it acts as a promoter under visible light or sacrificial agent under UV light. The visible light activity of the photocatalyst was attributed to the surface plasmon resonance effect (SPR) of the gold nanoparticles, whereas the UV light activity was due to the band gap excitation of TiO_2.

The results published by Zhou et al. [23] suggested that the Au/TiO_2 photocatalyst can be used to perform selective photo-oxidation reactions under alkaline conditions, however, the study shows an unexpected behaviour of the TiO_2 support during photocatalysis. The recent work reported by Colmenares [6, 17, 18, 20], Chong [25], Bellardita [26], and Da Vià [19, 21] showed that the TiO_2-supported photocatalysts and bare TiO_2 are able to convert glucose to specific products (i.e., gluconic acid, glucaric acid) under UV or visible light, but it has also been demonstrated that TiO_2 can promote side reactions or even degradation of the products formed. More recently, Jin et al. [8] reported the photo-oxidation of glucose into formate using Degussa P25 (commercial TiO_2) under alkaline conditions. Blank experiments were carried out in the presence and absence of the base (NaOH) under UV light. The results showed that the glucose conversion increased nearly eightfold in the presence of the base (NaOH), obtaining higher formate selectivity after 3 hours of irradiation at 50 °C. Optimisation studies showed a glucose conversion of 100% with a formate yield of 35% after 9 hours of reaction at 25 °C. The authors suggested that alkaline conditions promote the formation of oxidative radicals ($O_2^{\bullet-}$, $^{\bullet}OH$), which facilitates glucose oxidation. More interestingly, the results reported by Jin et

al. [8] about the role of the base during photocatalysis contradict the previous findings reported by Zhou et al. [23].

The previous results demonstrate that the current literature on the selective photo-oxidation of biomass derivatives such as glucose is still unclear and does not provide conclusive results to the scientific community. The results reported by Jin [8] and Zhou [23] motivated us to further study the photo-oxidation of glucose under alkaline conditions using gold-based photocatalysts.

4.2 Results and Discussion

4.2.1 Catalyst Testing

The photocatalytic oxidation of glucose was performed under visible and UV light conditions using two different systems. Tests under visible light conditions were carried out using a 300 W Xenon Oriel Arc Lamp (Mod. 6258, Newport, UK) equipped with UV filter with a cut-off value of 420 nm and with a water filter to remove the IR radiation and avoid overheating of the reaction mixture. A Luzchem Photoreactor (Mod. LZC-4, Luzchem Research Inc., CAN) equipped with 16 lamps (UVA or visible, 8 W per lamp), which provide a total power of 128 W was used to perform the reactions under both UV and visible light conditions. Control experiments (blank reactions) were carried out in the dark using the Luzchem Photoreactor (lights off) and the temperature was adjusted to the obtained value under visible light conditions (Chapter 2, Section 2.9.1.1). In a typical test, 14 mL of a glucose stock solution (20 mM) were transferred into a 16 mL borosilicate glass vial (reactor), then the catalyst (30 mg) was added to the solution. Subsequently, the appropriate amount of the base (Na_2CO_3) was added and the reactor was sealed. The temperature in the reaction mixture was recorded at fixed intervals using a thermocouple which was inserted in the vial. Initial tests were carried out for 24 hours with sampling every 30 minutes in the first 2 hours and after 4, 6 and 24 hours. In the optimized conditions, the tests were carried out for 6 hours. The products were separated from the slurry by filtration using a PTFE filter (GILSON®, 0.22 μm) and quantified using HPLC analysis (Chapter 2, Section 2.8.1).

4.2.1.1 TiO_2–based photocatalysts for the photo-oxidation of glucose

The photocatalytic conversion of glucose was carried out using the 2 wt% Au/TiO_2-SI and TiO_2 (Degussa P25) catalysts under UV and visible light conditions. The Au/TiO_2-SI catalyst was synthesized using the traditional sol immobilisation technique [28-30] as described in Chapter 3 (Section 3.2.2.2). Briefly, the method implies the preparation of metal nanoparticles by the reduction of the metal precursor ($HAuCl_4 \cdot 3H_2O$) in solution with a reducing agent (sodium borohydride-$NaBH_4$) in the presence of a stabilizing polymer (Polyvinyl alcohol-PVA). After sol generation, the colloid is immobilised on the support (TiO_2).

The ICP-OES analysis of the Au/TiO_2-SI catalyst showed that the real metal loading was 1.6 wt%, indicating that the amount of metal was slightly lower than the target value of 2 wt%. The Au/TiO_2-SI and TiO_2 catalysts were characterized by diffuse reflectance UV-Vis spectroscopy (DR UV-Vis) as shown in Figure 4.1. The DR UV-Vis spectrum of the bare TiO_2 (black line) shows a strong band in the range of 200-380 nm, indicating that the TiO_2 support can only be activated in the UV region (black line), whereas the UV-Vis spectrum of the Au/TiO_2-SI (red line) catalyst shows the UV light response of the TiO_2 and the visible light response of the gold nanoparticles. The absorption peak centered at 541 nm in the visible region is assigned to surface plasmon resonance (SPR) effect of the gold nanoparticles. Plasmonic peaks in the same range have been attributed to the presence of gold nanoparticles [31-34].

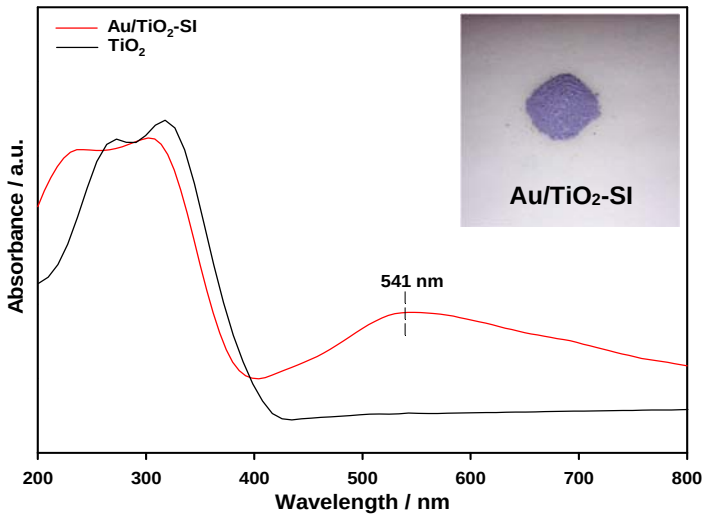

Figure 4.1 Solid UV-Vis spectra of the Au/TiO_2-SI and TiO_2 catalysts. The Au/TiO_2-SI catalyst showed the characteristic purple color of the gold nanoparticles (inset).

As reported by Zhou et al. [23] total glucose conversion with high yield to gluconic acid can be achieved after 4 hours of irradiation under UV or visible light by using the Au/TiO_2 in alkaline conditions. In order to corroborate the results reported by Zhou et al. [23], the photo-oxidation of glucose was carried out under UV and visible light using the Au/TiO_2-SI and TiO_2 catalysts in alkaline conditions. The reactions were performed by using a 20 mM glucose stock solution with a glucose/Na_2CO_3 = 1:1 molar ratio and 30 mg of catalyst. Figure 4.2 shows the results of the photo-oxidation of glucose after 4 hours of reaction time using the Au/TiO_2-SI and TiO_2 catalysts.

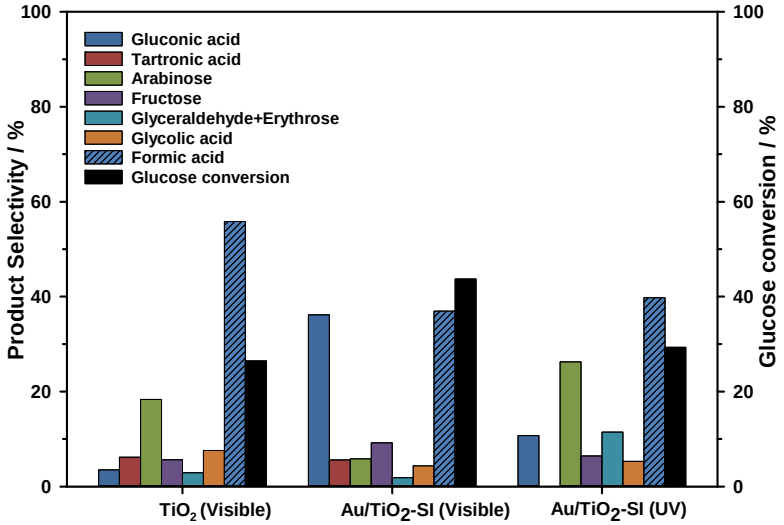

Figure 4.2 Glucose conversion and product selectivity values after 4 hours of reaction under UV and visible light in basic conditions. Glucose/Na_2CO_3 = 1:1 molar ratio, 30 mg catalyst, 20 mM glucose stock solution.

As it was expected the results show that the photo-oxidation of glucose under UV or visible light using TiO_2-based catalysts or bare TiO_2 leads to the formation of several products. The reaction under visible light using bare TiO_2 shows a glucose conversion of 26% with formic acid as the main product. This result confirms that the photo-oxidation of glucose can be performed under visible light using the TiO_2 catalyst as reported by Da Vià et al. [19]. Moreover, it was found that the presence of the base promotes the formation of fructose as a result of the isomerisation of glucose via the Lobry de Bruyn-Alberda van Ekenstein rearrangement [35]. In the case of the Au/TiO_2-SI catalyst, the glucose conversion was 43% under visible light with gluconic acid and formic acid as the main products. Comparing the results of the Au/TiO_2-SI catalyst with TiO_2, it is clear that the improved photoactivity of the

Au/TiO_2-SI catalyst is due to the presence of the gold nanoparticles and their visible light response as a result of the SPR effect. Remarkably, the selectivity to gluconic acid increased from 3.5% with TiO_2 as catalyst to 36% when the Au/TiO_2-SI catalyst was used in similar conditions. This result might indicate that the presence of gold nanoparticles promotes the selective photo-oxidation of glucose to gluconic acid. In fact, Au-based catalysts have shown exceptional activity for the glucose oxidation under "thermal" conditions [36-39] and more recently plasmon-driven photocatalysis has demonstrated to be a promising alternative for the glucose transformation [22, 23].

In order to examine the effect of light irradiation, the photo-oxidation of glucose was performed under UV light using the Au/TiO_2-SI catalyst. The results showed a glucose conversion of 29% with formic acid as the main product. Surprisingly, the selectivity to gluconic acid decreased from 36% under visible light to 10% under UV light. It is worth noting that supported gold nanoparticles might be used to perform chemical reactions under UV light: when the Au/TiO_2 catalyst is irradiated with UV light, electrons are photo-excited to the conduction band from the valence band of TiO_2 and then transferred to the gold nanoparticles which can activate various chemical species by an electron-transfer reaction. Also, gold nanoparticles exhibit modest UV absorption due to the intraband transition of the electrons from 5*d* to 6*sp* orbitals [40, 41] and therefore this excitation could be used in photocatalysis. Even though gold nanoparticles present significant UV light response, the results reported in Figure 4.2 shows that the Au/TiO_2-SI catalyst did not have a substantial effect on the photo-oxidation of glucose under UV light.

The results obtained for the photo-oxidation of glucose under UV or visible light using the Au/TiO_2-SI catalyst demonstrated that the presence of the base (Na_2CO_3) and gold nanoparticles did not impart the remarkable photoactivity reported by Zhou et al. [23]. In order to reproduce as close as possible the experimental conditions reported by Zhou et al. [23], the photo-oxidation was performed using a 1 mM glucose stock solution while the amount of catalyst (30 mg) and the volume of the solution (14 mL) were the same due to the experimental set-up used (Section 2.9.1.2). Table 4.1 shows the comparison between Zhou's [23] experimental set-up and this work as well as the reaction conditions used.

Table 4.1 Experimental set-up and reaction conditions used for the photo-oxidation of glucose using Au-based photocatalysts.

Parameter	Zhou et al. [23]	This work
Glucose concentration	1 mM	1 mM
Glucose/Na_2CO_3 molar ratio	1:1	1:1
Catalyst amount	25 mg	30 mg
Metal loading (wt %)	3 %	1.6 %
Irradiation time	4 h	6 h
Illuminated area	2 cm^2	4.5 cm^2
Light intensity	0.3 W/cm^2	0.45 W/cm^2
Lamp (Power)	Xenon (N/A)	Xenon (300 W)
Position of the light source	Top-irradiation	Side-irradiation
Volume of reaction mixture	1 mL	14 mL
Volume of reactor	10 mL	16 mL
Type of light	Visible	Visible
Temperature	30 °C	34±5 °C

N/A = Not available

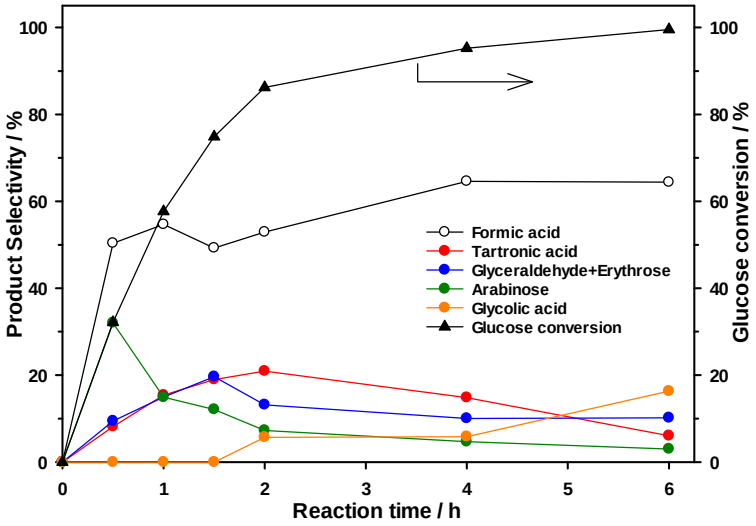

Figure 4.3 Glucose conversion and product selectivity values for the Au/TiO_2-SI catalyst after 6 hours of reaction under visible light in basic conditions. Glucose/Na_2CO_3 = 1:1 molar ratio, 30 mg catalyst, 1 mM glucose stock solution.

The results reported in Figure 4.2 showed that visible light irradiation displayed better performance on the glucose oxidation. Therefore, it was decided to use visible light to carry out the photoreaction. Figure 4.3 shows the results obtained with the Au/TiO_2-SI catalyst for the photo-oxidation of glucose in alkaline conditions. At low concentration of substrate, the Au/TiO_2-SI catalyst showed nearly total glucose conversion (99%) after 6 hours of reaction under alkaline conditions. Surprisingly, gluconic acid was not detected during the analysis of the products. This result might indicate that gluconic acid is converted into short-chain aldoses as soon as it forms. Despite higher glucose conversion, the photo-oxidation process did not

show any improvement in the product distribution, in fact, degradation of the organic compounds into formic acid was detected.

The results obtained under UV and visible light irradiation demonstrate that the Au/TiO_2 and TiO_2 catalysts are unable to perform the selective photo-oxidation of glucose in alkaline conditions. Even when the photo-oxidation of glucose was performed under similar reaction conditions (Table 4.1 and Figure 4.3) as reported by Zhou et al. [23], the Au/TiO_2 catalyst did not promote the formation of gluconic acid as the main product. These results confirm that the TiO_2 support actively participates in the reaction, allowing the formation of unwanted products. Therefore, it is clear that the search for new supports which present photoactivity but do not get directly involved in the reaction is desirable.

4.2.1.2 Conjugated Microporous Polymers (CMPs) as alternative support materials for the selective photo-oxidation of glucose

In Chapter 3, it was demonstrated that conjugated microporous polymers (CMPs) are suitable supports for the deposition of metal nanoparticles. These novel polymer-based catalysts showed good activity and stability during catalysis, even after several reuses. More interestingly, CMPs have shown potential for photocatalytic applications due to their extended π-conjugation, high surface area, chemical inertness, and photophysical properties [42-44]. In 2010 Chen et al. [45] demonstrated that CMPs with polyphenylene structures can serve as an antenna for light-harvesting. The authors suggested that the conjugated structure allows energy transfer from the CMPs framework to an energy acceptor. Recently, Cooper et al. [42] reported the synthesis of pyrene-based CMPs photocatalysts for the hydrogen production from water under visible light. The results showed that the optical gap (1.94–2.95 eV) and surface area (597–1710 $m^2\ g^{-1}$) can be modified by varying monomer composition allowing the formation of CMPs with unique photocatalytic properties. The authors also demonstrated that the polymers are capable of producing hydrogen from water in the absence of cocatalysts. Therefore, it is clear that the CMPs are promising materials with tunable properties which make them suitable supports for use in photocatalytic applications.

In this section, gold nanoparticles were immobilised on different polymeric structures (CMPs) and tested for the photo-oxidation of glucose under visible light in alkaline conditions. The gold catalysts were synthesized by the solvent-assisted sol immobilisation (SASI) method using acetonitrile as solvent, as reported in Chapter 3. Polymeric structures such as E-PAF, CMP-2, CMP-4, CMP-8, and CMP-10, kindly provided by the Cooper group (Prof A. I. Cooper FRS, University of Liverpool, UK) were used as support materials, whereas the CMP-1 structure was prepared as reported in Chapter 3.

Table 4.2 shows the photophysical properties and the apparent Brunauer–Emmett–Teller surface areas of the polymeric networks. The CMPs (1 to 10) show a read shift in the absorption onset from 420 to 532 nm, which is attributed to the increase of pyrene content in the polymeric network, thus the polymers are active under visible light.

Table 4.2 Photophysical properties and surface area of the CMPs.

Polymer	$\lambda_{on\text{-}set}$[a] (nm)	Optical gap[a] (eV)[a]	SA_{BET}[a,b] ($m^2\ g^{-1}$)	Comments
E-PAF	N/A[b]	3.24	1067	Non-conjugated
CMP-1	421	2.95	671	This work
CMP-2	463	2.69	682	[42]
CMP-4	489	2.54	684	[42]
CMP-8	512	2.42	1056	[42]
CMP-10	532	2.33	995	[42]

[a] Values obtained from Sprick et al. [42]
[b] N/A = Not available, SA = Surface area

Table 4.3 shows the ICP-OES analysis of the gold catalysts prepared by the SASI method using different polymeric networks. The results show that the required metal loading was achieved in some cases, however, in other cases an incomplete deposition of the gold nanoparticles was detected. This result might indicate that the nature of the support affects the immobilisation of the metal nanoparticles.

Table 4.3 Solid UV-Vis and ICP-OES analysis for the gold catalysts prepared by the SASI method using different porous networks.

Catalysts	$[Au]_{nominal}$ / wt%	$[Au]_{real}$ / wt%	$UV_{\lambda max}$ / nm
Au/E-PAF	2	1.2	531
Au/-CMP-1	2	1.6	550
Au/-CMP-2	2	1.0	529
Au/-CMP-4	2	2.0	N/D[a]
Au/-CMP-8	2	1.8	N/D[a]
Au/-CMP-10	2	2.1	571

[a] N/D= Not detected

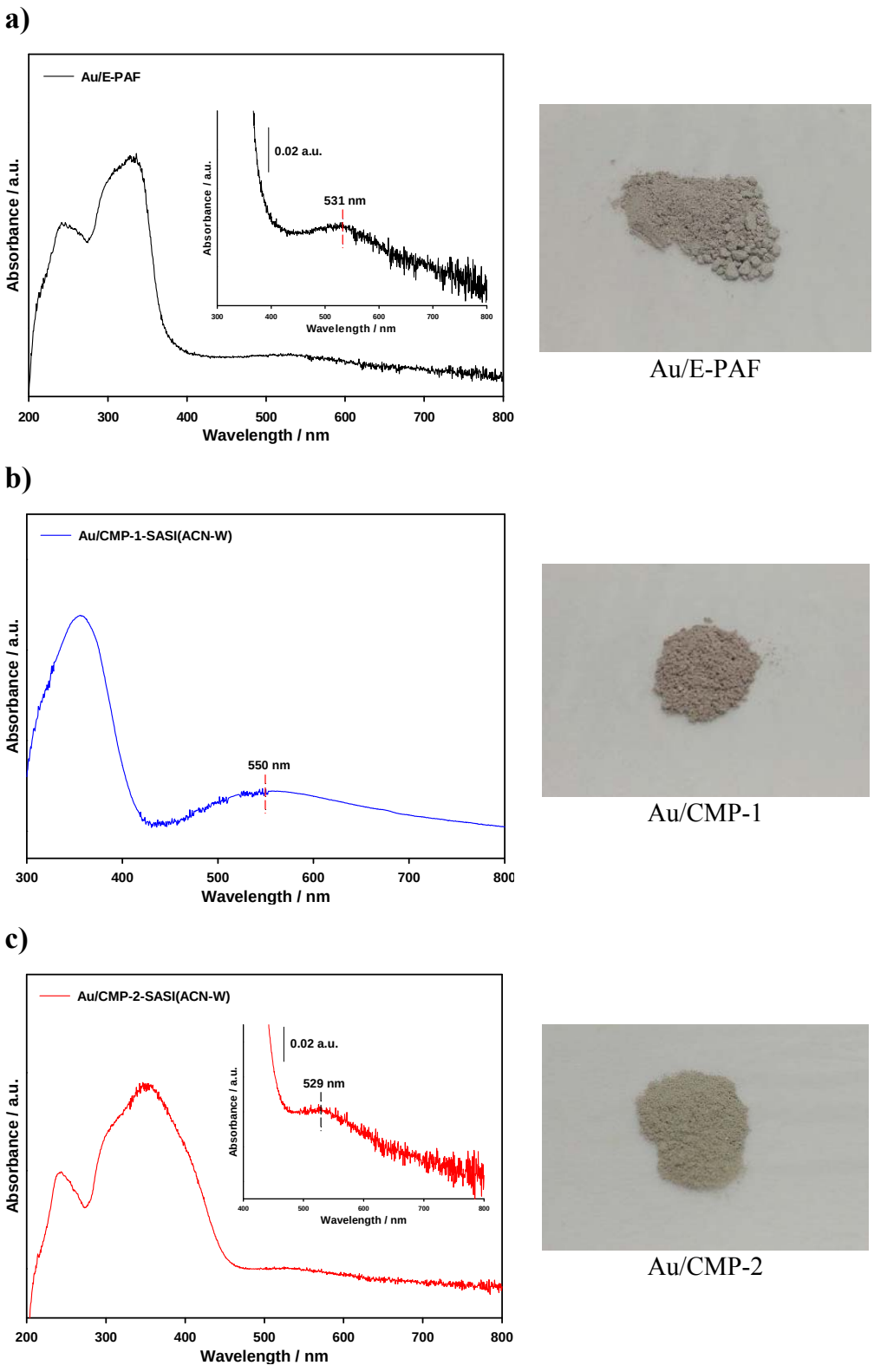

Figure 4.4 UV-Vis spectra of the (a) Au/E-PAF, (b) Au/CMP-1 and (c) Au/CMP-2 catalysts prepared by the SASI method and digital photographs of the corresponding samples.

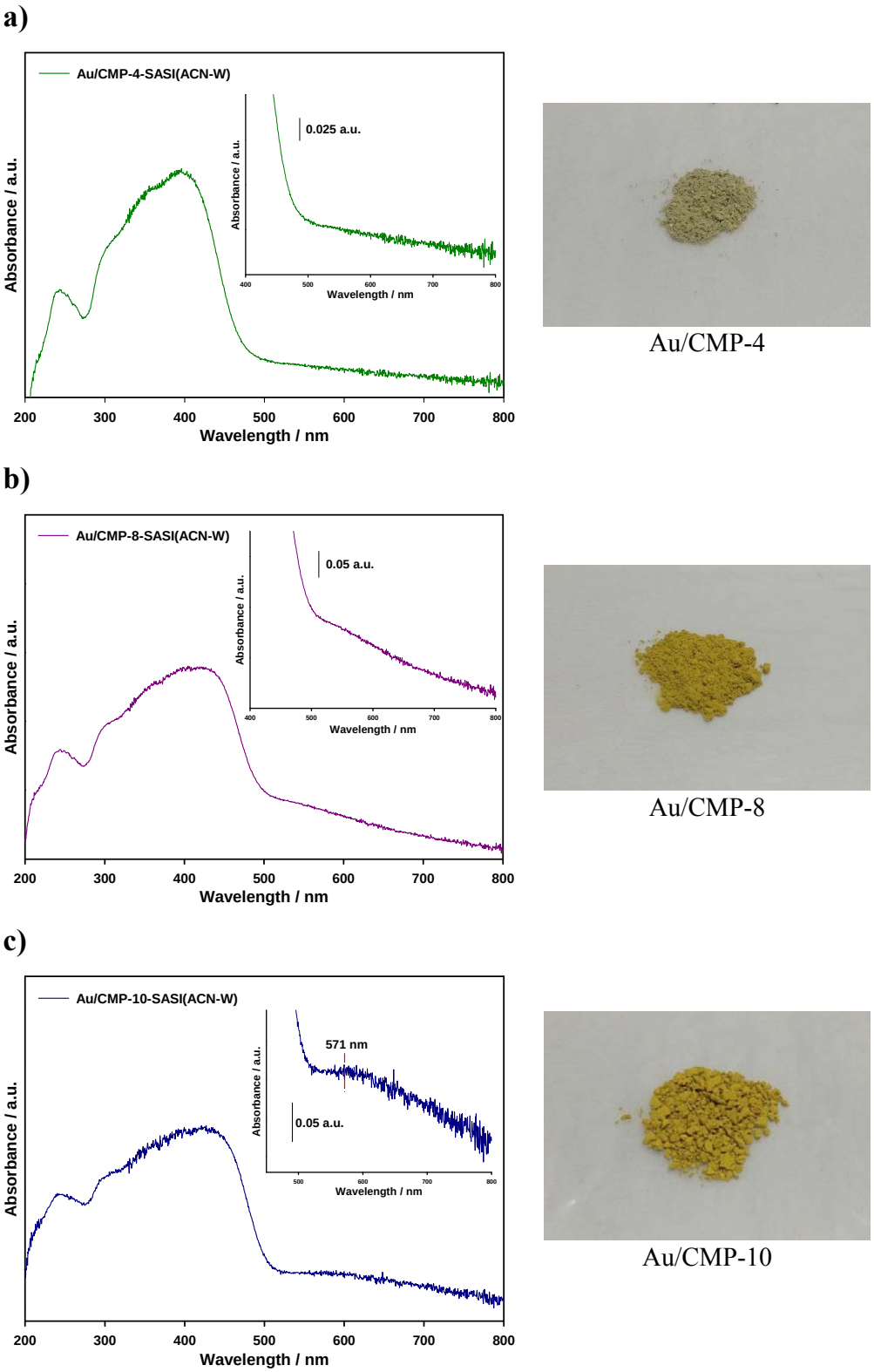

Figure 4.5 UV-Vis spectra of the (a) Au/CMP-4, (b) Au/CMP-8 and (c) Au/CMP-10 catalysts prepared by the SASI method and digital photographs of the corresponding samples.

The polymer-supported gold catalysts were characterized by diffuse reflectance UV-Vis spectroscopy (DR UV-Vis) as shown in Figures 4.4 and 4.5. The DR UV-Vis spectra of the gold catalysts show the presence of plasmonic peaks between 529 and 571 nm (Table 4.3). Plasmonic peaks in the same range have been attributed to the presence of gold nanoparticles [31-34]. Surprisingly, the Au/CMP-4 and Au/CMP-8 catalysts did not show the presence of plasmonic peaks (Figures 4.5a and 4.5b) despite the high metal content (Table 4.3). This result could be explained considering the interaction of the residual palladium from the synthesis of the polymers with the gold nanoparticles resulting in the formation of Au/Pd bimetallic nanoparticles. As reported by Wu et al. [46], the presence of Pd suppresses the formation of the surface plasmon of the gold structures in the Au/Pd systems. However, this is pure speculation and the presence of bimetallic nanoparticles in the Au/CMP-4 and Au/CMP-8 catalysts needs to be demonstrated.

The initial experiments in the photo-oxidation of glucose were carried out under visible light irradiation and dark conditions. The tests under visible light were performed using the 300 W Xenon Lamp and the Luzchem Photoreactor (equipped with 16 visible lamps, 128 W). Blank tests (dark conditions) were carried out using the Luzchem photoreactor with the lights off, while the temperature was adjusted to the one recorded for the reaction under visible light. The Au/CMP-1 catalyst was used as a representative sample to perform the reactions under visible light irradiation and dark conditions.

Figure 4.6 shows the results obtained for the glucose oxidation after 24 hours of reaction using the Au/CMP-1 catalyst. In this set of experiments, the effect of the light intensity (300W and 128W) and solvent composition (acetonitrile/water 50/50 v/v) were investigated. Surprisingly, it was found that the reactions did not show any difference in the photocatalytic activity when they were performed under visible light irradiation or dark conditions. The results obtained for the 300 W lamp show the highest glucose conversion (38.5%) with a gluconic acid selectivity of 95% after 24 hours of reaction, similar values of conversion (43.9%) and selectivity (95.2%) were found for the reaction under dark conditions. The same trend was observed when the light intensity decreased from 300 W to 128 W. The glucose conversion (29%) and selectivity to gluconic acid (>99%) under visible light irradiation showed similar values to the ones obtained under dark conditions after 24 hours of reaction, 23% and 98.8% respectively.

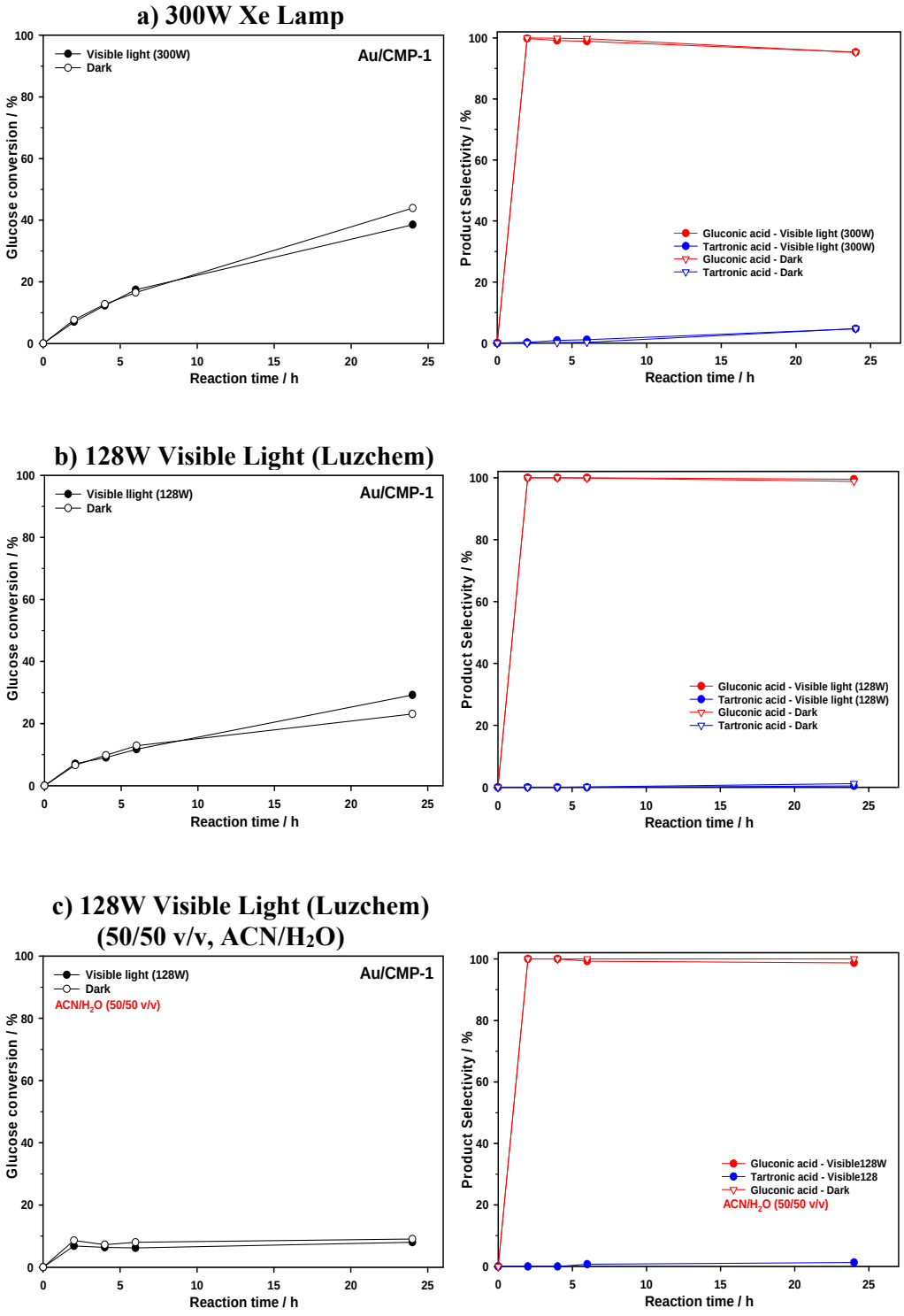

Figure 4.6 Glucose conversion and product selectivity values after 24 hours of reaction under visible light irradiation and dark conditions using the Au/CMP-1 catalyst. 20 mM glucose stock solution (14 mL), 30 mg of catalyst, atmospheric pressure. The mass balance in all cases was >99%.

The glucose oxidation with the 300 W lamp showed an increase of 9.5% with respect to the 128 W system (Luzchem photoreactor) under visible light. This result might indicate that the light intensity does not have an effect on the glucose oxidation using the Au/CMP-1 catalyst. In fact, the small increase in conversion could be associated with an increase in temperature. When the reaction was carried out using the 300 W lamp, the temperature was 38±4 °C. While the 128 W system (Luzchem photoreactor) kept the temperature at 30±1 °C.

On the other hand, the solvent composition was modified in order to promote the photo-oxidation of glucose. As reported by Shiraishi et al. [47], the presence of acetonitrile as co-solvent could be beneficial to prevent radical recombination reactions which might affect the photocatalytic activity. Recently, Colmenares et al. [17] reported that a water/acetonitrile 50/50 v/v mixture promotes the formation of organic compounds (gluconic acid, glucaric acid, and arabitol) during the photo-oxidation of glucose using TiO_2-based catalysts. Therefore, a 20 mM glucose stock solution was prepared by solubilising the appropriate amount of glucose in a water/acetonitrile mixture 50/50 v/v. The reaction was carried out using the Au/CMP-1 catalyst under visible light irradiation (128 W) and dark conditions. The results showed a glucose conversion of 8% with a gluconic acid selectivity of 98.7% under visible light after 24 hours of reaction, whereas the reaction in the dark showed a glucose conversion of 9% with a gluconic acid selectivity of >99%. Unfortunately, the results showed (Figure 4.6c) that the addition of acetonitrile did not have an effect on the glucose oxidation, in fact, the presence of the organic solvent was detrimental to the system.

These results revealed that the presence of visible light does not promote the photo-oxidation of glucose as the reaction in the dark showed similar results, even when the solvent composition was modified to improve the photoactivity. Moreover, the Au/CMP-1 catalyst has shown to be an effective material which promotes the formation of gluconic acid as the main product. At this stage of the work, we have demonstrated that the glucose oxidation might be a thermally driven process rather than a light-driven process. However, some authors have suggested that the photo-oxidation of glucose can be carried out using gold catalysts (i.e. Au/M, M= TiO_2, Al_2O_3, CeO_2) under visible light irradiation (0.3 W/cm^2 or 0.1 W/cm^2) and basic

conditions (Na_2CO_3 or NaOH) [22, 23]. Consequently, the next step was to prove that the addition of a base promotes the photo-oxidation of glucose under visible light irradiation. Similarly to the previous tests, the reaction was carried out using the Au/CMP-1 catalyst under visible light irradiation and dark conditions. A 20 mM glucose stock solution and a glucose/Na_2CO_3 = 1:1 molar ratio were used in these tests.

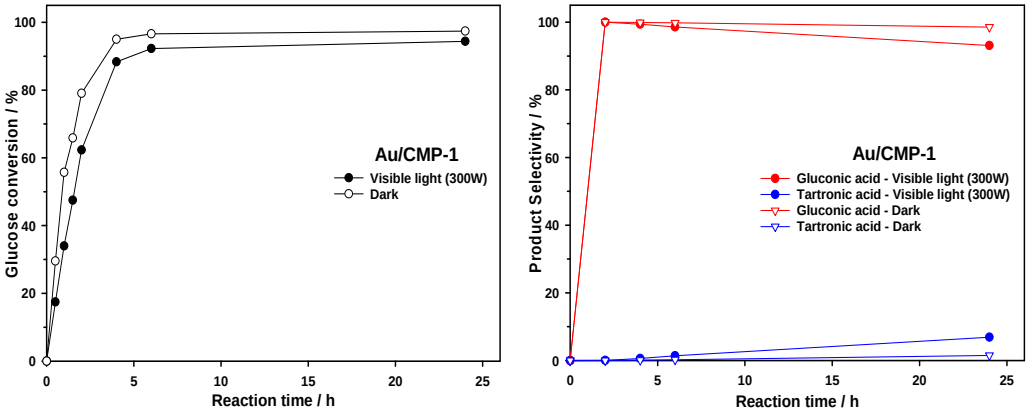

Figure 4.7 Conversion and product selectivity values for the glucose oxidation using the Au/CMP-1 catalyst under visible light irradiation and dark conditions. Glucose/Na_2CO_3 = 1:1 molar ratio, 20 mM glucose stock solution (14 mL), 30 mg of catalyst, atmospheric pressure. The mass balance in all cases was >99%.

Figure 4.7 shows the conversion and product selectivity values for the glucose oxidation after 24 hours of reaction using the Au/CMP-1 catalyst. Under visible light, the glucose conversion was 94% with a selectivity to gluconic acid of 93%, whereas the reaction in the dark showed 97% of conversion with a gluconic acid selectivity of 98% after 24 hours of reaction. Traces of tartronic acid were detected in both cases. As reported by Zhou et al. [23], the presence of a base accelerates the glucose oxidation under visible light. The results showed an increase in glucose conversion from 38.5% to 94% when alkaline conditions were used. More importantly, it is clear that the reaction time could be reduced from 24 to 6 hours as the glucose conversion increased slightly from 92% to 94% after 18 hours of reaction. Despite the increased conversion under visible light, the reaction in the dark showed slightly higher values of conversion and selectivity to gluconic acid under the same experimental conditions, indicating that the reaction could be a thermally driven process. Nevertheless, the use of the CMP-1 material as support for the gold nanoparticles has demonstrated superior performance on the glucose oxidation under

alkaline conditions. As shown in Figure 4.8, the Au/CMP-1 catalyst leads to the formation of gluconic acid as the main product, whereas the Au/TiO_2 promotes the formation of oxidation and degradation products as a result of the interaction of glucose with the TiO_2 support as reported by Chong et al. [25] and Da Vià et al. [19]. Therefore, the use of a conjugated microporous polymer (CMP-1) as support for the gold nanoparticles could be a promising alternative for the selective transformation of glucose into high-value chemicals. To further confirm that the CMPs can serve as support materials, the glucose oxidation was carried out using CMP-supported gold catalysts (Table 4.3) in alkaline conditions.

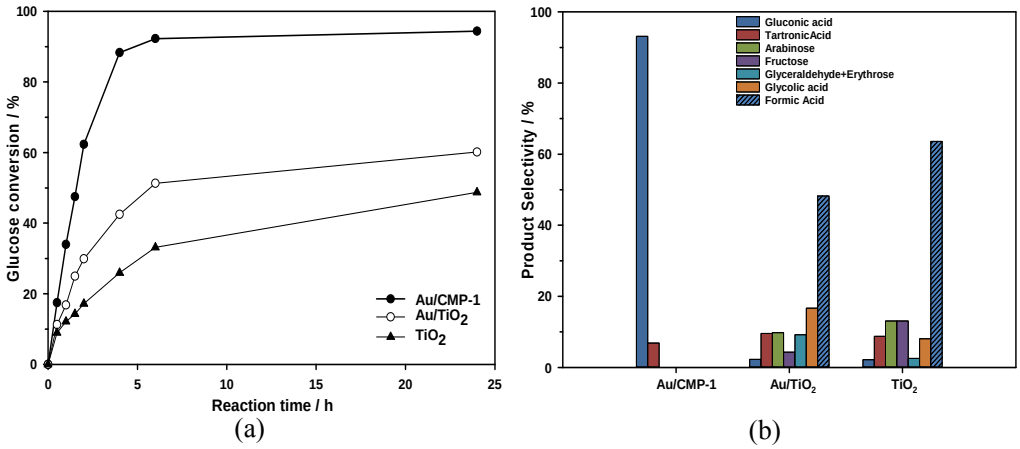

Figure 4.8 Conversion (a) and product distribution (b) values for the glucose oxidation using the Au/CMP-1, Au/TiO_2 and TiO_2 catalysts under visible light and basic conditions. Glucose/Na_2CO_3 = 1:1 molar ratio, 20 mM glucose stock solution (14 mL), 30 mg of catalyst, atmospheric pressure. The mass balance in all cases was >96%.

Glucose conversion and product selectivity values for the CMP-supported gold catalysts are reported in Table 4.4. The results show that gold nanoparticles supported on conjugated microporous polymers (CMPs) are active for the glucose oxidation, whereas non-conjugated structures such as E-PAF promotes the isomerisation of glucose to fructose. The formation of fructose might be due to the Lobry de Bruyn-Alberda van Ekenstein rearrangement [35]. For the CMP-supported gold catalysts, gluconic acid was the main product in all cases, however, small traces of tartronic acid and fructose were observed. In terms of activity, the Au/CMP-1 and Au/CMP-10 catalysts were the most active for the glucose oxidation with a TOF value of 41 h^{-1} in both cases, while the Au/CMP-4 showed the lowest activity with a TOF of 31 h^{-1}. These results corroborate our previous findings for the CMP-1

structure and emphasize the importance of support selection in oxidation reactions under basic conditions.

Table 4.4 Conversion and product selectivity values for the glucose oxidation using CMP-supported gold catalysts in alkaline conditions.[a]

Catalysts	Time (h)	Conv. (%)	Gluconic Acid (%)	Tartronic Acid (%)	Fructose (%)	TOF[b] (h^{-1})
Au/E-PAF	0.5	2.7	-	-	>99	-
	6	6.6	-	-	>99	-
	24	15	-	-	>99	-
Au/CMP-1	0.5	18	>99	-	-	41
	6	92	98	1.4	-	-
	24	94	93	6.9	-	-
Au/CMP-2	0.5	10	>99	-	-	36
	6	88	>99	-	0.4	-
	24	>99	94	-	4.4	-
Au/CMP-4	0.5	19	88	-	12	31
	6	95	94	-	6.0	-
	24	95	92	3.3	4.7	-
Au/CMP-8	0.5	18	>99	-	-	37
	6	>99	92	0.6	7.2	-
	24	>99	84	12	4.0	-
Au/CMP-10	0.5	25	94	-	5.7	41
	6	91	92	-	8.0	-
	24	>99	93	2.0	5.0	-

[a] Reaction conditions: 30 mg of catalyst, Glucose/Na_2CO_3 = 1:1 molar ratio, 20 mM glucose stock solution (14 mL), atmospheric pressure, visible light (300 W), The mass balance in all cases was >98%. [b] TOF values were calculated at 30 minutes reaction time. TOF = Moles of glucose converted / (Moles of metal x time).

In this section, the photo-oxidation of glucose under visible light irradiation in basic conditions was performed using gold nanoparticles supported on conjugated microporous polymers. For the first time, it was demonstrated that CMP-supported gold catalysts promote the formation of selective oxidation products such as gluconic acid from glucose. Although CMPs are suitable materials for light-harvesting [42] and do not interfere in the reaction mechanism, the results showed that the presence of visible light does not have any effect on the glucose oxidation as the reaction in the dark (thermal conditions) showed similar values of conversion and selectivity. Therefore, these results highlight the importance of careful evaluation of the reaction conditions (blank experiments) in order to avoid duplication of information and incorrect conclusions.

4.2.1.3 Carbon Nanotubes (CNTs) as support material for the selective photo-oxidation of glucose

Noble metal nanoparticles (i.e. Au, Ag) have been widely studied in different research areas such as catalysis [28-30], biotechnology [48], optics [49-51], and energy [52, 53], due to their unique physical and chemical properties. One of the most important features of the noble metal nanoparticles is its ability to absorb visible light due to the surface plasmon resonance (SPR), which can be tuned by varying the particle size, shape and refractive index of the surrounding medium [54-56]. Thus, this unique property (SPR) of the noble metal nanoparticles has provided an alternative route for the preparation of efficient visible light responding photocatalysts. Typically, plasmonic photocatalysts are often composed of noble metal nanoparticles deposited on semiconductor oxides (i.e. TiO_2, ZrO_2) [21-23, 25, 57], but recently carbonaceous materials such as carbon [58], graphene [59-61], and reduced graphene oxide [62-65], have attracted attention due to their electronic and structural properties. In this scenario, carbon nanotubes (CNTs) have emerged as a new class of carbon materials with exceptional properties such as high surface area, thermal stability, high electronic conductivity, etc. [66]. Particularly, it has been demonstrated that CNTs enhance light harvesting and/or promote charge transport in different photocatalytic processes [66-69]. More recently, noble metal nanoparticles have been incorporated into the CNTs' structure and used in photocatalytic applications.

Liu et al. [70] reported the selective photo-oxidation of cyclohexane under visible light using gold nanoparticles confined inside or outside CNTs. The results showed that the cyclohexane conversion increased nearly fourfold for the gold nanoparticles confined inside CNTs compared to the ones outside. Moreover, the confinement of the gold nanoparticles produced cyclohexanol as the main product and small traces of cyclohexanone, whereas gold nanoparticles outside CNTs showed low selectivity to cyclohexanol as a result of the formation of unknown products. The authors demonstrated that upon excitation of the SPR of the metal nanoparticles with visible light, electrons are transferred from the gold nanoparticles to the CNTs, reducing electron-hole recombination. On the other hand, Silva et al. [71] reported the photocatalytic reforming of methanol and bio-derived molecules using noble

metal nanoparticles (Au, Pt, Pd, Ir) supported on CNTs-TiO_2 composites. The results show that composites loaded with noble metals promote the hydrogen production compared to non-metal loaded composites. Particularly, Pt-based catalysts were the most active for hydrogen production from water/methanol solutions. The Pt/CNTs-TiO_2 catalyst displayed the highest rate of hydrogen evolution compared to the Pt/TiO_2 catalyst. The authors suggest that several factors might influence the photocatalytic activity, for example, particle size, the work function of the metal, the synthesis method, metal-support interaction, etc. Irrespective of this, the authors suggest that the synergistic effect of the CNTs-TiO_2 composite might be attributed to the CNTs acting as a photosensitizer as reported in the literature [68, 69]. Based on the previous reports, it is clear that carbon nanotubes are of great interest due to they have demonstrated their enormous potential for photocatalytic applications, ranging from hydrogen production to biological disinfection [66-73].

In this section, gold nanoparticles were immobilised on multi-walled carbon nanotubes (CNTs, Sigma-Aldrich) and tested for the photo-oxidation of glucose under visible light irradiation at atmospheric pressure. The Au/CNTs catalysts were prepared using the SASI method as described in Chapter 3 (section 3.2.2.3), but it was slightly modified (Figure 4.9). Prior to the thermal treatment under reflux conditions (step 2), the CNTs were sonicated in ethanol for 1 hour at room temperature in order to improve their dispersion in the liquid medium as reported in the literature [74-76]. Then, the synthesis was carried out in the same manner as described in Chapter 3.

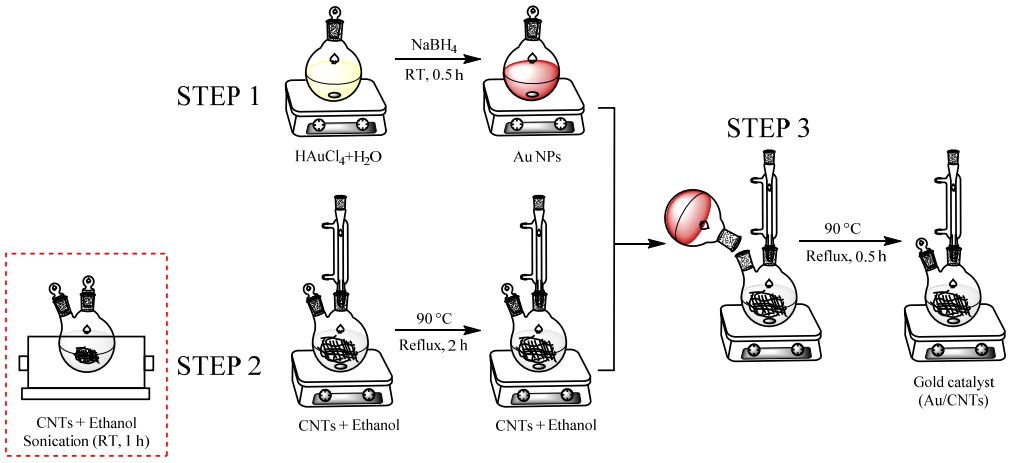

Figure 4.9 Schematic representation of the SASI method. 1) Preparation of the pre-formed metal nanoparticles, 2) sonication and thermal treatment, and 3) immobilisation of the colloid onto the support material.

The ICP-OES analysis of the Au/CNTs catalyst (a representative sample of all catalysts) showed that the real metal loading was 1.1 wt%, indicating that the amount of metal was lower than the target value of 2 wt%.

XRD analysis on the bare support and Au/CNTs catalyst is shown in Figure 4.10. Because of the nature of the CNTs, the characteristic XRD patterns of the CNTs are very similar to ones of graphite [77]. The diffraction patterns of the CNTs show the presence of reflection signals at $2\theta \approx 25.6°$ and 43.2° that correspond to the [0 0 2] and [1 0 0] planes of graphite structure [77-79]. Moreover, it is worth noting that the XRD patterns of the CNTs did not show any change after sonication, indicating that their structure was not damaged or modified. In the case of the Au/CNTs catalyst, reflection signals at $2\theta \approx 38.3°$, 66.7° and 78.1° that correspond to the [1 1 1], [2 0 0] and [3 1 1] planes of the gold crystalline structure were observed [80-82]. The average gold particle size for the Au/CNTs was calculated to be 9.3 nm using the Scherrer equation [83].

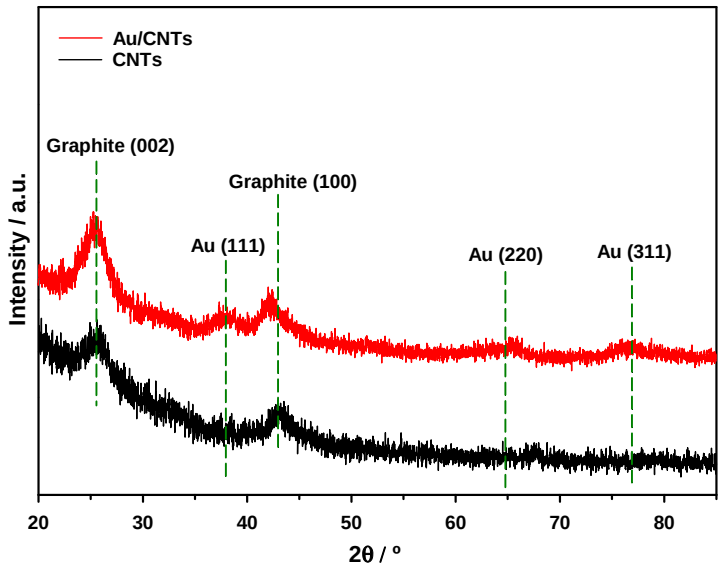

Figure 4.10 XRD patterns for the CNTs (black line) and Au/CNTs (red line) materials.

XPS analysis was performed on the 1.1 wt% Au/CNTs catalyst prepared by the SASI method. Figure 4.11 shows the spectrum (scattered points) of the Au/CNTs catalyst over the Au 4f region. The XPS analysis was performed using the CasaXPS software. The spectrum was fitted by using two spin-orbit split Au $4f_{7/2}$ (red line) and Au $4f_{5/2}$ (blue line) components. The XPS analysis of the Au/CNTs catalyst showed

binding energies of the Au $4f_{7/2}$ and Au $4f_{5/2}$ levels at 84.37 and 88.04 eV respectively. Binding energy values between 84.02 and 84.38 eV for the Au $4f_{7/2}$ level have been attributed to the presence of metallic gold (Au^0) [84-87]. Hence, the peak at 84.37 eV in the Au/CNTs catalyst is assigned to metallic gold (Au^0).

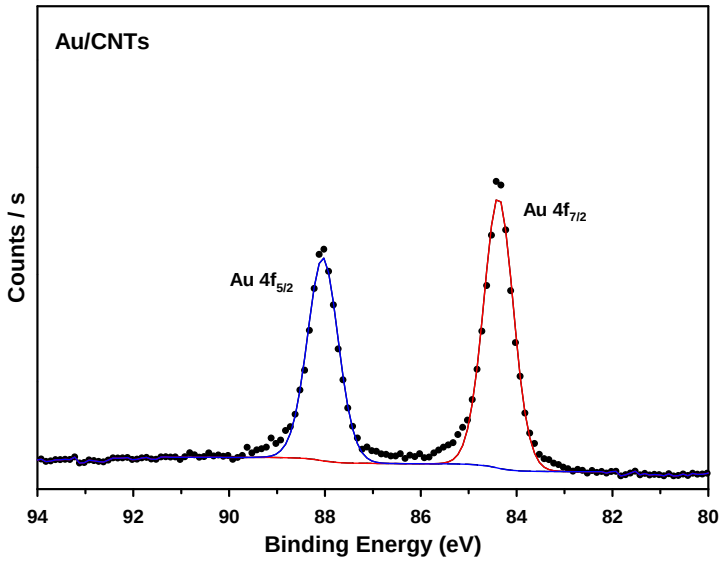

Figure 4.11 XPS spectrum of the Au 4f region for the Au/CNTs catalyst.

The photo-oxidation of glucose was carried out under visible light irradiation and dark conditions using the Au/CNTs catalyst. The tests under visible light were performed using a 300 W Xenon Lamp (Mod. 6258, Newport, UK), whereas the ones in the dark were performed using the Luzchem photoreactor with the lights off (Mod. LZC-4, Luzchem Research Inc., CAN). Under visible light, the temperature in the reaction mixture was recorded using a thermocouple which was inserted in the vial, while the temperature under dark conditions was adjusted to the one recorded under visible light using an internal temperature controller (FuzyPro 1/6 DIN, HCS Ltd, CAN).

Blanks experiments were carried out under visible light and dark conditions in order to investigate the effect of the base (Na_2CO_3) and support material on the photo-oxidation of glucose. In all cases, 14 mL of a 20 mM glucose stock solution were used. The reactions under alkaline conditions were performed using a glucose/Na_2CO_3 = 1:1 molar ratio.

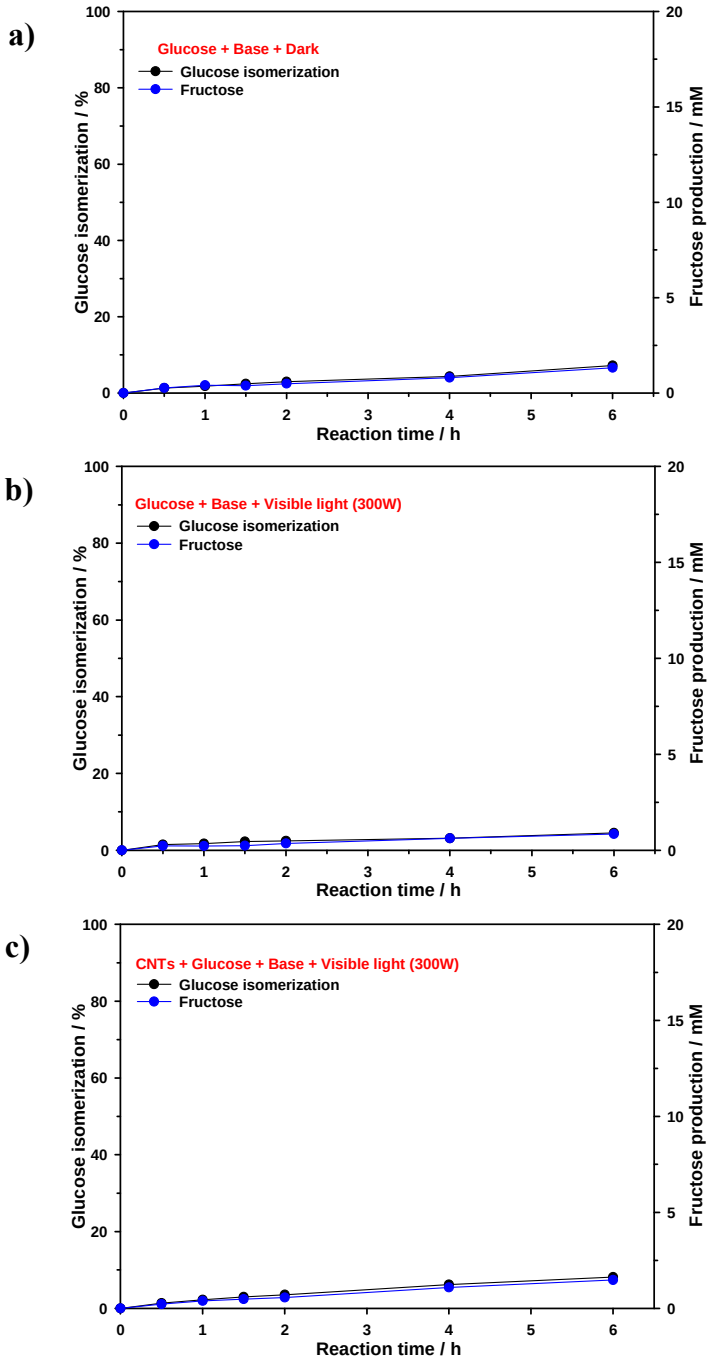

Figure 4.12 Blank experiments under visible light irradiation and dark conditions. All experiments were carried out under alkaline conditions with a Glucose/Na_2CO_3 = 1:1 molar ratio. The mass balance in all cases was >96%.

Figure 4.12 shows the results obtained for the blank reactions under alkaline conditions after 6 hours of reaction time at atmospheric pressure. Blank experiments showed no reaction under both visible light and dark conditions in the absence of the catalyst (Figures 4.12a and 4.12b). On the other hand, Luo et al. [88] reported for the

first time that CNTs after being purified and thermally treated, they can be used as photocatalysts under visible light. Although CNTs were used without purification in the synthesis of the gold catalysts, a blank test was carried out using the CNTs as the catalyst under visible light (Figure 4.12c). The results showed that the raw CNTs cannot perform the oxidation of glucose under visible light as no reaction was observed after 6 hours. In all cases, fructose was the main product as a result of the isomerisation of glucose via the Lobry de Bruyn-Alberda van Ekenstein rearrangement [35].

The previous results demonstrated that glucose cannot be oxidized using the bare support (CNTs) under visible light and the presence of the base did not produce large amounts of fructose after extended times. Hence, the next step was to investigate the photoactivity of the Au/CNTs catalyst on the photo-oxidation of glucose under visible light irradiation and dark conditions. Moreover, control experiments under base-free conditions were also performed. Figures 4.13 and 4.14 show the glucose conversion and product selectivity for the Au/CNTs catalyst after 6 hours of reaction time with and without the addition of the base. The results showed a glucose conversion of 21% with a selectivity of 95% to gluconic acid after 6 hours of reaction under visible light and base-free conditions, whereas the reaction under dark conditions showed a glucose conversion of 9% with a selectivity of 99% to gluconic acid.

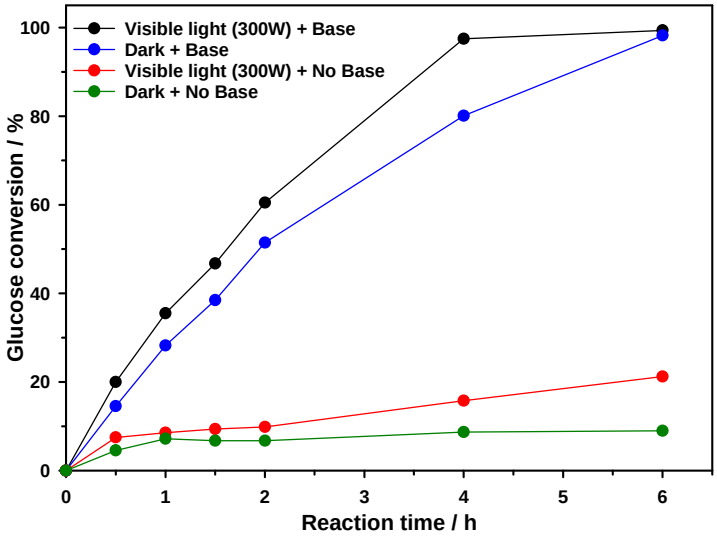

Figure 4.13 Conversion values for the photo-oxidation of glucose using the Au/CNTs catalyst under visible light irradiation and dark conditions. Reactions conditions: Glucose/Na_2CO_3 = 1:1 molar ratio, 30 mg of catalyst, 14 mL of a 20 mM glucose stock solution. The mass balance in all cases was >96%.

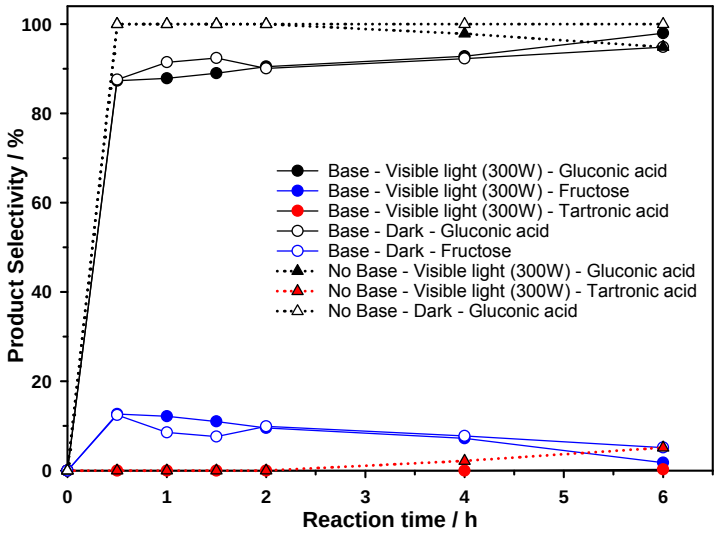

Figure 4.14 Product selectivity for the photo-oxidation of glucose using the Au/CNTs catalyst under visible light irradiation and dark conditions.

In the case of the reactions under alkaline conditions, the results showed a glucose conversion of 99% with a selectivity of 98% to gluconic acid under visible light after 6 hours, while the reaction under dark conditions showed a glucose conversion of 98% with a selectivity of 95% to gluconic acid. Traces of fructose were detected under both visible light (1.7%) and dark conditions (5%), while small traces of tartronic acid were only detected under visible light (0.2%).

These results demonstrate that the addition of the base promotes the oxidation of glucose in the presence of the Au/CNTs catalyst. However, the promotional effect of the base was observed under both visible light and dark conditions. Although an increase in the reaction rate was observed under visible light (Figure 4.13), the reaction in the dark reached the same conversion value under the same experimental conditions (glucose/base = 1:1 molar ratio, temperature and amount of catalyst). This result might indicate that the small increase in the reaction rate could be associated with a light-driven process. In fact, the experiments in the absence of the base showed an increase in the glucose conversion under visible light (21%) compared to the reaction in the dark (9%). In this scenario, it is clear that the Au/CNTs catalyst can promote the photo-oxidation of glucose under visible light, and the presence of the base accelerates the transformation of glucose as reported by Zhou et al. [23].

Despite the high catalytic activity of the Au/CNTs catalyst under visible light irradiation and alkaline conditions, the oxidation of glucose required long reaction times to achieve total conversion (6 hours). Consequently, the selective photo-oxidation of biomass-derived molecules such as glucose might not be considered an alternative route to produce high-value chemicals as many industrial processes require short reaction times to guarantee high production volumes. In most industrial processes, the oxidation stage is performed using toxic oxidants which produce large quantities of waste [89]. Therefore, the search for clean catalytic processes has become one of the main goals of academia and industry. An alternative approach for the oxidation of alcohols and carbohydrates is the use of air or molecular oxygen as eco-friendly oxidants [39, 90-92]. Particularly, molecular oxygen (O_2) can be activated by photocatalysts to produce reactive oxygen species (ROS) such as H_2O_2, $OH^{\bullet}$, $O_2^{\bullet-}$ and $^1O_2$, which are important oxidants in several organic reactions [93]. More interestingly, the selective photo-oxidation of alcohols such as aliphatic, aromatic and alicyclic, has been reported using molecular oxygen in the presence of a photocatalyst [94-98]. Based on the current literature, the use of molecular oxygen as the oxidant could potentially improve the efficiency of the Au/CNTs catalyst on the photo-oxidation of glucose. Therefore, we went one step further and decided to investigate the photo-oxidation of glucose using molecular oxygen under visible light irradiation and alkaline conditions. Briefly, the photocatalytic tests were performed using a Parr Stirred Reactor with oblong windows (Mod. 4590, Parr Instrument Company, Illinois, USA) and a 1000 W Xenon Oriel Arc Lamp (Mod. 6271, Newport, UK) as the light source. The lamp was equipped with a UV filter (Mod. FSQ-GG420, Newport, UK) with a cut-off value of 420 for visible light irradiation ($\lambda > 420$ nm) and a liquid filter (Mod. 6123NS, Newport, UK) to remove the infrared region and avoid overheating of the reaction mixture. The Au/CNTs catalyst (90 mg) was used in 40 mL of a glucose stock solution with a glucose/base = 1:1 molar ratio. The mixture was added to a 100 mL glass liner and then located on the photoreactor. Then, the vessel was sealed and purged with nitrogen and then pressurized with oxygen. The system was allowed to reach equilibrium for 10 minutes in the absence of light (section 2.9.1.1). Liquid samples were collected every 30 minutes in the first 2 hours and after 4, 6 and 24 hours. The temperature was set to 40 °C and monitored using a 4848 Reactor Controller (Parr Instrument Company, Illinois, USA).

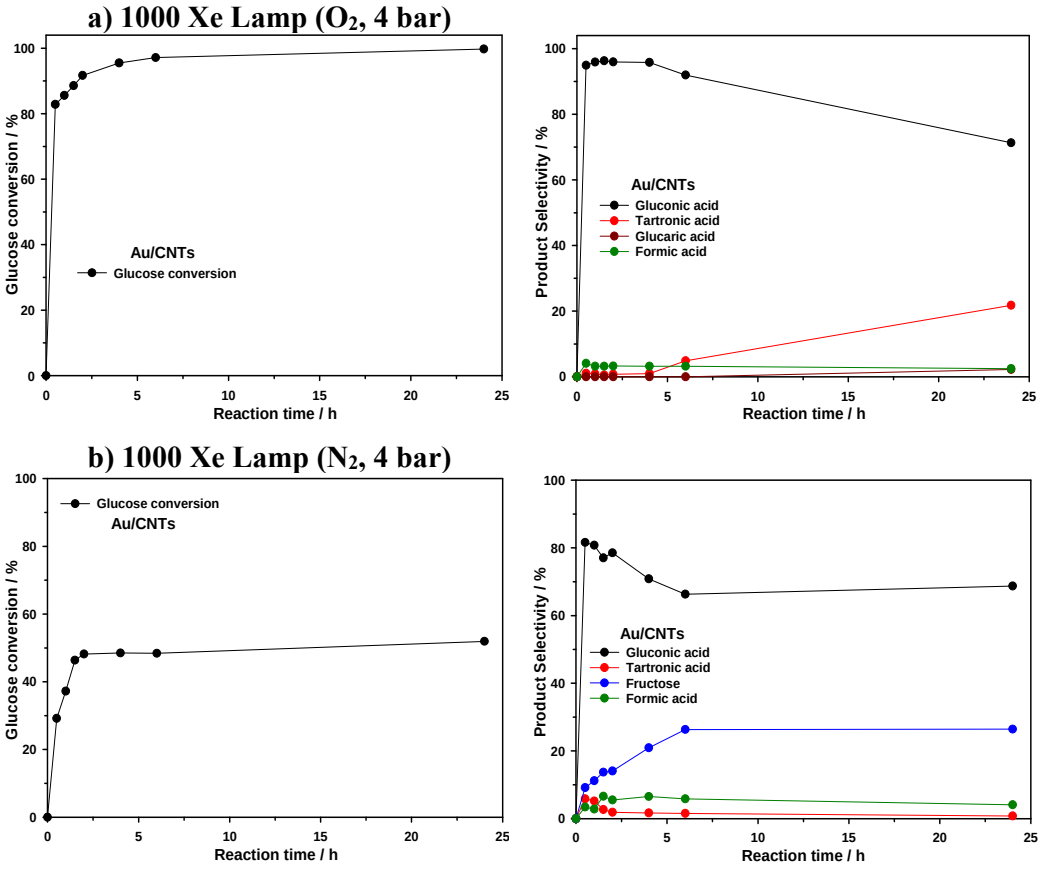

Figure 4.15 Glucose conversion and product selectivity values for the Au/CNTs catalyst under visible light irradiation and alkaline conditions. Reaction conditions: Visible light (1 kW), 90 mg of catalyst, Glucose/Na_2CO_3 = 1:1 molar ratio, 20 mM glucose stock solution (40 mL), T = 40±2 °C The mass balance in all cases was >97%.

The initial experiments were performed under oxygen or nitrogen atmosphere in the presence of visible light using the Au/CNTs catalyst. The reactions were carried out for 24 hours (Figure 4.15). The results showed a glucose conversion of 83% with a selectivity of 95% to gluconic acid after 30 minutes of reaction under 4 bar oxygen pressure (Figure 4.15a). When comparing these results with the ones obtained at atmospheric pressure (Figure 4.13), the effect of oxygen pressure on the oxidation of glucose showed an increase in conversion from 20% (atmospheric pressure) to 83% at the same reaction time (30 minutes). Moreover, it was found that the formation of tartronic acid was favoured at long reaction times. Tartronic acid is a high value-added chemical which is used in the pharmaceutical and food industry [99, 100]. These results clearly demonstrate the promotional effect of oxygen on the glucose oxidation in the presence of the Au/CNTs catalyst under visible light.

In order to further investigate the effect of oxygen, the reaction was carried out using nitrogen gas at a pressure of 4 bar under the same experimental conditions (temperature, glucose/base = 1:1 molar ratio and amount of catalyst). Interestingly, the results showed a drop in the glucose conversion from 83% (O_2, 4 bar) to 29% after 30 minutes of reaction when nitrogen was used under photocatalysis. The main products obtained were gluconic acid and fructose, with the latter, as a result of the isomerisation of glucose [35]. Clearly, the results showed that the use of nitrogen has a negative impact on the photo-oxidation of glucose as low conversion values and unwanted products (fructose) were observed.

The preliminary oxidation test demonstrated that the presence of oxygen improves the efficiency of the Au/CNTs catalyst, making photocatalysis an attractive route for the selective oxidation of biomass-derived molecules. Following this, we investigated the effect of the oxygen pressure on the photo-oxidation of glucose using the Au/CNTs catalyst under visible light irradiation and alkaline conditions. As it was found the oxidation of glucose showed high conversion values (83%) at short reaction times (Figure 4.15a) when a 20 mM glucose stock solution was used under 4 bar oxygen pressure. In order to properly evaluate the effect of oxygen pressure on the oxidation reaction, the glucose concentration was increased from 20 mM to 400 mM while keeping constant the amount of catalyst (90 mg). Moreover, the reaction time was reduced from 24 to 2 hours in order to avoid degradation of the products formed as it was observed in the preliminary test (Figure 4.15a).

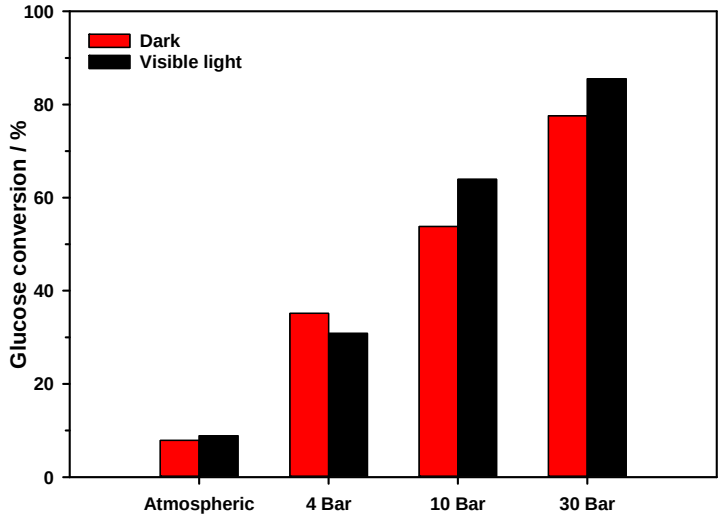

Figure 4.16 Effect of the oxygen pressure on the glucose conversion using the Au/CNTs catalyst under visible light irradiation and alkaline conditions.

Figure 4.16 and Table 4.5 show the glucose conversion and product selectivity values for the Au/CNTs catalyst respectively. As expected, the glucose conversion increased as the oxygen pressure did. For example, the results showed an increased in the conversion from 10% at atmospheric pressure to 85.5% at 30 bar oxygen pressure after 2 hours of reaction under visible light, thus showing the promotional effect of oxygen on the reaction rate. Furthermore, it was found that under atmospheric conditions the isomerization of glucose into fructose predominates over the oxidation reaction as a result of the low oxygen concentration. Gluconic acid was the main product in all cases, except for the reaction at atmospheric pressure (Table 4.5). It is worth noting that tartronic acid and formic acid were produced in low quantities despite the high oxygen concentration in some cases. This observation is notable as it suggests that the oxidation of glucose can be performed at short reaction times and high oxygen concentration using the Au/CNTs catalyst without loss of selectivity. Surprisingly, the reactions conducted in the dark showed conversion values very close to the ones for the reactions carried out under visible light (Figure 4.16). Once again, these results demonstrate the strong contribution of the thermal reaction (dark conditions) to the nonthermal one (light-driven process) and emphasize the importance of careful evaluation of the reaction conditions.

Table 4.5 Effect of the oxygen pressure on the glucose oxidation using the Au/CNTs catalyst under visible light irradiation and alkaline conditions. Conversion and product selectivity values after 2 hours of reaction time.[a]

	Pressure (Bar)	M.B. (%)	Conv. (%)	Selectivity[b] (%)			
				GL	TA	FT	FA
Dark	30	97.3	77.6	93.8	1.1	-	5.0
	10	96.3	53.7	91.1	1.0	-	7.8
	4	95.7	35.1	82.2	0.5	7.1	10
	Atmospheric	96.7	7.87	47.7	-	52	-
Visible Light	30	96.9	85.5	91.2	1.5	-	7.2
	10	95.9	63.9	84.9	1.2	-	13.7
	4	98.4	30.9	76.9	0.6	8.9	13.4
	Atmospheric	99.0	10.0	24.6	-	75	-

[a] Reaction conditions: Visible light (1 kW), 90 mg of catalyst, Glucose/Na_2CO_3 = 1:1 molar ratio, 400 mM glucose stock solution (40 mL), 2 hours reaction time, T = 40±2 °C.

[b] M.B.= Mass balance, Conv.= conversion, GL= Gluconic acid, TA= Tartronic acid, FT= Fructose, FA= Formic acid.

4.3 Conclusions

The photo-oxidation of glucose was carried out using gold metal nanoparticles supported on semiconductor materials such as titanium dioxide (TiO_2), conjugated microporous polymers (CMPs) and multi-walled carbon nanotubes (CNTs). The initial experiments were performed under basic conditions at atmospheric pressure, then a step forward was made by addition of molecular oxygen as the oxidant with the aim of improving the efficiency of the gold catalysts in the photo-oxidation of glucose.

The results obtained for the reactions carried out under visible light irradiation with the TiO_2 and Au/TiO_2 catalysts demonstrated the effect of the support on the oxidation reaction as it was found that both TiO_2 and Au/TiO_2 catalysts promoted the formation of several products such as gluconic acid, formic acid and short-chain aldoses (arabinose, erythrose, and glyceraldehyde). The presence of small sugars provides evidence of the α-scission mechanism which was first suggested by Chong et al. [25], and then later confirmed by Da Vià [19, 21]. These results contradict the work reported by Zhou et al. [23] and Omri et al. [22] as the authors claim that the selective photo-oxidation of glucose into gluconic acid (as the only product) can be performed using TiO_2-based gold catalysts under visible light irradiation and alkaline conditions.

The previous results provided useful information about the synergistic effect between the support and metal nanoparticles on the photo-oxidation of glucose. Therefore, we decided to use an organic semiconductor material as support for the gold nanoparticles due to their chemical inertness. Particularly, we focused on the conjugated microporous polymers (CMPs) as they have been used in photocatalytic applications due to their extended π-conjugation and remarkable photophysical properties [42-44]. The CMPs-supported gold catalysts were prepared using the SASI method developed in Chapter 3. The photo-oxidation of glucose was performed under the same experimental conditions as the TiO_2-based catalysts. Surprisingly, the results showed that under visible light irradiation or dark conditions the glucose oxidation displayed similar values of conversion and selectivity but more importantly, it was found that the use of CMPs inhibits the formation of side products compared to the TiO_2 support.

In order to further investigate the glucose oxidation under photocatalytic conditions. Multi-walled carbon nanotubes (CNTs) were used as support material for the gold nanoparticles. The Au/CNTs catalysts were prepared using the SASI method as reported in Chapter 3. The results showed an increase in the reaction rate when the oxidation was performed under visible light in alkaline conditions, however, similar glucose conversion was observed at the end of the reaction under dark conditions. Comparing these results with the ones under base-free conditions, it was clear that the presence of the base accelerates the glucose oxidation under visible light. Additional experiments were carried out using molecular oxygen as the oxidant under alkaline conditions. It was found that oxygen improves the reaction rate and the efficiency of the Au/CNTs under visible light irradiation. However, the results demonstrated once again the strong effect of the thermal reaction in the photocatalytic process.

4.4 References

[1] Y.-B. Huang, Y. Fu, Hydrolysis of cellulose to glucose by solid acid catalysts, Green Chem., 15 (2013) 1095-1111.

[2] L. Zhou, X. Yang, J. Xu, M. Shi, F. Wang, C. Chen, J. Xu, Depolymerization of cellulose to glucose by oxidation-hydrolysis, Green Chem., 17 (2015) 1519-1524.

[3] L. Hu, L. Lin, Z. Wu, S. Zhou, S. Liu, Chemocatalytic hydrolysis of cellulose into glucose over solid acid catalysts, Appl. Catal. B: Environ., 174–175 (2015) 225-243.

[4] G.L. Côté, 12 - Flavorings and other value-added products from sucrose**Mention of trade names or commercial products is solely for the purpose of providing specific information and does not imply recommendation or endorsement by the US Department of Agriculture, in: R. Rastall (Ed.) Novel Enzyme Technology for Food Applications, Woodhead Publishing2007, pp. 243-269.

[5] A. Fukuoka, P.L. Dhepe, Catalytic Conversion of Cellulose into Sugar Alcohols, Angew. Chem. Int. Ed., 118 (2006) 5285-5287.

[6] J.C. Colmenares, A. Magdziarz, Room temperature versatile conversion of biomass-derived compounds by means of supported TiO_2 photocatalysts, J. Mol. Catal. A: Chem., 366 (2013) 156-162.

[7] M. Besson, P. Gallezot, C. Pinel, Conversion of Biomass into Chemicals over Metal Catalysts, Chem. Rev., 114 (2014) 1827-1870.

[8] B. Jin, G. Yao, X. Wang, K. Ding, F. Jin, Photocatalytic Oxidation of Glucose into Formate on Nano TiO_2 Catalyst, ACS Sustainable Chem. Eng., 5 (2017) 6377-6381.

[9] Y. Sun, J. Cheng, Hydrolysis of lignocellulosic materials for ethanol production: a review, Bioresour. Technol., 83 (2002) 1-11.

[10] X. Fu, J. Long, X. Wang, D.Y.C. Leung, Z. Ding, L. Wu, Z. Zhang, Z. Li, X. Fu, Photocatalytic reforming of biomass: A systematic study of hydrogen evolution from glucose solution, Int. J. Hydrogen Energy, 33 (2008) 6484-6491.

[11] A.E. Koklin, T.A. Klimenko, A.V. Kondratyuk, V.V. Lunin, V.I. Bogdan, Transformation of aqueous solutions of glucose over the Pt/C catalyst, Kinet. Catal., 56 (2015) 84-88.

[12] A.M. Cañete-Rodríguez, I.M. Santos-Dueñas, J.E. Jiménez-Hornero, A. Ehrenreich, W. Liebl, I. García-García, Gluconic acid: Properties, production methods and applications—An excellent opportunity for agro-industrial by-products and waste bio-valorization, Process Biochem., 51 (2016) 1891-1903.

[13] U.R. Pillai, E. Sahle–Demessie, Selective Oxidation of Alcohols in Gas Phase Using Light-Activated Titanium Dioxide, J. Catal., 211 (2002) 434-444.

[14] K.J. Green, R. Rudham, Photocatalytic oxidation of propan-2-ol by semiconductor–zeolite composites, J. Chem. Soc., Faraday Trans., 89 (1993) 1867-1870.

[15] O.S. Mohamed, A.E.-A.M. Gaber, A.A. Abdel-Wahab, Photocatalytic oxidation of selected aryl alcohols in acetonitrile, J. Photochem. Photobiol. A: Chem., 148 (2002) 205-210.

[16] S. Farhadi, M. Afshari, M. Maleki, Z. Babazadeh, Photocatalytic oxidation of primary and secondary benzylic alcohols to carbonyl compounds catalyzed by $H_3PW_{12}O_{40}/SiO_2$ under an O_2 atmosphere, Tetrahedron Lett., 46 (2005) 8483-8486.

[17] J.C. Colmenares, A. Magdziarz, A. Bielejewska, High-value chemicals obtained from selective photo-oxidation of glucose in the presence of nanostructured titanium photocatalysts, Bioresour. Technol., 102 (2011) 11254-11257.

[18] J.C. Colmenares, A. Magdziarz, K. Kurzydlowski, J. Grzonka, O. Chernyayeva, D. Lisovytskiy, Low-temperature ultrasound-promoted synthesis of $Cr–TiO_2$-supported photocatalysts for valorization of glucose and phenol degradation from liquid phase, Appl. Catal. B: Environ., 134–135 (2013) 136-144.

[19] L. Da Già, C. Recchi, E.O. Gonzalez-Yañez, T.E. Davies, J.A. Lopez-Sanchez, Visible light selective photocatalytic conversion of glucose by TiO_2, Appl. Catal., B: Environ., 202 (2017) 281-288.

[20] J.C. Colmenares, A. Magdziarz, O. Chernyayeva, D. Lisovytskiy, K. Kurzydłowski, J. Grzonka, Sonication-Assisted Low-Temperature Routes for the Synthesis of Supported $Fe–TiO_2$ Econanomaterials: Partial Photooxidation of Glucose and Phenol Aqueous Degradation, ChemCatChem, 5 (2013) 2270-2277.

[21] L. Da Già, C. Recchi, T.E. Davies, N. Greeves, J.A. Lopez-Sanchez, Visible-Light-Controlled Oxidation of Glucose using Titania-Supported Silver Photocatalysts, ChemCatChem, 8 (2016) 3475-3483.

[22] M. Omri, F. Sauvage, Y. Busby, M. Becuwe, G. Pourceau, A. Wadouachi, Gold Catalysis and Photoactivation: A Fast and Selective Procedure for the Oxidation of Free Sugars, ACS Catalysis, (2018) 1635-1639.

[23] B. Zhou, J. Song, Z. Zhang, Z. Jiang, P. Zhang, B. Han, Highly selective photocatalytic oxidation of biomass-derived chemicals to carboxyl compounds over Au/TiO_2, Green Chem., 19 (2017) 1075-1081.

[24] B. Ohtani, O.O. Prieto-Mahaney, D. Li, R. Abe, What is Degussa (Evonik) P25? Crystalline composition analysis, reconstruction from isolated pure particles and photocatalytic activity test, J. Photochem. Photobiol. A: Chem., 216 (2010) 179-182.

[25] R. Chong, J. Li, Y. Ma, B. Zhang, H. Han, C. Li, Selective conversion of aqueous glucose to value-added sugar aldose on TiO_2-based photocatalysts, J. Catal., 314 (2014) 101-108.

[26] M. Bellardita, E.I. García-López, G. Marcì, B. Megna, F.R. Pomilla, L. Palmisano, Photocatalytic conversion of glucose in aqueous suspensions of heteropolyacid–TiO_2 composites, RSC Adv., 5 (2015) 59037-59047.

[27] J.A. Stapley, J.N. BeMiller, The Ruff degradation: a review of previously proposed mechanisms with evidence that the reaction proceeds by a Hofer–Moest-type reaction, Carbohydr. Res., 342 (2007) 407-418.

[28] J.A. Lopez-Sanchez, N. Dimitratos, C. Hammond, G.L. Brett, L. Kesavan, S. White, P. Miedziak, R. Tiruvalam, R.L. Jenkins, A.F. Carley, D. Knight, C.J. Kiely, G.J. Hutchings, Facile removal of stabilizer-ligands from supported gold nanoparticles, Nat. Chem., 3 (2011) 551.

[29] A. Villa, D. Wang, G.M. Veith, F. Vindigni, L. Prati, Sol immobilization technique: a delicate balance between activity, selectivity and stability of gold catalysts, Catal. Sci. Technol., 3 (2013) 3036-3041.

[30] S. Biella, L. Prati, M. Rossi, Selective Oxidation of D-Glucose on Gold Catalyst, J. Catal., 206 (2002) 242-247.

[31] A.M. Nadeem, G.I.N. Waterhouse, H. Idriss, The reactions of ethanol on TiO_2 and Au/TiO2 anatase catalysts, Catal. Today, 182 (2012) 16-24.

[32] Y. Borensztein, L. Delannoy, A. Djedidi, R.G. Barrera, C. Louis, Monitoring of the Plasmon Resonance of Gold Nanoparticles in Au/TiO_2 Catalyst under Oxidative and Reducing Atmospheres, J. Phys. Chem. C, 114 (2010) 9008-9021.

[33] X. Pan, Y.-J. Xu, Fast and spontaneous reduction of gold ions over oxygen-vacancy-rich TiO_2: A novel strategy to design defect-based composite photocatalyst, Appl. Catal. A: Gen., 459 (2013) 34-40.

[34] R. Zanella, S. Giorgio, C.-H. Shin, C.R. Henry, C. Louis, Characterization and reactivity in CO oxidation of gold nanoparticles supported on TiO_2 prepared by deposition-precipitation with NaOH and urea, J. Catal., 222 (2004) 357-367.

[35] A.A. Marianou, C.M. Michailof, A. Pineda, E.F. Iliopoulou, K.S. Triantafyllidis, A.A. Lappas, Glucose to Fructose Isomerization in Aqueous Media over Homogeneous and Heterogeneous Catalysts, ChemCatChem, 8 (2016) 1100-1110.

[36] P.J. Miedziak, H. Alshammari, S.A. Kondrat, T.J. Clarke, T.E. Davies, M. Morad, D.J. Morgan, D.J. Willock, D.W. Knight, S.H. Taylor, G.J. Hutchings, Base-free glucose oxidation using air with supported gold catalysts, Green Chem., 16 (2014) 3132-3141.

[37] Y. Cao, X. Liu, S. Iqbal, P.J. Miedziak, J.K. Edwards, R.D. Armstrong, D.J. Morgan, J. Wang, G.J. Hutchings, Base-free oxidation of glucose to gluconic acid using supported gold catalysts, Catal. Sci. Technol., 6 (2016) 107-117.

[38] M. Comotti, C.D. Pina, M. Rossi, Mono- and bimetallic catalysts for glucose oxidation, J. Mol. Catal. A: Chem., 251 (2006) 89-92.

[39] U. Prüße, M. Herrmann, C. Baatz, N. Decker, Gold-catalyzed selective glucose oxidation at high glucose concentrations and oxygen partial pressures, Appl. Catal. A. : Gen., 406 (2011) 89-93.

[40] S. Link, M.A. El-Sayed, Size and Temperature Dependence of the Plasmon Absorption of Colloidal Gold Nanoparticles, J. Phys. Chem. B, 103 (1999) 4212-4217.

[41] B. Balamurugan, T. Maruyama, Evidence of an enhanced interband absorption in Au nanoparticles: Size-dependent electronic structure and optical properties, Appl. Phys. Lett., 87 (2005) 143105.

[42] R.S. Sprick, J.-X. Jiang, B. Bonillo, S. Ren, T. Ratvijitvech, P. Guiglion, M.A. Zwijnenburg, D.J. Adams, A.I. Cooper, Tunable Organic Photocatalysts for Visible-Light-Driven Hydrogen Evolution, J. Am. Chem. Soc., 137 (2015) 3265-3270.

[43] R.S. Sprick, B. Bonillo, M. Sachs, R. Clowes, J.R. Durrant, D.J. Adams, A.I. Cooper, Extended conjugated microporous polymers for photocatalytic hydrogen evolution from water, Chem. Commun., 52 (2016) 10008-10011.

[44] S.R. Sebastian, B. Baltasar, C. Rob, G. Pierre, B.N. J., S.B. J., B. Frédéric, Z.M. A., A.D. J., C.A. I., Visible-Light-Driven Hydrogen Evolution Using Planarized Conjugated Polymer Photocatalysts, Angew.Chem. , 55 (2016) 1792-1796.

[45] L. Chen, Y. Honsho, S. Seki, D. Jiang, Light-Harvesting Conjugated Microporous Polymers: Rapid and Highly Efficient Flow of Light Energy with a Porous Polyphenylene Framework as Antenna, J. Am. Chem. Soc., 132 (2010) 6742-6748.

[46] M.-L. Wu, D.-H. Chen, T.-C. Huang, Synthesis of Au/Pd Bimetallic Nanoparticles in Reverse Micelles, Langmuir, 17 (2001) 3877-3883.

[47] Y. Shiraishi, T. Hirai, Selective organic transformations on titanium oxide-based photocatalysts, Journal of Photochemistry and Photobiology C: Photochemistry Reviews, 9 (2008) 157-170.

[48] J. Prakash, R.A. Harris, H.C. Swart, Embedded plasmonic nanostructures: synthesis, fundamental aspects and their surface enhanced Raman scattering applications, Int. Rev. Phys. Chem., 35 (2016) 353-398.

[49] J. Prakash, V. Kumar, R.E. Kroon, K. Asokan, V. Rigato, K.H. Chae, S. Gautam, H.C. Swart, Optical and surface enhanced Raman scattering properties of Au nanoparticles embedded in and located on a carbonaceous matrix, Phys.Chem.Chem.Phys., 18 (2016) 2468-2480.

[50] Y. Xia, N.J. Halas, Shape-Controlled Synthesis and Surface Plasmonic Properties of Metallic Nanostructures, MRS Bulletin, 30 (2011) 338-348.

[51] X. Huang, M.A. El-Sayed, Gold nanoparticles: Optical properties and implementations in cancer diagnosis and photothermal therapy, J. Adv. Res., 1 (2010) 13-28.

[52] X. Wu, A. Centeno, X. Zhang, D. Darvill, M.P. Ryan, D.J. Riley, N.M. Alford, F. Xie, Broadband plasmon photocurrent generation from Au nanoparticles/ mesoporous TiO_2 nanotube electrodes, Sol. Energy Mater. Sol. Cells, 138 (2015) 80-85.

[53] J. Zhu, Z. Xu, B. Lu, Ultrafine Au nanoparticles decorated $NiCo_2O_4$ nanotubes as anode material for high-performance supercapacitor and lithium-ion battery applications, Nano Energy, 7 (2014) 114-123.

[54] C. Wang, D. Astruc, Nanogold plasmonic photocatalysis for organic synthesis and clean energy conversion, Chem. Soc. Rev., 43 (2014) 7188-7216.

[55] J. Yang, X. Wang, Y. Chen, J. Dai, S. Sun, Enhanced photocatalytic activities of visible-light driven green synthesis in water and environmental remediation on Au/Bi_2WO_6 hybrid nanostructures, RSC Adv., 5 (2015) 9771-9782.

[56] J. Thomas, M. Yoon, Facile synthesis of pure TiO_2(B) nanofibers doped with gold nanoparticles and solar photocatalytic activities, Appl. Catal. B: Environ., 111-112 (2012) 502-508.

[57] A. Gołąbiewska, A. Malankowska, M. Jarek, W. Lisowski, G. Nowaczyk, S. Jurga, A. Zaleska-Medynska, The effect of gold shape and size on the properties and visible light-induced photoactivity of Au-TiO_2, Appl. Catal. B: Environ., 196 (2016) 27-40.

[58] R. Liu, H. Huang, H. Li, Y. Liu, J. Zhong, Y. Li, S. Zhang, Z. Kang, Metal Nanoparticle/Carbon Quantum Dot Composite as a Photocatalyst for High-Efficiency Cyclohexane Oxidation, ACS Catal., 4 (2014) 328-336.

[59] X. Guo, C. Hao, G. Jin, H.-Y. Zhu, X.-Y. Guo, Copper Nanoparticles on Graphene Support: An Efficient Photocatalyst for Coupling of Nitroaromatics in Visible Light, Angew. Chem. Int. Ed., 53 (2014) 1973-1977.

[60] M.E. Khan, M.M. Khan, M.H. Cho, Green synthesis, photocatalytic and photoelectrochemical performance of an Au–Graphene nanocomposite, RSC Adv., 5 (2015) 26897-26904.

[61] K. Ullah, S. Ye, L. Zhu, Z.-D. Meng, S. Sarkar, W.-C. Oh, Microwave assisted synthesis of a noble metal-graphene hybrid photocatalyst for high efficient decomposition of organic dyes under visible light, Mater. Sci. Eng. B, 180 (2014) 20-26.

[62] M.L.d.O. Pereira, D. Grasseschi, H.E. Toma, Photocatalytic Activity of Reduced Graphene Oxide–Gold Nanoparticle Nanomaterials: Interaction with Asphaltene and Conversion of a Model Compound, Energy Fuels, 32 (2018) 2673-2680.

[63] G. Darabdhara, P.K. Boruah, P. Borthakur, N. Hussain, M.R. Das, T. Ahamad, S.M. Alshehri, V. Malgras, K.C.W. Wu, Y. Yamauchi, Reduced graphene oxide nanosheets decorated with Au–Pd bimetallic alloy nanoparticles towards efficient photocatalytic degradation of phenolic compounds in water, Nanoscale, 8 (2016) 8276-8287.

[64] P. Kar, S. Sardar, B. Liu, M. Sreemany, P. Lemmens, S. Ghosh, S.K. Pal, Facile synthesis of reduced graphene oxide–gold nanohybrid for potential use in industrial waste-water treatment, Sci. Technol. Adv. Mater., 17 (2016) 375-386.

[65] H. Ali, N.R. Jana, Plasmonic photocatalysis: complete degradation of bisphenol A by a gold nanoparticle–reduced graphene oxide composite under visible light, Photochem. Photobiol. Sci., 17 (2018) 628-637.

[66] R.H. Baughman, A.A. Zakhidov, W.A. de Heer, Carbon Nanotubes--the Route Toward Applications, Science, 297 (2002) 787-792.

[67] A.C. Dillon, Carbon Nanotubes for Photoconversion and Electrical Energy Storage, Chem. Rev. , 110 (2010) 6856-6872.

[68] R. Leary, A. Westwood, Carbonaceous nanomaterials for the enhancement of TiO2 photocatalysis, Carbon, 49 (2011) 741-772.

[69] K. Woan, G. Pyrgiotakis, W. Sigmund, Photocatalytic Carbon-Nanotube–TiO_2 Composites, Adv. Mater. , 21 (2009) 2233-2239.

[70] J. Liu, R. Liu, H. Li, W. Kong, H. Huang, Y. Liu, Z. Kang, Au nanoparticles in carbon nanotubes with high photocatalytic activity for hydrocarbon selective oxidation, Dalton Trans., 43 (2014) 12982-12988.

[71] C.G. Silva, M.J. Sampaio, R.R.N. Marques, L.A. Ferreira, P.B. Tavares, A.M.T. Silva, J.L. Faria, Photocatalytic production of hydrogen from methanol and saccharides using carbon nanotube-TiO_2 catalysts, Appl. Catal. B: Environ., 178 (2015) 82-90.

[72] V. Krishna, S. Pumprueg, S.H. Lee, J. Zhao, W. Sigmund, B. Koopman, B.M. Moudgil, Photocatalytic Disinfection with Titanium Dioxide Coated Multi-Wall Carbon Nanotubes, Process Saf. Environ. Prot., 83 (2005) 393-397.

[73] S.-H. Lee, S. Pumprueg, B. Moudgil, W. Sigmund, Inactivation of bacterial endospores by photocatalytic nanocomposites, Colloids Surf. B, 40 (2005) 93-98.

[74] Y. Yu, J.C. Yu, J.-G. Yu, Y.-C. Kwok, Y.-K. Che, J.-C. Zhao, L. Ding, W.-K. Ge, P.-K. Wong, Enhancement of photocatalytic activity of mesoporous TiO_2 by using carbon nanotubes, Appl. Catal. A: Gen., 289 (2005) 186-196.

[75] W. Wang, P. Serp, P. Kalck, J.L. Faria, Photocatalytic degradation of phenol on MWNT and titania composite catalysts prepared by a modified sol–gel method, Appl. Catal. B: Environ., 56 (2005) 305-312.

[76] Y. Luo, J. Liu, X. Xia, X. Li, T. Fang, S. Li, Q. Ren, J. Li, Z. Jia, Fabrication and characterization of TiO_2/short MWNTs with enhanced photocatalytic activity, Mater. Lett., 61 (2007) 2467-2472.

[77] T. Belin, F. Epron, Characterization methods of carbon nanotubes: a review, Mat. Sci. Eng. B, 119 (2005) 105-118.

[78] S. Akbayrak, S. Özkar, Ruthenium(0) Nanoparticles Supported on Multiwalled Carbon Nanotube As Highly Active Catalyst for Hydrogen Generation from Ammonia–Borane, ACS Appl. Mater. Interfaces, 4 (2012) 6302-6310.

[79] Z. Sun, X. Zhang, Na, Z. Liu, B. Han, G. An, Synthesis of ZrO_2−Carbon Nanotube Composites and Their Application as Chemiluminescent Sensor Material for Ethanol, J. Phys. Chem. B, 110 (2006) 13410-13414.

[80] M.H. Majles Ara, Z. Dehghani, R. Sahraei, A. Daneshfar, Z. Javadi, F. Divsar, Diffraction patterns and nonlinear optical properties of gold nanoparticles, J. Quant. Spectrosc. Radiat. Transfer, 113 (2012) 366-372.

[81] Y. Chen, X. Gu, C.-G. Nie, Z.-Y. Jiang, Z.-X. Xie, C.-J. Lin, Shape controlled growth of gold nanoparticles by a solution synthesis, Chem. Commun., (2005) 4181-4183.

[82] N. Vo Ke Thanh, H. Trong Phat, N. Dang Giang, N. Hoang Phuong Uyen, L. Quang Vinh, H. Thanh Dat, Synthesis and spectroscopic characterization of gold nanobipyramids prepared by a chemical reduction method, Adv. Nat. Sci.: Nanosci. Nanotechnol., 6 (2015) 045017.

[83] I.B.C. Gallo, E.A. Carbonio, H.M. Villullas, What Determines Electrochemical Surface Processes on Carbon-Supported PdAu Nanoparticles?, ACS Catal., 8 (2018) 1818-1827.

[84] C. Gentilini, F. Evangelista, P. Rudolf, P. Franchi, M. Lucarini, L. Pasquato, Water-Soluble Gold Nanoparticles Protected by Fluorinated Amphiphilic Thiolates, J. Am. Chem. Soc., 130 (2008) 15678-15682.

[85] Y. Du, R. Hu, Y. Jia, Q. Zhou, W. Meng, J. Yang, $CuCl_2$ promoted low-gold-content Au/C catalyst for acetylene hydrochlorination prepared by ultrasonic-assisted impregnation, J. Ind. Eng. Chem., 37 (2016) 32-41.

[86] L. Ilieva, G. Pantaleo, I. Ivanov, R. Zanella, J.W. Sobczak, W. Lisowski, A.M. Venezia, D. Andreeva, Preferential oxidation of CO in H_2 rich stream (PROX) over gold catalysts supported on doped ceria: Effect of water and CO_2, Catal. Today, 175 (2011) 411-419.

[87] L. Abis, L. Armelao, D. Belli Dell'Amico, F. Calderazzo, F. Garbassi, A. Merigo, E.A. Quadrelli, Gold molecular precursors and gold–silica interactions, J. Chem. Soc., Dalton Trans., (2001) 2704-2709.

[88] Y. Luo, Y. Heng, X. Dai, W. Chen, J. Li, Preparation and photocatalytic ability of highly defective carbon nanotubes, J. Solid State Chem., 182 (2009) 2521-2525.

[89] M. Haruta, Gold rush, Nature, 437 (2005) 1098.

[90] P.N. Amaniampong, X. Jia, B. Wang, S.H. Mushrif, A. Borgna, Y. Yang, Catalytic oxidation of cellobiose over TiO_2 supported gold-based bimetallic nanoparticles, Catal. Sci. Technol., 5 (2015) 2393-2405.

[91] P.N. Amaniampong, K. Li, X. Jia, B. Wang, A. Borgna, Y. Yang, Titania-Supported Gold Nanoparticles as Efficient Catalysts for the Oxidation of Cellobiose to Organic Acids in Aqueous Medium, ChemCatChem, 6 (2014) 2105-2114.

[92] S.E. Davis, M.S. Ide, R.J. Davis, Selective oxidation of alcohols and aldehydes over supported metal nanoparticles, Green Chem., 15 (2013) 17-45.

[93] Y. Nosaka, A.Y. Nosaka, Generation and Detection of Reactive Oxygen Species in Photocatalysis, Chem. Rev., 117 (2017) 11302-11336.

[94] F.J. López-Tenllado, A. Marinas, F.J. Urbano, J.C. Colmenares, M.C. Hidalgo, J.M. Marinas, J.M. Moreno, Selective photooxidation of alcohols as test reaction for photocatalytic activity, Appl. Catal., B: Environ., 128 (2012) 150-158.

[95] V. Augugliaro, H. Kisch, V. Loddo, M.J. López-Muñoz, C. Márquez-Álvarez, G. Palmisano, L. Palmisano, F. Parrino, S. Yurdakal, Photocatalytic oxidation of aromatic alcohols to aldehydes in aqueous suspension of home-prepared titanium dioxide: 1. Selectivity enhancement by aliphatic alcohols, Appl. Catal. A: Gen., 349 (2008) 182-188.

[96] P.R. Harvey, R. Rudham, S. Ward, Photocatalytic oxidation of liquid alcohols and binary alcohol mixtures by rutile, J. Chem. Soc., Faraday Trans. 1, 79 (1983) 2975-2981.

[97] A. Lüken, M. Muhler, J. Strunk, On the role of gold nanoparticles in the selective photooxidation of 2-propanol over Au/TiO_2, Phys. Chem. Chem. Phys., 17 (2015) 10391-10397.

[98] W. Schilling, D. Riemer, Y. Zhang, N. Hatami, S. Das, Metal-Free Catalyst for Visible-Light-Induced Oxidation of Unactivated Alcohols Using Air/Oxygen as an Oxidant, ACS Catal., 8 (2018) 5425-5430.

[99] X. Tian, Z. Wang, P. Yang, R. Hao, S. Jia, N. Li, L. Li, Z. Zhu, Green oxidation of bio-lactic acid with H_2O_2 into tartronic acid under UV irradiation, RSC Adv., 6 (2016) 41007-41010.

[100] P.M. Bizot, B.R. Bailey, P.D. Hicks, Use of tartronic acid as an oxygen scavenger, Patent US5750037, (1998).

Chapter 5

Photocatalytic Conversion of Polysaccharides by Noble Metals Supported on TiO_2

5.1 Introduction

Titania or Titanium dioxide (TiO_2) is the most studied semiconductor since the discovery of the photoelectrochemical water splitting by Fujishima and Honda [1]. The TiO_2 photocatalyst presents some advantages such as high stability, nontoxicity, low cost, and remarkably photoactivity [2]. Despite the intrinsic properties that make it an ideal photocatalyst, TiO_2 cannot be activated under visible light as it only absorbs wavelengths below 380 nm due to the wide bandgaps of its components (rutile-3.2 eV and anatase-3.0 eV) and therefore, UV light irradiation is required to generate electron-hole pairs [3, 4]. The use of UV light is the major drawback of the TiO_2 photocatalyst as it comprises only ~5% of the solar spectrum. Therefore, several strategies have been used to extend the TiO_2 photoresponse to the visible region of the solar spectrum, for example, sensitization using organic dyes [5] or metal complexes [6], doping with nonmetallic impurities [7, 8], coupling with a narrow-band-gap semiconductor [9, 10], and deposition of noble metals (i.e. Au, Ag, Pt) [11-13].

On the other hand, photocatalysis has emerged as an alternative route for the photodegradation of organic pollutants from the pulp and paper industry. Particularly, the combination of UV light irradiation and the TiO_2 catalyst has been used in the purification and treatment of cellulose bleaching effluents [14-16]. However, most of these studies were dedicated to the photodegradation of the organic matter. In an attempt to produce valuable chemicals, early studies showed the production of CO and CO_2 from cellulose [17], while others reported the production of volatile hydrocarbons under UV light irradiation [18, 19]. In 2011 Fan et al. [20] reported for the first time the selective photoconversion of cellulose into 5-hydroxymethylfurfural (HMF) using TiO_2 thin films in the presence of a concentrated $ZnCl_2$ solution. Later, Wang et al. [21] demonstrated for the first time the conversion of microcrystalline cellulose (previously treated with 1-ethyl-3-methylimidazolium chloride) into glucose and HMF under visible light irradiation using an Au/HY-zeolite/TiO_2 hybrid photocatalysts at 140 °C for 6 hours. More recently, in 2016 Zhang et al. [22] reported the hydrogen production along with small traces of sugars and acids from cellulose under UV light conditions. Although these studies have demonstrated that cellulose can be converted into high-valuable chemicals under light irradiation, the use of high temperatures and expensive solvents limits the application of photocatalysis as an environmentally friendly alternative.

In this chapter, we present a new approach for the photocatalytic conversion of polysaccharides into valuable chemicals under light irradiation. This section will focus on the photoconversion of complex feedstocks (α-cellulose, Avicel® PH-101, starch soluble) in the presence of light irradiation using TiO_2-supported noble metal catalysts under oxygen pressure. Parameters such as nature of the substrate, light intensity, reaction time and solvent composition were investigated in order to get the best reaction conditions for the photocatalytic conversion of polysaccharides.

5.2 Results and discussion

The photocatalytic conversion of polysaccharides (α-cellulose, Avicel® PH-101, starch soluble) was carried out using noble metals supported on TiO_2 under UVA and visible light irradiation. The reactions were performed using three different systems: a 300 W Xenon Oriel Arc Lamp (Mod. 6258, Newport, UK), a 1000 W Xenon Oriel Arc Lamp (Mod. 6271, Newport, UK), and a Luzchem Photoreactor (Mod. LZC-4, Luzchem Research Inc., CAN). The lamps were equipped with a UV filter with a cut-off value of 420 nm and with a water filter to remove the IR radiation and avoid overheating of the reaction mixture. The Luzchem Photoreactor was equipped with 16 UVA lamps, which provide a total power of 128 W. In a typical test, the appropriate amount of the polysaccharide was suspended in water or a water/acetonitrile mixture 50/50 v/v, then the catalyst was added and the reactor sealed. For the experiments under pressure, the reaction vessel was purged with nitrogen three times and then pressurized with the appropriate gas (O_2 or H_2). Reactions under alkaline conditions were carried out using NaOH as the base with a substrate/base = 1:1 molar ratio. In all cases, the reaction mixture was allowed to reach equilibrium for 10 minutes in the absence of light. The temperature was recorded using a thermocouple and an internal temperature controller (FuzyPro 1/6 DIN, HCS Ltd., CAN) for the 300 W Xenon Lamp and the Luzchem photoreactor respectively. For the pressurized system, the temperature was set to 40 °C and monitored using a 4848 Reactor Controller (Parr Instrument Company, Illinois, USA). Liquid products were separated from the reaction mixture using a PTFE filter (GILSON®, 0.22 μm) and quantified using HPLC analysis. Gas phase products (H_2 and CO_2) were collected using a Tedlar® PLV Gas Sampling Bag (Sigma-Aldrich) and quantified using GC analysis.

5.2.1 Catalyst Testing

The photocatalytic conversion of polysaccharides was performed using TiO_2-supported noble metal catalysts under UVA and visible light conditions. The catalysts were prepared using the traditional wet impregnation method (section 2.4.1). Briefly, the support (TiO_2) was suspended in water under vigorous stirring, then the appropriate amount of the aqueous solution of the metal salt was added ($HAuCl_4 \cdot 3H_2O$, $AgNO_3$, $H_2PtCl_6 \cdot xH_2O$, $Pd(NO_3)_2 \cdot 2H_2O$, $RuCl_3 \cdot xH_2O$) and finally, the solution was left to evaporate at constant temperature until it became a paste. The obtained solid was dried under reduced pressure for 12 hours and calcined under static air for 3 hours at 400 °C with a heating rate of 2 °C min^{-1}. The Pt/TiO_2 and Ru/TiO_2 catalysts were reduced under H_2 flow (50 mL/min^{-1}) with a heating rate of 2 °C min^{-1} for 4 hours before reaction.

The ICP-OES analysis of the TiO_2-based catalysts is reported in Table 5.1. The results showed that the real metal loading was lower than the nominal value in some cases, indicating an incomplete metal deposition. However, the traditional wet impregnation method was chosen for the preparation of the catalysts because of its simplicity and low-level waste, making it attractive for scale-up production.

Table 5.1 ICP-OES analysis for the TiO_2-supported noble metal catalysts prepared by the traditional impregnation method.

Catalysts	$[Au]_{nominal}$ / wt%	$[Au]_{real}$ / wt%
Au/TiO_2	1.5	1.52
Ag/TiO_2	1.5	1.16
Pt/TiO_2	1.5	1.14
Pd/TiO_2	1.5	1.27
Ru/TiO_2	1.5	1.41

The catalysts were characterized by diffuse reflectance UV-Vis spectroscopy (DR UV-Vis) as shown in Figure 5.1. The DR UV-Vis spectrum of the TiO_2 support showed a strong band in the range of 200-380 nm, indicating that the TiO_2 support can only be activated in the UV region (purple line). In the case of the Au/TiO_2 catalyst, the UV-Vis spectrum showed an absorption peak located at 580 nm in the visible region, which is assigned to the surface plasmon resonance effect (SPR) of

the gold nanoparticles (dark red line). Plasmonic peaks in the same region have been attributed to the presence of gold nanoparticles [23-26]. The solid UV-Vis spectrum of the Ag/TiO_2 catalysts showed a plasmonic peak in the visible range at 450 nm (green line), which is attributed to the presence of silver nanoparticles [27-29].

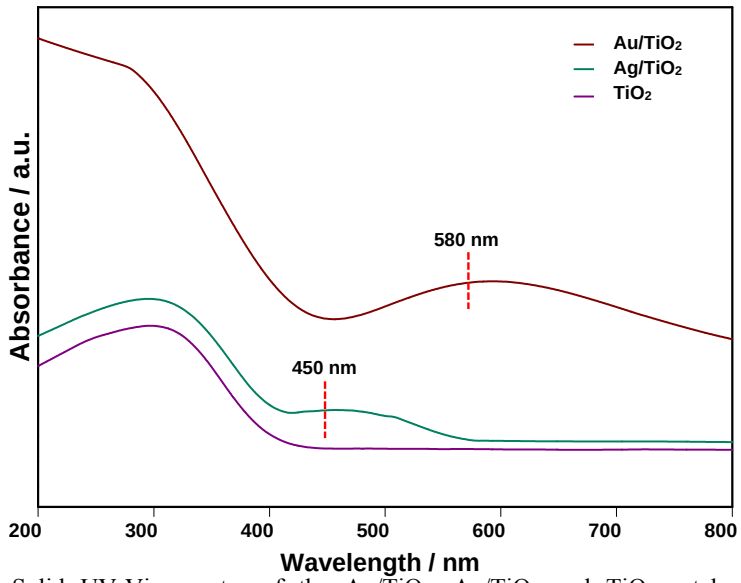

Figure 5.1 Solid UV-Vis spectra of the Au/TiO_2, Ag/TiO_2 and TiO_2 catalysts used for the photoconversion of polysaccharides under UVA and visible light conditions.

5.2.1.1 Photocatalytic Conversion of α-Cellulose Under Light Irradiation

Cellulose is a polymer which consists of several glucose units linked via β-1,4-glycosidic bonds. Due to the high amount of hydroxyl groups in the structure, cellulose can easily form intra- and intermolecular hydrogen bonds, leading to the formation of a rigid structure [30, 31], which is insoluble in water and most common solvents [32]. Therefore, the cellulose's crystalline structure limits its reactivity to be depolymerized it into soluble oligosaccharides and glucose. In order to reduce the crystallinity of cellulose and increase its reactivity, several pretreatment methods

have been used to facilitate the transformation of cellulose, for example, acid treatment, solubilisation in ionic liquids and nonthermal atmospheric plasma among others [33-35]. In this work, the ball-milling method [36-38] was used to reduce the crystallinity of cellulose and improve the efficiency of the TiO_2-based catalysts. The sample (α-cellulose, 2.5 g) was pulverized with ZrO_2 balls (10 mm, 18 balls) in a 45 mL grinding bowl (ZrO_2) for 48 hours at 600 rpm using a Planetary Micro Mill (Fritsch GmbH, PULVERISETTE 7 premium line).

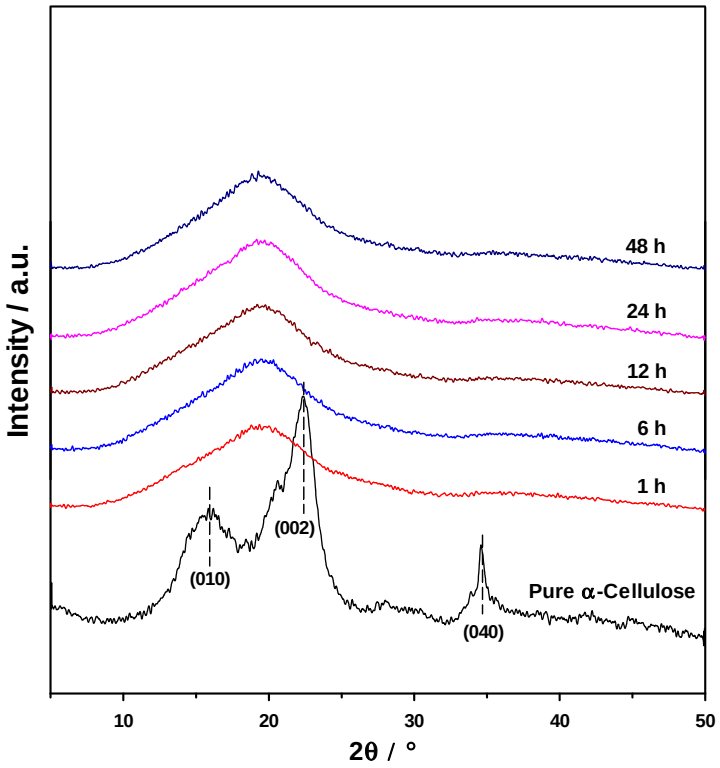

Figure 5.2 XRD patterns of the Pure α-Cellulose and Milled α-Cellulose.

XRD analysis of the pure α-cellulose and milled α-cellulose is shown in Figure 5.2. The XRD pattern of the pure α-cellulose showed the presence of reflection signals at $2\theta \approx 16.1°$, 22.4° and 34.5° that correspond to the [0 1 0], [0 0 2] and [0 4 0] planes of the cellulose crystalline structure [37, 39]. For the milled α-cellulose, the XRD analysis did not show the presence of peaks for crystalline cellulose in the samples, indicating that amorphous cellulose was formed in all cases.

To date, cellulose has only been investigated in photocatalysis for the purification and abatement of organic pollutants from the pulp and paper industry using TiO_2 as the photocatalyst under UV light irradiation [14-16]. The importance of TiO_2 as the photocatalyst in the photodegradation of organic pollutants in the cellulose bleaching effluents is associated with the production of strong oxidant species which are used to degrade the organic matter. In addition to the formation of highly oxidative species by the TiO_2 photocatalyst, it has been reported that the use of molecular oxygen accelerates the photodegradation of organic matter due to the formation of reactive oxygen species (ROS) by the photocatalytic reduction and oxidation processes of oxygen and water [40-42]. The combination of TiO_2 and molecular oxygen in the presence of UV light irradiation, it appears to be the most feasible alternative to degrade the rigid structure of cellulose. Therefore, we decided to carry out the photocatalytic conversion of the milled α-cellulose under UV light irradiation using TiO_2-based catalysts with molecular oxygen.

The initial experiments were carried out using bare TiO_2 (90 mg) as the photocatalyst in the presence of molecular oxygen (10 bar) under UV light irradiation (1000 W) for 24 hours. Pure water and a 50/50 v/v water/acetonitrile mixture were used as a solvents for the milled α-cellulose (50 mg). The water/acetonitrile mixture has been reported to promote selective oxidations as lower water content might hinder the formation of highly reactive radicals as reported by Colmenares et al. [43, 44].

Prior to the photocatalytic experiments, HPLC analysis of the pure α-cellulose and milled α-cellulose was carried out in order to determine the presence of oligomers or impurities in the samples. The tests were performed using 50 mg of pure α-cellulose and milled α-cellulose which were suspended separately in 40 mL of water, then the mixtures were stirred in the absence of light. Liquid samples were taken from the respective mixture after 24 hours and separated from the solid phase using a PTFE filter (GILSON®, 0.22 μm). Product analysis was carried out using an Agilent 1260 Infinity HPLC with an Aminex HPX-87H column using a refractive index detector (RID) and a diode array detector (DAD). For the photocatalytic tests, the obtained products were identified by comparison with the known standards (Chapter 2, section 2.8.1).

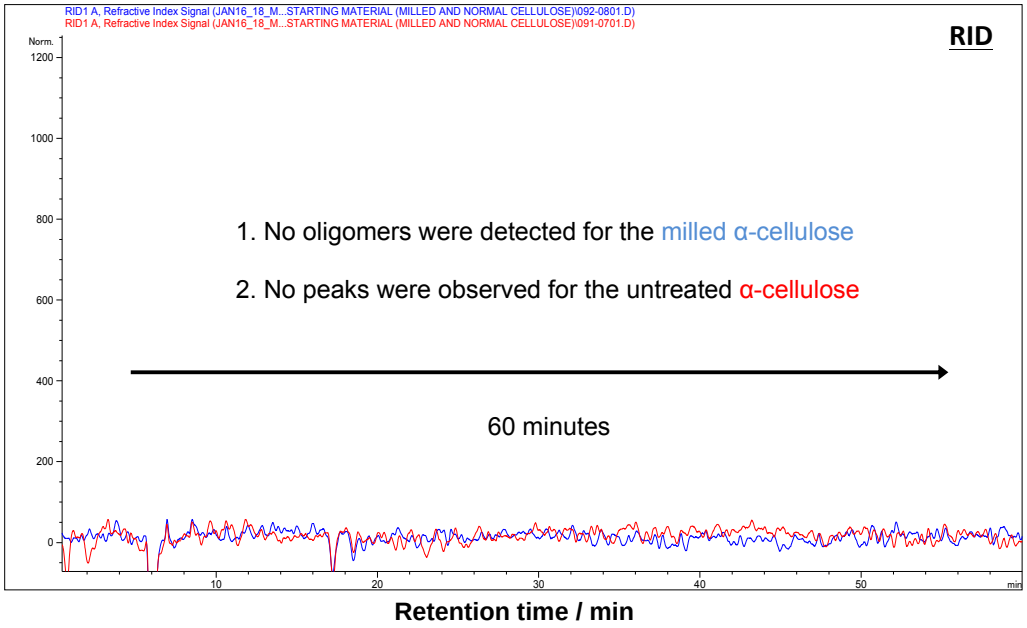

Figure 5.3 HPLC-RID chromatograms for the liquid phase of the α-cellulose/water (red line) and milled α-cellulose/water (blue line) mixtures.

Figure 5.3 shows the HPLC-RID chromatograms for the analysis of the liquid phase of the milled α-cellulose/water/acetonitrile and pure α-cellulose/water mixtures. The results showed that no oligomers were detected for the milled α-cellulose, and no peaks for the untreated α-cellulose were observed. For the photocatalytic experiments, milled α-cellulose will be used throughout this section, unless stated otherwise.

The initial photocatalytic tests for the cellulose conversion using TiO_2 as the photocatalyst and molecular oxygen under UV light irradiation with pure water or a water/acetonitrile mixture are shown in Figure 5.4. The results showed that the use of a 50/50 v/v water/acetonitrile mixture in the photoconversion of milled α-cellulose leads to the formation of several products such as tartronic acid, arabinose, and erythrose (Figure 5.4a). Moreover, the presence of unknown products (denoted 1, 2 and 3) was observed in both detectors (RID and DAD). When pure water was used as a solvent, small traces of glucose were observed after 24 hours of reaction (Figure 5.4b). From these results, it is clear that the presence of acetonitrile contributes to the formation of aldoses and acids, while pure water might promote the total mineralization of the products formed due to the presence of highly reactive radicals.

A)

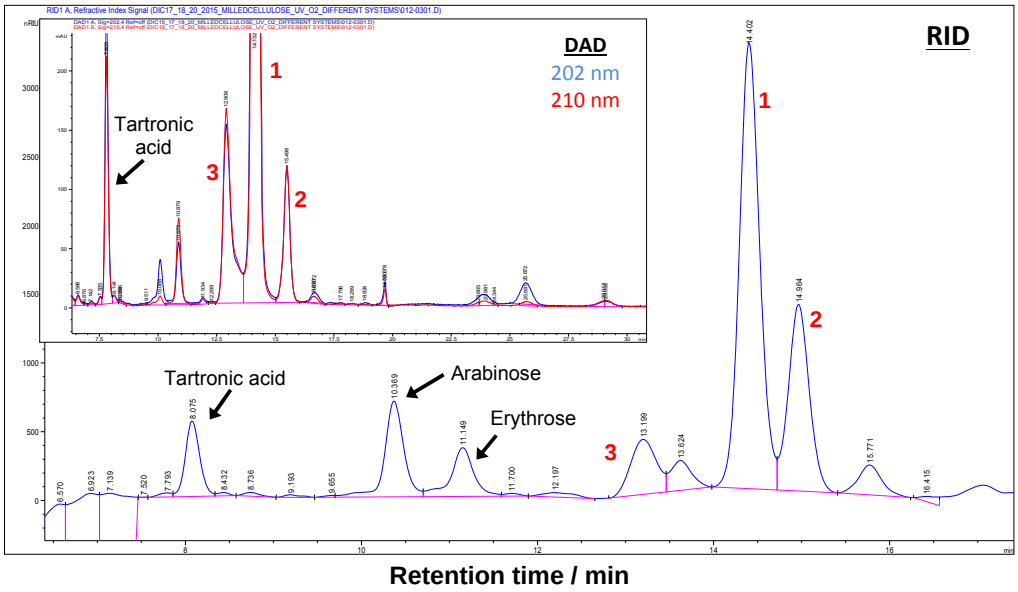

B)

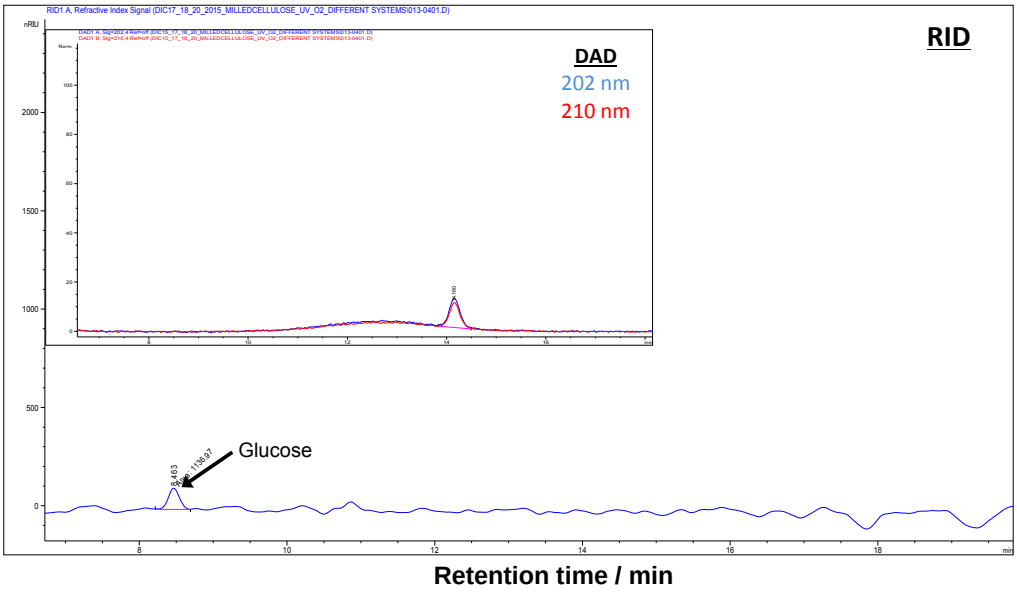

Figure 5.4 HPLC-RID/DAD chromatograms for the photocatalytic conversion of milled α-cellulose with TiO_2 as photocatalyst under UV light irradiation and oxygen pressure using (A) water or (B) water/acetonitrile as a solvents. Reaction conditions: milled α-cellulose =50 mg, catalyst =90 mg, $P(O_2)$ =10 bar, T =40±4 °C, t =24 hours, solvent =40 mL.

Interestingly, the analysis of the formation of products throughout the reaction shows that the aldoses and acids are formed after 12 hours when a water/acetonitrile mixture is used as a solvent, and they became more evident after 24 hours of reaction time (Figure 5.5). These results demonstrate that the photoconversion of cellulose requires long reaction times under these experimental

conditions, and therefore new strategies must be devised to improve the reaction performance.

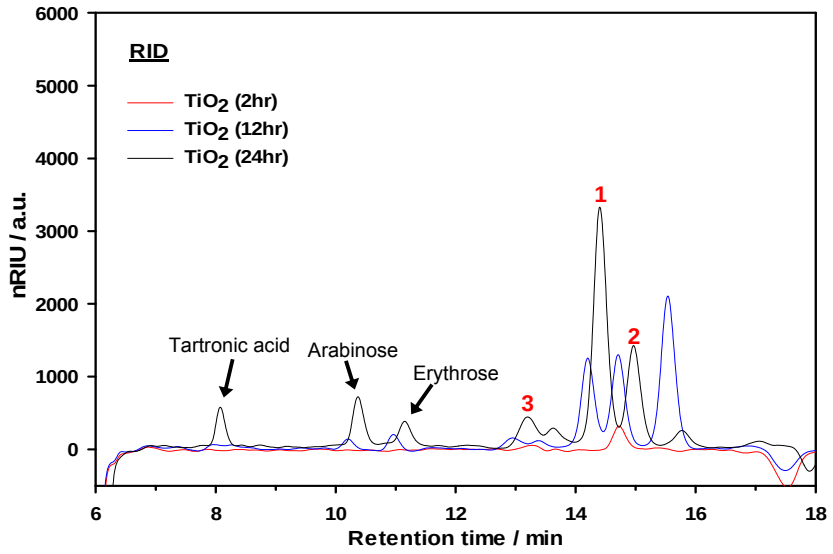

Figure 5.5 HPLC-RID chromatograms for the photocatalytic conversion of milled α-cellulose with TiO_2 as a photocatalyst under UV light irradiation and oxygen pressure using a 50/50 v/v water/acetonitrile mixture as a solvent.

It is well documented that the deposition of noble metal nanoparticles on a semiconductor improves the photocatalytic activity due to the formation of a Schottky junction which increases electron-hole separation and facilitates electron transfer to reducible species [45]. Therefore, the photocatalytic conversion of milled α-cellulose was carried out using TiO_2-supported noble metal catalysts under UV light irradiation in the presence of molecular oxygen with a water/acetonitrile mixture as a solvent. Figure 5.6 shows the HPLC-RID chromatograms for the photo-oxidation of milled α-cellulose using the TiO-based photocatalysts (TiO_2, Au/TiO_2, Ag/TiO_2, and Pt/TiO_2) after 24 hours of reaction time. The results showed that the formation of the same unknown products (denoted 1, 2, and 3) was observed in all cases, even though a clear shift in the retention time among the samples was observed. More surprisingly, it was found that aldoses (arabinose and erythrose) and acids (tartronic acid) were exclusively produced when TiO_2 was used as the photocatalyst. In this scenario, the presence of noble metal nanoparticles supported on the TiO_2 surface might not have an effect on the cellulose conversion into high-value products, however, these results do not provide conclusive evidence of the lack of catalytic activity of the metal nanoparticles under such conditions. At this point, it

was speculated that the power of light source (1000 W) could promote the mineralization of the products formed due to the high density of radical species in the reaction medium. Hence, it was decided to investigate the effect of the power of light source by using a 300 W lamp.

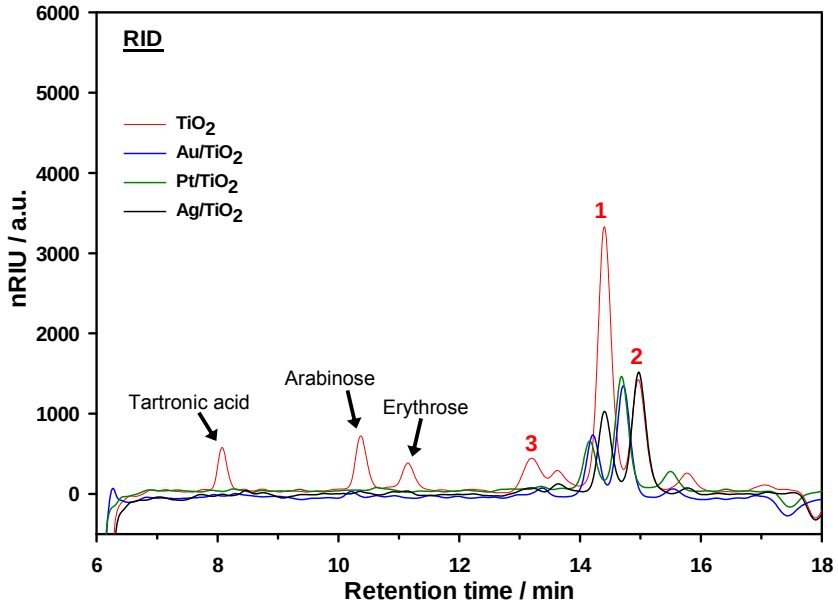

Figure 5.6 HPLC-RID chromatograms for the photocatalytic conversion of milled α-cellulose using TiO_2-supported noble metal catalysts under UV light irradiation and oxygen pressure using a 50/50 v/v water/acetonitrile mixture as a solvent.

The Au/TiO_2 photocatalyst was used as a representative sample for the photocatalytic conversion of milled α-cellulose under UV light irradiation and oxygen pressure. Figure 5.7 shows the HPLC-RID chromatograms for the Au/TiO_2 photocatalyst using the 300 W and 1000 W lamps in the photoconversion of cellulose. The results show that the formation of the same unknown products (denoted 1, 2, and 3) was observed after 24 hours of reaction time. Moreover, it is also evident from Figures 5.6 and 5.7 that the presence of metal nanoparticles do not lead to the formation of products such as aldoses and acids compared to the bare TiO_2. These observations are very unusual for the TiO_2-supported noble metal catalysts as it was expected a positive effect of the noble metals on the photocatalytic activity. In fact, some reports have shown that metal nanoparticles might have a negligible effect on the photocatalytic activity, particularly in the case of gold-modified TiO_2 photocatalysts [46-48]. Despite the apparent lack of activity of the TiO_2-supported noble metal catalysts, the effect of the solvent composition,

temperature, oxygen concentration, light intensity, have demonstrated to have sometimes a decisive role on the photocatalytic activity. Therefore, we speculated that the apparent lack of photoactivity of the catalysts might be associated with the use of the water/acetonitrile mixture as it has been reported that lower water content might hinder the formation of radical species [43, 44].

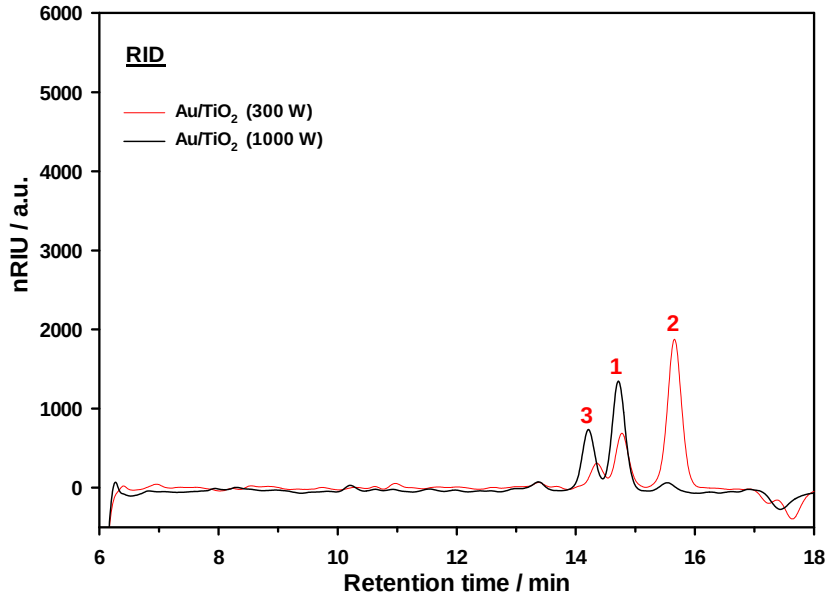

Figure 5.7 HPLC-RID chromatograms for the photocatalytic conversion of milled α-cellulose under UV light using a 300 W and 1000 W lamps in the presence of molecular oxygen and the Au/TiO_2 catalyst with a 50/50 v/v water/acetonitrile mixture as a solvent.

In order to investigate the stability of the water/acetonitrile mixture under photocatalytic conditions, blank tests were carried out using the TiO_2 catalyst under UV light irradiation in an inert (N_2) or reactive (O_2) atmosphere. For the blank experiments, 90 mg of the catalyst was suspended in 40 mL of the water/acetonitrile mixture, then the reactor was sealed and pressurized with the appropriate gas (O_2 or N_2). Figure 5.8 shows the HPLC-RID chromatograms for the water/acetonitrile mixture after 24 hours of UV light irradiation in the presence of TiO_2 as a catalyst under oxygen or nitrogen pressure. Surprisingly, the results showed the presence of the same unknown peaks (denoted 1, 2, and 3) under both oxygen and nitrogen pressure. Particularly, the HPLC analysis of the water/acetonitrile mixture under oxygen pressure showed more intense peaks for the unknown products compared to the analysis for the system under nitrogen pressure. This result demonstrated that the

water/acetonitrile mixture was subjected to an oxidation reaction. In this case, the organic component (acetonitrile) was responsible for the formation of the products observed at 14.2, 14.7 and 15.5 minutes (denoted 1, 2, and 3 respectively) in the HPLC analysis. Unfortunately, it was demonstrated that acetonitrile can be oxidized under both oxygen and nitrogen pressure in the presence of UV light irradiation and the TiO_2 catalyst.

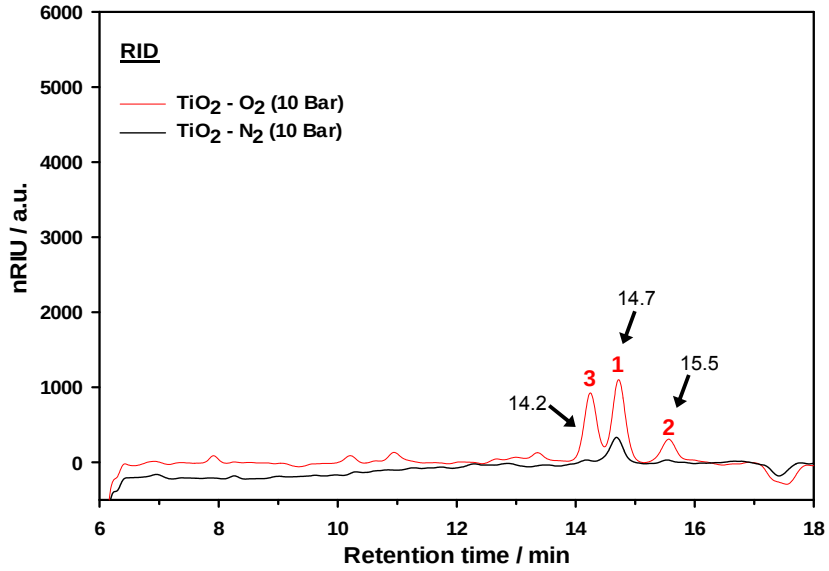

Figure 5.8 HPLC-RID chromatograms for the water/acetonitrile mixture after 24 hours of UV light irradiation in the presence of the TiO_2 catalyst.

Acetonitrile has been used in different applications [43, 49-51], and more particularly the photo-oxidation of glucose towards glucaric acid and gluconic acid [43]. In this paper, the authors suggest that in the presence of a water/acetonitrile mixture the selectivity to desired products increases, as acetonitrile provides a protective environment for the products formed, however, no more details were provided to support the evidence.

On the other hand, it has been found that acetonitrile can be presented in both molecularly (in Ti^{4+} sites) and dissociatively (by the influence of surface OH groups) during its exposure on the TiO_2 surface, after the adsorption, $CH_3C(O)NH_2$ and $CH_3C(O)NH$ surface species are formed. Chuang et al. [52] have proposed that these species can be photodecomposed on the surface to adsorbed CH_3COO^-, $HCOO^-$, NCO, and CN-containing species (Figure 5.9). Based on the previous reports and the

obtained results, the presence of the peaks at 14.2, 14.7 and 15.5 minutes (denoted 1, 2, and 3 respectively) in the HPLC analysis are due to the photo-oxidation of acetonitrile on the TiO_2 surface. Moreover, it was confirmed that the most intense peak with a retention time of 14.7 minutes corresponds to acetic acid, as the photo-oxidation of acetonitrile can promote the formation of the acetate ion ($CH3COO^-$) on the TiO_2 surface. The injection of the acetic acid standard solution into the Aminex HPX-87H column confirms the presence of the acid (Figure 5.10).

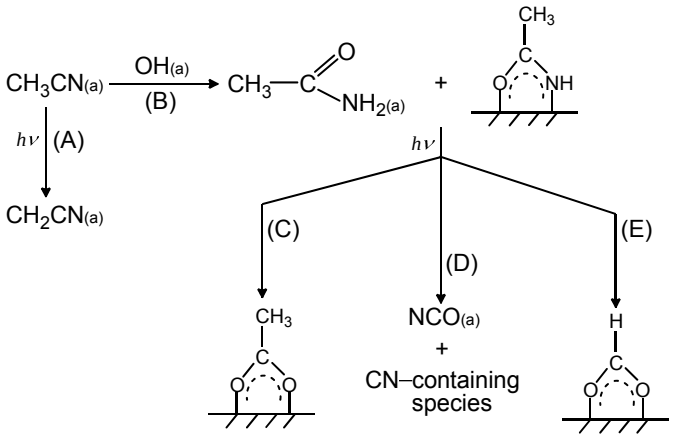

Figure 5.9 Mechanism proposed for the thermal and photochemical reactions of acetonitrile on the TiO_2 surface. Adapted from Chuang et al. [52].

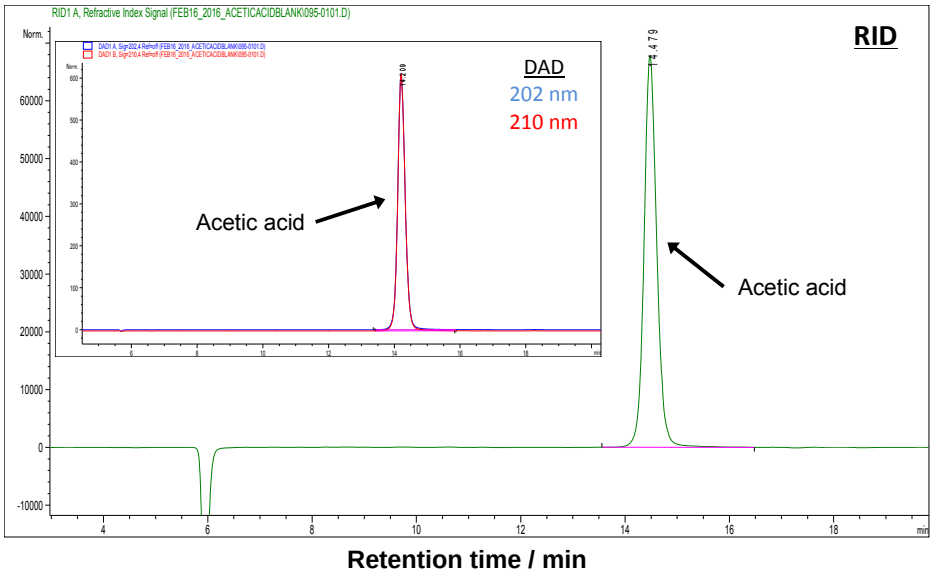

Figure 5.10 HPLC-RID/DAD chromatogram for the acetic acid standard solution.

To further investigate the photoconversion of milled α-cellulose, the reaction was performed using pure water as a solvent in the presence of UV light irradiation and molecular oxygen with TiO_2, Pt/TiO_2, and Au/TiO_2 as the catalysts. Figure 5.11 shows the HPLC-RID/DAD chromatograms for the products formed after 24 hours of reaction. The results showed small traces of glucose and formic acid in all cases, and no other products were detected under these conditions. Despite considerable efforts to try to transform cellulosic biomass (α-cellulose) by light irradiation, the use of model substrates might be more suitable for practical application in photocatalysis.

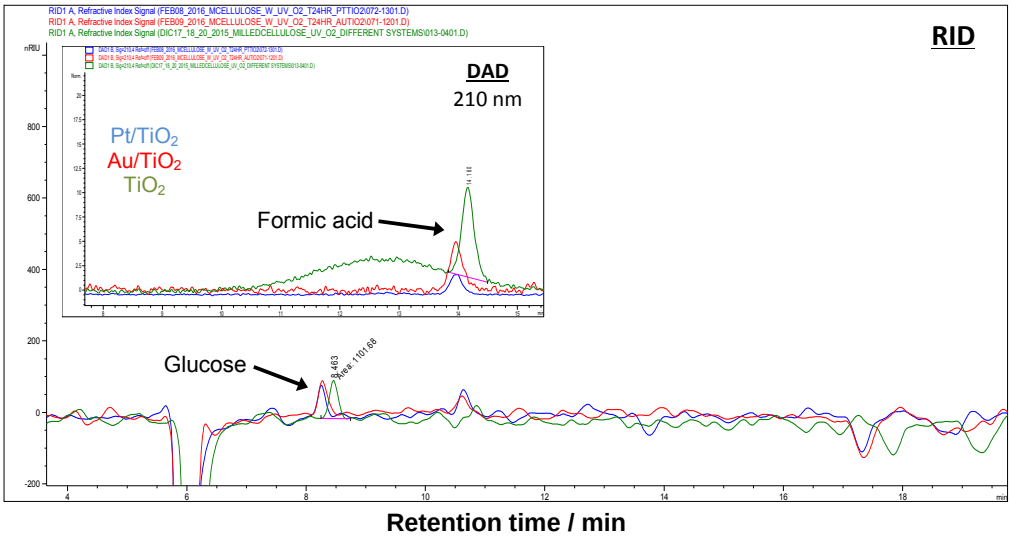

Figure 5.11 HPLC-RID/DAD chromatograms for the photocatalytic conversion of milled α-cellulose with the TiO_2, Pt/TiO_2, and Au/TiO_2 catalysts under UV light irradiation and oxygen pressure using pure water as a solvent. Reaction conditions: milled α-cellulose =50 mg, catalyst =90 mg, $P(O_2)$ =10 bar, T =40±4 °C, t =24 hours, water =40 mL.

5.2.1.2 Photocatalytic Conversion of Cellulose Microcrystalline (Avicel® PH-101) Under Light Irradiation

In the previous section, the photocatalytic conversion of α-cellulose was studied using TiO_2-supported noble metal catalysts under UV light irradiation in the presence of molecular oxygen. Several strategies were applied in order to transform α-cellulose into valuable chemicals, however, due to the complex nature of the substrate our efforts were unsuccessful. Therefore, we decided to investigate a model substrate which can partially mimic the natural physical properties of the α-cellulose. In this case, microcrystalline cellulose [53] (Avicel® PH-101, Sigma-Aldrich) was used as a model compound for the photocatalytic experiments. Prior to the reaction, the microcrystalline cellulose (MCC) was pulverized for 48 hours using the ball-milling method with a Planetary Micro Mill (Fritsch GmbH, PULVERISETTE 7 premium line) as described in the previous section. Subsequently, 50 mg of milled MCC was suspended in 40 mL of water under vigorous stirring for 24 hours in the absence of light, then a liquid sample was analysed by HPLC.

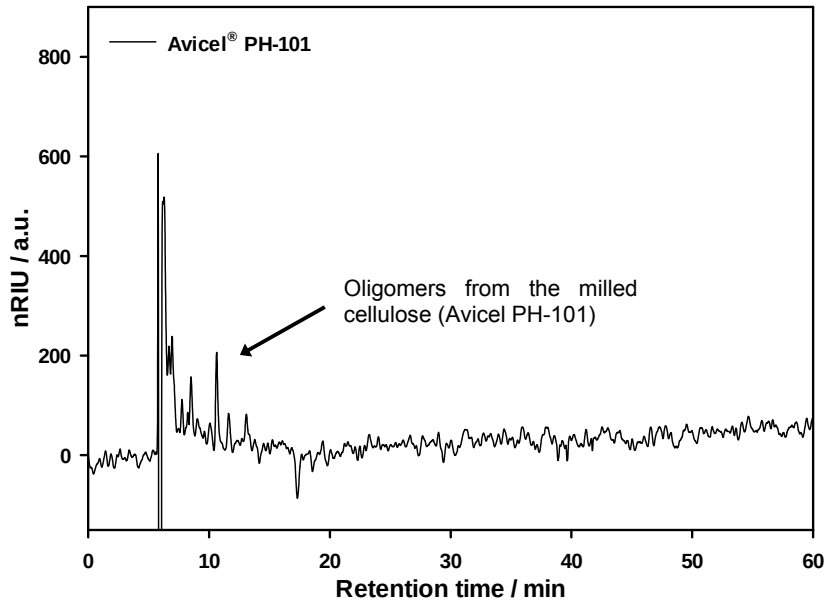

Figure 5.12 HPLC-RID chromatograms for the liquid phase of the milled MCC/water mixture.

Figure 5.12 shows the HPLC-RID chromatogram for the liquid phase of the milled MCC/water mixture after 24 hours of vigorous stirring. The results showed that the mechanical treatment of MCC produced soluble oligomers which can also be used as starting material for the formation of valuable chemicals.

The photocatalytic conversion of milled MCC was carried out using TiO_2 as a catalyst under both oxygen and nitrogen pressure in the presence of UV light irradiation. The reactions were performed using water as a solvent. The results showed that the soluble oligomers from the milled MCC were consumed during the photoreaction under both nitrogen and oxygen pressure. In both cases, traces of glucose were detected after 24 hours (Figure 5.13). Furthermore, the analysis of the gas phase products showed the presence of carbon dioxide (CO_2) under both oxygen and nitrogen pressure (Figure 5.14), whereas hydrogen (H_2) was only detected in the presence of a nitrogen atmosphere (see Appendix B: Figure B.1). Hence, these results showed the effect of the reaction atmosphere on the photoconversion of the soluble oligomers, however, despite the harsh conditions used (i.e. O_2 pressure, UV light), no other products were observed.

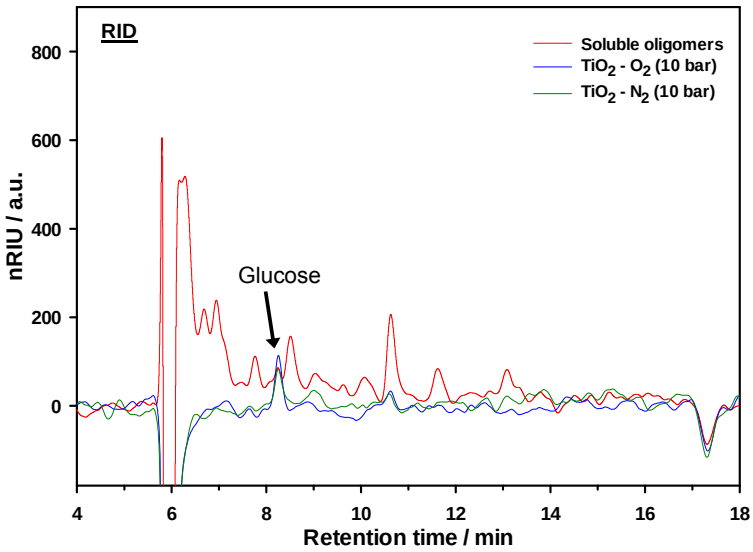

Figure 5.13 HPLC-RID chromatograms for the photocatalytic conversion of milled MCC using TiO_2 as a catalyst under UV light irradiation and N_2/O_2 pressure. Reaction conditions: milled MCC =50 mg, catalyst =90 mg, P =10 bar, T =40±4 °C, t =24 hours, water =40 mL, UV light =1000 W.

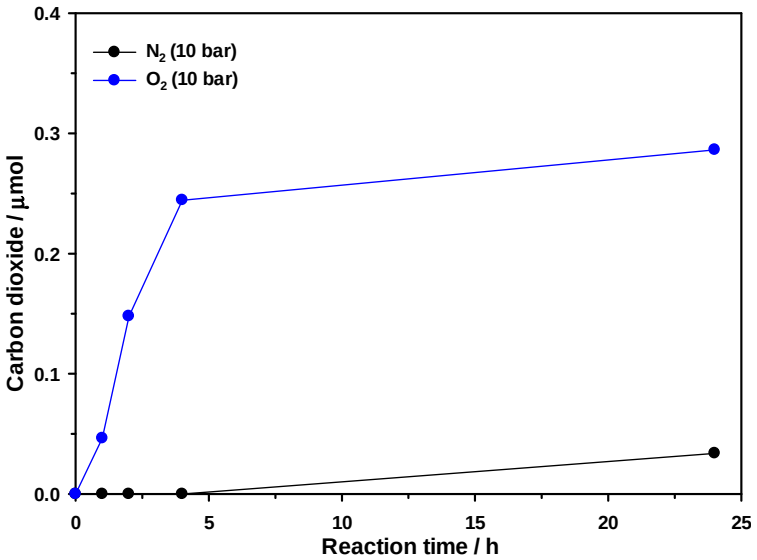

Figure 5.14 Carbon dioxide evolution for the photocatalytic conversion of milled MCC using TiO_2 as a catalyst under UV light irradiation and N_2/O_2 pressure. Reaction conditions: milled MCC =50 mg, catalyst =90 mg, T =40±4 °C, t =24 hours, water =40 mL, UV light =1000 W.

In an attempt to transform the milled MCC into valuable chemicals, further tests were carried out at different conditions: lamp power (300 and 128 W), solvent composition (water, 50/50 v/v water/acetonitrile), reaction time (2 and 24 h), type of light (UVA and visible light). However, the photodegradation of the soluble oligomers was observed in all cases, and no other products were obtained from the milled MCC (see Appendix B: Figures B.2-B.4).

On the other hand, the photocatalytic hydrogenation of the milled MCC was also carried out using the 1.4 wt% Ru/TiO_2 catalyst under UV light irradiation. Particularly, Ru-based catalysts have been widely used in hydrogenation [54] and oxidation [55] reactions, and more recently, ruthenium nanoparticles were used as a co-catalyst for the ammonia decomposition ($2NH_3 \rightarrow N_2 + 3H_2$) under photocatalytic conditions [56]. Therefore, we attempted to produce sorbitol or mannitol [57, 58] from the hydrogenation of milled MCC using the 1.4 wt% Ru/TiO_2 catalyst under UV light irradiation.

Figure 5.15 shows the HPLC-RID chromatograms for the photocatalytic hydrogenation of milled MMC using the 1.4 wt% Ru/TiO_2 catalyst under UV light irradiation after 24 hours of reaction. The results showed the presence of small traces of glucose and an unknown product at 4 hours of reaction, however, soluble oligomers were observed in the reaction mixture after 24 hours. Also, the presence of traces of CO_2 was observed after 4 hours, similar to the formation of the products

(see Appendix B: Figure B.5). Unfortunately, these results demonstrated the poor activity of the Ru/TiO_2 catalyst for the hydrogenation of the milled MMC under photocatalytic conditions.

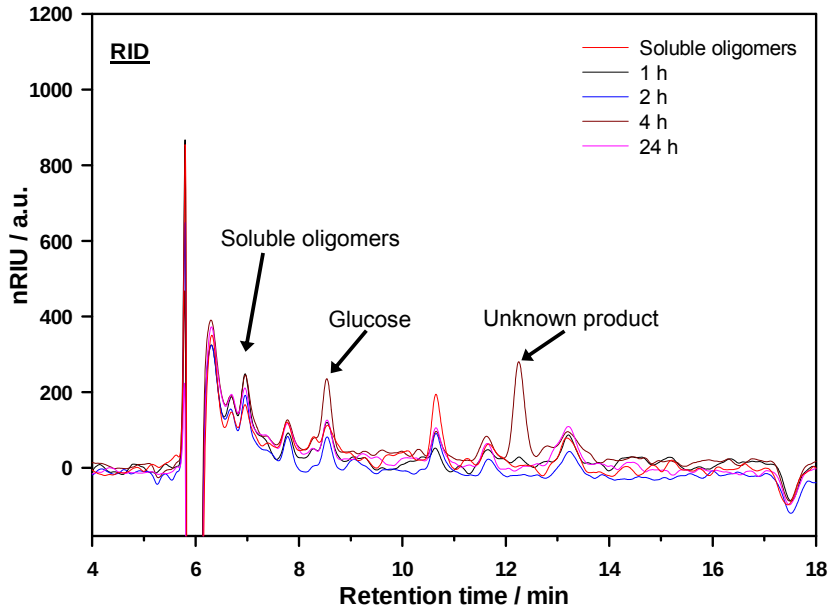

Figure 5.15 HPLC-RID chromatograms for the photocatalytic hydrogenation of milled MCC using the 1.4 wt% Ru/TiO_2 catalyst under UV light irradiation. Reaction conditions: milled MCC =50 mg, catalyst =90 mg, P (H_2) =10 bar, T =40±4 °C, t =24 hours, water =40 mL, UV light =1000 W.

5.2.1.2.1 Photoconversion of milled MMC (Avicel® PH-101) Under Light Irradiation and Basic Conditions

Cellulose is a complex polysaccharide which is composed of several glucose units linked via β-1,4-glycosidic bonds. Typically, the average number of glucose units in the cellulose's structure is defined as the degree of polymerization (DP). In native cellulose, the DP can vary from 2000-9000 glucose units, depending on the source [59]. Due to the high amount of hydroxyl groups in the structure, the glucose units are stuck together, forming strong hydrogen bonds which create a rigid structure [30, 31]. In order to facilitate the transformation of cellulose, various pretreatment methods such as mechanical, alkaline or acid treatment, solubilisation in ionic liquids, nonthermal atmospheric plasma among others, have been investigated by several authors [33-38, 60-62]. In this section, alkaline conditions were used in combination with the ball-milling method for the photocatalytic conversion of milled MCC under UV light irradiation. Particular, it has been demonstrated that the use of basic conditions at low temperatures improves the cellulose reactivity by promoting the hydrolysis (alkaline scission) of the glycosidic linkages resulting in a decrease in the degree of polymerization [62].

The photocatalytic experiments were carried out using the TiO_2, Ag/TiO_2 and Au/TiO_2 catalysts under UV light irradiation and oxygen pressure. In a typical test, 150 mg of milled MCC was added to 40 mL of water, then the appropriate amount of the catalyst (42 mg) was suspended in the mixture, followed by the addition of the base (NaOH) with a substrate/base = 1:1 molar ratio. Subsequently, the reactor was purged with nitrogen and then pressurized with molecular oxygen. In all tests, the reaction mixture was allowed to reach equilibrium for 10 minutes in the absence of light. The temperature was set to 40 °C and monitored using a 4848 Reactor Controller (Parr Instrument Company, Illinois, USA).

Figures 5.16-5.19 shows the HPLC-RID chromatograms for the photocatalytic conversion of milled MCC using the TiO_2-based catalysts after 24 hours of reaction time. Figures 5.16-5.18 shows the products obtained for the photoconversion of milled MCC with the TiO_2, Ag/TiO_2, and Au/TiO_2 catalysts respectively, under UV light irradiation and oxygen pressure. The results showed that

the presence of the base (NaOH) promoted the formation of a wide range of products such as aldoses, carboxylic acids, sugar alcohols, and unknown products in some cases. In addition, it was found that some peaks of these compounds overlap each other as a broad peak was observed in the same range, 8 to 9 min (Figures 5.16-5.18).

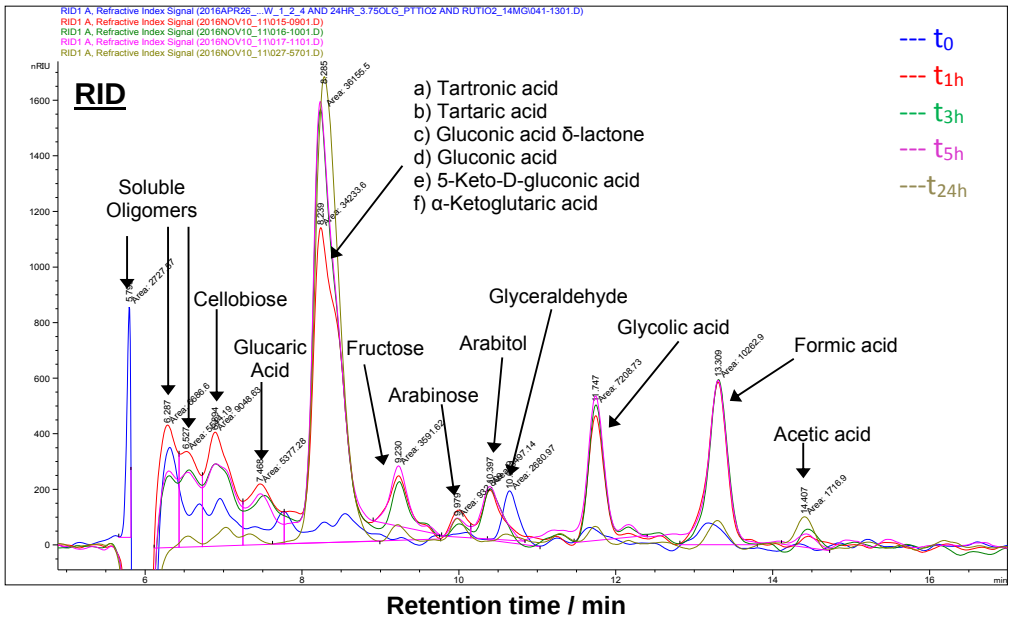

Figure 5.16 HPLC-RID chromatograms for the photoconversion of milled MCC using the TiO_2 catalyst with molecular oxygen under UV light irradiation and basic conditions.

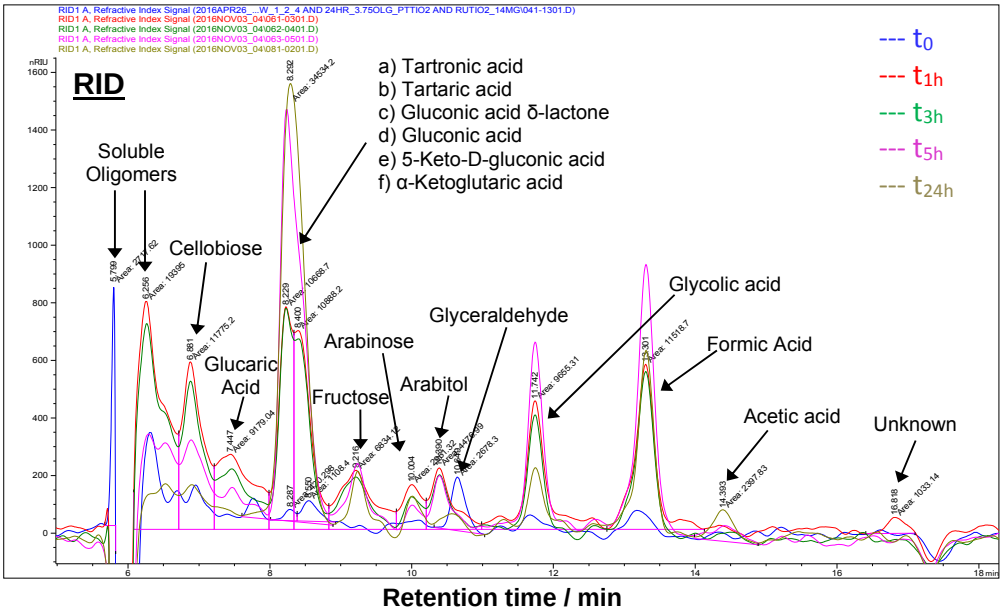

Figure 5.17 HPLC-RID chromatograms for the photoconversion of milled MCC using the Ag/TiO_2 catalyst with molecular oxygen under UV light irradiation and basic conditions.

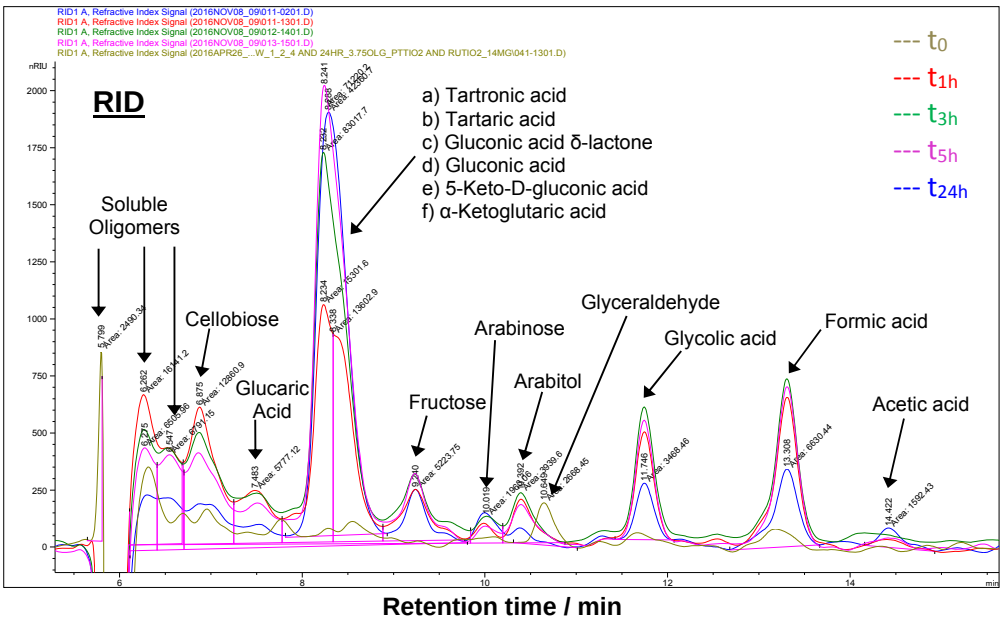

Figure 5.18 HPLC-RID chromatograms for the photoconversion of milled MCC using the Au/TiO_2 catalyst with molecular oxygen under UV light irradiation and basic conditions.

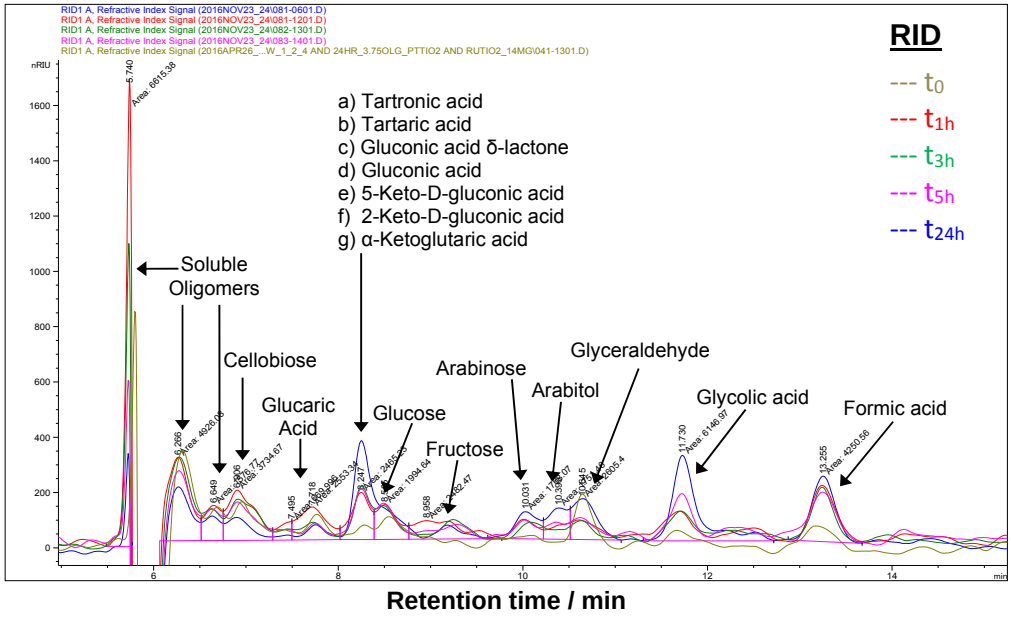

Figure 5.19 HPLC-RID chromatograms for the photoconversion of milled MCC using the Au/TiO_2 catalyst with molecular oxygen under visible light irradiation (1000 W) and basic conditions.

More interestingly, the photoconversion of milled MCC demonstrated the effect of both UV and visible light on the formation of the products with the Au/TiO_2 catalyst (Figures 5.18 and 5.19). In the case of the reaction under visible light, the results showed low-intensity peaks for the products formed using the Au/TiO_2

catalyst. Also, the HPLC-RID chromatograms showed the presence of soluble oligomers after 24 hours of reaction, suggesting the poor activity of the Au/TiO_2 catalyst under visible light (Figure 5.19). This result might indicate that the incident irradiation was not sufficient to promote the formation of electron-hole pairs on the Au/TiO_2 surface. When the reaction was performed under UV light irradiation, more intense peaks were observed for the products formed (Figure 5.18). The HPLC-RID chromatograms confirmed that soluble oligomers were not detected after 24 hours of reaction time. Furthermore, the peak with a retention time between 8–9 min was more intense than the one under visible light, suggesting the presence of high amounts of oxidation products.

An additional test was carried out under dark conditions using the Au/TiO_2 catalyst and milled MCC in the presence of molecular oxygen and alkaline conditions. The results showed low-intensity peaks for the products formed after 24 hours of reaction for the Au/TiO_2 catalyst. Due to the absence of light irradiation, especially UV light, small traces of oxidation products were detected (Figure 5.20).

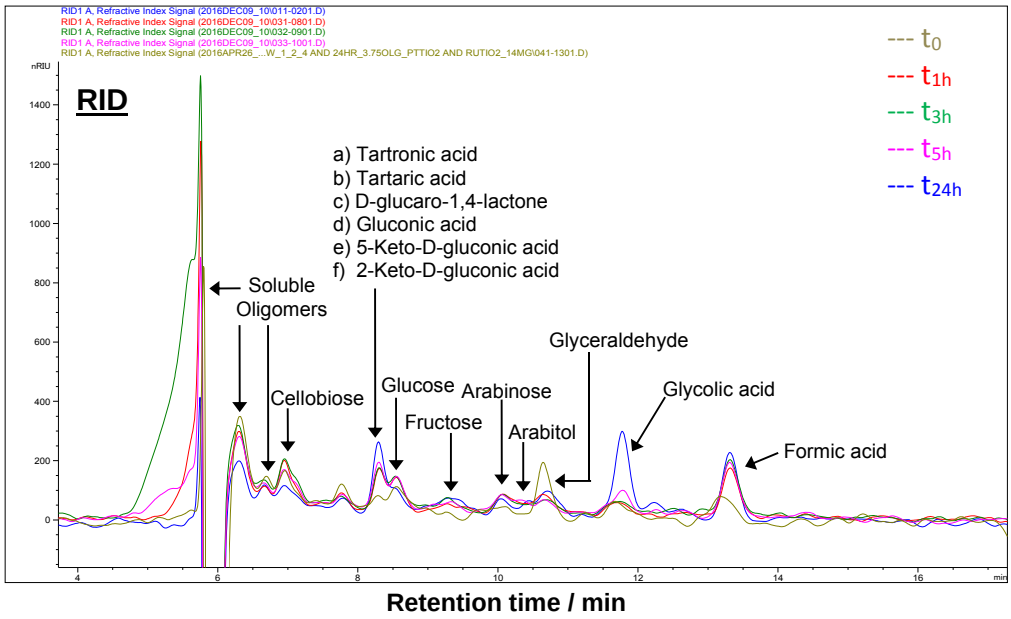

Figure 5.20 HPLC-RID chromatograms for the photoconversion of milled MCC using the Au/TiO_2 catalyst with molecular oxygen under basic conditions in the absence of light (dark).

Due to the complex nature of the cellulose, it was not possible to identify and quantify all the products, however, cellulose conversion and yields were calculated using the response factor of the known standards which are reported in Chapter 2,

section 2.8.1. For the soluble oligomers and unknown product (8.2 min), the glucose's response factor was used to calculate their concentration in the reaction mixture. For comparison, the blank reaction was carried out using TiO_2 as a catalyst in the absence of light under alkaline conditions and oxygen pressure (see Appendix B: Figure B.6).

Table 5.2 Conversion and yield values for the photocatalytic transformation of milled cellulose (Avicel PH-101) into valuable chemicals using TiO_2-supported noble metal catalysts under oxygen pressure and alkaline conditions.**

	TiO_2[a]	Au/TiO_2[a]	Au/TiO_2[b]	TiO_2[c]	Au/TiO_2[c]	Ag/TiO_2[c]
Conversion %	**3.77**	**0.99**	**4.80**	**6.64**	**14.51**	**18.05**
	Yield (%)					
Acetic Acid	0.65	0.48	0.77	1.32	2.13	6.84
Formic Acid	1.12	0.97	1.21	0.86	3.38	5.82
Glycolic Acid	1.88	1.67	1.79	0.28	1.53	1.27
Arabitol	0.47	0.48	0.91	0.55	0.77	0.55
Arabinose	0.55	0.37	0.62	0.33	0.52	0.58
Fructose	0.75	0.39	0.55	0.29	0.70	0.79
Glucaric Acid	0.32	ND	0.25	0.20	0.28	ND
Cellobiose	0.55	0.60	0.50	0.23	0.85	0.19
Glucose	0.20	0.17	0.34	ND	ND	ND
Glyceraldehyde	062	0.25	0.75	0.13	0.01	0.07
Gluconic Acid	ND	ND	ND	ND	ND	ND
Erythrose	ND	ND	ND	0.15	ND	ND
Unknown (8.241s)*	2.01	0.61	2.36	8.36	9.52	8.01
Oligomers*	0.44	0.69	0.57	ND	0.36	ND

*Based on the glucose's calibration curve, No detected = ND, [a] Dark, [b] Visible light, [c] UV light.
**Reaction conditions: milled MCC =150 mg, catalyst =42 mg, $P(O_2)$ =10 bar, T =40±4 °C, t =24 hours, water =40 mL, Lamp power =1000 W, milled MCC/NaOH =1:1 molar ratio.

Table 5.2 shows the summarized results on the photocatalytic conversion of milled MCC (Avicel PH-101) using TiO_2-supported noble metal catalysts. As expected, the reactions performed under visible light irradiation (b) and dark (a) conditions showed low conversion values for the TiO_2 and Au/TiO_2 catalysts. Also, the presence of soluble oligomers after 24 hours of reaction confirms the poor activity of the materials as the TiO_2 catalyst cannot be activated under visible light and the incident irradiation was not sufficient to generate electron-hole pairs on the Au/TiO_2 surface. In the case of UV light irradiation, high conversion values were achieved with the TiO_2, Ag/TiO_2, and Au/TiO_2 catalysts after 24 hours of reaction. Soluble oligomers were only detected for the Au/TiO_2 catalyst, while they were not presented for the TiO_2 and Ag/TiO_2. This result suggests that the TiO_2 and Ag/TiO_2 catalysts improve the conversion of milled MCC, more particularly, the formation of

oxidation products. In fact, the Ag/TiO_2 showed the highest yield of acetic and formic acids which are over-oxidation products, demonstrating the highly oxidizing environment. Therefore, these results demonstrated that TiO_2-supported noble metal catalysts can be used for the photoconversion of milled MCC into valuable chemicals with molecular oxygen under light irradiation and alkaline conditions.

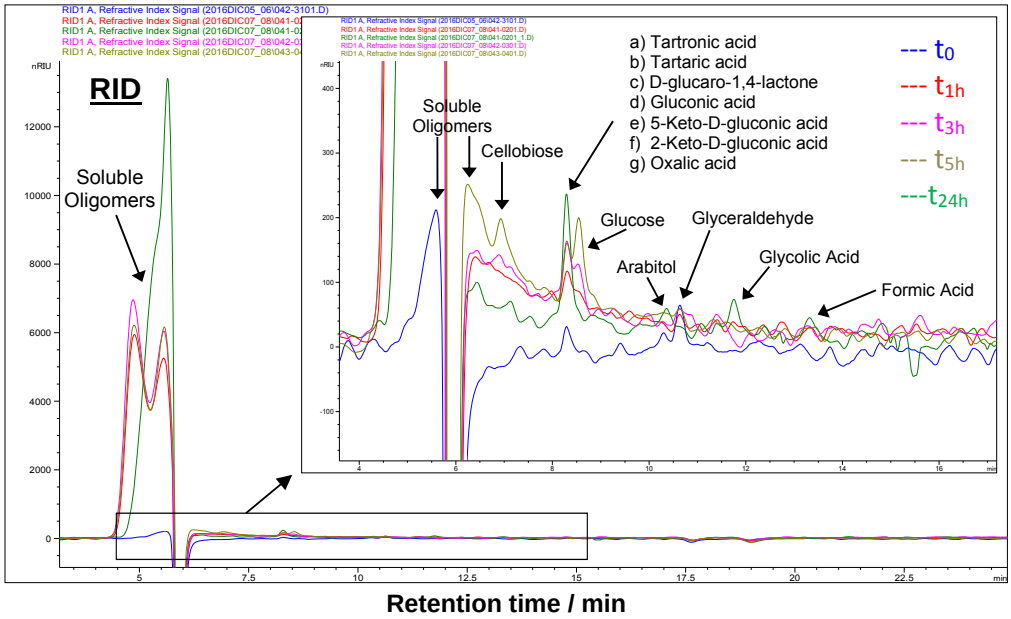

Figure 5.21 HPLC-RID chromatograms for the photoconversion of water-soluble starch using the Au/TiO_2 catalyst under visible light irradiation and oxygen pressure. Reaction conditions: Startch =150 mg, catalyst =42 mg, T =40±4 °C, t =24 hours, water =40 mL, Lamp power =1000 W, P (O_2) =10 bar.

In an attempt to further investigate the photoconversion of polysaccharides using TiO_2-based catalysts, the conversion of water-soluble starch (Sigma-Aldrich) was carried out under visible light irradiation and oxygen pressure. Preliminary tests were performed using the TiO_2 and Au/TiO_2 catalysts under base-free conditions, however, traces of the products and high amounts of soluble oligomers were observed in both cases (see Appendix B: Figures B.7 and B.8). On the other hand, the reaction performed under alkaline conditions using the Au/TiO_2 catalyst showed the highest amount of soluble oligomers and small quantities of products, despite the long reaction times (Figure 5.21). Although the photoconversion of water-soluble starch was unsuccessful with the Au/TiO_2 catalyst, these results highlight how the nature of the substrate and the reaction conditions play an important role in the activity of the photocatalysts.

5.3 Conclusions

In this study, the photocatalytic conversion of polysaccharides was investigated using TiO_2-supported noble metal catalysts under light irradiation and oxygen pressure. Polysaccharides such as microcrystalline cellulose – Avicel PH-101, α-cellulose, and water-soluble starch were used as a starting material for the photocatalytic studies. The initial experiments demonstrated that the solvent composition plays an important role on the photoactivity of the catalysts as it was found that the presence of an organic solvent, particularly in a 50/50 v/v water/acetonitrile mixture, promotes the formation of aldoses and carboxylic acid from α-cellulose under UV light irradiation. But at the same time, the organic solvent can undergo photodegradation over noble metal-loaded TiO_2 catalysts and the bare TiO_2, limiting the availability of active sites for the photocatalytic processes.

Due to the complex nature of the α-cellulose, it was decided to investigate a model substrate which could partially mimic the physical properties of the native cellulose. Particularly, microcrystalline cellulose (Avicel® PH-101, Sigma-Aldrich) was used as a model substrate in an attempt to produce valuable chemicals using light irradiation and TiO_2-based catalysts. The results showed that microcrystalline cellulose was not transformed into valuable chemicals under photocatalytic conditions and the presence of carbon dioxide can be attributed to the total mineralization of the soluble oligomers produced during the pretreatment step. In order to improve the cellulose reactivity, the reactions were carried out under basic conditions (NaOH) in the presence of molecular oxygen. It was found that in the presence of the base, several products were formed, especially oxidation products which were favoured by the presence of noble metal-loaded TiO_2 catalysts under UV light irradiation (Table 5.2).

In order to further investigate the application of TiO_2-based catalysts on the photoconversion of polysaccharides, the photocatalytic transformation of water-soluble starch was carried out using the TiO_2 and Au/TiO_2 catalysts under visible light irradiation and alkaline conditions. This approach was aimed to produce valuable chemicals (i.e. gluconic acid) at mild conditions by taking advantage of the high solubility of the starch in water, however, small traces of oxidation products and high amounts of soluble oligomers were detected after reaction. Therefore, these

results highlight the complex nature of polysaccharides and the difficulty in identifying the products formed under light irradiation, but at the same time, they offer new insights for the selection of reaction conditions in the photocatalytic conversion of polymeric carbohydrates using TiO_2-supported noble metal catalysts.

5.4 References

[1] A. Fujishima, K. Honda, Electrochemical Photolysis of Water at a Semiconductor Electrode, Nature, 238 (1972) 37-38.

[2] M.A. Henderson, A surface science perspective on TiO_2 photocatalysis, Surf. Sci. Rep., 66 (2011) 185-297.

[3] L. Yan, L. Zhe, G. Michael, J. Michael, L. Yang Yang, C. Xiaobo, Titanium dioxide nanomaterials for photocatalysis, J. Phys. D: Appl. Phys., 50 (2017) 193003.

[4] R. Leary, A. Westwood, Carbonaceous nanomaterials for the enhancement of TiO2 photocatalysis, Carbon, 49 (2011) 741-772.

[5] P. Chowdhury, H. Gomaa, A.K. Ray, Dye-Sensitized Photocatalyst: A Breakthrough in Green Energy and Environmental Detoxification, Sustainable Nanotechnology and the Environment: Advances and Achievements, American Chemical Society(2013), pp. 231-266.

[6] G. Kim, W. Choi, Charge-transfer surface complex of EDTA-TiO_2 and its effect on photocatalysis under visible light, Appl. Catal. B: Environ., 100 (2010) 77-83.

[7] R. Asahi, T. Morikawa, T. Ohwaki, K. Aoki, Y. Taga, Visible-Light Photocatalysis in Nitrogen-Doped Titanium Oxides, Science, 293 (2001) 269-271.

[8] S.U.M. Khan, M. Al-Shahry, W.B. Ingler, Efficient Photochemical Water Splitting by a Chemically Modified n-TiO_2, Science, 297 (2002) 2243-2245.

[9] J.C. Yu, L. Wu, J. Lin, P. Li, Q. Li, Microemulsion-mediated solvothermal synthesis of nanosized CdS-sensitized TiO_2 crystalline photocatalyst, Chem. Commun., (2003) 1552-1553.

[10] C. Yu, L. Wei, J. Chen, Y. Xie, W. Zhou, Q. Fan, Enhancing the Photocatalytic Performance of Commercial TiO_2 Crystals by Coupling with Trace Narrow-Band-Gap Ag_2CO_3, Ind. Eng. Chem. Res. , 53 (2014) 5759-5766.

[11] B. Zhou, J. Song, Z. Zhang, Z. Jiang, P. Zhang, B. Han, Highly selective photocatalytic oxidation of biomass-derived chemicals to carboxyl compounds over Au/TiO_2, Green Chem., 19 (2017) 1075-1081.

[12] L. Da Già, C. Recchi, T.E. Davies, N. Greeves, J.A. Lopez-Sanchez, Visible-Light-Controlled Oxidation of Glucose using Titania-Supported Silver Photocatalysts, ChemCatChem, 8 (2016) 3475-3483.

[13] Z. Yu, S.S.C. Chuang, The effect of Pt on the photocatalytic degradation pathway of methylene blue over TiO_2 under ambient conditions, Appl. Catal. B: Environ., 83 (2008) 277-285.

[14] M. Cristina Yeber, J. Rodríguez, J. Freer, N. Durán, H. D. Mansilla, Photocatalytic degradation of cellulose bleaching effluent by supported TiO_2 and ZnO, Chemosphere, 41 (2000) 1193-1197.

[15] R.S. Sonawane, B.B. Kale, M.K. Dongare, Preparation and photo-catalytic activity of Fe–TiO_2 thin films prepared by sol–gel dip coating, Mater. Chem. Phys., 85 (2004) 52-57.

[16] A.E.H. Machado, J.A. de Miranda, R.F. de Freitas, E.T.F.M. Duarte, L.F. Ferreira, Y.D.T. Albuquerque, R. Ruggiero, C. Sattler, L. de Oliveira, Destruction of the organic matter present in effluent from a cellulose and paper industry using photocatalysis, J. Photochem. Photobiol., A, 155 (2003) 231-241.

[17] R.A. Stillings, R.J.V. Nostrand, The Action of Ultraviolet Light upon Cellulose. I. Irradiation Effects. II. Post-Irradiation Effects1, J. Am. Chem. Soc., 66 (1944) 753-760.

[18] R.L. Desai, J.A. Shields, Photochemical degradation of cellulose material, Makromol. Chem., 122 (1969) 134-144.

[19] E. Greenbaum, C.V. Tevault, C.Y. Ma, New Photosynthesis: Direct Photoconversion of Biomass to Molecular Oxygen and Volatile Hydrocarbons, Energy & Fuels, 9 (1995) 163-167.

[20] H. Fan, G. Li, F. Yang, L. Yang, S. Zhang, Photodegradation of cellulose under UV light catalysed by TiO2, J. Chem. Technol. Biotechnol., 86 (2011) 1107-1112.

[21] L. Wang, Z. Zhang, L. Zhang, S. Xue, W.O.S. Doherty, I.M. O'Hara, X. Ke, Sustainable conversion of cellulosic biomass to chemicals under visible-light irradiation, RSC Adv., 5 (2015) 85242-85247.

[22] G. Zhang, C. Ni, X. Huang, A. Welgamage, L.A. Lawton, P.K.J. Robertson, J.T.S. Irvine, Simultaneous cellulose conversion and hydrogen production assisted by cellulose decomposition under UV-light photocatalysis, Chem. Commun., 52 (2016) 1673-1676.

[23] A.M. Nadeem, G.I.N. Waterhouse, H. Idriss, The reactions of ethanol on TiO_2 and Au/TiO_2 anatase catalysts, Catal. Today, 182 (2012) 16-24.

[24] Y. Borensztein, L. Delannoy, A. Djedidi, R.G. Barrera, C. Louis, Monitoring of the Plasmon Resonance of Gold Nanoparticles in Au/TiO_2 Catalyst under Oxidative and Reducing Atmospheres, J. Phys. Chem. C, 114 (2010) 9008-9021.

[25] X. Pan, Y.-J. Xu, Fast and spontaneous reduction of gold ions over oxygen-vacancy-rich TiO2: A novel strategy to design defect-based composite photocatalyst, Appl. Catal. A: Gen., 459 (2013) 34-40.

[26] R. Zanella, S. Giorgio, C.-H. Shin, C.R. Henry, C. Louis, Characterization and reactivity in CO oxidation of gold nanoparticles supported on TiO_2 prepared by deposition-precipitation with NaOH and urea, J. Catal., 222 (2004) 357-367.

[27] I. Tunc, M. Bruns, H. Gliemann, M. Grunze, P. Koelsch, Bandgap determination and charge separation in Ag@TiO_2 core shell nanoparticle films, Surf. Interface Anal., 42 (2010) 835-841.

[28] C. Suwanchawalit, S. Wongnawa, P. Sriprang, P. Meanha, Enhancement of the photocatalytic performance of Ag-modified TiO_2 photocatalyst under visible light, Ceram. Int., 38 (2012) 5201-5207.

[29] Q. Xiang, J. Yu, B. Cheng, H.C. Ong, Microwave-Hydrothermal Preparation and Visible-Light Photoactivity of Plasmonic Photocatalyst Ag-TiO_2 Nanocomposite Hollow Spheres, Chem. Asian J., 5 (2010) 1466-1474.

[30] H. Wang, G. Gurau, R.D. Rogers, Ionic liquid processing of cellulose, Chem. Soc. Rev., 41 (2012) 1519-1537.

[31] K.M. Gupta, J. Jiang, Cellulose dissolution and regeneration in ionic liquids: A computational perspective, Chem. Eng. Sci., 121 (2015) 180-189.

[32] M.E. Himmel, S.-Y. Ding, D.K. Johnson, W.S. Adney, M.R. Nimlos, J.W. Brady, T.D. Foust, Biomass Recalcitrance: Engineering Plants and Enzymes for Biofuels Production, Science, 315 (2007) 804-807.

[33] R.P. Swatloski, S.K. Spear, J.D. Holbrey, R.D. Rogers, Dissolution of Cellose with Ionic Liquids, J. AM. CHEM. SOC., 124 (2002) 4974-4975.

[34] J. Zhang, B. Zhang, J. Zhang, L. Lin, S. Liu, P. Ouyang, Effect of phosphoric acid pretreatment on enzymatic hydrolysis of microcrystalline cellulose, Biotechnol. Adv., 28 (2010) 613-619.

[35] M. Benoit, A. Rodrigues, Q. Zhang, E. Fourré, K. De Oliveira Vigier, J.-M. Tatibouët, F. Jérôme, Depolymerization of Cellulose Assisted by a Nonthermal Atmospheric Plasma, Angew. Chem. Int. Ed., 50 (2011) 8964-8967.

[36] D.K. Sidiras, E.G. Koukios, Acid saccharification of ball-milled straw, Biomass, 19 (1989) 289-306.

[37] M. Yabushita, H. Kobayashi, K. Hara, A. Fukuoka, Quantitative evaluation of ball-milling effects on the hydrolysis of cellulose catalysed by activated carbon, Catal. Sci. Technol., 4 (2014) 2312-2317.

[38] P. Dornath, H.J. Cho, A. Paulsen, P. Dauenhauer, W. Fan, Efficient mechano-catalytic depolymerization of crystalline cellulose by formation of branched glucan chains, Green Chem., 17 (2015) 769-775.

[39] K. Lefatshe, C.M. Muiva, L.P. Kebaabetswe, Extraction of nanocellulose and in-situ casting of ZnO/cellulose nanocomposite with enhanced photocatalytic and antibacterial activity, Carbohydr. Polym., 164 (2017) 301-308.

[40] H.D. Mansilla, M. Cristina Yeber, J. Freer, J. Rodríguez, J. Baeza, Homogeneous and heterogeneous advanced oxidation of a bleaching effluent from the pulp and paper industry, Waf. Sci. Tech., 35 (1997) 273-278.

[41] M. Yeber, J. Rodríguez, J. Freer, J. Baeza, N. Durán, H.D. Mansilla, Advanced oxidation of a pulp mill bleaching wastewater, Chemosphere, 39 (1999) 1679-1688.

[42] Y. Nosaka, A.Y. Nosaka, Generation and Detection of Reactive Oxygen Species in Photocatalysis, Chem. Rev., 117 (2017) 11302-11336.

[43] J.C. Colmenares, A. Magdziarz, A. Bielejewska, High-value chemicals obtained from selective photo-oxidation of glucose in the presence of nanostructured titanium photocatalysts, Bioresour. Technol., 102 (2011) 11254-11257.

[44] J.C. Colmenares, A. Magdziarz, Room temperature versatile conversion of biomass-derived compounds by means of supported TiO_2 photocatalysts, J. Mol. Catal. A: Chem., 366 (2013) 156-162.

[45] M. Jakob, H. Levanon, P.V. Kamat, Charge Distribution between UV-Irradiated TiO_2 and Gold Nanoparticles: Determination of Shift in the Fermi Level, Nano Lett., 3 (2003) 353-358.

[46] H. Li, Z. Bian, J. Zhu, Y. Huo, H. Li, Y. Lu, Mesoporous Au/TiO_2 Nanocomposites with Enhanced Photocatalytic Activity, J. Am. Chem. Soc., 129 (2007) 4538-4539.

[47] B.K. Min, J.E. Heo, N.K. Youn, O.S. Joo, H. Lee, J.H. Kim, H.S. Kim, Tuning of the photocatalytic 1,4-dioxane degradation with surface plasmon resonance of gold nanoparticles on titania, Catal. Commun., 10 (2009) 712-715.

[48] E. Kowalska, R. Abe, B. Ohtani, Visible light-induced photocatalytic reaction of gold-modified titanium(iv) oxide particles: action spectrum analysis, Chem. Commun., (2009) 241-243.

[49] Y. Shiraishi, M. Morishita, T. Hirai, Acetonitrile-assisted highly selective photocatalytic epoxidation of olefins on Ti-containing silica with molecular oxygen, Chemical Communications, (2005) 5977-5979.

[50] Y. Shiraishi, T. Hirai, Selective organic transformations on titanium oxide-based photocatalysts, Journal of Photochemistry and Photobiology C: Photochemistry Reviews, 9 (2008) 157-170.

[51] K.E. O'Shea, S.H. Jannach, I. Garcia, The reactions of substituted acyclic 1,3-butadienes on photoexcited TiO_2 in acetonitrile, Journal of Photochemistry and Photobiology A: Chemistry, 122 (1999) 127-131.

[52] C.-C. Chuang, W.-C. Wu, M.-X. Lee, J.-L. Lin, Adsorption and photochemistry of CH_3CN and CH_3CONH_2 on powdered TiO_2, Phys. Chem. Chem. Phys., 2 (2000) 3877-3882.

[53] M.T. Holtzapple, CELLULOSE, in: B. Caballero (Ed.) Encyclopedia of Food Sciences and Nutrition (Second Edition), Academic Press, Oxford, 2003, pp. 998-1007.

[54] P. Kluson, L. Cerveny, Selective hydrogenation over ruthenium catalysts, Appl. Catal. A: Gen., 128 (1995) 13-31.

[55] S. Muthusamy, N. Kumarswamyreddy, V. Kesavan, S. Chandrasekaran, Recent advances in aerobic oxidation with ruthenium catalysts, Tetrahedron Lett., 57 (2016) 5551-5559.

[56] L. Zhou, D.F. Swearer, C. Zhang, H. Robatjazi, H. Zhao, L. Henderson, L. Dong, P. Christopher, E.A. Carter, P. Nordlander, N.J. Halas, Quantifying hot carrier and thermal contributions in plasmonic photocatalysis, Science, 362 (2018) 69-72.

[57] W. Deng, X. Tan, W. Fang, Q. Zhang, Y. Wang, Conversion of Cellulose into Sorbitol over Carbon Nanotube-Supported Ruthenium Catalyst, Catal. Lett., 133 (2009) 167-174.

[58] A. Fukuoka, P.L. Dhepe, Catalytic Conversion of Cellulose into Sugar Alcohols, Angew. Chem. Int. Ed., 118 (2006) 5285-5287.

[59] H. Krässig, J. Schurz, R.G. Steadman, K. Schliefer, W. Albrecht, Cellulose, Ullmann's Encyclopedia of Industrial Chemistry (2004).

[60] G. Bali, X. Meng, J.I. Deneff, Q. Sun, A.J. Ragauskas, The Effect of Alkaline Pretreatment Methods on Cellulose Structure and Accessibility, ChemSusChem, 8 (2015) 275-279.

[61] C.J. Knill, J.F. Kennedy, Degradation of cellulose under alkaline conditions, Carbohydr. Polym., 51 (2003) 281-300.

[62] J. Xu, J.J. Cheng, R.R. Sharma-Shivappa, J.C. Burns, Sodium Hydroxide Pretreatment of Switchgrass for Ethanol Production, Energy & Fuels, 24 (2010) 2113-2119.

Chapter 6

Conclusions and Future Work

The aim of this Thesis was to investigate the selective valorization of bio-derived molecules using metal nanoparticles supported on different materials such as conjugated microporous polymers, multi-walled carbon nanotubes, and titanium dioxide. The catalytic activity of the supported metal catalysts was evaluated under thermal and photocatalytic conditions aiming to produce high-valuable chemicals from model molecules. In this Thesis, the experimental work was focused on three main directions: the development and testing of novel polymer-based catalysts, catalytic studies under light irradiation, and the photocatalytic conversion of polysaccharides at high-pressure conditions. This chapter presents the conclusions for the research projects reported in Chapters 3–5.

6.1 Chapter 3

For the first time, we have synthesized gold nanoparticles supported on conjugated microporous polymers (CMPs), and the resulting gold catalysts were assessed for the glucose oxidation reaction. Conventional methods were explored for the preparation of the gold catalysts, however, it was required to develop a new synthetic procedure which could take advantage of the intrinsic properties of the

CMPs (swellability and microporosity). As a result, the organic solvent-assisted sol immobilisation (SASI) method was developed to prepare gold catalysts. The TEM and XPS analyses of a representative sample of the Au/CMP-SASI(ACN-W) catalyst showed well-defined spherical gold nanoparticles (3.7 nm) and the presence of $Au^{\delta-}$ species, which are associated with the electron transfer from the support to the metal nanoparticles. The SASI method produced highly active catalysts compared to the conventional methods, and the presence of acetonitrile as a solvent during the preparation of the catalysts demonstrated to be a fundamental part of their superior activity. Under optimized conditions, the 2.1 wt% Au/CMP-SASI(ACN-W) catalyst displayed the highest catalytic activity with a TOF value of 327.7 min^{-1} in the glucose oxidation. Moreover, it was found that the Au/CMP-SASI(ACN-W) catalyst can be reused several times without losing activity. Therefore, we have demonstrated for the first time that conjugated microporous polymers can be used as a support material for the deposition of metal nanoparticles, and the synthesis method has a strong effect on the catalytic activity of the resulting catalyst.

Future Work

In this chapter, it was showed that CMPs-supported gold catalysts can be used in heterogeneous catalysis, particularly in the glucose oxidation reaction. However, it would be desirable to extend the use of the CMPs as support material for various metals, in order to explore their application in reactions of interest. For example, as they are mainly composed of carbon-carbon bonds and presented aromaticity in their structure, the use of the CMPs for the toluene and benzyl alcohol oxidation could be advantageous due to the presence of similar properties, however, this speculation needs to be demonstrated. On the other hand, it is required to investigate the role of the acetonitrile during the synthesis of the catalysts in order to gain more control over the final material as it was found a solvent-dependent catalytic activity. Moreover, the investigation of additional parameters on the synthesis of the polymer-based catalysts might be useful to improve their activity, for example, solvent composition, PVA/metal ratio, and the method for the removal of the stabilising agent. In order to optimize the catalyst synthesis and loading procedure, it would be required to determine the spatial position and distribution of

the metal nanoparticles within the CMP network. Particularly, this analysis is important for metal nanoparticles with size-dependent catalytic activity as their confinement inside the pores could potentially limit particle aggregation. Therefore, the synthesis of polymer-based catalysts could be improved by knowing the exact position of the nanoparticles within the polymeric network. In this case, electron microscopy techniques such as high-angle annular dark-field scanning transmission electron microscopy and electron tomography can be used to characterize metal nanoparticles within porous structures [1, 2].

6.2 Chapter 4

The aim of Chapter 4 was to investigate the oxidation of glucose under light irradiation conditions using gold nanoparticles supported on different semiconductor materials. The photo-oxidation of glucose under both UV and visible light irradiation showed the formation of several products such as tartronic acid, gluconic acid, formic acid, and short-chain aldoses when the TiO_2 and 1.6 wt% Au/TiO_2 catalysts were used under alkaline conditions. The presence of these products was also reported by Chong et al. [3] and Da Vià et al. [4] under both UV and visible light irradiation using TiO_2-based catalysts. The results obtained in this work confirmed the previous findings [3, 4], but at the same time contradict the work reported by Zhou et al. [5] and Omri et al. [6]. The authors suggest that the selective photo-oxidation of glucose to gluconic can be performed using TiO_2-based catalysts in alkaline medium under both UV and visible light irradiation, and the presence of side products is not even considered under such conditions.

In this scenario, it was clear that a new approach should be taken in order to understand such discrepancies, and more particularly the synergistic effect between the metal nanoparticles and the support material should be avoided. Therefore, we decided to investigate the use of conjugated microporous polymers (CMPs) as a support material for the gold nanoparticles due to their chemical inertness, but more importantly, due to their extended π-conjugation which provides the driving force for the light-harvesting process [7]. The initial experiments were performed using the 1.6 wt% Au/CMP-1 catalyst under visible light irradiation and base-free conditions. As

expected, the main product was gluconic acid along with small traces of tartronic acid in all cases, but more surprisingly, it was found that the photo-oxidation of glucose under both visible light irradiation and dark conditions showed almost identical values of conversion and selectivity. These results might indicate that the oxidation process is thermally-driven rather than a photocatalytic process. However, this is purely speculation and needs to be demonstrated. In an attempt to influence the reaction mechanism by the presence of light irradiation, the photo-oxidation of glucose was performed using the 1.6 wt% Au/CMP-1 catalyst under visible light and alkaline conditions. As reported by Zhou et al. [5] and Omri et al. [6], the photo-oxidation of glucose under light irradiation can be strongly influenced by the presence of a base. Surprisingly, the results showed almost complete glucose conversion after 6 hours of reaction under visible light irradiation and thus confirming the promotional effect of the alkaline conditions. Despite the remarkable improvement in the glucose oxidation, the reaction under dark conditions showed similar values of conversion and selectivity to the reaction in the presence of visible light. Hence, we have demonstrated that the use of CMPs as a support material inhibits the formation of side products compared to the TiO_2 support, but at the same time, these studies suggest that the glucose oxidation over CMPs-supported gold catalysts is governed by thermal catalysis.

In an attempt to further investigate the photo-oxidation of glucose under light irradiation, multi-walled carbon nanotubes (CNTs) were used as a support material for the gold nanoparticles. Particularly, CNTs have emerged as promising materials for photocatalytic applications due to their electronic and structural properties [8]. Under visible light, the results showed complete glucose conversion with a selectivity of 98% to gluconic acid when the 1 wt% Au/CNTs catalyst was used under alkaline conditions. However, the results obtained in the dark showed similar values of conversion and selectivity at the end of the reaction. Once again, our results confirmed the promotional effect of the base and highlighted the inevitable thermal contribution to the glucose oxidation. Additional experiments were carried using the 1 wt% Au/CNTs catalyst under visible light irradiation in the presence of molecular oxygen at high-pressure conditions. The results showed that the presence of molecular oxygen improved the reaction rate and the efficiency of the catalyst, however, the synergistic effect between photocatalysis and thermal catalysis could not be avoided.

Future Work

In Chapter 4, the photo-oxidation of glucose was studied under light irradiation conditions using metal nanoparticles supported on semiconductor materials. Interestingly, we have found considerable discrepancies between this work and the literature. At this point, the apparent discrepancies could be attributed to the different experimental conditions; for example, substrate concentration, illumination time, temperature, light intensity, additives, metal loading, and experimental setup among others. In this scenario, future work should be considered on a case-by-case basis, however, we suggested additional experiments from a more general perspective. For example, it would be useful to investigate the apparent activation energies of both the thermal (dark conditions) and photocatalytic reaction in order to determine whether the oxidation of glucose is favoured under light irradiation conditions or by thermal catalysis. Moreover, it would be required to identify the radical species produced by the photocatalysts under light irradiation conditions with the aim to determine the active species. As the photocatalytic and thermal reaction follow different mechanisms, it would be interesting to investigate the role of O_2 in both systems.

6.3 Chapter 5

The aim of Chapter 5 was to investigate the photocatalytic conversion of polysaccharides using TiO_2-supported noble metal catalysts at high-pressure conditions. The results showed the formation of small traces of organic acids (gluconic and formic acids) and short-chain aldoses (arabinose and erythrose) from the milled α-cellulose when the TiO_2 catalyst was used under UV light irradiation and oxygen pressure. Particularly, it was found that the use of a 50/50 v/v water/acetonitrile mixture as solvent promoted the formation of sugars and acids, while the reaction conducted with water as a solvent produced small traces of glucose, suggesting the presence of highly reactive radicals which led to the total mineralization of the products formed. Unfortunately, it was found that acetonitrile

can undergo photodegradation when TiO_2-supported noble metal catalysts are used. Therefore, the photoconversion of milled α-cellulose was performed with water as a solvent. After 24 hours of reaction, traces of formic acid and glucose were detected under UV light conditions.

Due to the complex structure of the α-cellulose and its poor activity under light irradiation, it was decided to investigate the photoconversion of a model substrate such as microcrystalline cellulose (MCC, Avicel® PH-101). The tests were carried out using milled MCC under alkaline conditions and oxygen pressure with the TiO_2, Au/TiO_2, and Ag/TiO_2 catalysts. The results showed that under UV light conditions, the highest conversion was 18% for the Ag/TiO_2 catalyst, whereas the conversion of MCC over the TiO_2 support was 6.6%. Hence, these results demonstrated that noble metal nanoparticles (i.e. Ag and Au) supported on TiO_2 can perform the photoconversion of milled MCC under UV light irradiation and oxygen pressure in alkaline conditions. However, despite promising results with the metal catalysts, it was evident that the photoconversion of milled MCC is an unselective process for the production of valuable chemical, and therefore more work will be needed in order to tune the selectivity to the desired products.

On the other hand, preliminary tests were carried out using water-soluble starch using the TiO_2 and Au/TiO_2 catalysts under visible light irradiation and oxygen pressure in alkaline conditions. The aim was to produce carboxylic acids such as gluconic and glucaric acids at moderate conditions taking advantage of the low crystallinity and high solubility of the starch. Our results showed that the TiO_2 and Au/TiO_2 catalysts produced small traces of soluble oligomers and organic acids under base-free conditions and visible light irradiation. When the photoconversion of starch was performed using a base as a promoter under similar experimental conditions with Au/TiO_2 catalyst, the results showed high amounts of soluble oligomers and small traces of acids and sugars. Unfortunately, the soluble oligomers were not converted into molecules of interest even after 24 hours of reaction at moderate conditions. Despite these results, this work presents an initial approach for the photoconversion of polysaccharides using TiO_2-supported noble metal catalysts and emphasizes how the nature of the substrate contributes to the photocatalysis.

Future Work

In Chapter 5, the photoconversion of polysaccharides was carried out using noble metal-loaded TiO_2 catalysts. In most cases, it was found that the identification of the products (i.e. soluble oligomers, organic acids) was limited to the known standards, and therefore it would be desirable to determine and quantify the molecules formed after photocatalysis. In this case, several analytical techniques could be useful to solve the problem: for example, total organic carbon analysis (TOC), gel permeation chromatography (GPC), time-of-flight mass spectrometry coupled with liquid chromatography (HPLC-QTOF) among others. However, the use of these techniques is not straightforward, and sample derivatization might be required before analysis. On the other hand, it was found that the photoconversion of polysaccharides in alkaline conditions produces soluble oligomers which could be further oxidized and formed unwanted products. An alternative approach for the overoxidation process might involve the separation of the soluble compounds (i.e. oligomers, sugars) as they are formed, and therefore it would be needed to develop a continuous flow process. With the aim of improving the photoconversion of the polysaccharides using metal catalysts, the polymeric carbohydrates could be subjected to various treatments before reaction, for example, ball milling, mix-milling (substrate-catalyst), ultrasound, and acid treatment among others. Regarding the photocatalyst, the situation is more complicated as it would be required to prepare a multifunctional photocatalyst which can perform simultaneous hydrolysis and oxidation along with light-harvesting.

6.4 References

[1] S. Turner, O.I. Lebedev, F. Schröder, D. Esken, R.A. Fischer, G.V. Tendeloo, Direct Imaging of Loaded Metal−Organic Framework Materials (Metal@MOF-5), Chem. Mater., 20 (2008) 5622-5627.

[2] F. Wang, J. Mielby, F.H. Richter, G. Wang, G. Prieto, T. Kasama, C. Weidenthaler, H.-J. Bongard, S. Kegnæs, A. Fürstner, F. Schüth, A Polyphenylene Support for Pd Catalysts with Exceptional Catalytic Activity, Angew. Chem. Int. Ed., 53 (2014) 8645-8648.

[3] R. Chong, J. Li, Y. Ma, B. Zhang, H. Han, C. Li, Selective conversion of aqueous glucose to value-added sugar aldose on TiO_2-based photocatalysts, J. Catal., 314 (2014) 101-108.

[4] L. Da Già, C. Recchi, T.E. Davies, N. Greeves, J.A. Lopez-Sanchez, Visible-Light-Controlled Oxidation of Glucose using Titania-Supported Silver Photocatalysts, ChemCatChem, 8 (2016) 3475-3483.

[5] B. Zhou, J. Song, Z. Zhang, Z. Jiang, P. Zhang, B. Han, Highly selective photocatalytic oxidation of biomass-derived chemicals to carboxyl compounds over Au/TiO_2, Green Chem., 19 (2017) 1075-1081.

[6] M. Omri, F. Sauvage, Y. Busby, M. Becuwe, G. Pourceau, A. Wadouachi, Gold Catalysis and Photoactivation: A Fast and Selective Procedure for the Oxidation of Free Sugars, ACS Catal., (2018) 1635-1639.

[7] L. Chen, Y. Honsho, S. Seki, D. Jiang, Light-Harvesting Conjugated Microporous Polymers: Rapid and Highly Efficient Flow of Light Energy with a Porous Polyphenylene Framework as Antenna, J. Am. Chem. Soc., 132 (2010) 6742-6748.

[8] R.H. Baughman, A.A. Zakhidov, W.A. de Heer, Carbon Nanotubes--the Route Toward Applications, Science, 297 (2002) 787-792.

Table A.1 Conversion, Product Yield and Mass Balance values in the catalytic oxidation of glucose using the Au/CMP and Au/PPO catalysts under microwave-assisted heating.

Catalyst	Reaction Time (min)	Glucose Conversion (%)	Gluconic Acid (%)	Tartronic Acid (%)	Glycolic Acid (%)	Formic Acid (%)	Mass Balance (%)
Au/CMP-SASI(ACN-W)	5	32.2	31.4	0.09	-	0.23	99.51
	10	66.0	61.4	0.65	-	0.86	96.87
	20	71.9	64.4	1.17	-	2.57	96.26
	30	86.8	71.5	2.67	-	7.72	95.13
Au/CMP-SASI(DMF-W)	5	40.8	37.4	0.18	-	0.36	97.2
	10	58.4	52.7	0.45	-	0.78	95.5
	20	80.4	69.7	1.66	0.07	3.03	94.1
	30	85.3	70.6	2.31	0.22	6.14	94.0
Au/CMP-SI	5	15.9	16.0	-	-	-	100.1
	10	21.1	22.2	0.02	-	-	101.4
	20	45.6	41.8	0.34	-	0.28	96.73
	30	52.3	48.5	0.32	-	0.70	97.31
Au/CMP-WI(ACN)	5	0.26	0.42	-	-	-	100.1
	10	1.33	1.62	-	-	-	100.2
	20	2.17	1.76	-	-	-	99.58
	30	2.36	1.84	-	-	-	99.48
Au/PPO-SASI(ACN-W)	5	0.03	0.03	-	-	-	100.1
	10	0.03	0.03	-	-	-	100.8
	20	1.02	1.00	-	0.02	-	99.98
	30	2.25	2.21	-	0.03	-	99.10
Au/PPO-SASI(DMF-W)	5	4.18	4.93	-	-	-	100.7
	10	21.5	21.9	-	-	-	100.3
	20	26.0	26.0	-	-	-	99.92
	30	28.5	27.4	-	-	-	98.93
Au/PPO-SI	5	7.44	8.14	-	-	-	100.6
	10	19.5	19.2	-	0.02	-	99.66
	20	30.8	29.3	-	0.05	-	98.61
	30	35.4	33.8	-	0.13	-	98.56
Au/PPO-WI(ACN)	5	0.70	0.13	-	-	-	100.7
	10	1.44	0.14	-	-	-	101.4
	20	1.58	0.15	-	-	-	101.5
	30	2.35	0.17	2.13	-	-	102.3

Reaction conditions = Glucose/Au = 438 molar ratio, T = 130 ºC, $P(O_2)$ = 10 bar.

Table A.2 Conversion, Product Yield and Mass Balance values in the catalytic oxidation of glucose using the Au/CMP-SASI(ACN-W) catalyst under microwave-assisted heating. Effect of the temperature on the synthesis method.

Catalyst	Reaction Time (min)	Glucose Conversion (%)	Gluconic Acid (%)	Tartronic Acid (%)	Glycolic Acid (%)	Formic Acid (%)	Mass Balance (%)
Au/CMP-SASI(ACN-W) - 90°C	5	58.93	55.08	0.64	-	0.30	97.09
	10	80.35	72.74	1.22	-	1.20	94.83
	20	86.18	72.47	2.39	0.24	4.10	93.03
	30	87.08	73.92	2.45	0.40	6.40	96.10
Au/CMP-SASI(ACN-W) - 45°C	5	61.70	56.11	0.47	-	0.26	95.14
	10	73.62	67.29	0.86	-	0.81	95.34
	20	85.73	72.11	2.59	0.32	4.14	93.44
	30	90.30	72.66	3.02	0.38	7.58	93.34
Au/CMP-SASI(ACN-W) - RT[a]	5	42.88	38.37	0.34	0.05	0.14	96.03
	10	83.83	71.74	1.95	0.15	3.03	93.05
	20	85.74	72.03	2.29	0.23	3.48	92.30
	30	89.27	72.73	2.68	0.52	5.95	92.62

Reaction conditions = Glucose/Au = 438 molar ratio, T = 130 ºC, $P(O_2)$ = 10 bar. [a] RT = Room Temperature.

Table A.3 Conversion, Product Yield and Mass Balance values in the catalytic oxidation of glucose using the Au/CMP-SASI(ACN-W) catalyst under microwave-assisted heating. Effect of the immobilisation time on the synthesis method.

Catalyst	Reaction Time (min)	Glucose Conversion (%)	Gluconic Acid (%)	Tartronic Acid (%)	Glycolic Acid (%)	Formic Acid (%)	Mass Balance (%)
Au/CMP-SASI(ACN-W)-0.5h	5	32.26	31.45	0.09	-	0.23	99.51
	10	66.06	61.42	0.65	-	0.86	96.87
	20	71.97	64.48	1.17	-	2.57	96.26
	30	86.84	71.58	2.67	-	7.72	95.13
Au/CMP-SASI(ACN-W)-2h	5	69.25	62.26	0.49	-	0.34	93.85
	10	75.22	68.97	0.79	-	0.81	95.36
	20	88.52	75.93	2.26	0.25	4.03	93.97
	30	91.70	73.10	3.08	0.37	9.88	94.75
Au/CMP-SASI(ACN-W)-5h	5	63.82	61.81	0.86	-	0.66	99.50
	10	75.68	67.06	1.36	-	1.35	94.09
	20	80.16	72.91	0.81	0.08	1.04	94.69
	30	92.44	73.30	3.27	0.29	8.76	93.18
Au/CMP-SASI(ACN-W)-24h	5	50.26	46.29	1.03	-	0.84	97.91
	10	68.56	58.17	1.50	-	1.72	92.82
	20	69.58	63.05	1.34	0.10	3.04	97.96
	30	81.14	67.71	2.45	0.39	8.13	97.55

Reaction conditions = Glucose/Au = 438 molar ratio, T = 130 ºC, $P(O_2)$ = 10 bar.

Table A.4 Conversion, Product Yield and Mass Balance values in the catalytic oxidation of glucose using the Au/CMP-SASI(ACN-W) catalyst under microwave-assisted heating. Effect of the metal loading on the oxidation of glucose.

Catalyst	Reaction Time (min)	Glucose Conversion (%)	Gluconic Acid (%)	Tartronic Acid (%)	Glycolic Acid (%)	Formic Acid (%)	Mass Balance (%)
0.57 wt% Au/CMP-SASI(ACN-W)	5	32.91	27.48	0.79	-	0.34	95.71
	10	48.22	38.48	1.76	-	0.88	92.90
	20	53.55	42.08	2.06	0.32	1.39	92.30
	30	59.79	45.20	2.11	0.74	1.91	90.19
1.18 wt% Au/CMP-SASI(ACN-W)	5	33.15	28.92	0.46	-	0.48	96.72
	10	28.88	29.28	0.41	-	0.88	101.69
	20	55.17	46.13	1.27	0.22	2.76	95.22
	30	72.31	57.73	2.26	0.44	6.21	94.35
2.19 wt% Au/CMP-SASI(ACN-W)	5	69.25	62.26	0.49	-	0.34	93.85
	10	75.22	68.97	0.79	-	0.81	95.36
	20	88.52	75.93	2.26	0.25	4.03	93.97
	30	91.70	73.10	3.08	.0.37	9.88	94.75
3.39 wt% Au/CMP-SASI(ACN-W)	5	53.03	50.79	0.28	-	0.28	98.33
	10	61.21	54.88	0.38	-	0.63	94.68
	20	82.52	71.99	1.41	0.17	2.91	93.97
	30	88.46	73.23	2.30	0.42	7.45	94.96

Reaction conditions = Glucose/Au = 438 molar ratio, T = 130 ºC, $P(O_2)$ = 10 bar.

Table A.5 Comparison of the catalytic activity of the Au/CMP catalyst and bare CMP in the glucose oxidation under microwave conditions. Conversion, product yield and mass balance values after 10 minutes of reaction time.[a]

Catalyst	Reaction Time (min)	Glucose Conversion (%)	Gluconic acid (%)	Tartronic acid (%)	Fructose (%)	Mass Balance (%)
[b] Au/CMP	2	19	17	–	–	98
	5	40	37	–	–	96
	10	68	56	–	–	87
CMP	2	4.3	–	–	3.7	99
	5	6.7	–	–	5.8	99
	10	8.1	–	–	6.5	97

[a] Reaction conditions: Glucose/Au = 438 molar ratio, T = 160 ºC, $P(O_2)$ = 7 bar, t = 10 min.
[b] Catalyst: 1.6 wt % Au/CMP-SASI(ACN-W)

Appendix B

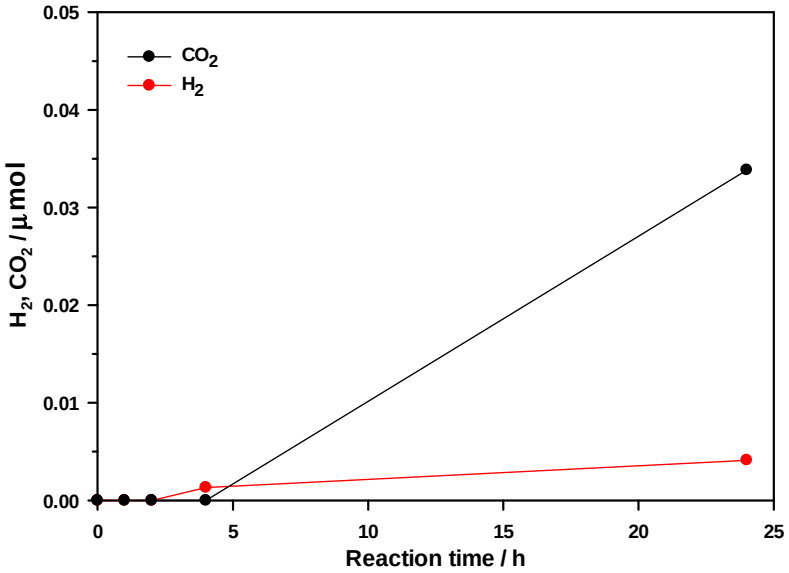

Figure B.1 Hydrogen and carbon dioxide evolution for the photocatalytic conversion of milled MCC using TiO_2 as a catalyst under UV light irradiation and nitrogen pressure. Reaction conditions: milled MCC =50 mg, catalyst =90 mg, T =40±4 °C, t =24 hours, water =40 mL, UV light =1000 W.

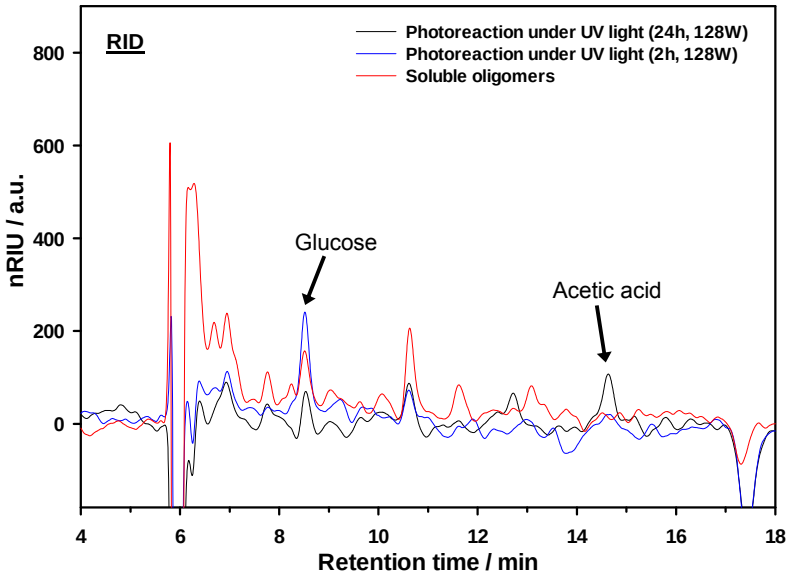

Figure B.2 HPLC-RID chromatograms for the photocatalytic conversion of milled MCC under UV light irradiation (128W) utilising TiO_2 as a catalyst in the presence of a 50/50 v/v water/acetonitrile mixture at atmospheric pressure.

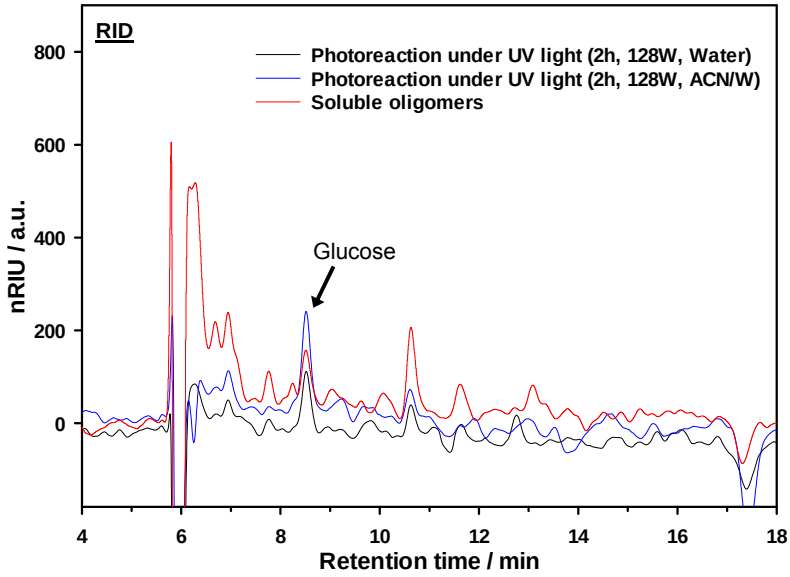

Figure B.3 HPLC-RID chromatograms for the photocatalytic conversion of milled MCC under UV light irradiation (128W) utilising TiO_2 as a catalyst at atmospheric pressure. Comparison of the obtained products between the water (black line) and water/acetonitrile mixture (red line).

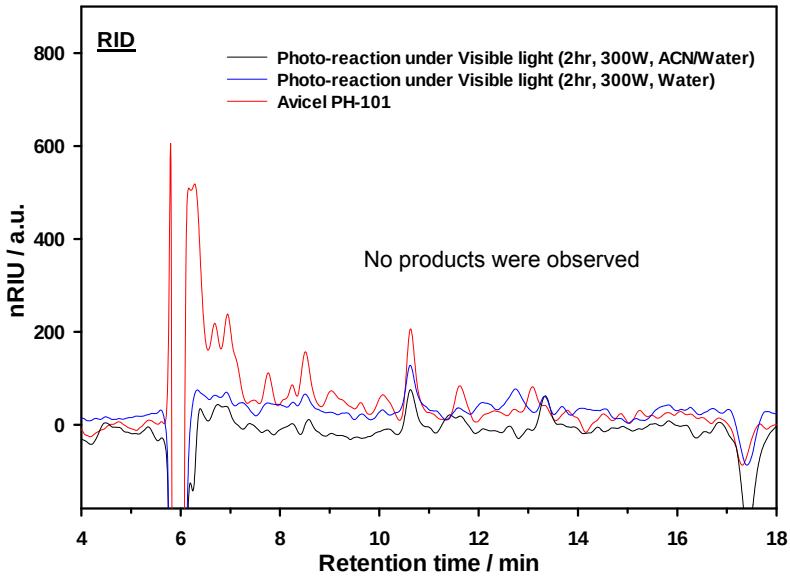

Figure B.4 HPLC-RID chromatograms for the photocatalytic conversion of milled MCC under Visible light irradiation (300 W) utilising the TiO_2 catalyst at atmospheric pressure. The reactions were carried out using water (red line) and a 50/50 v/v water/acetonitrile mixture (black line).

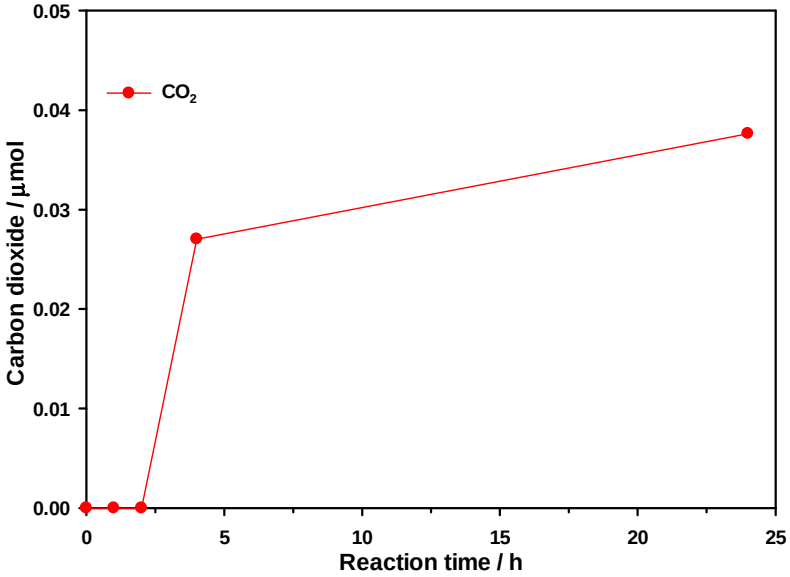

Figure B.5 Carbon dioxide evolution for the photocatalytic hydrogenation of milled MCC using the 1.4 wt% Ru/TiO_2 catalyst under UV light irradiation. Reaction conditions: milled MCC =50 mg, catalyst =90 mg, T =40±4 °C, t =24 hours, water =40 mL, UV light =1000 W, P (H_2) =10 bar.

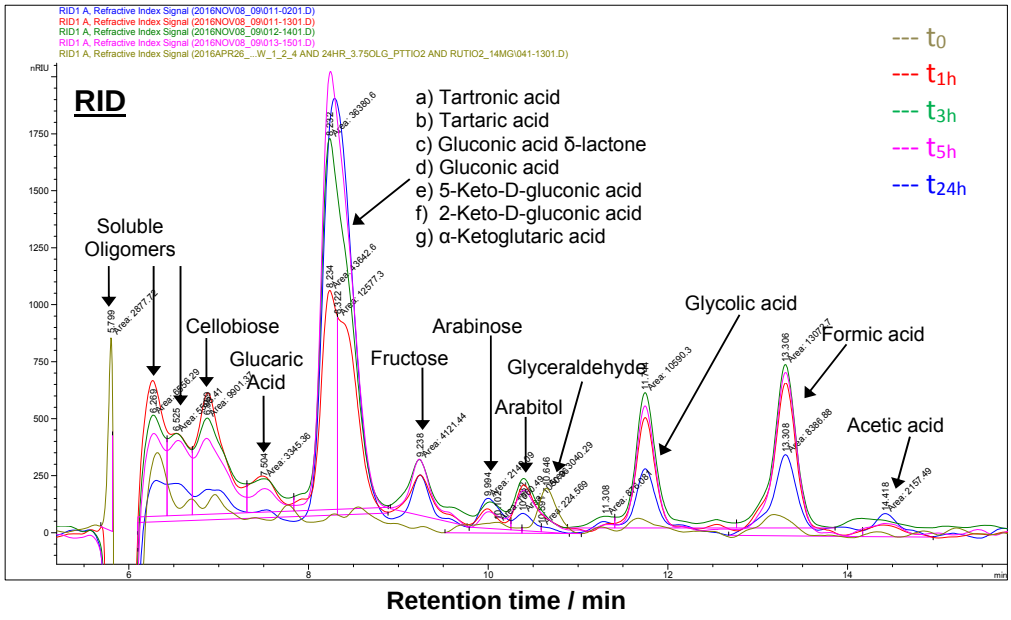

Figure B.6 HPLC-RID chromatograms for the conversion of milled MCC using the TiO_2 catalyst with molecular oxygen under basic conditions in the absence of light.

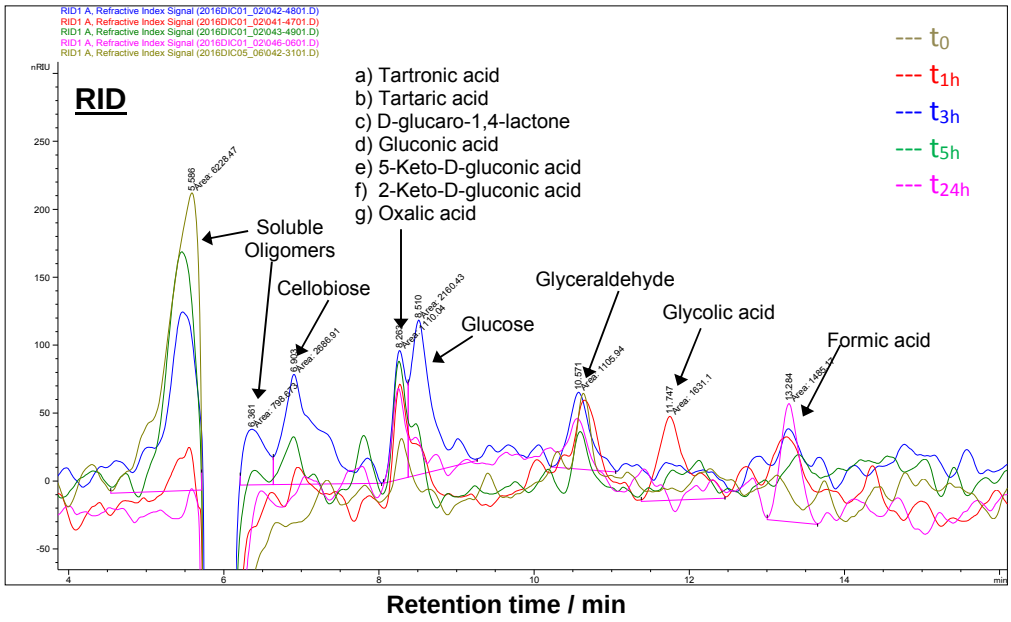

Figure B.7 HPLC-RID chromatograms for the photoconversion of water-soluble starch using the TiO_2 catalyst under visible light irradiation and oxygen pressure. Reaction conditions: Startch =150 mg, catalyst =42 mg, T =40±4 °C, t =24 hours, water =40 mL, Lamp power =1000 W, P (O_2) =10 bar.

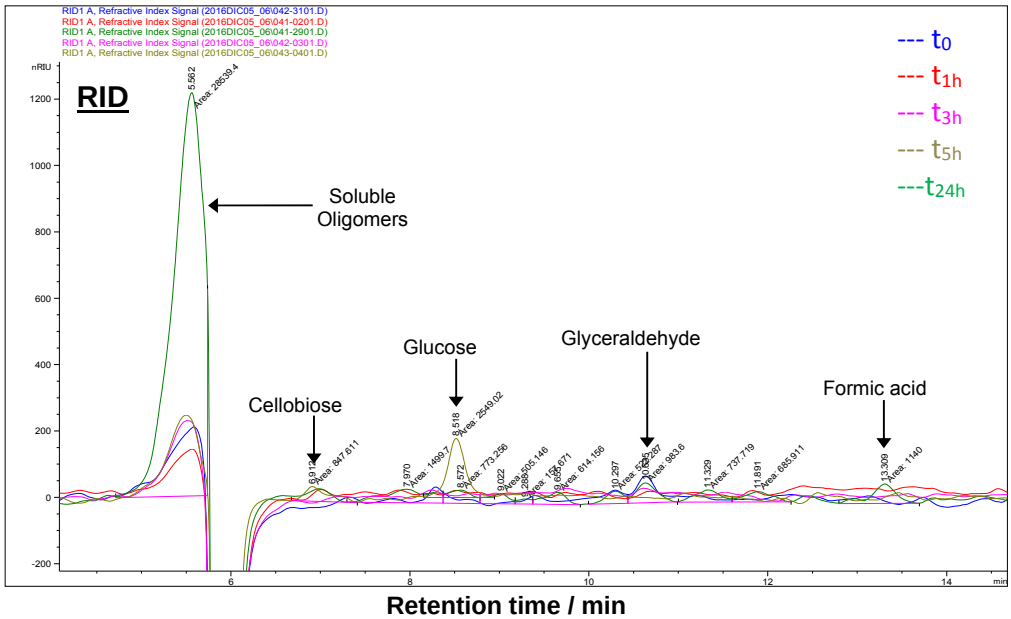

Figure B.8 HPLC-RID chromatograms for the photoconversion of water-soluble starch using the Au/TiO_2 catalyst under visible light irradiation and oxygen pressure. Reaction conditions: Startch =150 mg, catalyst =42 mg, T =40±4 °C, t =24 hours, water =40 mL, Lamp power =1000 W, P (O_2) =10 bar.